ACTIVITY-REGULATED GENES IN PANCREATIC ISLETS AND NEURONS OF THE ARCUATE NUCLEUS

by

Ji Soo Yoon

B.Sc., The University of British Columbia, 2016

A THESIS SUBMITTED IN PARTIAL FULFILLMENT OF THE REQUIREMENTS FOR THE DEGREE OF

DOCTOR OF PHILOSOPHY

in

THE FACULTY OF GRADUATE AND POSTDOCTORAL STUDIES

(Cell and Developmental Biology)

THE UNIVERSITY OF BRITISH COLUMBIA

(Vancouver)

August 2023

© Ji Soo Yoon, 2023

The following individuals certify that they have read, and recommend to the Faculty of Graduate and Postdoctoral Studies for acceptance, the dissertation entitled:

Activity-regulated genes in pancreatic islets and neurons of the arcuate nucleus

submitted by Ji Soo Yoon in partial fulfillment of the requirements for

the degree of Doctor of Philosophy

in Cell and Developmental Biology

Examining Committee:

Francis C. Lynn, Associate Professor, Cell and Developmental Biology, UBC
Supervisor

Jacqueline A. Quandt, Assistant Professor, Pathology and Laboratory Medicine, UBC
Supervisory Committee Member

Mark S. Cembrowski, Assistant Professor, Cell and Developmental Biology, UBC
University Examiner

C. Bruce Verchere, Professor, Pathology and Laboratory Medicine, UBC
University Examiner

Additional Supervisory Committee Members:

Shernaz X. Bamji, Professor, Cell and Developmental Biology, UBC
Supervisory Committee Member

Elizabeth J. Rideout, Associate Professor, Cell and Developmental Biology, UBC
Supervisory Committee Member

Abstract

Both pancreatic islets and hypothalamic arcuate nucleus neurons are critical for energy homeostasis and depend on activity-regulated genes to respond to stimuli. NPAS4 is one such gene that is expressed in both sites and is important for proper function of islets and neurons. The overall goals of my thesis are to profile activity-regulated genes in pancreatic islets and arcuate nucleus neurons, and characterize the functional role of NPAS4 in arcuate nucleus neurons in order to reveal novel mechanisms in cells important in energy homeostasis.

To identify calcium-dependent activity-regulated genes in human islet cell types, I used single cell RNA sequencing on islets that had experimentally induced or inhibited intracellular calcium signalling. In addition to identifying activity-regulated genes in each islet cell type, I found that beta cells with the most calcium-regulated genes expressed the marker PCDH7 and had enhanced glucose-stimulated insulin secretion. In order to study the role of NPAS4 in the arcuate nucleus, I first determined that *Npas4* mRNA was expressed and was induced in AgRP and POMC neurons in the arcuate nucleus in response to peripheral nutrient and endocrine stimuli. Next, I characterized mice with NPAS4 knockout in either AgRP or POMC neurons, with or without high-fat diet, and found that mice with POMC-specific NPAS4 knockout gained less body weight on high-fat diet due to an early reduction in food intake. To determine the molecular mechanism behind this phenotype, I performed single cell RNA sequencing on arcuate nuclei from fasted and refed NPAS4 knockout and control mice fed high-fat diet. I found that the POMC neurons with NPAS4 knockout had reduced *Pomc* expression, increased feeding-regulated genes, and reduced inhibitory GABAergic synapse genes, which could explain the reduced body weight over time. Future experiments would involve assessing

electrophysiological changes in POMC neurons from NPAS4 knockout mice to confirm functional alterations as a result of reduced inhibitory synapses.

Overall, this thesis shows the importance of activity-regulated genes in both pancreatic islets and arcuate nucleus neurons, and shows a novel role of the transcription factor NPAS4 in POMC neurons in regulating energy homeostasis.

Lay Summary

Obesity can result from problems in different organs. The gene NPAS4 is found in the brain and the pancreas, activated by calcium, and is important for responding to changes in the environment. In this thesis, I investigated what other genes are activated by calcium in different types of pancreatic cells, and the role of NPAS4 in brain cells during obesity. In the pancreas, I found that cells that had the most genes activated by calcium secreted more hormones when they were stimulated by sugar. In the brain, I found the NPAS4 gene is in appetite-controlling neurons. NPAS4 deletion from these neurons caused mice to gain less weight by eating less, because of decreased genes that were important in turning off these neurons. Overall, the work in my thesis shows that NPAS4 and other genes activated by calcium in the brain and pancreas play important roles in metabolism and weight gain.

Preface

All experiments were designed by Ji Soo Yoon and Dr. Francis C. Lynn. All experiments were carried out in the BC Children's Hospital Research Institute. Animal protocols were approved by the University of British Columbia Animal Care Committee. All animal work was carried out under breeding certificates A13-0184, A17-0158, and A21-0187, or under the experimental certificates A14-0163, A18-0213, and A22-0202. Unless indicated otherwise below, all experiments and analyses were performed by Ji Soo Yoon.

Chapter 3:

Parts of chapter 3 were published in: Yoon, J.S., Sasaki, S., Velghe, J., Lee, M.Y.Y., Winata, H., Nian, C., Lynn, F.C. Calcium-dependent transcriptional changes in human pancreatic islet cells reveal functional diversity in islet cell subtypes. *Diabetologia.* 2022;65(9):1519–1533. doi:10.1007/s00125-022-05718-1.

The manuscript was written by Ji Soo Yoon and edited by all authors. All data pertaining to the single-cell RNA-sequencing was analyzed by Ji Soo Yoon, Jane Velghe, Michelle Lee, and Helena Winata. The experiments were performed by Ji Soo Yoon, Dr. Shugo Sasaki, Michelle Lee, and Cuilan Nian. Data shown in figures 3.1 and 3.11c-f represent experiments performed and analyzed by Dr. Shugo Sasaki. Michelle Lee performed library generation and sequencing for human islets from donor R282. Cuilan Nian contributed technical expertise in manual picking and dissociation of human islets.

Chapter 4:

For data shown in figure 4.1, the brains of NPAS4$^{-/-}$ and littermate NPAS4$^{+/+}$ mice were kindly gifted by Dr. Jacqueline Quandt (University of British Columbia). The euthanasia, perfusions, and brain harvests for these mice were performed by Pierre Becquart in the laboratory of Dr. Jacqueline Quandt.

Chapter 5:

The original founder mice of the AgRP-CreER and POMC-CreER lines were kindly gifted by Dr. Joel Elmquist (University of Texas Southwestern). For data shown in figures 5.11 and 5.12, metabolic cages in the laboratory of Dr. William T. Gibson were used. All metabolic cage experiments were performed and analyzed by Dr. Daniel Gamu. For figures 5.12d and 5.14c, the body compositions were measured using the EchoMRI-100 in the laboratory of Dr. William T. Gibson. The body composition measurements and analyses were performed by Ji Soo Yoon with the assistance of Dr. Daniel Gamu.

Table of Contents

List of Tables

List of Figures

List of Abbreviations

ADP	Adenosine diphosphate
AgRP	Agouti-related peptide
AMPAR	α-amino-3-hydroxy-5-methyl-4-isoxazolepropionate acid receptor
ARC	Arcuate nucleus
ARG	Activity-regulated genes
ARNT	Aryl hydrocarbon receptor nuclear translocator
ARNT2	Aryl hydrocarbon receptor nuclear translocator protein 2
ATP	Adenosine triphosphate
BDNF	Brain-derived neurotrophic factor
bHLH	Basic helix-loop-helix
BMAL1	Aryl hydrocarbon receptor nuclear translocator-like protein 1
BMAL2	Basic helix-loop-helix ARNT-like protein 2
BMI	Body mass index
CaM	Calmodulin
CaMK	Calcium/calmodulin-dependent protein kinase
cAMP	Cyclic adenosine monophosphate
CART	Cocaine- and amphetamine-related transcript
CHOP	C/EBP homologous protein
CNS	Central nervous system
CREB	cAMP response element-binding protein
CRY	Cryptochrome
CT	POMC-CreER
db/db mice	*Diabetes* mice
DEG	Differentially expressed gene
dH_2O	Distilled water
DMH	Dorsomedial hypothalamus

EDTA	Ethylenediaminetetraacetic acid
EGTA	Egtazic acid
ER	Endoplasmic reticulum
FFA	Free fatty acids
FFAR1	Free fatty acid receptor 1
FFAR2	Free fatty acid receptor 2
FFAR3	Free fatty acid receptor 3
FISH	Fluorescent *in situ* hybridization
FTO	Fat mass and obesity associated
GABA	γ-aminobutyric acid
$GABA_AR$	γ-aminobutyric acid type A receptor
GHSR	Growth hormone secretagogue receptor
GLP-1	Glucagon-like peptide-1
GLP1R	Glucagon-like peptide-1 receptor
GLUT1	Glucose transporter 1
GLUT2	Glucose transporter 2
GLUT3	Glucose transporter 3
GSIS	Glucose-stimulated insulin secretion
GWAS	Genome-wide association studies
HAB	Hibernate® AB complete
HFD	High fat diet
HIF	Hypoxia-inducible factor
hr	Hour
IEG	Immediate early genes
IKKβ	Inhibitor of nuclear factor kappa-B kinase subunit beta
IRE1	Inositol-requiring enzyme 1
K_{ATP} channels	ATP-sensitive potassium channels
KO	POMC-NPAS4 KO

KRBH	Krebs-Ringer bicarbonate HEPES
LEP	Leptin (gene)
LEPR	Leptin receptor (gene)
LH	Lateral hypothalamus
LRG	Late response genes
MAPK	Mitogen-activated protein kinase
MBH	Mediobasal hypothalamus
MC3R	Melanocortin 3 receptor
MC4R	Melanocortin 4 receptor
ME	Medial eminence
MEF2	Myocyte enhancer factor 2
mins	Minutes
NFAT	Nuclear factor of activated T-cells
NF-κB	Nuclear factor kappa-light-chain-enhancer of activated B cells
NMDAR	N-methyl-D-aspartate receptor
NPAS4	Neuronal PAS domain protein 4
$NPAS4^{-/-}$ mice	Germline NPAS4 knockout mice
NPY	Neuropeptide Y
NPY2R	Neuropeptide Y 2 receptor
ob/ob mice	*Obese* mice
PCDH7	Protocadherin 7
PCSK1	Prohormone convertase 1 (gene)
PER	Period
PER	Period
PFA	Paraformaldehyde
PHD	Prolyl hydroxylase domain
PI3K	Phosphatidylinositol 3-kinase
POMC	Proopiomelanocortin

PVN	Paraventricular nucleus
PYY	Peptide tyrosine tyrosine
qPCR	Quantitative real-time PCR
RER	Respiratory exchange ratio
REST	Repressor element 1 silencing transcription factor
ROS	Reactive oxygen species
SCN	Suprachiasmatic nucleus
SF-1	Steroidogenic factor-1
SIM	Simple-minded
SIM1	Single-minded 1
SRF	Serum response factor
STAT3	Signal transducer and activator of transcription 3
tdT	tdTomato
TLR4	Toll like receptor 4
TrkB	Tropomyosin receptor kinase B
VHL	Von Hippel Lindau
VMH	Ventromedial hypothalamus
α-MSH	Alpha melanocortin stimulating hormone

Acknowledgements

First and foremost, I would like to thank my supervisor and mentor, Dr. Francis Lynn. I would not have started nor completed my PhD without his guidance, patience, and his (reasonable) acceptance of my crazy ideas for experiments. It could not have been easy for him to mentor a pessimistic and stubborn student who was working on a project that was so far removed from the expertise of the lab. I was truly lucky that he decided to let me pursue my doctoral studies in his lab, and I hope future students in the lab can feel the same way when they complete their studies.

I would also like to thank my advisory committee members Dr. Shernaz Bamji, Dr. Jacqueline Quandt, Dr. Elizabeth Rideout, and the late Dr. Susie Clee. I was grateful for their kind but constructive support and scientific insights, especially during the pandemic. I hope they continue to inspire future generations of female scientists.

Of course, I would not have completed my PhD without all Lynn lab members, past and present. To Nicole, Eric, and Thilo – Lynn Lab 1.0 – all of you were my mentors, regardless of whether your advice was about science or life. Paul, I only met you once, but your thesis saved me a lot of time on literature searches, so thank you. To Alex, Marcus, and Shan – Lynn Lab 2.0 – we might not have been perfect students, but I think we all found our way in life, one way or another. I'm glad to have met you, and I hope we're all happy in the future, whatever we end up doing in life. To Lynn Lab 3.0, especially Helen, Sam, and Ekaterina: you made the last few years of my degree incredibly enjoyable with your shenanigans, and helped me stay sane. Sorry for not being any sort of role model, since I didn't work with stem cells, but hopefully I was of some help to you over the years. To my previous undergraduate students – Michelle, Helena,

Jane, and James – thank you so much for your help, especially to the ladies who helped me get over my fear of R and coding. Last but not least, to Cuilan, Shugo, and Dahai – I think you all are the most capable people I've ever met during my academic career, and I have nothing but the utmost respect for you. Thank you for helping me run experiments and for listening to me complain when I had too many mice.

Thanks to my brilliant friends: Natasha, Charlotte, Amelia, Atefeh, Lianna, Mriga, Sarah, Meghan, and Priya. I know I wouldn't have been the same person I am today without your support and love. Thanks to the brilliant scientists I met in the BCCHR 4th floor and Canadian diabetes research community, especially Steph, Ben, Austin, Sigrid, Sau, Kevin, and Noa. Thank you to my mother and father, for being the best parents you could've been for me. I know you still don't really get what I worked on for a good chunk of my twenties, but please know that your support and unconditional love was always appreciated. Finally, to Sterling Megas, my partner in life who put up with me before and during my PhD life – I love you, and I hope we continue to be happy together.

Dedication

To my parents and Sterling, who I love very much.

Chapter 1: Introduction

1.1 Obesity

Obesity is now recognized as a metabolic disease where the excessive accumulation of fat impairs normal bodily functions[1]. It was recently reported from the Global Burden of Diseases, Injuries, and Risk Factors Study of 2019 that the prevalence of obesity and type 2 diabetes increased but unlike other metabolic diseases, mortality rates did not decrease over the past 10 years[2]. Most concerningly, the global prevalence of obesity has tripled since the 1970s, alongside an increase in mean body mass index (BMI) in children, adolescents, and adults[3,4]. In 2016, it was reported that 39% of the global adult population was estimated to be overweight (BMI ≥ 25kg/m^2) and 13% of adults was estimated to be obese (BMI ≥ 30 kg/m^2)[3]. The reason why the rising rate of obesity is a serious public health concern is because obesity is a major risk factor for developing additional non-communicable diseases. Obesity is one of the highest risk factors for metabolic diseases such as type 2 diabetes and cardiovascular diseases[5–8]. In addition, it has been found during the ongoing COVID-19 pandemic that obesity was a significant risk factor for developing more severe symptoms in patients[9].Due to its additional association with an overall increase in risk of mortality[5,10–12], obesity requires additional attention in order to alleviate this burden to global health, especially in today's "obesogenic" environment.

1.2 Characteristics of obesity

A defining feature of obesity is the abundance of fat mass in the body and altered adipocyte biology. White adipocytes normally accumulate triglycerides as an important source of stored energy for survival in times of nutrient deficit. In an obese state, the amount of triglycerides stores is increased and the rate of triglyceride removal is decreased[13]. The expression levels of

hormone-sensitive lipase and adipose triglyceride lipase, which are enzymes important for lipolysis, are decreased in obese adipocytes[14]. This has also been observed in insulin-resistant states independent of obesity[15]. Adipocyte numbers are also altered during obesity, further influencing the accumulation of fat mass[16]. It has been reported that adipocyte numbers are likely pre-determined at a young age and usually remain constant independent of BMI, but obese adults are known to have more adipocytes than non-obese adults[13,16,17]. Adipocytes also act as an endocrine organ, which secretes multiple adipokines that are important in whole-body regulation of metabolism. There is considerable research showing that adipocyte function is altered during obesity, including altered levels of adipokine secretion[18,19]. One example is adiponectin, which normally circulates at levels inversely proportional to the adiposity in the body[20]. In humans with increased adiposity, there is a reduction in adiponectin levels, and this has been associated with lower insulin sensitivity and higher risk of type 2 diabetes[20–22]. Another example is leptin, which circulates at levels proportional to fat mass, and is increased in people with obesity [23,24]. Obesity has also been described as a state of chronic low-grade inflammation. Macrophages accumulate in the adipose tissue in obese states and are known to secrete inflammatory cytokines such as interleukin 6 and tumor necrosis factor alpha[25–27].

In addition to altered adipose tissue biology, further features of obesity include hyperinsulinemia and insulin resistance, which are also associated with type 2 diabetes. Generally, people with obesity show greater insulin secretion even without pronounced insulin resistance, so increased basal and postprandial insulin levels have been associated with obesity[28]. It has been shown that these elevated insulin levels are sufficient to overcome the decreased efficiency of insulin action and to maintain normal glucose homeostasis, provided the insulin-secreting beta cells are still

functional[29,30]. It has been shown that one of the more important determinators of insulin resistance is free fatty acids (FFA). People with obesity have been shown to have elevated levels of FFA in the bloodstream, despite the lower rate of FFA release compared to people who are lean[31]. This is due to the overall larger amount of fat mass, so the rate of FFA release relative to fat-free mass is actually greater in people with obesity[31]. Even acutely increasing plasma levels of FFA leads to insulin resistance in humans[32], while lowering plasma FFA levels have been shown to improve insulin sensitivity[33]. This hyperlipidemia present in obesity, along with hyperglycemia, can lead to beta cell dysfunction through nutrient-induced stress [34,35]. Taken together, obesity is a systemic disease in which multiple tissues crucial to maintaining normal metabolism, such as adipose tissue and pancreatic beta cells, are affected and dysregulated.

1.3 Genetics of obesity

While the stigmatized view of obesity development frames the causes of obesity as solely environment/lifestyle drivers and frames obesity as a consequence of "poor willpower", there is now evidence to support the genetic causes of obesity. First, the heritability of obesity, or heritability in BMI in general, has been estimated to be between 40% and 70%[36,37]. Twin studies have shown that body weight, height, BMI, and fat distribution all show high heritability and support a genetic basis of obesity[36–39]. Second, there have been multiple genome-wide association studies (GWAS) that have reported genetic variations that increase the risk of developing obesity, specifically polygenic obesity; a famous example is the intronic single nucleotide polymorphism rs9939609 in the fat mass and obesity-associated (*FTO*) gene that is associated with increased BMI[40]. Following the identification of *FTO*, numerous GWAS have

been conducted on increasingly larger populations, and now have included hundreds of thousands of individuals to identify hundreds of loci of interest[41]. Not all of these GWAS have focused on BMI because it is a rather crude indicator of adiposity, and have instead focused on other indicators of obesity such as body fat mass[42,43], lean body mass[44], and circulating leptin levels[45]. Others have even focused on the opposite phenotype, thinness, to determine GWAS loci for preventing obesity and body weight gain[46,47]. Finally, there are cases of human monogenic obesity that are caused by a single mutation in a single gene. These cases of monogenic obesity in humans are rare but severe early-onset cases of obesity. The genes that are confirmed to be human obesity genes include leptin (*LEP*)[48], leptin receptor (*LEPR*)[49], prohormone convertase 1 (*PCSK1*)[50], proopiomelanocortin (*POMC*)[51,52], and melanocortin 4 receptor (*MC4R*)[53,54]. The above evidence provides support for the genetic basis of obesity and justifies studying the roles of various genes that are potentially important in obesity development, whether they are further influenced by environmental factors or not.

1.4 Hypothalamic control of energy homeostasis

Obesity is fundamentally a state of sustained impaired energy homeostasis. Energy homeostasis is a concept where energy intake is balanced by energy expenditure. Energy intake is composed of feeding and subsequent nutrient absorption for storage, while energy expenditure is achieved through a combination of physical activity, adaptive thermogenesis, and basal metabolism[55]. Obesity is a state of positive energy balance, in which the total energy intake exceeds total energy expenditure, causing an increase in storage of the excess energy. Studying the mechanisms of energy balance, particularly energy intake in the form of feeding, may be the key in progressing the understanding of obesity.

Mammalian energy homeostasis is regulated by the central nervous system (CNS) through the control of feeding and activity in response to changes in nutrient availability and endocrine signalling[56]. In the CNS, the hypothalamus regulates the homeostatic process of feeding, and is comprised of distinct regions such as the arcuate nucleus (ARC), paraventricular nucleus (PVN), ventromedial hypothalamus (VMH), and lateral hypothalamus (LH)[57]. Classical experiments of creating bilateral lesions implicated the hypothalamus in the control of energy homeostasis as early as 1940[58]. Later studies showed that lesions in the VMH caused obesity through increased food intake, while lesions in the LH caused decreased food intake, implying the VMH promotes satiety and the LH promotes food intake[59]. Lesions to the PVN also resulted in overeating and obesity, implying the PVN is a site that promotes satiety, similar to the VMH[60]. Finally, the ARC is adjacent to the 3rd ventricle and the median eminence (ME), a circumventricular organ that is an interruption in the blood-brain barrier, which allows endocrine and nutrient signals to reach ARC neurons[23]. The anatomical arrangement of these hypothalamic nuclei important in feeding regulation are found in Figure 1.1. Although the initial crude lesion studies highlighted the general role of hypothalamic nuclei in regulating food intake, more precise methods in the following decades revealed specific neuronal populations within hypothalamic nuclei that are now known to be critical in maintaining energy homeostasis.

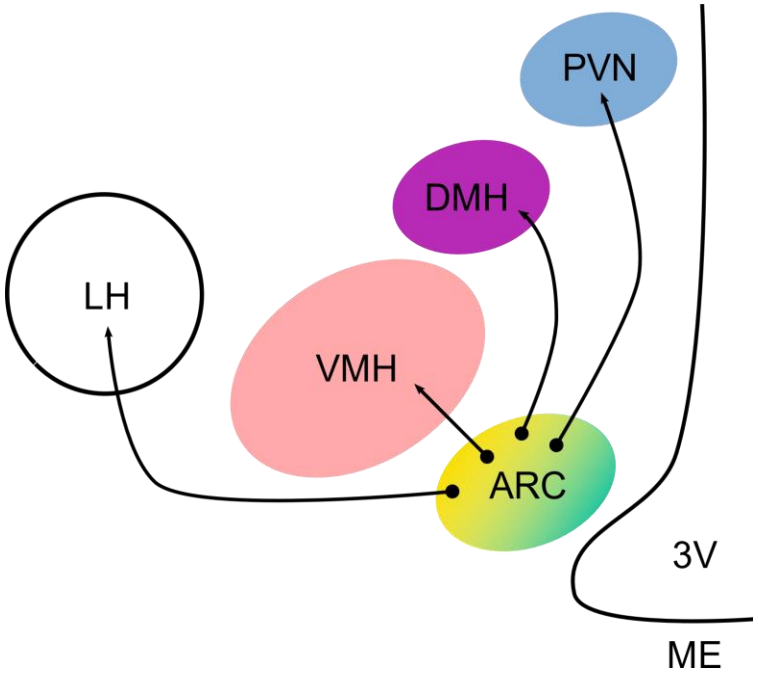

Figure 1.1 | The hypothalamic nuclei involved in regulation of feeding. Black lines represent projections that arise from the arcuate nucleus to other hypothalamic nuclei. ARC = arcuate nucleus, VMH = ventromedial hypothalamus, DMH = dorsomedial hypothalamus, PVN = paraventricular nucleus, LH = lateral hypothalamus, 3V = 3rd ventricle, ME = median eminence.

1.5 Neurons of the arcuate nucleus

The ARC is the site of first-order neurons that sense nutrient availability and endocrine signals from the periphery. There are two functionally opposing neuronal populations in the ARC. One orexigenic population expresses neuropeptides agouti-related peptide (AgRP) and neuropeptide Y (NPY)[56,61]. The other anorexigenic population expresses the neuropeptides cocaine- and amphetamine-regulated transcript (CART) and alpha melanocortin stimulating hormone (α-MSH), which is derived through proteolytic processing of the precursor POMC protein[56,62,63]. These AgRP/NPY neurons and POMC/CART neurons are two populations that are part of the central melanocortin system. The ARC neurons project into the PVN, where second-order neurons express the melanocortin 3 (MC3R) and melanocortin 4 (MC4R) receptors[64]. α-MSH from POMC/CART neurons is an agonist ligand for these receptors, while AgRP from

AgRP/NPY neurons is a competitive antagonist for the same receptors[64–66]. Neurons of the PVN respond to the neuropeptides from the ARC by controlling sympathetic outflow to the periphery and increasing lipolysis, and neurons that express the transcription factor single-minded 1 (SIM1) in the PVN are critical for inhibiting food intake and increasing energy expenditure[60,67,68]. In addition to the PVN, ARC neurons project into the VMH, a satiety-promoting region containing MC4R-expressing neurons[69]. Downstream of the melanocortin signalling from the ARC, neurons in the VMH that express the transcription factor steroidogenic factor-1 (SF-1) are activated and secrete the neuropeptide brain-derived neurotrophic factor (BDNF), which signals through the tropomyosin receptor B (TrkB) receptor to promote satiety[70,71]. A schematic of this system is represented in figure 1.2.

Overall, this melanocortin system is reliant on AgRP and POMC neurons detecting endocrine and nutrient signals from the periphery, then secreting their respective neuropeptides to activate or inhibit MC4R-expressing neurons. Activation of AgRP neurons leads to secretion of AgRP and promotion of food intake, while activation of POMC neurons leads to secretion of α-MSH and inhibition of food intake[72,73]. In addition, AgRP neurons are known to directly inhibit POMC neuronal activity by releasing the inhibitory neurotransmitter γ-aminobutyric acid (GABA)[74], further contributing to the regulatory circuit of food intake.

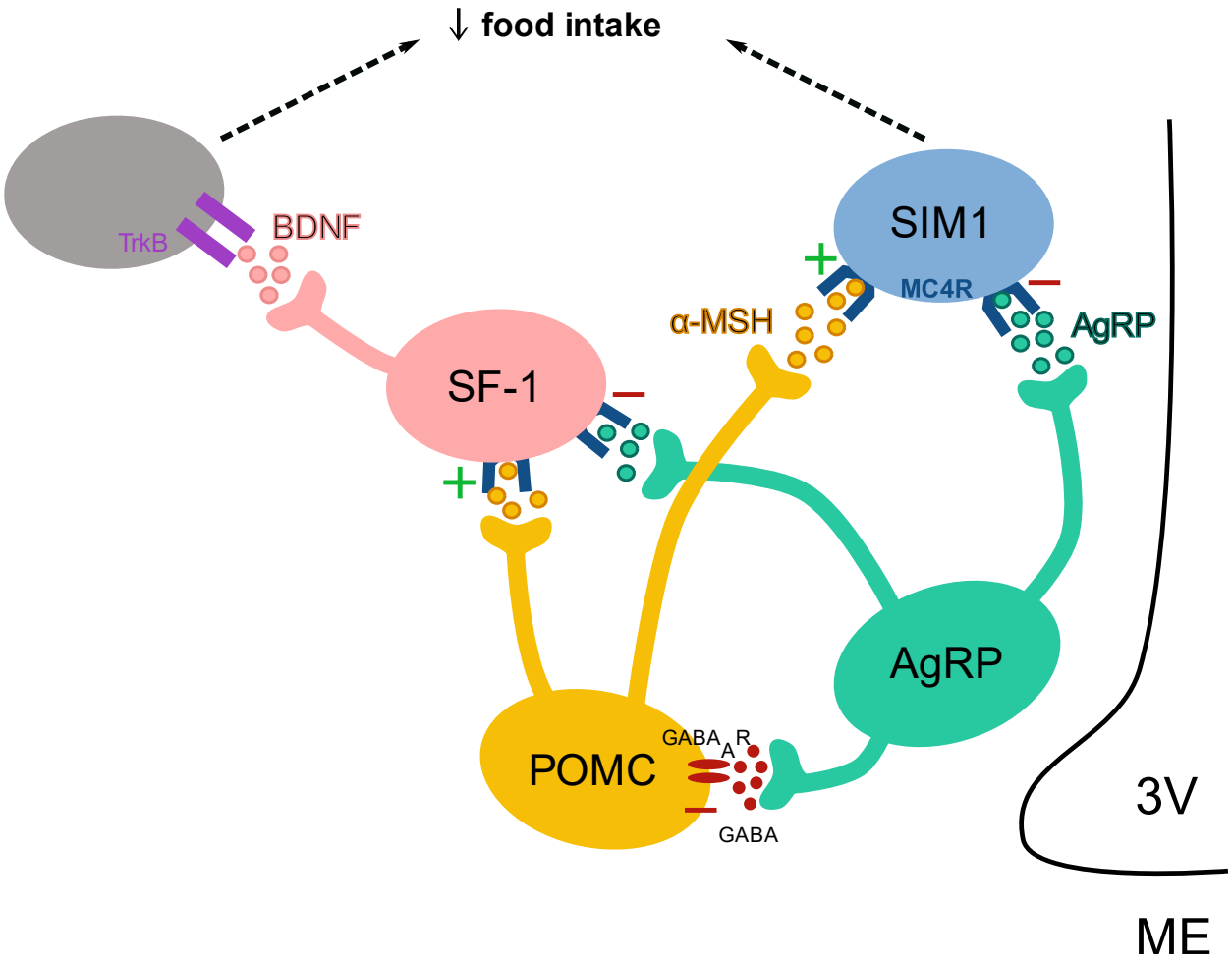

Figure 1.2 | A simplified schematic of food intake regulation by POMC and AgRP neurons through neuropeptide signalling to higher-order neurons. 3V = 3rd ventricle, ME = median eminence, POMC = proopiomelanocortin, AgRP = agouti-related peptide, SF-1 = steroidogenic factor-1, SIM1 = single-minded 1, BDNF = brain-derived neurotrophic factor, TrkB = tropomyosin receptor kinase B, α-MSH = alpha melanocortin stimulating hormone, GABA = γ-aminobutyric acid, $GABA_AR$ = GABA type A receptor.

1.6 Mouse models of obesity

As discussed above in section 1.5, genes that encode factors of the melanocortin signalling pathways in the hypothalamus are crucial for food intake regulation and are often the causal mutated genes in rare human cases of monogenic obesity (discussed in section 1.3). Many of these genes, such as *LEP*, *LEPR*, *MC4R*, or *POMC*, were initially identified and studied in mice, which led to the discovery and generation of various obese mouse models. For instance, the

discovery of the leptin and leptin receptor genes stemmed from the *obese* (*ob/ob*) and *diabetes* (*db/db*) mouse lines which are still used for obesity studies today. The *ob/ob* mouse was a spontaneously arisen mutant mouse that displayed severe hyperphagia and obesity, and was first reported in 1950[75]. The *db/db* mouse was similarly reported in the 1960's as a new mutation that resulted in a profound diabetes-like phenotype and abnormal fat accumulation[76]. However, the identities of the genes were not identified until the 1990's, when the *obese* gene was shown to be the leptin gene[77], and *diabetes* was shown to be the leptin receptor gene with reverse genetics[78], implicating the critical role of leptin signalling in the brain for maintenance of healthy body weight. While both *ob/ob* and *db/db* mice displayed early-onset hyperphagia and reduced energy expenditure, leptin treatment caused reduced food intake and body weight in the *ob/ob* mouse, but not in the *db/db* mouse due to the mutated leptin receptor[79,80]. The gene *Agrp*, encoding for the orexigenic AgRP peptide, was also first discovered from a mouse that had an obese and diabetic phenotype termed "lethal yellow" due to its coat colour, which was the result of a mutation that caused constitutive *Agrp* expression[81,82]. It was later found that the AgRP peptide was an antagonist of MC4R, connecting the role of melanocortin signalling to regulating food intake and body weight[65,66,83].

Following the implication of the hypothalamic melanocortin pathways in obesity, mouse models were generated with genetic knockout of key genes involved in melanocortin signalling downstream of leptin. One example was a transgenic POMC-deficient mouse ($POMC^{-/-}$), which not only lacked α-MSH, but all peptide products of the *Pomc* gene[84,85]. As expected of mice lacking an anorexigenic peptide, $POMC^{-/-}$ mice were reported to be obese, hyperphagic, and showed altered pigmentation[84]. Even heterozygous $POMC^{+/-}$ mice developed an intermediate

obese phenotype, indicating the importance of this locus in food intake regulation[85]. Interestingly, mice with genetic knockout of *Agrp* (AgRP$^{-/-}$), or *Npy* (NPY$^{-/-}$), or both, show minimal changes to food intake and body weight[86]. Follow-up studies also generated an AgRP and POMC double knockout mouse, which showed a phenotype very similar to the POMC$^{-/-}$ mouse[87]. While both the double knockout and POMC$^{-/-}$ mouse respond to α-MSH treatment by reducing food intake, AgRP administration caused no effects in the double knockout mouse, confirming the role of AgRP peptide as a melanocortin antagonist[85,87]. Similar to humans with MC4R mutations, MC4R-deficient (MC4R$^{-/-}$) mice have been shown to be obese, hyperinsulinemic, hyperleptinemic, hyperglycemic, and resistant to the satiety-inducing effects of leptin administration because MC4R is downstream of leptin signalling in the ARC[88,89]. In contrast to MC4R$^{-/-}$ mice, MC3R-deficient (MC3R$^{-/-}$) mice were shown to not have significantly increased significantly body weight, but instead showed a specific increase in relative fat mass with reduced fat oxidation[90]. Mice with double knockouts of the MC3R and MC4R displayed significantly heavier body mass than MC4R$^{-/-}$ mice, showing that the downstream of actions of signalling through the MC3R and MC4R are not redundant[91].

As methods of ablating specific populations of neurons were developed, it became possible to selectively remove entire neuronal subtypes from a specific region of interest instead of performing genetic knockouts. Mice with ablated POMC neurons displayed a reduction in food intake, but still developed obesity and hyperglycemia, alongside reduced energy expenditure[92]. A more specific model where only POMC neurons in the ARC were ablated showed increased food intake, reduced energy expenditure, and the development of obesity[73]. In contrast to AgRP$^{-/-}$ mice, ablation of AgRP neurons in adult mice caused reduction in feeding to the point of

starvation[93,94]. However, ablation of AgRP neurons in neonatal mice showed minimal effects on food intake, suggesting potential compensation for the loss AgRP neurons on feeding regulation during development[94]. Taken together, the above studies clearly showed that the individual genes and neuronal subtypes involved in central melanocortin signalling are crucial for proper food intake. The disruption of any of the anorexigenic factors, including peripheral signals like leptin, result in obesity, which showed the importance of endocrine signalling on the CNS in the maintenance of energy homeostasis.

1.7 Endocrine signalling on ARC neurons

Classically, AgRP/NPY neurons are activated by stimuli indicating low energy states such as fasting and POMC/CART neurons are activated by stimuli indicating high energy states such as feeding. In fact, due to their location in the mediobasal hypothalamus (MBH) adjacent to the ME, a circumventricular organ, these neurons are in an ideal location to access circulating endocrine signals that convey information about the body's energy states, secreted from peripheral tissues such as adipose tissue, pancreatic islets, and the gut enteroendocrine cells. One such signal is the adipokine leptin, which was briefly mentioned in section 1.2. Leptin secreted from white adipocytes in proportion to body fat mass signals through the leptin receptor, which is located on both AgRP and POMC neurons. Leptin has been shown to directly activate POMC neurons and promote secretion of α-MSH[63,95,96] but inhibits AgRP neurons through the same leptin receptors[97–99]. Mice with leptin receptor knockout specifically in POMC neurons (POMC-Lepr KO) or in AgRP neurons (AgRP-Lepr KO) both displayed obesity[100,101]. However, the increased fat mass in POMC-Lepr KO mice was not due to a food intake or energy expenditure difference[100], but AgRP-Lepr KO mice showed increased fat mass and food intake[101]. Insulin

secreted from pancreatic beta cells can also directly signal to these neurons via the insulin receptor, which is also located on both AgRP and POMC neurons. The effects of insulin, however, was not found to be as clear as leptin. Insulin was initially characterized to cause hyperpolarization in AgRP neurons, which could be reversed by tolbutamide, a blocker of ATP-sensitive potassium (K_{ATP}) channels[102]. Through knockout studies of leptin receptor specifically in AgRP and POMC neurons, it was found that insulin signalling in AgRP neurons only was necessary for suppression of hepatic glucose production[102]. However, there were no effects of knocking out insulin receptor in either cell type on body weight or food intake regulation. Direct injection of insulin into the 3rd ventricle was found to increase *Pomc* gene expression[103], but there is also data to suggesting insulin inhibits POMC activity by hyperpolarization through the K_{ATP} channels, similar to insulin action on AgRP neurons[104,105]. More recent studies show that whether insulin activates or inhibits POMC neurons is plastic and actively regulated depending on the fasted or fed state of the animal[106,107].

Gut hormones, secreted from enteroendocrine cells of the intestine, have also been found to regulate food intake by signalling to ARC neurons[108]. Peptide tyrosine tyrosine (PYY) is a gut hormone that is present at very low levels in circulation during fasting conditions, but is elevated postprandially[109]. Both peripheral and central administration of PYY have been shown to reduce food intake and body weight in rodents, signalling through the NPY 2 receptor (NPY2R)[110–112]. PYY has also been shown to activate POMC neurons by inhibiting NPY neuron terminals and increasing *Pomc* mRNA expression in the ARC[110,111]. The incretin glucagon-like peptide-1 (GLP-1) also has been shown to affect food intake and body weight. Acute peripheral and central administration of GLP-1 have been shown to decrease food intake and body weight, and these

effects can be sustained chronically with repeated administrations of GLP-1 in rats[113,114]. In humans, it has been reported that intravenous administration of GLP-1 reduced *ad libitum* food intake in a dose-dependent manner, in both people with obesity and people who are lean[115]. The receptor for GLP-1, GLP-1 receptor (GLP1R), was found to be expressed in multiple feeding regulatory nuclei, including the ARC, VMH, and PVN[116], suggesting GLP-1 can signal to multiple neuronal subpopulations. Specifically in the ARC, GLP-1 has been found to directly activate POMC/CART neurons and inhibit AgRP/NPY neurons, and this is likely one of the mechanisms by which the GLP-1 analog drug liraglutide induces weight loss[117]. Among the anorexigenic peripheral hormones, ghrelin is the lone orexigenic gut hormone that operates in the opposite manner as leptin. Both central and peripheral administration of ghrelin has been found to rapidly induce feeding behaviour in rodents by activating neurons of the ARC, PVN, DMH, and the LH[118–120]. Ghrelin signalling through the growth hormone secretagogue receptor (GHSR) in the ARC has been shown to be the primary site of its action to increase food intake, and mice with diet-induced obesity show ghrelin resistance in their AgRP/NPY neurons[121,122]. In humans, ghrelin is induced in a fasting-dependent manner and people with obesity have lower fasting ghrelin than people who are lean[123,124]. In addition to leptin, insulin, PYY, GLP-1, and ghrelin, there are numerous other peripheral hormones that are known to act on the brain to influence food intake[108]. The established roles of these peripheral hormones further show how the ARC acts as center of feeding regulation, and its importance in integrating these signals to maintain energy homeostasis.

1.8 Nutrient sensing in ARC neurons

In addition to responding to peripheral endocrine signals, ARC neurons also respond to the

fluctuating energy states by directly detecting nutrient levels in circulation. All cells naturally have the capability of taking up nutrients for survival and proper function, but the activity of neurons have been shown to be coupled to nutrient sensing to some degree[125]. The idea that the hypothalamus was able to monitor the glucose levels in the body somehow and translate these glucose levels into electrical activity was suggested as early as 1953[126]. In the years that followed, two groups identified the "glucose-sensing neurons" in the hypothalamus independently and showed that extracellular glucose concentrations affects neuronal firing[127,128]. Since these early studies, the presence of largely two populations of neurons has been established within the hypothalamus: glucose-excited neurons and glucose-inhibited neurons[125,129,130]. As the names imply, glucose-excited neurons are neurons that increase their activity in response to rising glucose concentrations, and glucose-inhibited neurons are neurons that are activated in response to hypoglycemic conditions. Although the focus here will be the ARC neurons, glucose-excited and glucose-inhibited neurons are located throughout the hypothalamic nuclei[130]. Within the ARC, there are both glucose-excited and glucose-inhibited neurons that respond to higher and lower ranges of glucose, respectively[131–133]. It's important to note that unlike peripheral glucose levels in circulation, glucose levels in the CNS are much lower, ranging from 1mM to 2.5mM normally, never exceeding 5mM in physiological conditions, and falling as low as 0.5mM during hypoglycemia[133] . In rats, it has been found that during a plasma glucose range of 2mM to 18mM, the equivalent in the ARC and VMH is 0.2mM to 4.5mM, with a steady state around 2.5mM[134]. At least 40% of AgRP/NPY neurons in the ARC are known to be glucose-inhibited neurons, and lower concentrations of glucose have been shown to cause calcium oscillations and depolarization[132,135,136]. In fasting conditions when glucose levels are lowered, it has been shown that incubation in 0.7mM glucose enhanced neuronal activity and NPY release

rate, and the neurons can be activated by a smaller magnitude of glucose flux[137]. This makes sense, as AgRP/NPY neurons are responsible for increasing food intake in response to negative energy states, and activation in lower glucose levels would promote food intake to restore normoglycemia. As expected, POMC neurons are mostly glucose-excited and increasing extracellular glucose concentrations have been shown to activate POMC neurons[138]. The electrical activity of POMC neurons is modulated in response to changes in extracellular glucose, and the secretion of α-MSH increases with increasing glucose[132,139]. The glucose-sensing mechanism in glucose-excited POMC neurons has been shown to be quite similar to the mechanism in pancreatic beta cells[140–143]. Briefly, this mechanism relies on glucose uptake through glucose transporters (GLUT), glucokinase, and closure of K_{ATP} channels that leads to depolarization and calcium influx, triggering neurotransmitter release. Although the widespread glucose transporters in the CNS are thought to be GLUT1 and GLUT3, the expression of GLUT2 has also been reported on ARC neurons[144,145]. It has also been shown that glucose-sensing depends on an increase in mitochondrial reactive oxygen species downstream of glucose uptake, acting as a short-lived signal in addition to the rise in ATP/ADP ratio[131,141,143,146]. With regards to regulating energy intake, it has been shown that there is a drop in blood glucose levels before the act of feeding, and a sustained central administration of glucose leads to an inhibition of feeding along with a reduction in body weight over time[147,148]. However, inhibition of glucose metabolism with central administration of 2-deoxy-D-glucose can induce food intake[149,150]. Given the known roles of AgRP/NPY and POMC/CART neurons, it seems likely that the glucose-excited and glucose-inhibited neurons in each population detect a rise or drop in local glucose concentrations and respond accordingly by secreting their orexigenic and anorexigenic neuropeptides, respectively.

Traditionally, lipids were not thought of as a nutrient signal for neurons because they are not the conventional fuel source for the central nervous system. Peripherally administered FFAs have been found to cross the blood-brain barrier to the CNS[151,152]. Depending on the nature of FFA, they were shown to be either oxidized or incorporated into phospholipids once in the brain[153]. Once it was established that fatty acids were able to reach the neurons, the possibility of fatty acids as another nutrient signal that is sensed by neurons became appealing, particularly in studies of diet-induced obesity that used a high fat diet (HFD). Similar to glucose, central administration of fatty acids has been shown to decrease food intake[154]. Infusion of FFA into the carotid artery of rats showed activation in the LH, but an inhibition of neurons in the ARC, PVN, DMH, and VMH[155]. Specifically in the ARC, oleic acid has been shown to modulate neuronal firing in distinct populations and demonstrated minimal overlap between neurons that were glucose-sensing and neurons that were lipid-sensing[156]. Specifically, at least 40% of POMC neurons have been shown to be directly excited by oleic acid through inhibition of K_{ATP} channels, while AgRP neurons were unaffected by oleic acid[157]. This effect was shown to be rather specific for a long-chain fatty acid and could not be shown with a short-chain fatty acid like octanoic acid. In obesity-prone mice, palmitate infusion causes a rapid increase in ARC *Pomc* expression and *Pcsk1* expression, and inhibition of PCSK1 enzyme (encoded by *Pcsk1*) caused increased caloric intake and body weight in these mice[158]. In humans, it was found that the levels of β-endorphin, another product of POMC processing, but not α-MSH, decreased significantly in some individuals after consumption of a high-fat meal and this was possibly correlated with less body weight gain over time, based on similar rodent studies[159].

In summary, it is well-established that the neurons of the ARC are able to detect and respond to a variety of systemic nutrient signals as well as peripheral endocrine signals. This further supports the role of the ARC neurons as primary regulators of energy homeostasis that respond to both positive and negative energy states. Preservation of function or protection of these neurons will be critical in prevention of obesity, especially when the system is under chronic exposure to high glucose or high fats.

1.9 Consequences of diet-induced obesity in the ARC

Whether or not diets high in fat primarily cause human obesity has been debated[160,161], but HFD is commonly used in rodent obesity studies due to the commercial availability and reproducible induction of weight gain. It has been demonstrated that mice fed HFD display both increased body weight and fat mass, sometimes accompanied by altered glucose homeostasis as well[162,163]. Specifically within the hypothalamus, it has been shown that diet-induced obesity leads to hypothalamic inflammation[164,165]. Hypothalamic inflammation has been reported to occur within one to three days of HFD feeding before any significant weight gain, whereas peripheral inflammation occurs in response to overt obesity[166]. Saturated fatty acids that can cross the blood-brain barrier have been shown to trigger inflammatory signalling in the hypothalamus through toll like receptor 4 (TLR4) and downstream inhibitor of nuclear factor kappa-B kinase subunit beta (IKKβ) and nuclear factor kappa-light-chain-enhancer of activated B cells (NF-κB) activation, leading to increased expression of pro-inflammatory genes[165,167,168]. Activation of the inflammatory signalling cascade across the MBH has been shown to increase food intake and negatively affect insulin and leptin signalling, but specific activation of IKKβ and NF-κB in AgRP neurons protected against obesity[165]. Hypothalamic inflammation in obesity has also been

shown to cause direct hypothalamic injury and neuronal apoptosis in the ARC[166,169]. Specifically in POMC neurons, chronic HFD feeding caused mitochondrial stress in addition to inflammation, which eventually resulted in a decreased number of POMC neurons[170,171]. HFD has also been shown to decrease levels of reactive oxygen species (ROS) in POMC neurons, which leads to a decrease in ROS-induced activation of POMC neurons and overall increase in food intake[172]. Finally, the increased FFA has been shown to increase intracellular ATP concentrations in POMC neurons, but the neurons displayed membrane hyperpolarization instead of the expected depolarization, decreasing overall POMC firing[157].

Another consequence of diet-induced obesity is endoplasmic reticulum (ER) stress, which contributes to central insulin and leptin resistance[173,174]. Directly triggering ER stress by centrally administering thapsigargin has been shown to induce food intake, increase body weight, inhibit insulin and leptin action, and increase ER stress markers inositol-requiring enzyme 1 (IRE1) and C/EBP homologous protein (CHOP)[175]. Conversely, chemically reducing ER stress by central administration of tauroursodeoxycholic acid or 4-phenyl butyric acid sensitized the hypothalamus to leptin action[173]. ER stress can also directly affect POMC neuronal function in diet-induced obesity by reducing levels of prohormone convertase 2, which is necessary for proper processing of the POMC precursor peptide into the anorexigenic α-MSH.

HFD feeding also impacts synaptic organization within the hypothalamus[176,177]. Even before exposure to HFD, rats that are prone to obesity possess greater numbers of inhibitory synaptic inputs on POMC neurons than rats that are resistant to obesity[176]. After 3 months of HFD feeding, POMC neurons in obesity-resistant rats had an increased total number of synapses,

while obesity-prone rats had a decreased total number of synapses[176]. Even in a genetic obesity model, leptin-deficient *ob/ob* mice showed increased inhibitory synapses on POMC neurons and increased excitatory synapses on AgRP/NPY neurons, while the opposite was observed in wild type lean mice[177]. Upon leptin treatment, the synaptic densities on POMC and NPY neurons of *ob/ob* mice were reversed within 6 hours to resemble those of wild type mice, but ghrelin administration in wild type mice reorganized synapses to suppress POMC neuronal tone[177].

In rodent models of diet-induced obesity using HFD, the resulting inflammation, stress, cell death, and synaptic organization greatly impacts POMC neurons over AgRP neurons. The negative effects of obesity not only impact the function and survival of these ARC neurons, but also impair their ability to respond to peripheral signals. In particular, the insulin and leptin resistance in obese rodents and the ability of leptin and ghrelin to regulate synaptic organization within the ARC show the importance of endocrine crosstalk between the periphery and CNS in the maintenance of energy homeostasis.

1.10 Pancreatic islets and glucose homeostasis

Outside of the CNS, the pancreas is another metabolically critical site that has been studied in the settings of healthy and dysfunctional metabolism. Specifically, the endocrine compartment of the pancreas is composed of clusters of multiple endocrine cell types, and these clusters are called the “islets of Langerhans”, or islets[178]. Each islet is composed of at least four different endocrine cell types, each characterized by a defining hormone with a different role in regulating glucose homeostasis: insulin-secreting beta cells, glucagon-secreting alpha cells, somatostatin-secreting delta cells, and pancreatic polypeptide-secreting PP cells (or gamma cells). The human islet is

composed of 50-75% beta cells, 25-35% alpha cells, 10% delta cells, and < 1% other endocrine cell types[179]. It is also highly vascularized to allow islet cells sufficient oxygenation and access to circulating factors[180,181], and innervated to a lesser degree to allow for some nervous control[182–184]. The primary role of islets is to maintain glucose homeostasis. In humans, blood glucose is maintained within a tight range of 4mM to 5.5mM as a result of the interplay between the aforementioned islet hormones. When blood glucose rises following a meal, beta cells sense the elevated glucose and respond by secreting insulin[185,186]. This process of glucose-stimulated insulin secretion (GSIS) is highly similar to the mechanism of activation in glucose-excited neurons, as mentioned in section 1.7. Glucose uptake occurs through the glucose transporter GLUT1[187,188] and is metabolized through oxidative phosphorylation, increasing the intracellular levels of ATP that causes a closure of the K_{ATP} channels[189,190]. The resulting depolarization of the cell membrane causes calcium influx through the L-type and P/Q-type voltage-gated calcium channels, which in turn triggers exocytosis of insulin-containing granules[191,192]. The secreted insulin signals through the insulin receptor on peripheral tissues such as muscle and adipose tissue to promote glucose uptake into these tissues, thus restoring the physiological range of glucose in circulation[193–195]. Much like AgRP and POMC neurons that act in a functionally opposing manner to each other, insulin action is opposed by glucagon action. Alpha cells are activated in response to low glucose conditions, when beta cells are less active and insulin levels decrease, and secrete glucagon. While the mechanism of GSIS has been well-studied, the mechanism behind glucagon secretion has been less clear. It has been suggested that high glucose can inhibit alpha cells because the closure of K_{ATP} channels leads to inactivation of voltage-gated sodium channels, which leads to a net inhibition of membrane depolarization[196]. In low glucose conditions, alpha cells can be activated due to low levels of K_{ATP} channel activity

that selectively opens the P/Q-type calcium channels for glucagon secretion[196]. Glucagon primarily targets the liver to promote hepatic gluconeogenesis to raise glucose levels back to the physiological range, but can also signal in adipose tissue to promote lipolysis[197]. Delta cells, on the other hand, are mostly studied in the context of paracrine signalling within the islet. Somatostatin secretion has been shown to increase with increasing glucose concentration, which suggests mechanisms similar to those in beta cells[198,199]. However, somatostatin locally inhibits both alpha and beta cells to modulate glucagon and insulin secretion, respectively[200].

Glucose is the most important upstream signal of islet activity, but islet cells are also able to respond to circulating FFA. It has been clearly shown that beta cells are able to be stimulated and activated by FFA signalling through specialized FFA receptors, which are G protein-coupled receptors[201,202]. In both mouse and human islets, acute activation of free fatty acid receptor 1 (FFAR1) with FFA administration increased insulin secretion when ambient glucose concentrations were high[203,204]. However, chronic administration of palmitate leads to decreased insulin secretion after a few days due to a decoupling between the voltage-gated calcium channels and insulin granules, showing the detrimental effects of prolonged high fat on beta cell function[205]. FFA are also able to diffuse into beta cells independent of the FFAR1, to feed into GSIS amplification pathways and increase insulin secretion[206]. In addition to FFAR1, FFAR2 and FFAR3 have been shown to inhibit insulin secretion[207] and beta cell survival[208]. In contrast to the pool of knowledge in beta cells, the effects of lipids on alpha cells and glucagon signalling are once again unclear by comparison. Studies have shown both activating[209,210] and inhibitory[211] roles of lipids on alpha cells. Alpha cells also express FFAR1, and long-chain fatty acids have been shown to stimulate glucagon secretion from alpha cells by increasing cytosolic

concentrations of calcium[210].

In summary, pancreatic islet cell types are critical for maintaining glucose homeostasis, and they achieve this by secretion of their characteristic glucoregulatory hormones. These hormones not only signal centrally to affect energy homeostasis (discussed in section 1.6), but signal in peripheral tissues to regulate processes that affect whole-body energy states, such as gluconeogenesis and lipolysis. Overall, islet cell types are an important peripheral site of incorporating nutrient signals throughout different energy states, as they are capable of detecting and responding to both glucose and lipids in circulation.

1.11 Similarities between ARC neurons and pancreatic islets

Although the ARC neurons and pancreatic islets originate from entirely different germ layers and are physically located in very different compartments of the body, numerous similarities between the two cell types have been pointed out[212,213], especially regarding their gene expression and mechanistic function. Islets and neurons share expression of many genes, even genes that were initially thought to be specific to the CNS. Part of this is due to the fact that neither cell type expresses the repressor element 1 silencing transcription factor (REST), which is typically expressed in non-neuronal cell types to suppress a neuronal fate[214]. It has also been shown that the gene activity state of beta cells closely resembles that of neurons[215]. Neurons have been shown to express characteristic islet genes like insulin and glucagon[216,217] across species. Transcription factors that are known to be critical in islet development and identity are also expressed in neuronal development. Some examples of these include neurogenin3[218,219], paired-box protein 6[220,221], and Nk6 homeobox 1[222,223]. This wide overlap in gene expression is also

partially problematic when working with transgenic mouse Cre-lox lines, as many mouse Cre lines developed for pancreas- or islet-specific recombination display Cre enzymatic activity in the brain. Famous examples of this include the *RIP-Cre* transgenic lines and the *Pdx1-Cre* lines, both of which show Cre-mediated recombination in the hypothalamus[213,224].

There are also clear parallels in their overall organization and homeostatic roles. Both islets and ARC are composed of multiple cell types that functionally oppose each other to some degree. Alpha cells and beta cells, with the opposing actions of glucagon and insulin on peripheral tissues, resemble the AgRP and POMC neurons of the ARC and their opposing roles on food intake. Mechanistically, it has already been highlighted that the glucose-sensing machinery in glucose-excited neurons and pancreatic beta cells in particular are incredibly similar, except for their respective local concentrations of glucose[225]. The way in which islet cells receive and integrate external nutritional stimuli to secrete hormones from granules mimics the way in which neurons release neurotransmitters from synaptic vesicles. Furthermore, various neuronal "features" like the neurotransmitter glutamate[226], glutamate receptors[227], the enzyme glutamic acid decarboxylase, and the neurotransmitter GABA[228] have all been detected in beta cells.

Due to their general similarities in gene expression and function, cellular pathways and mechanisms identified in neurons are likely to be also found in islets, and vice versa. Since both cell types have surveillance roles of sorts, coupling their ability to detect nutrient signals to cellular activation, studying the changes that occur in response to activity in general will further our understanding of their physiology.

1.12 Calcium signalling in neurons and islets

All excitable cells depend on calcium to some degree. Calcium ions not only act as a broad secondary messenger that regulates many intracellular processes, but often trigger important cellular functions like exocytosis, as mentioned in previous sections. In and around a cell, there are normally pools of calcium that are maintained at certain concentrations through various ionic channels, pumps, and exchangers. A physiological range of cytosolic calcium concentrations range from 10nM to 100nM, whereas extracellular calcium concentrations range from 1-2mM, which ensures passive influx of calcium ions across the plasma membrane if entry was allowed[229]. Both neurons and islet cells actively maintain lower basal intracellular calcium concentrations in order to utilize the large influx of calcium as an "on" switch to induce cellular processes such as transcription through similar kinase cascades and signalling proteins[230,231]. Following depolarization, calcium influx in islet cells occurs through L-type and P/Q-type voltage-gated calcium channels[191,196]. In neurons, calcium influx can occur through voltage-gated calcium channels, but calcium can also enter the cell through the N-methyl-D-aspartate receptor (NMDAR) or α-amino-3-hydroxy-5-methyl-4-isoxazolepropionate acid receptor (AMPAR)[232,233]. The importance of these receptors for neuronal activation has been demonstrated in the hypothalamus and in ARC AgRP and POMC neurons as well[234–236]. When intracellular calcium concentrations rise upon calcium entry, calcium ions bind to the protein calmodulin (CaM), which undergoes a conformational change to activate different effector proteins[237,238]. These effector proteins include the calcium/calmodulin-dependent protein kinases (CaMK) and calcineurin. Specifically in islet beta cells, many isoforms of CaMK have been identified, including CaMKI, CaMKII, and CaMKIV[239–241]. In neurons, CaMKII, CaMKK, CaMKI, and CaMKIV have been studied and found to have numerous regulatory roles[242].

Following activation, calcineurin activates the transcription factor myocyte enhancer factor 2 (MEF2) by dephosphorylation, and CaMKII phosphorylates the calcium-dependent transcription factor cAMP response element-binding protein (CREB)[230,243–245]. Another target of calcineurin is the nuclear factor of activated T-cells (NFAT), which is dephosphorylated by calcineurin to translocate to the nucleus for transcriptional regulation[246,247]. Additionally, the transcription factor NF-κB is a target of CaMKII, which phosphorylates NF-κB to induce its nuclear translocation[248,249]. By these pathways, an influx of calcium ions can be rapidly translated into regulation of gene expression in response to stimuli within minutes, an essential mechanism of quickly responding to changes in the environment[250,251].

1.13 Immediate early genes

Both neurons and islets constantly detect and respond to the environment, and regulating gene expression for long-term and short-term responses is critical for their survival and adaptation[252]. As both cell types depend on coupling nutrient sensing to cellular activity, they naturally depend on activity-regulated genes (ARG), which were characterized in neurons as genes that are induced in response to neuronal activity[253]. Following the idea that transcription was linked to neuronal activity, the first immediate early genes (IEG) were characterized in neurons. IEGs are defined as genes that display a rapid and transient increase in expression, that is independent of protein synthesis, in response to extracellular stimuli[254]. The first IEG to be characterized was *Fos*, from the observation that agonizing nicotinic acetylcholine receptors or causing depolarization and calcium influx through L-type voltage-gated calcium channels in any way, caused a rapid and transient induction of the proto-oncogene in a neuronal cell lines[255]. More IEGs were identified over time, and today, it is relatively easy to identify hundreds of IEGs,

especially with applications of RNA-seq technology[256]. Many of the identified IEGs encoded for transcription factors that could target their own downstream target genes once induced and translated into protein[250]. Most IEGs are significantly upregulated within the first hour following stimuli, regardless of whether the stimuli is sustained or brief, and their expression levels can range from 2- to 10-fold[257]. Meanwhile, the targets of the IEGs, sometimes called late response genes (LRG), do not show a significant induction until 3-4 hours after stimulus.

As more and more IEGs were identified, it became apparent that IEGs were not strictly limited to neuronal cell types, and there may be differentially regulated IEGs across cell types that carry out different roles. An example of this is the NR4A orphan nuclear receptor genes, which are involved in differentiation and developmental processes in adipocytes, but macrophage NR4A genes have roles in inflammation[258]. In islet cells, it would be expected that IEGs would be induced by different stimuli in each cell type, as different cell types have different activating conditions. In islets, most of the studies on IEGs have focused on beta cells, and well-studied IEGs like *Fos, Egr1, Junb,* and *Nr4a1* have been shown to be expressed and regulated by glucose[259–261]. In beta cells, hundreds of IEGs have been identified at once by stimulating with high glucose and a membrane-permeable cAMP analogue, then isolating out IEGs by comparing to gene expression profiles obtained from cells that received cycloheximide[262]. Since cycloheximide blocks protein synthesis, this method allows for the specific identification of IEGs, which will still show induction, from their target genes, which will not be induced without their IEG transcription factor.

1.14 bHLH-PAS proteins

The basic helix-loop-helix (bHLH) superfamily of proteins contains several transcription factors that contain the PAS domain and act as sensors of environmental stimuli that regulate a wide range of cellular processes to adapt to the environment[263,264]. Their characteristic PAS domain was named after the original three proteins that were found to contain the domain: Period (PER), aryl hydrocarbon receptor nuclear translocator (ARNT), and Simple-minded (SIM)[265]. This family of proteins is further characterized by the presence of a basic DNA-binding domain and the helix-loop-helix dimerization domain, both of which are needed for their function as transcription factors[263]. Due to the different binding interactions amongst the family members, mammalian bHLH-PAS proteins can be divided into class I and class II. Class I proteins act as the receptors for specific stimuli and must heterodimerize with a class II protein, but class II proteins are ubiquitously expressed and can heterodimerize or homodimerize[264]. Class II proteins that are known to act as general binding partners for class I proteins include ARNT, its more tissue-restricted paralog ARNT2, and the circadian rhythm proteins aryl hydrocarbon receptor nuclear translocator-like protein 1 (BMAL1 or ARNTL), and basic helix-loop-helix ARNT-like protein 2 (BMAL2)[263,264]. Some of the best-studied class I bHLH-PAS proteins include circadian rhythm clock proteins and hypoxia-inducible proteins[263,264,266], which recently received renewed attention due to the Nobel prizes in 2017 and 2019 being awarded for the discovery of their molecular mechanisms. These two processes have also been studied in the context of metabolism, as disrupting their pathways have been shown to cause metabolic disease[267,268], and will be briefly discussed here.

The maintenance of circadian rhythm occurs in the CNS and is particularly important for the

regulation of food intake. The “master clock”, or central clock mechanism that controls the body’s overall circadian rhythm is located in the suprachiasmatic nucleus (SCN) of the hypothalamus[267]. During the light cycle, the class I bHLH-PAS protein CLOCK and class II protein BMAL1 begin the cycle of circadian rhythm by heterodimerizing and translocating to the nucleus to induce the expression of their downstream targets, the *Period* and *Cry* family genes[266,267]. The translated Period (PER) and Cryptochrome (CRY) proteins heterodimerize and inhibit the activity of the CLOCK-BMAL1 dimer, decreasing the levels of *Period* and *Cry* transcription over time[263,269]. Over the rest of the cycle, PER and CRY proteins are steadily phosphorylated by the casein kinase I epsilon and delta, and degraded over time[263,270,271]. The depletion of PER and CRY lifts the repression of CLOCK-BMAL1 activity, beginning the cycle anew over 24 hours. In other areas of the hypothalamus, circadian rhythm and its associated proteins have been shown to play important roles in food intake regulation[272]. Food-seeking and food intake are behavioural processes that have been shown to negatively impact metabolic health when misaligned or mistimed[273,274]. In the context of energy homeostasis, orexigenic pathways that promote food intake have been reported to be generally more active during the organism’s active phase (light cycle for humans and dark cycle for nocturnal rodents) when food-seeking and food intake behaviour is possible[275,276]. Specifically within the ARC, circadian rhythm genes have been shown to be differentially expressed in response to different feeding restriction schedules in rodents[277]. It has been shown that this region operates under a distinct, independent rhythm using PER2-driven luciferase reporters in ARC tissue explants[278]. Restricting feeding in mice to the light cycle showed a rhythmic change in AgRP neuronal activity measured by *c-fos*[279]. In mice that were deprived of food, POMC neurons were enriched for clock pathway genes during the light cycle, when mice are typically fasting[280]. Genetic

deletion of BMAL1 from AgRP neurons to disrupt the molecular clock pathway resulted in mice that had increased food intake over 24 hours, increased meal sizes, and increased light cycle hepatic gluconeogenesis and respiratory exchange ratio (RER)[281]. These studies showed the importance of circadian rhythm bHLH-PAS proteins in the regulation of food intake.

The ability to sense oxygen depletion in the environment and respond to it accordingly is critical for cell survival, which highlights the importance of the bHLH-PAS proteins involved in the hypoxia response pathway. In mammals, the hypoxia-inducible factor (HIF) proteins that are class I bHLH-PAS proteins are HIF1α[282], HIF2α[283], and HIF3α[284]. In normoxia, HIF proteins are hydroxylated by the prolyl hydroxylase domain (PHD) enzymes PHD1, PHD2, and PHD3, which promotes an association with the Von Hippel-Lindau (VHL) protein that is part of the E3 ubiquitin ligase protein complex[285,286]. Therefore, HIF proteins are constantly ubiquitinated and degraded by the proteasome in normoxia[287]. In hypoxia, the oxygen-dependent PHD enzymes are inactive due to the low availability of oxygen and cannot hydroxylate HIF proteins, which results in HIF stabilization. HIF is then able to heterodimerize with ARNT, and the heterodimer translocates to the nucleus to act as a transcription factor, specifically binding to hypoxia response elements[288]. It has been shown that intermittent hypoxia can directly affect energy homeostasis and feeding. Rats that were exposed to 8 hours of intermittent hypoxia showed reduced body weight and food intake with no changes to fat mass, and displayed elevated circulating leptin levels[289]. The rise in leptin levels in response to hypoxic conditions have also been reported in humans[290,291]. Within the ARC, intermittent hypoxia is known to increase POMC protein levels and cause increased activation of POMC neurons[289]. However, in leptin-deficient animals, the increase in plasma leptin, the increased activation of ARC phosphorylated

signal transducer and activator of transcription 3 (STAT3) downstream of leptin signalling, and the elevated levels of POMC protein were not seen[292]. Interestingly, HIF1α expression in the ARC and ME has been observed in POMC neurons and glial cells, but not AgRP neurons[293]. In a model of diet-induced obesity, HFD feeding was shown to upregulate HIF1α and downregulate VHL, and the knockdown of its binding partner ARNT in the ARC caused increased body weight due to decreased basal metabolic rate and thermogenesis[293]. This inhibition of ARNT in HFD-fed mice also caused an increase in *Agrp* expression, worsened hypothalamic inflammation, and impaired glucose tolerance, showing an overall exacerbated diet-induced obesity phenotype[293]. The hypoxia pathway is also important for glucose metabolism and sensing in the hypothalamus, as high glucose availability in the ARC upregulated HIF1α and HIF2α, and HIF proteins directly upregulate the expression of *Pomc*[294]. Genetic knockout of ARNT in POMC neurons to impair the HIF complex resulted in the failure of HIF-mediated *Pomc* upregulation, lack of glucose-mediated feeding suppression, and increased feeding[294]. Of course, the caveat with the approach of knocking out ARNT is that it does not only bind to HIF, and a cell with ARNT knockout most likely has more disrupted pathways that involve more than HIF proteins. There have also been approaches to increase HIF activity through ROS, a common biproduct of glucose metabolism that is elevated in diet-induced obesity[172] and has been shown to stabilize HIF[295,296]. The increased ROS in glucose-stimulated POMC neurons that promote POMC firing[172,297] could be connected to the glucose-induced HIF stabilization and downstream effects in these neurons.

The above studies showed that bHLH-PAS proteins are important for a variety of cellular processes, including their roles in the context of energy homeostasis, ARC neurons, and food

intake. Given the wide range of cellular processes that they are involved in, it is possible that bHLH-PAS proteins other than HIF and CLOCK have important roles in the regulation of food intake in the ARC.

1.15 Neuronal PAS domain protein 4

Neuronal PAS domain protein 4 (NPAS4) is one of the four NPAS proteins in the bHLH-PAS family, and was originally discovered in 2004 by two separate groups in neuronal tissues[298,299]. Despite containing the basic helix-loop-helix (bHLH) domain and both the PAS A and PAS B domains, NPAS4 has a very low sequence homology to other members of the bHLH-PAS family[263,298,299]. As the name implies, NPAS4 was first characterized in neurons and is expressed in neurons within the CNS, showing negligible expression in glial cells[300,301]. The neuronal specificity of NPAS4 expression is due to active repression of NPAS4 expression in non-neuronal cell types by REST/NRSF binding to the multiple sites in the promoter and intron 1[302]. Being a class I bHLH-PAS protein, NPAS4 must form a heterodimer in order to carry out its function as a transcription factor. NPAS4 has been reported to heterodimerize with both ARNT and ARNT2 in the CNS[303,304]. Interestingly, it has been shown that the differential dimerization of NPAS4 with either ARNT or ARNT2 in response to stimuli leads to heterodimers with distinct DNA-binding activity[304]. Within the brain, *Npas4* mRNA is expressed throughout various sites including the cortex, olfactory bulb, and the hippocampus, where it shows the highest levels of expression[298,299]. Of note, *Npas4* expression has also been shown in the PVN and ARC of the hypothalamus[305]. Like other IEGs, *Npas4* expression is normally very low at basal levels, but it is induced in response to stimuli. However, NPAS4 is selectively induced in response to neuronal activity and the resulting depolarization, while other IEGs can also be

induced by neurotrophins and growth factors[300,306]. This activity-regulated induction of was found to be calcium-dependent, establishing NPAS4 as a calcium-dependent IEG[300,307]. In neurons, the exact calcium-responsive effector proteins that are responsible for *Npas4* transcription are not fully determined, but it is known that *Npas4* lacks CREB-responsive elements, suggesting that CREB is not likely to be required[307]. Mitogen-activated protein kinase (MAPK) and phosphatidylinositol 3-kinase (PI3K) pathways have been shown to be required for pharmacological *Npas4* induction in hippocampal slices[308]. Serum response factor (SRF) has also been proposed to be an upstream regulator of *Npas4* expression, because SRF deletion leads to a downregulation in *Npas4* levels and there are SRF binding sites located in the *Npas4* promoter[309]. In beta cells, it has been shown that the upstream effectors of transcription of *Npas4* are Akt, CaMK, and calcineurin[310].

Within the brain, NPAS4 is implicated in a wide range of processes such as neuroprotection, contextual memory formation, and neuronal development[311–313,306,314]. At the molecular level, the main role of NPAS4 is to modulate synaptic connections in an activity-dependent manner. The first study of the synaptic functions of NPAS4 showed that NPAS4 induced the expression of other ARGs to form and maintain GABAergic synapses on excitatory neurons[300]. In later studies, it was found that NPAS4 activates distinct genes in both excitatory and inhibitory neurons, promoting the formation of inhibitory synapses onto excitatory neurons and excitatory synapses onto inhibitory neurons[256]. In this manner, NPAS4 can regulate inhibitory-excitatory balance within neural circuits, which is partially through the regulating the transcription of its direct downstream target BDNF[315,316]. Furthermore, NPAS4 has an important role in neuroprotection. Germline NPAS4 knockout ($NPAS4^{-/-}$) mice are viable, but show higher mortality when they are

3 months old, which was attributed to apoptotic neurodegeneration in the hippocampus[299]. Additional *in vivo* studies where the excitotoxic drug kainate was administered to mice show accelerated neurodegeneration in NPAS4$^{-/-}$ mice compared to controls[299]. In a mouse model of ischemic stroke, NPAS4$^{-/-}$ mice showed larger lesions and increased neurodegeneration[317]. Finally, *in vitro* studies show that NPAS4 is upregulated in response to a variety of stressors, including endoplasmic reticulum stress, oxidative stress, and osmotic stress[299].

Despite its name, there have been reports of NPAS4 in non-neuronal cell types in the periphery. In addition to the CNS neurons, NPAS4 is also expressed in endothelial cells[318] and pancreatic beta cells, where it is also induced in response to depolarization in a calcium-dependent manner[319]. In pancreatic beta cells, NPAS4 was found to be a negative regulator of insulin expression, and shown to protect beta cells from cell stress and death caused by ER stressor thapsigargin and palmitate[319]. In addition, NPAS4 overexpression was sufficient to prevent cell death caused by the cytotoxic calcineurin inhibitor tacrolimus[310]. These findings reflect the neuroprotective roles of NPAS4 in the CNS. Finally, NPAS4 was found to maximize energy production in beta cells by preventing HIF1α stabilization and promoting maximal oxidative phosphorylation[320]. Knockout of NPAS4 in beta cells led to increased HIF1α action, which led to beta cell dedifferentiation and reduced oxidative phosphorylation during chronic high glucose conditions[320].

The above studies show that in both neurons and beta cells, NPAS4 is important for proper function and survival of cells, but in different ways mechanistically. There are clearly functions and downstream targets of NPAS4 that are specific to each cell type. In addition to the pancreatic

beta cells, it will be interesting to determine if NPAS4 has further roles in metabolically important cell types.

1.16 Thesis objectives

In today's obesogenic environment, there are a variety of stresses that threaten cell types that are critical for energy balance. The combination of an inflammatory environment, sustained elevations in nutrient intake, and genetic predisposition increases the workload of these cells and exacerbates overall pathophysiology over time. Thus, it is important to study factors such as activity-regulated genes that respond to the changing environment, particularly during metabolic stress. Since calcium signalling is a crucial process in all excitable cells that is modulated by disease, and there are overlapping functional mechanisms between pancreatic islets and nutrient-sensing neurons, there is merit to studying genes that are regulated downstream of cell activation and calcium signalling in both cell types.

In the islet, it is already known that calcium signalling is crucial for proper function, and activity-coupled calcium signalling regulates transcriptional changes in order to respond to the rapidly changing environment. The majority of studies in islet cell types have focused on the insulin-producing beta cell, due to its well-characterized mechanism of glucose-stimulated insulin secretion that is coupled to calcium influx. In chapter 3 of this thesis, I extended the investigation of calcium-regulated transcription to all endocrine cell types of the adult human islet to address this gap in knowledge. Therefore, the primary aim in chapter 3 was to profile activity-regulated genes that are specifically regulated in a calcium-dependent manner in healthy human islet endocrine cell types at the single cell level.

In neurons, commonly known IEGs have already been studied and are traditionally used as markers of neuronal activation. Physiologically relevant roles of bHLH-PAS proteins like NPAS4 have been identified in several regions of the brain, but NPAS4 has not been studied within the ARC. In chapter 4, I determined the expression and conditions of *Npas4* induction in the AgRP and POMC neurons of the ARC. In chapter 5, I investigated the effects of genetic NPAS4 knockout specifically in either AgRP and POMC neurons of adult mice in an obesogenic environment. In chapter 6, I apply the single cell transcriptomics approaches used in chapter 3 to broadly profile activity-regulated genes in mouse POMC neurons that are regulated specifically in response to an acute feeding stimulus and are potentially regulated by NPAS4 in diet-induced obesity.

Collectively, this thesis highlights how activity-regulated genes in general, and NPAS4 in particular, are regulated in pancreatic islets and ARC neurons, as well as how they contribute to the function of these cell types during conditions of high nutrient stress.

Chapter 2: Materials & Methods

2.1 Animal husbandry

All mice were housed at the Animal Care Facility in the British Columbia Children's Hospital Research Institute. All experiments and measurements were performed in adult male mice between 6 to 37 weeks old. Up to four littermates of the same sex were housed per cage, in Optimice® cages (Animal Care Systems) with *ad libitum* access to food and water. All cages were held in temperature-controlled rooms with a 12-hour light/dark cycle at 22°C.

2.2 Mouse strains

All mouse strains used in this thesis and the genotyping primers used for each strain are found in Table 2.1. All mutant mice were maintained on a B6 background and all CreER alleles were kept hemizygous. For studies involving the POMC-CreER strain, $Npas4^{flox/flox}$ mice and POMC-$CreER^{+}$ mice were used as controls, and POMC-$CreER^{+}$;$Npas4^{flox/flox}$ mice were used as KO (POMC-NPAS4 KO). For studies involving the AgRP-CreER strain, $Npas4^{flox/flox}$ mice and AgRP-$CreER^{+}$ mice were used as controls, and AgRP-$CreER^{+}$;$Npas4^{flox/flox}$ mice were used as KO (AgRP-NPAS4 KO). $Npas4^{flox/flox}$ mice and KO were littermates. Some, but not all, of the AgRP-CreER and POMC-CreER offspring also had a tdTomato (tdT) sequence downstream of a loxP-flanked STOP sequence in their Rosa26 locus ($Rosa26^{LSL\text{-}tdT}$) to act as a CreER-activated lineage marker. This was not a separate mouse strain, as AgRP-CreER and POMC-CreER parental mice originally received in the lab for this study already contained this transgene.

Table 2.1 Mouse strains and genotyping primers

Strain nomenclature (Strain designation)	**Original source**	**Genotyping primers (5' → 3')**
Npas4^{tm2Meg} (Npas4 flox) MGI: 3828100	Michael E. Greenberg laboratory[300]	LL41: CCCTGCCCTAATCAGAC LL42: GGCATTGTTCTTTCTGTCTCC
NPAS4$^{-/-}$	Michael E. Greenberg laboratory[300]	WT forward: TGCTGAGAGGGTCTTTCTATGCG WT reverse: TCCAGGTAGTGCTGCCACAATG KO forward: AAAGACCCCAACGAGAAGCG KO reverse: GCAAGTAAAACCTCTACAAATGTGG
C57Bl/6J (B6)	Jackson Laboratory (000664)	NA
AgRP-CreER^{T2} (AgRP-CreER)	Joel Elmquist laboratory	For AgRP-CreER: LL645: GCTCTACTTCATCGCATTCCTTG LL646: CAGATACCATCATCTCTCCC LL647: CCTTAAACTCGCCCATATATGTGG For Rosa26$^{LSL-tdT}$: LL172: CTCTGCTGCCTCCTGGCTTCT LL173: CGAGGCGGATCACAAGCAATA LL174: TCAATGGGCGGGGGTCGTT
POMC-CreER^{T2} (POMC-CreER) MGI: 5569339	Joel Elmquist laboratory[321]	For POMC-CreER: LL643: GGAAACAGAGAGGGAAACTGCC LL644: CTCTTCCCTTTGCTCTGTAC LL645: GCTCTACTTCATCGCATTCCTTG For Rosa26$^{LSL-tdT}$: LL172: CTCTGCTGCCTCCTGGCTTCT LL173: CGAGGCGGATCACAAGCAATA LL174: TCAATGGGCGGGGGTCGTT

2.3 Genotyping

Ear punch biopsies were taken from mice for genotyping at 3 to 4 weeks of age. Biopsies were immediately placed into 200uL mixture of chelex beads (Bio-Rad; 1421253), DEPC water, and proteinase K (Roche; 3115879001), and incubated overnight (> 10 hours) at 55°C. For long-term storage, samples were stored at 4°C until genotyping was completed, then moved to room temperature (22°C). 1.5µL of sample DNA was added to 23.5µL of PCR genotyping master mix made of: 18µL molecular biology grade water (GE Life Sciences; SH30538.02), 2.5µL 10x buffer E, 0.5µL 10mM dNTP mix (FroggaBio; DN001025-5), 1µL DMSO (Fisher; BP231-1), 1µL 10mM primer mix, and 0.5µL Taq polymerase. 10x Buffer E for PCR was made by mixing 33.5mL of 1M tris (pH 9.01), 75µL of 1M $MgSO_4$, 4.5mL of 2M $AmSO_4$, and 350µL of 14M β-mercaptoethanol, which was topped up to 50mL with water and filter-sterilized before using. PCR products were run on a 1.2% agarose gel to confirm band sizes specific for each allele.

2.4 Diets

All mice were weaned at 3 weeks of age onto standard rodent Chow (Chow; Teklad 2918). Chow caloric value was composed of 58% carbohydrate, 18% fat, and 24% protein. For mice that were fed HFD in Chapters 4, 5, and 6, mice were switched to HFD (Research Diets D12331) at 7 weeks of age, after tamoxifen administration when applicable. HFD caloric value was composed of 25% carbohydrate, 58% fat, and 17% protein.

2.5 Tamoxifen preparation and administration

At 6 weeks of age, 8mg of tamoxifen (Toronto Research Chemicals; T006000) was administered to each mouse every other day, for a total of 3 times over 5 days. Tamoxifen solution was

prepared fresh before each administration. Corn oil (ACH Food Companies Inc.; 100% pure Mazola corn oil) was added to the appropriate mass of tamoxifen powder for a concentration of 60mg/mL and the tamoxifen was dissolved by sonication for 10 cycles of 30s at 80% power in a cup horn Misonix Sonicator S-4000 (Fisher Scientific; 13101353). 133µL of tamoxifen solution was administered to each mouse via oral gavage. Mice remained in a cytotoxin shedding room with an internal water bottle and food hopper until 72 hours after the last dose of tamoxifen administration, then underwent a full cage change before being switched onto HFD (or remaining on Chow).

2.6 Body weight and blood glucose measurements

Body weights of mice were measured using a digital scale. For mice in chapter 5, body weight and blood glucose were measured between 09:00 and 10:00 each week. Body weights and blood glucose were measured biweekly from mice that were random-fed or fasted overnight for 10 hours starting at 7 weeks of age. For all blood glucose measurements, the left hind leg of the mouse was shaved to expose the skin when needed, and the saphenous vein was pricked with a 27½ gauge needle (VWR; BD305109). Blood glucose was measured using a handheld OneTouch UltraMini glucometer (LifeScan Europe; AW 06720302A) and OneTouch Ultra glucose strips (LifeScan Europe; AW 06858804A). For fast-refeed experiments, body weights were measured before and after the refeeding.

2.7 Plasma collection and ELISA

All blood collection was performed on the saphenous vein after a prick with a 27½ gauge needle (VWR; BD305109). A heparinized microcapillary tube (Fisherbrand; 22-362-566) was filled

with blood. The blood was transferred to a 1.5mL microcentrifuge tube (Diamed; SPE155-N) and stored on ice for up to 30 minutes before being centrifuged at 5000g for 10 minutes at 4°C. Plasma was collected and transferred to a clean 1.5mL tube. Plasma samples were stored frozen at -20°C until assayed on a rodent insulin ELISA (Alpco; 80-INSMR-CH10) according to manufacturer's instructions.

2.8 Oral glucose tolerance tests

Mice were fasted for 10 hours overnight before the tolerance test. In the morning, body weight and blood glucose were measured, and one microcapillary tube of blood was taken from each mouse. 2g/kg glucose was administered to each mouse by oral gavage, using a sterile-filtered 40% D-glucose solution prepared by dissolving D-glucose (Sigma; G7021-1KG) in water. Blood glucose was measured at 10, 30, 60, 90, and 120 minutes post-gavage, and 1 microcapillary tube of blood was taken at 10 minutes post-gavage.

2.9 Insulin tolerance tests

Mice were fasted for 2 hours during the light cycle before the tolerance test. Body weight and blood glucose was measured, and 0.75U/kg insulin was administered to mice via intraperitoneal injection with a 27½ gauge needle, using a sterile-filtered 150mU/mL insulin stock solution in PBS). Blood glucose was measured at 10, 30, 60, 90, and 120 minutes post-injection.

2.10 Glycerol tolerance tests

Mice were fasted for 10 hours overnight before the tolerance test. In the morning, body weight and blood glucose were measured. 2g/kg of glycerol was administered to mice via intraperitoneal

injection with a 27½ gauge needle, using a sterile-filtered 40% w/v glycerol solution in water. Blood glucose was measured at 10, 30, 60, 90, and 120 minutes post-injection.

2.10 Body composition and metabolic cages

In chapter 5, lean and fat mass was quantified in 2 and 6 weeks HFD-fed mice. Body composition was measured using quantitative magnetic resonance technology on the EchoMRI-100 (Echo Medical Systems) in collaboration with the laboratory of Dr. William T Gibson.
In chapter 5, mice fed HFD for 6 weeks underwent metabolic cage analyses in collaboration with the laboratory of Dr. William T. Gibson. All mice were singly housed in metabolic cages (LabMaster TSE systems). Mice were allowed to acclimate to the metabolic cages for 24 hours before recording for the following 72 hours. Indirect calorimetry was used to measure CO_2 production and O_2 consumption from the cages, and the RER was calculated from volume of CO_2 produced to volume of O_2 consumed during the day. Food intake and water intake was measured by weight sensors linked to the food hopper and water bottle in each cage. Locomotor activity was measured with infrared beam breakage inside the cages.

2.11 Fast-refeeding

In Chapters 4, 5, and 6, mice underwent a fast-refeed at various ages. Mice were fasted overnight for 10 hours by transferring to a clean cage with no food hopper and only *ad libitum* access to water. In the morning, a pre-weighed food hopper with Chow or HFD was placed in the cage and mice were allowed to eat *ad libitum* for 1 hour. At the end of 1 hour, the food hopper and any uneaten crumbs of food on the cage floor were removed from the cage and weighed. Before and after the refeeding period, body weight and blood glucose were measured for each mouse. If

euthanizing for tissue harvest after refeeding, stomach contents were also checked after euthanasia during the dissection to confirm the mouse had eaten.

2.12 Manual food intake measurements

All mice undergoing manual food intake measurements were singly housed. Body weights of mice were measured weekly. Weekly food intake was calculated by subtracting the weight of food in the hopper and food crumbs on the cage floor from the weight of the freshly added food given the week before. Approximately 10 fresh pellets of HFD were given to each mouse every week, and the old pellets were discarded every week.

2.13 Mouse transcardial perfusion and tissue harvest

Mice were anesthetized with isoflurane under presence of O_2 and euthanized by asphyxiation with CO_2. After visually confirming that breathing had stopped, the mouse was removed from the isoflurane chamber, sprayed with 70% ethanol, and dissected to expose the liver and stomach in the abdominal cavity within one minute of removal from the chamber. The diaphragm was cut through and the ribcage was cut vertically on the left, right, and middle to expose the heart. The mouse carcass was transported into a 2cm-deep plastic dish inside a fume hood, and the right atrium was punctured with surgical scissors to create an exit point for blood. A 27½ gauge needle with tubing (1mm diameter, 12cm long) attached to a syringe was gently inserted into the left ventricle, and the carcass was flushed of blood with 5mL of ice-cold PBS. The 5mL syringe was replaced with a 30mL syringe containing 20mL of 4% paraformaldehyde (PFA), and the carcass was perfused at a rate of 1mL/min until all PFA had been dispensed.

2.14 Tissue processing for histology

For mouse liver and pancreas collection, tissues were dissected out with fine surgical scissors and blunt-ended forceps following transcardial perfusion of the mouse carcass. The liver and pancreas were post-fixed in 5-10mL of 4% PFA overnight at 4°C. The next morning, the PFA was removed, and tissues were washed three times with PBS, 5 minutes each, and transferred to a clean tube containing enough 50% ethanol to submerge the tissue for 24 hours at 4°C. The 50% ethanol was removed and replaced with enough 70% ethanol to submerge the tissue for another 24 hours at 4°C. Tissues were secured in histology processing cassettes and dehydrated through a series of: 95% ethanol (two 30 minute incubations), 100% ethanol (three 30 minute incubations), xylenes (two 30 minute incubations), and paraffin (two 1 hour incubations). Following dehydration, tissues were embedded in paraffin blocks for long-term storage at room temperature.

For human islets, 100-200 islets were fixed in 1mL of 4% PFA for 1 hour at room temperature. The islets were manually picked into 500µL of PBS in a 1.5mL microcentrifuge tube. Islets were allowed to settle for 1 minute, or briefly pulse centrifuged. The majority of the PBS was removed, leaving the islets in approximately 30-50µL of PBS. Using a 10µL pipette tip, islets were transferred with minimal PBS into a mold, forming a bubble of PBS containing islets. A 2% agarose solution in water was prepared, allowed to cool until warm to the touch, and a pre-warmed 200µL pipette tip was used to pipette enough warm agarose into the mold containing islets until the mold was filled. Once the agarose hardened, the agarose-embedded islets were transferred back to the 4% PFA overnight at 4°C. The next morning, the PFA was removed, and the agarose block was washed three times with PBS, 5 minutes each, and transferred to 3mL of

50% ethanol for 6-8 hours at 4°C. The 50% ethanol was removed and replaced with 3mL of 70% ethanol for 16 hours at 4°C. The agarose block was transferred to a histology cassette, dehydrated, and paraffin-embedded in the same way as mouse liver and pancreas. For immunofluorescence, 5μm-thick paraffin sections of islets were mounted onto Superfrost Plus glass slides (Fisherbrand; 12-550-17) using a microtome.

For brain harvests, the perfused mouse carcass was decapitated using heavy scissors. The skin of the head was peeled away towards the snout, and turned inside-out to expose the skull. Using fine surgical scissors and blunt-ended forceps, the dorsal half of the skull was carefully removed from the brain, starting from the posterior end of the skull and cutting anteriorly. Once the brain was visible, forceps were used to gently scoop underneath the ventral surface of the brain, severing cranial nerves, and to remove the whole brain including olfactory bulbs from the remaining skull. The brain was post-fixed in 5-10mL of 4% PFA overnight at 4°C. The next morning, the PFA was removed, and tissues were washed three times with PBS, 5 minutes each, and transferred to a clean tube containing enough 20% sucrose (w/v solution in water) to submerge the tissue for 24 hours, or until the brain had sunk to the bottom of the tube, at 4°C. The 20% sucrose solution was removed and replaced with enough 30% sucrose (w/v solution in water) to submerge the tissue for another 24 hours, or until the brain had sunk to the bottom of the tube, at 4°C. Next, the brain was removed from the sucrose solution, transferred to a small dish containing OCT cryomatrix (Epredia; ref 6502), and thoroughly coated in OCT using blunt-ended forceps. The brain was bisected coronally at the level of the caudal edge of the hypothalamus, visible on its ventral surface, and the caudal portions of tissue were discarded. The remaining brain tissue was embedded in a cryomold with fresh OCT with the olfactory bulbs

pointing up, and the tissue was frozen within the cryomold on a bed of dry ice. After the OCT had completely frozen and turned opaque white, the frozen samples were stored at -80°C.

2.15 Cryosectioning

The frozen samples were removed from -80°C and allowed to equilibrate at -20°C for at least 2 hours before sectioning. The cryostat (Leica; CM 1950) was set to -21°C and the blade, brushes, and slide box were allowed to equilibrate within the cryostat for at least 15 minutes. The frozen samples were removed from the cryomolds and mounted onto cryostat sample discs using OCT cryomatrix. The blocks were trimmed at 50µm until tissue became visible, then 15µm-thick sections were collected once the block had been trimmed to reach the level of the middle of the arcuate nucleus, where the 3rd ventricle showed its characteristic shape (shown in figure 1.1 and 1.2). Sections were collected directly onto Superfrost Plus glass slides and placed into the slide box. Once sectioning was complete, blocks were re-sealed and re-frozen with OCT cryomatrix, and the blocks and slide box were placed at -80°C.

2.16 Hypothalamus dissociation

Mice were anesthetized with isoflurane and euthanized by cervical dislocation. The head and neck were sprayed down with 70% ethanol, and heavy surgical scissors were used to decapitate the mouse. The brain was rapidly removed from the skull, placed onto a petri dish with its ventral side facing upwards, rinsed in 15mL of PBS, and wetted with 5mL of Hibernate® AB complete medium (BrainBits; HAB). A clean razor blade was used to bisect the brain coronally at the caudal edge of the hypothalamus, visible on its ventral surface, and the caudal portions of tissue were discarded. The remaining brain tissue was placed into 7mL of HAB medium and

placed on ice until all samples had been collected. Using a clean razor blade, two 1mm-thick coronal sections were collected from each brain and moved to a petri dish with HAB medium. Under a dissection microscope (Olympus; SZX16), the ARC was roughly dissected out from each thick section. For some mice with recombined tdTomato lineage marker, a red fluorescent filter on the microscope and fluorescence illumination lamp (Excelitas Technologies; X-cite 120Q) were used to dissect out visibly tdTomato-positive regions from each section.

From this point, the dissected neural tissue was dissociated following an adjusted version of a published protocol[322], keeping the tissues on ice whenever possible. The tissue was placed into a 15mL polystyrene tube (VWR; 21008-212) containing 2mL of sterile-filtered 2mg/mL papain solution, made by dissolving solid papain (BrainBits; PAP) in Hibernate® A medium without calcium (BrainBits; HACA) for 20-30 minutes at 37°C. The tube containing papain and tissue was placed in a shaking water bath (VWR) set to 32°C, and the tissue was dissociated by shaking at 170-180rpm for 40 minutes. The tissue was removed from the papain using a wide-bore pipette tip, transferred to a clean tube containing 2mL of HAB medium, and incubated for 5 minutes on ice. Fire-polished siliconized 9-inch glass Pasteur pipettes were prepared by polishing the tip to 0.6-0.8mm diameter over a bunsen burner and siliconizing with Sigmacote® (Sigma; SL2-100ML). Using the fire-polished pipettes, the tissue was triturated ten times over one minute, then allowed to settle for one minute on ice. The supernatant was transferred to an empty 15mL tube, and the remaining tissue was resuspended in a fresh 2mL of HAB medium. The trituration was repeated 2 more times, for a total of 6mL of dissociated cells. The 6mL of dissociated cell solution was carefully applied to the top of the prepared OptiPrep™ (Sigma; D1556-250ML) density gradient (see Table 2.2), and the gradient was centrifuged at 800g for 15

minutes at 4°C. The top 7mL of the centrifuged gradient, containing debris and oligodendrocytes, were aspirated. The next 2.5mL, excluding the microglia pellet at the bottom, were collected and diluted with 5mL of HAB medium. The cell solution was centrifuged for 2 minutes at 200g at 4°C, and the supernatant was removed. The cell pellet was resuspended in 1mL of PBS- (cytiva; SH30028.02) and filtered through a 30µm strainer (Miltenyi Biotec; 130-041-407) into a clean tube. An additional 500µL of PBS- was used to rinse the tube and this was also filtered. The cell solution was centrifuged for 2 minutes at 200g at 4°C, the supernatant was removed, the cells were resuspended in 100µL of PBS-, and transferred to a nuclease-free 1.5mL microcentrifuge tube, which was kept on ice. 10µL of the single cell solution was stained with 10µL of trypan blue dye, and 10µL of this mixture was visualized on a hemacytometer to confirm successful dissociation with minimal debris and high cell viability. A final cell count was calculated by manually counting the total number of bright visible cells in all quadrants, calculating the average number of cells per quadrant, and multiplying by 10^4, the dilution factor, and the resuspension volume in mL.

Table 2.2 OptiPrep density gradient preparation for one gradient

Layer	OptiPrep (µL)	HABG medium (µL)	Total (µL)
1 (bottom)	173	827	1000
2	124	876	1000
3	99	901	1000
4 (top)	74	926	1000

2.17 Human islets

Human islets were isolated by the University of Alberta Islet Research or Clinical Cores as described (dx.doi.org/10.17504/protocols.io.x3mfqk6, accessed 20 January 2021). Details of donor metrics are summarised in Table 3.1 and some functional data are available at https://www.epicore.ualberta.ca/IsletCore/. Upon receiving human islets, desired islets were manually picked from remaining exocrine tissue with a dissecting microscope into 10mL of CMRL 1066 (VWR; CA45001–114) medium in a petri dish and incubated overnight at 37°C in a humidified CO_2 incubator.

2.18 Human islet stimulation and dissociation

450 islets per donor were manually picked into three wells (150 islets/well) of a 12-well plate containing Krebs-Ringer bicarbonate HEPES (KRBH) medium with 2.8mM glucose and incubated at 37°C for 1 h. Next, the islets were incubated for 1 hour in a new well containing KRBH under one of three experimental conditions: Low (2.8mM glucose); Positive (25mM glucose, 40mM KCl); or Negative (25mM glucose, 40mM KCl, 5mM EGTA). Islets were washed with PBS (Mg2+/calcium-free) containing 0.5 mM EDTA, then dispersed for 12-15 minutes in 200µl of 0.25% trypsin/EDTA at 37°C. Trypsinization was quenched with 25% FBS (1ml in PBS). Cells were centrifuged for 3 minutes at 200 g, the supernatant fraction was removed, and cells were resuspended in 300µl of PBS with 2% FBS. Cells were filtered through a 40µm cell strainer (Corning; 352340) and counted with a hemacytometer (see 2.16) prior to centrifugation and resuspension in PBS at the desired concentration.

2.19 FACS and reaggregation

Human islets were dissociated (see 2.18), washed with PBS, and incubated with rabbit AlexFluor647-labelled anti-protocadherin7 (PCDH7) antibodies (Bioss Antibodies; bs-11085R-A647) on ice for 30 minutes. Cells were washed with PBS, filtered (40μm), resuspended in 500μl of 2% FBS in PBS, and sorted using a BD FACSAria IIu (BD Biosciences). Sorted PCDH7+ and PCDH7− cells were plated onto a Corning Elplasia 96-well round bottom ultra-low attachment microcavity microplate (Corning; 4442) at 80 aggregates/well (1000 cells/aggregate) and cultured in CMRL medium for 48 hours prior to the GSIS assay. For qPCR, sorted PCDH7+ and PCDH7- cells were used for RNA isolation immediately following the sorting.

2.20 Glucose-stimulated insulin secretion assay

The sorted and reaggregated cells from islets of donors R366, R367, R369, H2330, H2337 and H2338 were pre-incubated in KRBH with 2.8mM glucose for 1 hour. Islets were sequentially stimulated with 2.8mM glucose, 16mM glucose, and 2.8mM glucose with 40mM KCl in KRBH for 1 hour at 37°C. The supernatant was collected after each stimulation and secreted human C-peptide was measured as a surrogate measurement for insulin using C-peptide ELISA kits (Mercodia; 10-1136-01). The stimulation index was calculated by normalizing to values at 2.8mM glucose.

2.21 Immunostaining

For paraffin-embedded samples, the sections were de-paraffinized and rehydrated through a series of xylenes (two 5 minute incubations), 100% ethanol (three 2 minute incubations), 95% ethanol (two 2 minute incubations), 75% ethanol (two 2 minute incubations), 50% ethanol (two 2

minute incubations), and dH_2O (one 2 minute incubation). For antigen retrieval, the sections were placed into 220mL citraconic anhydride buffer, prepared by diluting 130µL of 98% citraconic anhydride in 300mL of dH_2O and adjusting the pH to 7.4 with 1M sodium hydroxide. The sections were heated to 95°C in the buffer with the microwave, maintained at 95°C for 10 minutes, and cooled at room temperature for 1 hour. After cooling, the sections were washed with dH_2O once and twice with PBS, 5 minutes per wash. A hydrophobic barrier was drawn around each tissue section with a pap-pen (Cedarlane; MU22-A) and the sections were blocked with 5% horse serum in PBS for 30 minutes at room temperature in a humidified staining box. After blocking, the sections were washed three times with PBS, 5 minutes per wash. Primary antibodies (see Table 2.3) were diluted in PBS with 5% horse serum and sections were incubated with primary antibodies overnight at 4°C. The next morning, the sections were washed three times with PBS, 5 minutes per wash. Secondary antibodies (see Table 2.4) and nuclear stains TO-PRO-3 or DAPI were diluted in PBS with 5% horse serum, and sections were incubated with secondary antibodies and nuclear stain for 1-2 hours in the dark at room temperature. Sections were washed three times with PBS, 5 minutes per wash, and mounted with Diamond antifade mounting media and glass coverslips. Mounted slides were stored in a slide box at 4°C until they were imaged using a Leica SP8 confocal microscope.

For fixed frozen sections of mouse brain for ARC immunostaining, the sections were washed for 5 minutes in PBS to remove OCT cryomatrix before permeabilizing for 7 minutes with 1% SDS. Sections were washed three times with PBS, 5 minutes each, before proceeding with the rest of the protocol as stated above for paraffin-embedded sections.

2.22 RNAscope fluorescent in situ hybridization

Fluorescent *in situ* hybridization (FISH) was performed with the RNAscope multiplex fluorescent v2 kit (ACDbio) according to manufacturer's instructions. Briefly, cryosections were washed in PBS to remove OCT, baked in the HybEZ oven (ACDbio) at 60°C for 1 hour to improve tissue adherence, and placed into target retrieval buffer (ACDbio; 322000) heated to 95-98°C in a steamer for five minutes before being immersed in 100% ethanol for three minutes. A hydrophobic barrier was drawn around the sections with the ImmaEdge pen (Vector Laboratories; H-4000), and sections were incubated with protease III (ACDbio; 322337) in the HybEZ oven at 40°C for 30 minutes. Sections were washed with dH_2O and incubated with probes (see Table 2.5) in the HybEZ oven at 40°C for 2 hours. A technical positive and negative control was included for every RNAscope experiment using the provided positive and negative control probe mixtures. Sections were washed with 1X wash buffer (ACDbio; 310091) and left overnight in 5X SSC buffer, diluted in water from 20X SSC buffer (Ambion; AM9763), at room temperature. The next day, sections were washed with wash buffer and underwent amplification and development of each channel signal with provided channel-specific HRP reagents and fluorescent Opal dyes 520, 570, or 650 (Perkin Elmer FP1487001KT, FP1488001KT, or FP1496001KT). After a 5 minute incubation with provided DAPI, slides were washed and mounted with Diamond antifade mounting media (see section 2.20) and stored at 4°C until imaged with a Leica SP8 confocal microscope.

2.23 Quantification of RNAscope images

At least three sections of RNAscope images were quantified per mouse. For each RNAscope experiment, the technical positive control section was used to confirm successful protocol

completion, and the technical negative control section was used to designate the imaging settings to prevent any background signal in any channel. The left and right sides of the arcuate nucleus were imaged as Z-stacks separately for each section using the Leica SP8 confocal microscope 20X objective. The resulting image files were converted to .ims file formats and quantified with Imaris v9 (Oxford Instruments). The Cells with Vesicles feature was used on the image, specifying Cells as the areas with *Agrp* or *Pomc* signal that marked the neuronal cell bodies, and specifying Vesicles as the *Npas4* punctate signals. For each image, the threshold for Cells was manually set to completely cover all areas with detectable *Agrp* or *Pomc* signal, and cell boundaries were automatically calculated by the software when cell diameter was set to 10μm. Cells that had detectable *Agrp* or *Pomc* signal but no nucleus were manually removed from the final quantifications. Vesicle diameter was set to 2μm, and thresholds for Vesicles was manually set to count all *Npas4* punctate signals within the regions covered by *Agrp* or *Pomc* signal. Final statistics reports were exported as counts of vesicles per cell, and exported data was manually organized on Microsoft Excel to quantify the number of *Npas4* spots per *Agrp*+ or *Pomc*+ cell and the proportion of *Npas4+/Agrp*+ or *Npas4+/Pomc*+ cells. Due to the relatively low numbers of *Npas4* puncta in the ARC, *Npas4*+ cells were classified into 4 levels of *Npas4* expression based on the number of spots in a cell of interest: *Npas4*- (no puncta), *Npas4*-low (1-3 puncta/cell), *Npas4*-medium (4-9 puncta/cell), or *Npas4*-high (10 or more puncta/cell).

2.24 RNA isolation and reverse transcription PCR

100-200 human islets or sorted PCDH7+ and PCDH7- cells were counted and picked into 500μL of TRIzol (Thermo Fisher Scientific; 15596018). The samples were vortexed and frozen at -80°C. To extract RNA from samples preserved in TRIzol, 100μL of chloroform (Sigma; C2432-

250ML) was added to the thawed TRIzol sample before the samples were vortexed and centrifuged for 15 minutes at 12000g at 4°C. Keeping the samples on ice as much as possible, the supernatant was removed from the samples and 1mL of 70% ethanol was added to the samples. The samples were mixed by inverting 2-3 times and centrifuged at 12000g at room temperature. The supernatant was removed and the ethanol wash was repeated once. Residual ethanol was pipetted out and samples were air-dried for 1-2 minutes until ethanol traces had evaporated. The RNA pellet was resuspended in 21.5µL of water, 1µL DNAse and 2.5µL 10X DNAse buffer from the TURBO DNA-free™ kit (Thermo Fisher Scientific; AM1907) was added to each sample. Samples were incubated at 37°C for 30 minutes before adding 5µL of stop solution to each sample. Samples were vortexed, centrifuged at 12000g for 3 minutes at room temperature, and only the clear layer containing RNA was transferred to clean nuclease-free tubes. RNA concentration (ng/µL) was quantified with the Nanodrop 2000c (Thermo Scientific) and frozen at -80°C for long-term storage if necessary.

For reverse transcription PCR (RT-PCR), 1µg of RNA from each sample was mixed with 1µL of a mixture of random hexamers (10µg/25µL reaction) and oligodT (200ng/25µL reaction), then topped up to 14.62µL with water. A master mix was prepared with (per sample): 0.5µL water, 5µL 5X First Strand buffer (Invitrogen; Y02321), 2.5µL 0.1M DTT (Invitrogen; Y00147), 1.25µL 10mM dNTP mixture, 0.625µL 40U/µL RNAseOUT, and 0.5µL 200U/µL Superscript reverse transcriptase III (Invitrogen; 18080093). For a negative control, RNAseOUT and reverse transcriptase was not added, and 1.625µL of water was used instead. Diluted samples were heated at 70°C for 10 minutes and 10.38µL of master mix was added to each sample before running on a thermocycler (Eppendorf; Mastercycler pro S) with the following cycle: 15°C for

10 minutes, 25°C for 10 minutes, 37°C for 15 minutes, 42°C for 45 minutes, 50°C for 10 minutes, 55°C for 5 minutes, 95°C for 3 seconds, and 4°C for holding. Resulting cDNA was frozen at -20°C for storage.

2.25 Quantitative real-time PCR

All samples were run in triplicate for all target genes for quantitative real-time PCR (qPCR). Samples were diluted 1:2 in water. For each target gene, enough master mix was prepared for technical triplicates of each sample. Master mix was prepared at a larger volume for all replicates and samples within each gene, and each well was estimated to have: 5.9375µL water, 1µL 10X buffer A (), 0.3125µL 10mM dNTP mixture, 0.5µL 10µM primers, and 0.25µL DNA Taq polymerase. 8µL of master mix was dispensed into each well of a 384-well plate, and 2µL (40ng) of sample was added to each well. For no template negative control wells, 2µL of water was added instead of diluted sample. Taqman qPCR was performed on the Viia7 real-time PCR system (Applied Biosystems) using the 384-well/TaqMan/fast-run settings. All reactions used FAM as the reporter dye, ZEN and IBFQ as quenching dyes, and the relative gene expression was calculated using the ΔΔCt method with *TBP* as the reference gene. All primers and probes used in qPCR are found in Table 2.6.

2.26 Nanostring

50 human islets were manually picked into 100µl Buffer RLT (Qiagen) containing 1% beta-mercaptoethanol for lysis. Whole islet gene expression was measured by the Nanostring nCounter assay according to manufacturer's instructions, using a custom nCounter XT Gene Expression Reporter Codeset and Capture Probeset as described[323], on the nCounter SPRINT

Profiler. Gene expression was analyzed using the nSolver 4.0 Analysis Software and normalized to reference genes *B2M, GAPDH, GUSB, HPRT1, POLR2A,* and *TBP*.

2.27 Single cell RNA sequencing

For stimulated human islets, dissociated islet cells from each experimental condition (Low, Positive, Negative; see section 2.18) for each donor was processed as a separate sample. Libraries were generated for 5000 target cells per sample with the Chromium Single Cell 3' reagent kits (10x Genomics) according to the manufacturer's instructions. Version 2 reagent kits were used for donors R253 and R282, and Version 3 was used for donor R317. For dissociated mouse hypothalamic cells (see 2.16), cells from each mouse were processed as a separate sample. Libraries were generated for 10000 target cells per sample with the Chromium Next GEM Single Cell 3' version 3.1 reagent kits (10x Genomics) according to the manufacturer's instructions. Library quality assessment was performed twice during the library generation protocol with the Agilent Bioanalyzer High Sensitivity dsDNA kit (Agilent; 5067-4626).

Completed libraries were quantified with both the Qubit high sensitivity dsDNA kit (Thermo Fisher Scientific; Q32854) and KAPA library quantification kit for Illumina platforms (KAPA Biosystems; KK4824). For stimulated human islet libraries, libraries for each donor were diluted to 4nM and pooled before sequencing. For mouse hypothalamic cells libraries, two to four samples' libraries were diluted to 4nM and pooled before sequencing, depending on chronological order of mouse availability. All libraries were sequenced with the Illumina NextSeq500 on manual mode using a 75-cycle High Output v2 or v2.5 kit (Illumina FC-404-

2005). For libraries generated using Chromium v2 kits, cycle numbers were: 8 for index 1 (i7), 0 for index 2 (i5), 28 for read 1, and 50 for read 2. For libraries generated using Chromium v3 kits, cycle numbers were: 8 for index 1 (i7), 0 for index 2 (i5), 28 for read 1, and 56 for read 2. For libraries generated using Chromium Next GEM v3.1 kits, cycle numbers were: 10 for index 1 (i7), 10 for index 2 (i5), 28 for read 1, and 44 for read 2. Sequencing was repeated for all libraries until all samples reached a minimum read depth of 20000 reads/cell as determined by downstream processing of sequencing data.

2.28 Analysis of scRNA-seq data

Binary base call (BCL) files of sequencing data were obtained as outputs from the Illumina NextSeq500. Cell Ranger v7.0 (10x Genomics) was used for processing of all scRNA-seq data. FASTQ files from sequencing outputs with *cellranger mkfastq*. Alignment, demultiplexing, filtering, barcode counting, and UMI counting was performed with *cellranger count* separately for each sample, combining multiple sequencing runs' worth of FASTQ files for the same sample. For human islet samples, FASTQ files were aligned to reference human genome GRCh38. For mouse hypothalamus samples, FASTQ files were aligned to the reference mouse genome GRCm38. Reads/cell, genes/cell, and number of cells per sample were obtained at the end of the Cell Ranger pipeline.

Outputs of Cell Ranger were carried forward to the R package Seurat[324] v4.0.4 for further filtering and downstream analysis. First, Seurat objects were created from the Cell Ranger outputs and cells that expressed more than 20% mitochondrial genes or more than 6000 genes/cell were filtered out. For human islet data, metadata was edited to include experimental

conditions and donor ID. For mouse hypothalamus data, metadata was edited to include mouse number (sample ID), fasted or refed status, and genotype. Next, the objects were normalized with SCTransform and integrated to form one Seurat object with all samples, and clustered in UMAP space at an initial resolution of 0.6. The biological identities of clusters were manually determined with known marker gene expression. Differentially expressed gene (DEG) analysis was performed using *FindMarkers* or *FindAllMarkers* functions when needed. For identifying calcium-regulated genes in the human islet data, only cells from the Positive and Negative conditions were subsetted from populations of interest, and *FindMarkers* was used to identify DEGs across the two conditions in each cluster within the subsetted population. Glucose-regulated genes were identified in the same manner, using cells from the Positive and Low condition. For identifying DEGs across fasted vs refed states or genotypes in the mouse hypothalamus data, cells expressing *Pomc* were subsetted first, and only cells from the targeted combination of fasted and refed states, POMC-CreER (CT) and POMC-NPAS4 KO (KO), or combinations of the metadata were used in the DEG analysis with *FindMarkers.* Gene ontology (GO) analysis was performed through EnrichR[325–327] using the libraries GO: Biological Process 2021 and Molecular Function 2021, with the R function *DEenrichRPlot*. All code used for analysis of scRNA-seq data in chapter 3 and chapter 6 can be found in Appendix B and Appendix C, respectively.

2.29 Statistical analyses

Statistical calculations were performed in Rstudio or GraphPad Prism v8.0.1. Data are shown as mean ± SEM unless otherwise stated in figure legends. In general, statistical significance was determined using the Student's t-test for two groups or genotypes, one-way ANOVA with

Tukey's multiple comparisons for three groups or genotypes, and two-way ANOVA with Tukey's multiple comparisons for three groups or genotypes for multiple time points or conditions. Statistical tests used for each figure are stated in the figure legends. For scRNA-seq data in Chapters 3 and 6, cutoffs for all statistically significant DEGs were $P_{adjusted} < 0.05$ using Wilcoxon rank-sum tests. In Chapters 4 and 5, all RNAscope quantifications are shown with each dot representing one biological replicate, as a sum of quantifications from a minimum of 3 ARC sections from a biological replicate.

Table 2.3 Primary antibodies and dilutions used for immunofluorescence

Target	Species	Dilution	Source
Insulin	Guinea pig	1:500	Dakocytomation (A0564)
Glucagon	Rabbit	1:100	Abcam (ab92517)
Glucagon	Mouse	1:2000	Sigma-Aldrich (G2654-100UL)
Neuropeptide Y	Rabbit	1:400	Cell Signalling Technology (11976S)
Insulin-like growth factor-binding protein 2	Rabbit	1:200	Thermo Fisher Scientific (15699-1-AP)
Protocadherin 7	Rabbit	1:100	Abcam (ab139274)
Neuronal PAS domain protein 4	Rabbit	1:500	Activity Signalling (AS-AB18A-100)

Table 2.4 Secondary antibodies and dilutions used for immunofluorescence

Target	Host	Fluorophore	Dilution	Source
Guinea pig IgG	Donkey	FITC	1:450	Jackson ImmunoResearch (706-096-148)
Guinea pig IgG	Donkey	Cy3	1:250	Jackson ImmunoResearch (711-096-152)
Rabbit IgG	Donkey	FITC	1:450	Jackson ImmunoResearch (706-166-148)
Rabbit IgG	Goat	Alexa Fluor 647	1:200	Invitrogen (A27040)
Mouse IgG	Donkey	Cy3	1:250	Jackson ImmunoResearch (715-166-150)

Table 2.5 RNAscope probes

Target gene	Species	NCBI reference sequence	Target region (bp)	Channel	RNAscope probe catalogue #
INS	Human	NM_000207.2	20 - 399	2	313571-C2
GCG	Human	NM_002054.4	26 - 1265	3	556741-C3
Npas4	Mouse	NM_153553.4	1860 - 3067	1	461631
Pomc	Mouse	NM_008895.3	19 - 995	2	314081-C2
Agrp	Mouse	NM_001271806.1	11 - 764	3	400711-C3
tdtomato	NA	LC311026.1	910 - 2285	3	317041-C3

Table 2.6 qPCR primers

All primers are targeted to human mRNA sequences

Target	Primer 1	Primer 2	Probe
PCDH7	GTG GAA TTC AGC CAA ACA CAG	ATT TGT GGG AGC AGG AGA C	ACA GCA AAC AGA TGC GTC TAC ATC CA
INS	CTA GTG TGC GGG GAA CG	CAC GCT TCT GCA GGG AC	CGG CGG GTC TTG GGT GTG TA
ERO1B	GGG TGA GTT GGA AGC CTT TAG	TGG ACT GTG TTG GAT GTG AC	ACA GAC TCA GGG TTT AGG AAC TGC C
NKX6-1	TCG TTT GGC CTA TTC GTT GG	TGT CTC CGA GTC CTG CTT C	TGC TTC TTC CTC CAC TTG GTC CG
SLC30A8	AGG TCA ATT AAG AGG TGG GC	AAT GAG TAC GCC TAT GCC AAG	CAC ATT GCT GGG AGT CTT GCT GTT G
TBP	GAG AGT TCT GGG ATT GTA CCG	ATC CTC ATG ATT ACC GCA GC	TGG GAT TAT ATT CGG CGT TTC GGG C

Chapter 3: Using single cell transcriptomics to identify calcium-regulated transcriptional changes in human pancreatic islets

3.1 Rationale

Due to the heterogeneous nature of the islet, using scRNA-seq has become a favourable method to study the transcriptomes multiple cell types simultaneously in an unbiased manner. Within the past decade, there have been a number of human islet scRNA-seq experiments. Most have focused on how diabetes alters the islet transcriptome or identifying rare cell types[328–334]. A more recent addition to the field of islet single-cell studies have been coupling functional data to transcriptomes[328,329,331–333,335]. However, there has not been an attempt focused on using scRNA-seq to profile the activity-regulated transcriptome of human islet cell types.

Like all excitable cells, all islet cell types rely on intracellular calcium signalling to some degree of function. Due to the complexities of calcium signalling and the ready availability of mouse and human beta cell lines, most studies have focused on calcium signalling specifically in beta cells[240,336,243]. As discussed in section 1.12, calcium signalling in beta cells triggers two main pathways that are known to regulate transcription: 1) the CAMK/CREB pathway[231,237,337,338,240,339] and 2) the CaN/NFAT pathway[231]. In islet cells, the process of calcium-regulated transcription is coupled to depolarization and activation of the cell downstream of glucose stimulation and metabolism, which is vital for the biological role of islets. Therefore, there is merit to studying the rapid changes in activity-regulated gene expression that occur as the islet responds to changes in the environment.

In this chapter, I used scRNA-seq to profile the rapidly responding calcium-regulated

transcriptome in human islet cell types, focusing on the endocrine cell types. I hypothesized that like previous islet scRNA-seq studies, there would be significant heterogeneity within a single cell type, due to the different identities of calcium-regulated genes across these subtypes.

3.2 Human islet multi-conditional scRNA-seq data clustering is not affected by experimental conditions

To study islet cell calcium-regulated genes, I generated islet single-cell libraries from three healthy male, BMI- and age-matched donors R253, R282, and R317 (Table 3.1). In order to confirm that donor islets were healthy and showed expected islet gene expression, 50 islets were picked from each donor prep and used for Nanostring gene expression analysis using a custom islet gene expression panel. Compared to the average expression of previously collected 107 donor preps, the islets from the three donors showed similar expression levels of 56 adult human islet genes (Fig. 3.1). Prior to library preparation, I stimulated islets from each donor for 1 hour under the following conditions: 1) “Low” glucose to activate alpha cells and inhibit beta cells; 2) “Positive”, a high glucose and high KCl stimulus to directly depolarise all cells and trigger maximal calcium influx and downstream calcium signaling; and 3) “Negative”, a control condition with high glucose/high KCl stimulus and extracellular calcium chelator EGTA (Fig. 3.2a). The relatively short stimulation time of 1 hour was to ensure that only the most robustly and acutely calcium-regulated genes would be detected. The short stimulation time would also allow for existing biological heterogeneity to remain unaffected by the transcriptional changes that occur due to the induction of activity-regulated genes.

Downstream of the pre-processing of raw sequencing files, the 10x Genomics Cell Ranger

software detected 59,791 sequenced cells, with each donor having a minimum of 20,000 average reads/cell (Table 3.1). After the dataset was converted into a Seurat object for further analysis, 50,194 cells remained (Table 3.1). After filtering out cells that did not meet the QC cutoffs of less than 6,000 genes/cell (nFeature_RNA) and less than 20% mitochondrial genes (percent.mt), 43,909 cells were carried forward as 30 clusters (Table 3.1, Fig. 3.2b). All clusters showed similar proportions of Low, Positive and Negative cells, implying that clustering was minimally influenced by experimental conditions and that existing biological heterogeneity was preserved (Fig. 3.2d). This supported the goal of designing experimental conditions that would allow us to investigate calcium-regulated genes and islet heterogeneity with the same dataset.

In the 30 clusters, there were 37,436 endocrine and 6,473 non-endocrine cells. I determined cluster identities using expression of known marker genes for each cell type: *INS* for beta cells, *GCG* for alpha cells, *SST* for delta cells, *PPY* for Pancreatic Polypeptide (PP) cells, *KRT19* for duct cells, *CPA1* for acinar cells, *PECAM1* for endothelial cells, *PDGFRB* for mesenchymal cells, and *FCER1G* for immune cells[340] (Fig. 3.2c, e). For further validation of non-endocrine cell types, I carried out a more in-depth DEG analysis, and found that *INHBA* and *TIMP1* expression were restricted to mesenchymal cells, while *PLVAP* and *ESM1* were endothelial cell marker genes (Fig 3.3a-b). In addition to known cell types, there was a cluster expressing *INS*, *GCG*, and *SST* ("polyhormonal") and a cluster that did not seem to express robust levels of any of the known marker genes ("unknown"). Furthermore, I detected ghrelin (*GHRL*)-expressing cells located near the PP and alpha cells, but these cells did not form a whole cluster by themselves, presumably due to their low cell number (Fig 3.3c).

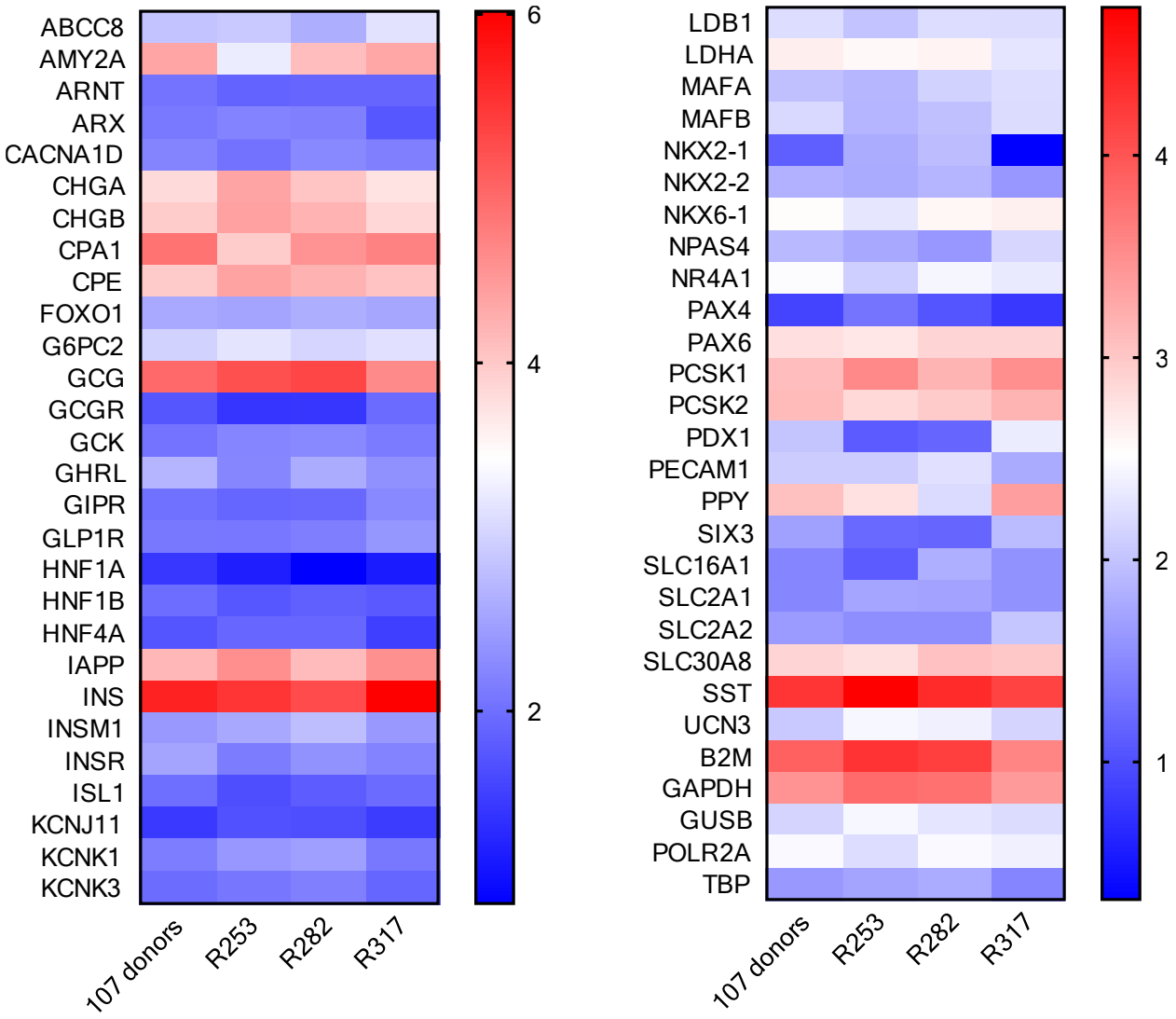

Figure 3.1 | Islets from donors R253, R282, and R317 show similar islet gene expression. Nanostring gene expression panel of 56 adult human islet genes, shown as a heatmap depicting log-transformed expression with a colour scale of blue (low) to red (high). The gene expression profiles of islets from donors R253, R282, and R317 used for scRNA-seq were compared to the average gene expression profile of 107 human islet donors collected previously (https://www.epicore.ualberta.ca/IsletCore/).

Table 3.1 Human islet donor information and cell numbers during key analysis steps

Donor ID	**R253**	**R282**	**R317**
Age (years)	57	57	54
Sex	male	male	male
Diabetes	none	none	none
BMI (kg/m^2)	25.5	26.4	26.4
HbA_{1c} (%)	5.0	6.0	5.1
Number of sequenced cells (Cell Ranger v.7)	9,008	17,182	25,601
Average reads/cell (Cell Ranger v.7)	74,262	42,154	28,427
After creating Seurat object	8,698	16,942	24,514
After filtering based on QC cutoffs (Figure 3.2)	7,756	16,180	19,973
After subsetting endocrine cells only	6,842	13,724	17,715
After removal of poorly integrated clusters (Figure 3.4)	6,035	11,080	15,371

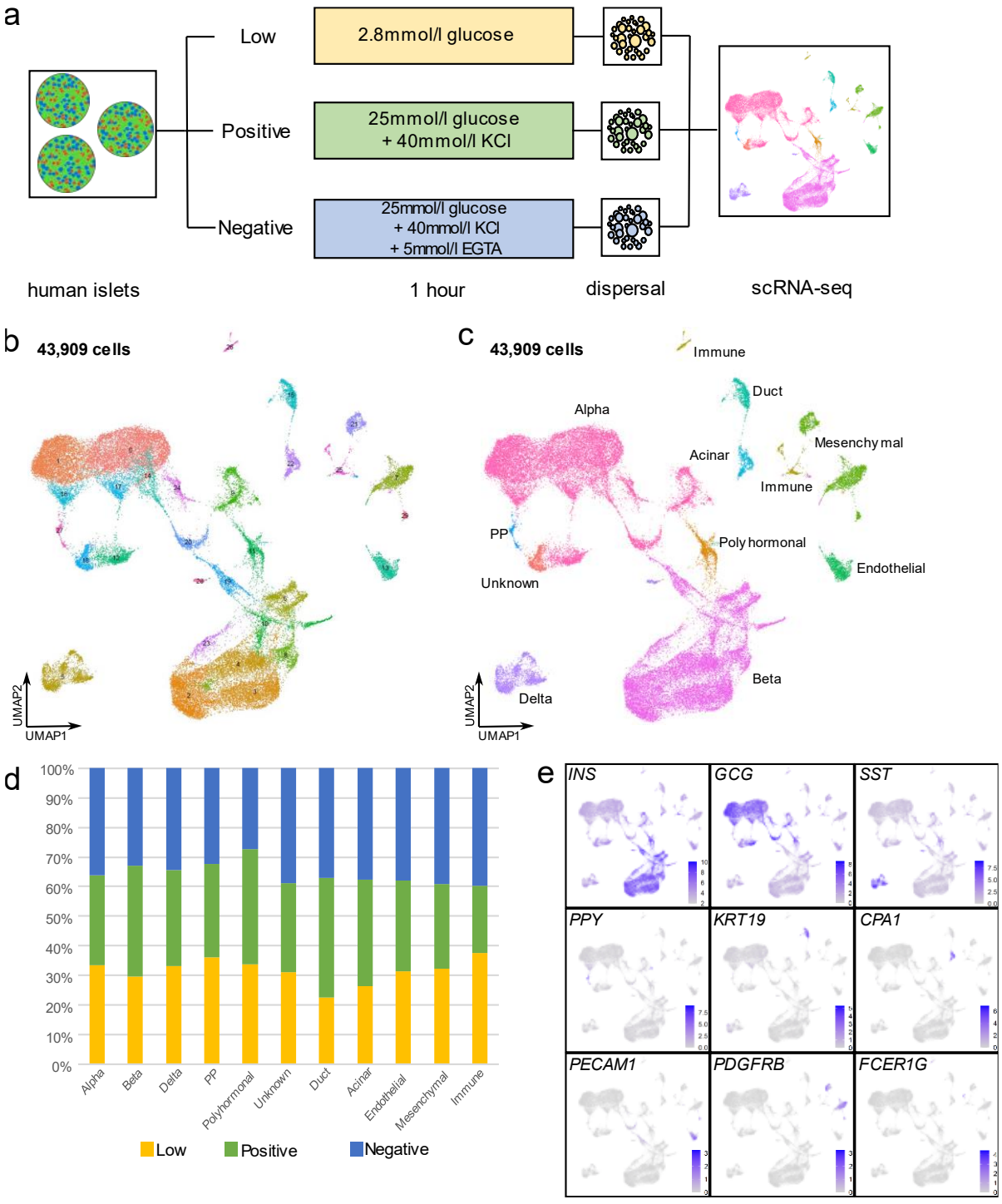

Figure 3.2 | Human pancreatic islet single cell RNA-seq dataset contains all expected cell types. a, Depiction of the experimental procedures leading up to the library preparation. **b-c,** UMAP plots of 43,909 human islet cells that passed quality control and filtering thresholds shown in 30 clusters (a) and cell types (b). **d,** Stacked bar plots showing the proportion of cells from Low, Positive, and Negative conditions in each cell type. **e,** Featureplots showing the expression of marker genes specific for each cell type, with higher expression levels shown as darker shades of blue.

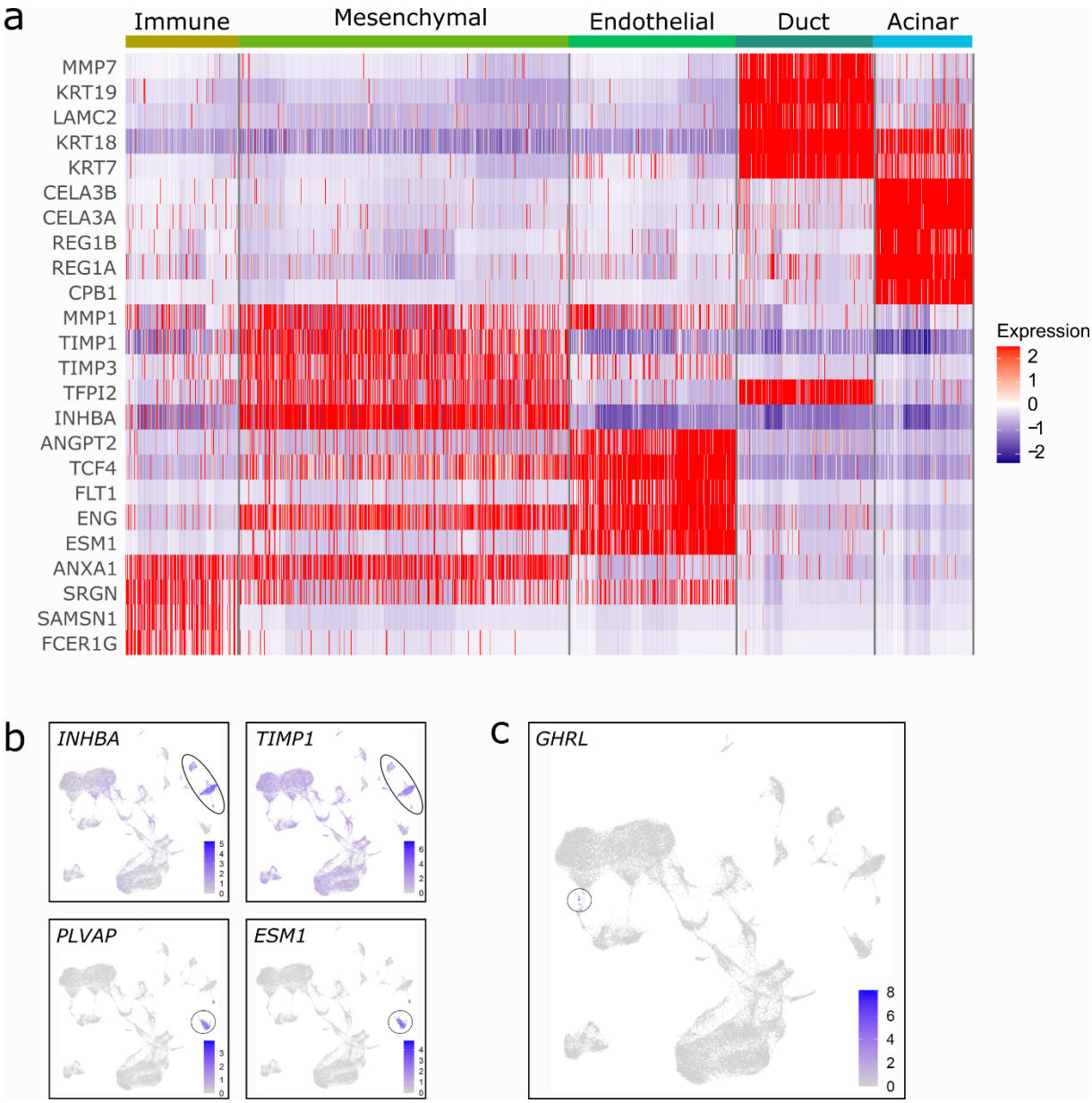

Figure 3.3 | DEGs that identify non-endocrine cell types. a, Heatmap showing the top 5 DEGs in the non-endocrine cell types, with relative gene expression shown from blue (low) to red (high). **b,** Featureplots of representative DEGs identified as markers for mesenchymal cells (*INHBA*, *TIMP1*) and endothelial cells (*PLVAP*, *ESM1*) from the heatmap above (a). **c,** Featureplot showing the expression of *GHRL*-expressing cells that did not cluster distinctly.

3.3 Reclustering of endocrine cells reveals heterogeneity within alpha and beta cells

I subsetted and reclustered 38,281 alpha, beta, delta, PP, and polyhormonal cells for further analysis. After reclustering, I removed clusters that were poorly integrated across donors, leaving 32,486 cells in 15 clusters (Fig 3.4a). Like before, expression of the key endocrine cell type marker genes *INS, GCG, SST,* and *PPY* were used to identify the clusters (Fig 3.4b). While delta, PP, and polyhormonal cells remained as single clusters, there were five clusters within alpha cells and seven clusters within beta cells, which I named α1–α5 and β1–β7, respectively (Fig. 3.4a). Overall, the dataset was now composed of 43% alpha cells, 46% beta cells, 6.5% delta cells, 3.8% polyhormonal cells, and less than 1% PP cells.

To examine cluster heterogeneity among alpha and beta cells and potentially uncover new cluster-specific marker genes, I performed a DEG analysis in each cell type (Fig. 3.4c-d). Within the top 10 DEG in each alpha cell cluster, α1 and α4 expressed similar panels of marker genes, including *RSAD2* and *CLDN4* (Fig. 3.4c, 3.5a). Cluster α2 was enriched for some alpha cell marker genes such as *ALDH1A1*, *CRYBA2*, *TM4SF4*[329], and *LOXL4* (Fig. 3.4a, d). Notably, none of the detected marker genes for cluster α3 seemed to be particularly robust. Despite its small cell numbers, the α5 cluster DEG list showed robust marker genes, including *CTNNA3* and *CHGB* (Fig. 3.4c, 3.5a). The α5 cluster also expressed the highest levels of *GCG* and *TTR* among the alpha cell clusters (Fig. 3.5d). Finally, the gene *IGFBP2* was expressed in a small proportion of all alpha cell clusters and showed high alpha cell specificity when compared with other cell types (Fig. 3.5a). To confirm this, I immunostained human islet sections and found IGFBP2 protein was restricted to a small number of GCG-positive alpha cells (Fig. 3.5b).

Within beta cells, the β1 cluster had elevated levels of genes such as *CNTN5*, *SPP1*, *NPY* and *IGFBP5* (Fig. 3.4d, 3.5a). Immunostaining for NPY, which has been suggested to mark immature beta cells[341], showed expression in a subset of INS-expressing beta cells (Fig. 3.5c). Cluster β2 showed the highest expression levels of *IAPP* among all clusters (Fig. 3.4d, 3.5a). High protein levels of human islet amyloid polypeptide are associated with a pathological islet, beta cell maturity or beta cell dysfunction[342,343]. Similar to α3, clusters β3 and β4 did not show robustly elevated levels of any DEG, but cluster β4 uniquely expressed reduced levels of *KCNMA1*, which encodes for an α-subunit of a calcium-sensitive potassium channel (Fig 3.5a). Cluster β5 was enriched for metallothionein genes such as *MT2A*, *MT1X* and *MT1E*, suggesting increased protective capacity against oxidative stress[344]. Notably, β6 was characterised by low expression of key beta cell maturation markers such as *NKX2-2*, *UCN3* and *ERO1B*, and could comprise transcriptionally immature beta cells, such as virgin beta cells[345] (Fig. 3.5e).

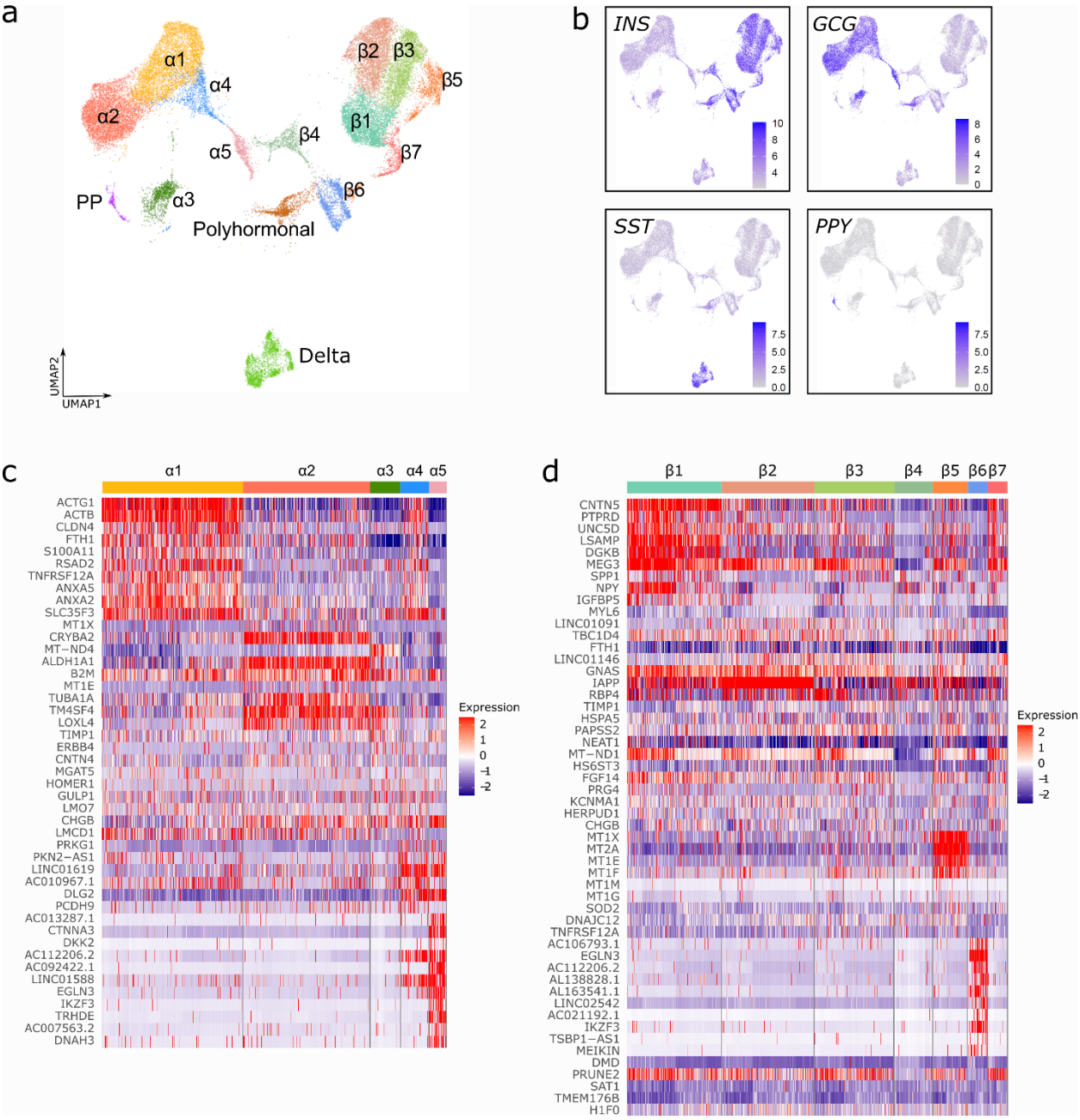

Figure 3.4 | Multiple alpha and beta cell clusters with distinct gene expression profiles are present in human islets. a, UMAP plot showing re-clustered endocrine cells only, with individual clusters labelled if present within cell types. **b,** Featureplots showing expression of endocrine cell type marker genes *INS*, *GCG*, *SST*, and *PPY*. **c-d,** Heatmaps showing the top 10 DEGs in clusters α1- α5 in alpha cells (c) and clusters β1-β7 in beta cells (d), with relative expression shown from red (low) to blue (high).

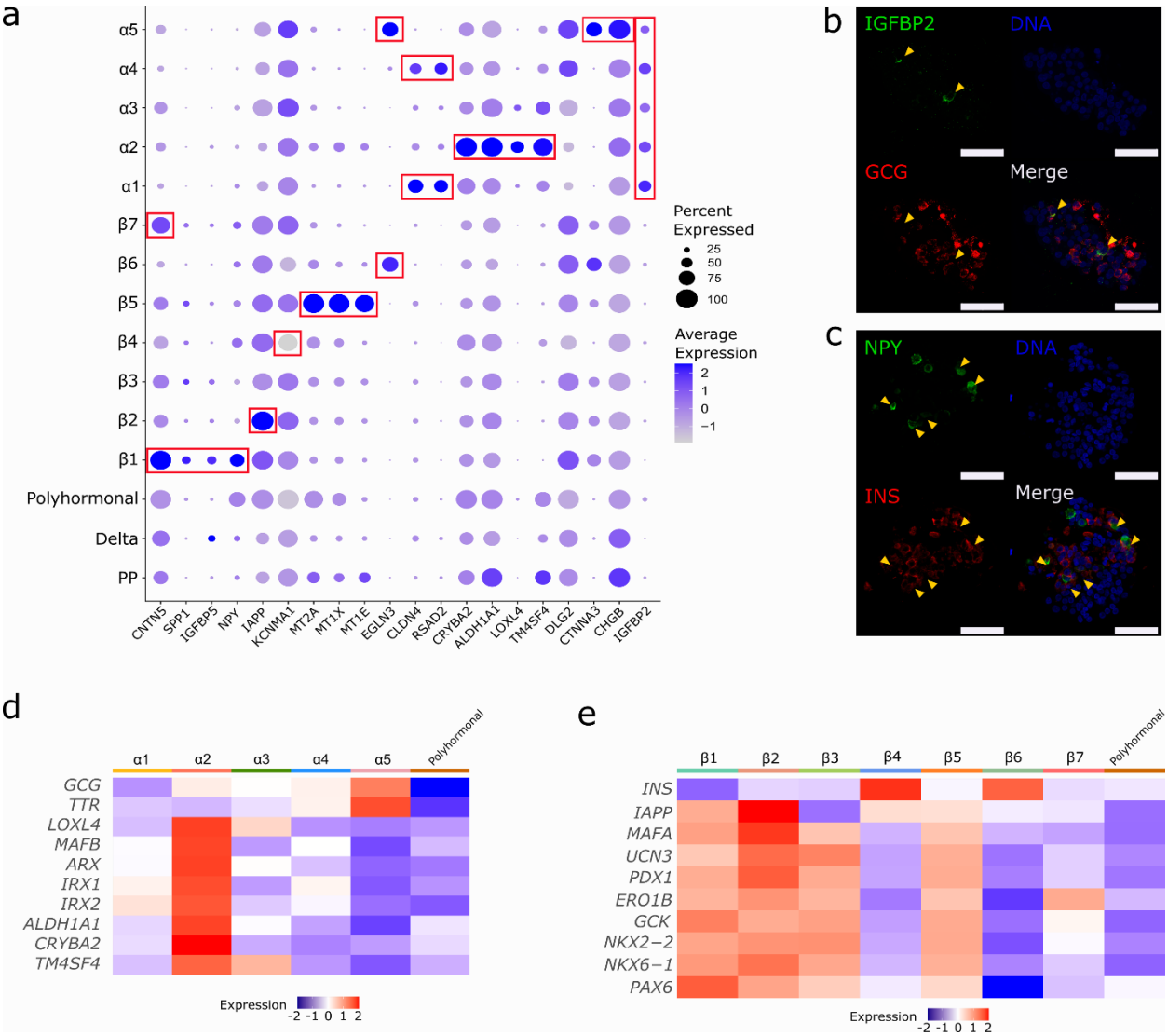

Figure 3.5 | Alpha and beta cell clusters show heterogeneous marker genes and different levels of cell type-specific genes. a, Dot plot showing selected representative potential marker genes for certain clusters, with highlighted genes in red boxes. The proportion of cells in each cluster expressing a gene is represented by the size of the dot, and higher expression of a gene is shown as darker shades of blue. **b-c,** Images of immunostained human islet sections, stained for IGFBP2 (green), GCG (red), and DNA (blue) (f); or NPY (green), INS (red), and DNA (blue) (g). Yellow arrowheads indicate regions of overlap between IGFBP2 and GCG (f) or NPY and INS (g). Scale bars = 100μm. **d-e,** Heatmaps showing the average expression of alpha cell marker genes (a) and beta cell marker genes (b) in clusters α1- α5 (a) and clusters β1-β7 (b) and polyhormonal cells. Expression levels are shown from blue (low) to red (high).

3.4 Alpha cell clusters regulate unique sets of calcium-regulated genes

I next focused on identifying calcium- and glucose-regulated genes by paired comparisons of transcriptomes from different conditions. Within each cluster of a certain cell type, I identified calcium-regulated genes as those that had a higher expression in either the Positive or Negative condition when the two transcriptomes were compared. In the same manner, in the Low vs Positive comparison, genes that were significantly elevated in either condition would be glucose-induced. An ideal calcium-regulated gene would be expressed at lower levels in low glucose (Low), higher levels in response to depolarisation and calcium signalling (Positive), and at reduced levels when calcium signalling is inhibited by EGTA (Negative) (Fig. 3.6a).

In alpha cells, only the enzyme-encoding gene *PAM* was detected as calcium-regulated in all five alpha cell clusters (Fig. 3.6b). Cluster α2, which expressed the highest levels of alpha cell marker genes, had the highest number of cluster-specific calcium-regulated genes. α1 and α2 also had the highest number of calcium-regulated genes overall compared to all other alpha cell clusters (Fig. 3.6c). Interestingly, both α1 and α2 regulated typical beta cell genes such as *IAPP* and *INS*. Overall, there were five calcium-regulated genes common to four out of five clusters, and nine calcium-regulated genes common to three out of five clusters. By the absolute number of calcium-regulated genes, I suspect that α1 and α2 are the most calcium-responsive clusters, while α5 may have a blunted calcium response. Since alpha cells secrete glucagon under low glucose conditions, I also compared Low and Negative conditions. As expected, most clusters had more genes expressed at higher levels in the Low condition, with the exception of α3 (Fig. 3.6d). Once again, α5 showed a minimal response, with only one gene unique to the cluster. In contrast to the comparison between Positive and Negative conditions, the Low vs Negative comparison showed

only the gene *PTEN* as a commonly regulated gene between all five clusters (Fig. 3.6e). From these results, I conclude that while most alpha cells show a transcriptional response in response to calcium and glucose, a small subset (α5) is less responsive or slower to respond.

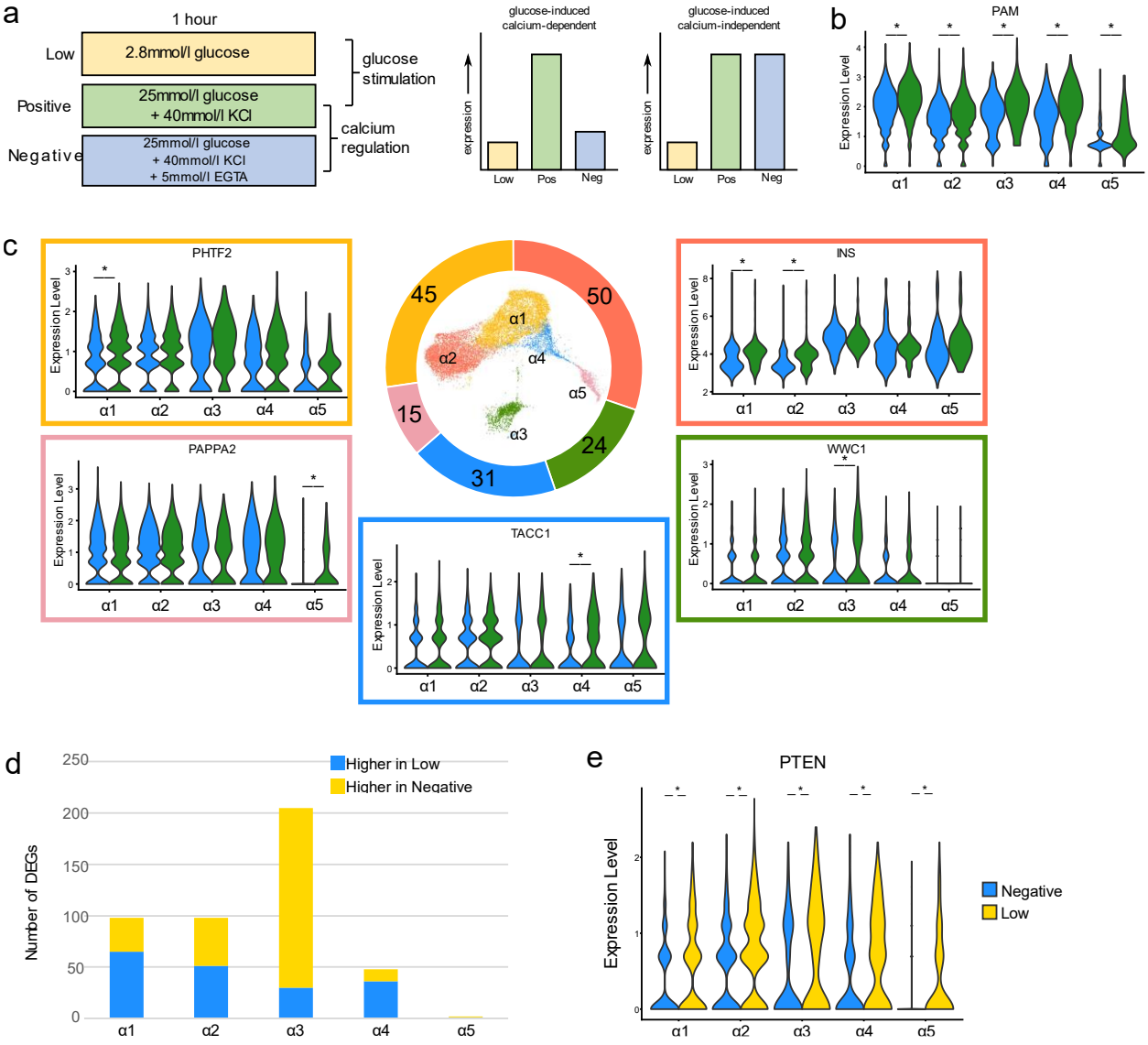

Figure 3.6 | Alpha cell clusters show heterogeneity in calcium-regulated genes. a, Diagram showing the expression levels of an ideal calcium-regulated gene and a calcium-independent gene across the Low, Positive, and Negative experimental conditions. **b,** Violin plot showing the expression of the core alpha cell calcium-regulated gene *PAM* in clusters α1- α5 across the Positive (green) and Negative (blue) condition. **c,** Donut pie chart showing the total number of calcium-regulated genes in each alpha cell cluster, with violin plots of a representative calcium-regulated gene in the square colour-coded for each cluster. **d,** Stacked bar plot showing the

number of DEGs per cluster from the Low vs Negative comparison in each alpha cell cluster, with genes expressed higher in the Low condition shown in blue and genes expressed higher in the Negative condition shown in yellow. **e,** Violin plot showing the expression of the gene *PTEN* significantly upregulated in the Low (yellow) vs the Negative (blue) condition in clusters α1- α5. Non-parametric Wilcoxon rank sum test, $*P_{adjusted} < 0.05$.

3.5 Beta cell clusters regulate unique sets of calcium-regulated and glucose-regulated genes

Unlike alpha cells, beta and delta cells secrete hormones when ambient glucose levels are high, and have similar intracellular mechanisms downstream of glucose uptake[346]. Therefore, I focused on first identifying the calcium-regulated genes by comparing Positive vs Negative conditions. Cluster β6 had only three detectable calcium-regulated genes: *ELMO1, MT-ND3,* and *ZNF331* (Fig. 3.7a-b). These were all commonly regulated in all seven beta cell clusters and made up the "Core" list of calcium-regulated genes. This meant that β6 did not have any cluster-specific calcium-regulated genes, further supporting the idea that β6 could be dysfunctional or immature compared with other beta cells. Six clusters all regulated four genes in addition to the Core list: *C2CD4B, ELL2, SIK2,* and *SIK3* (Fig. 3.7c). Following the Core list, there are several known IEGs shared between four or five clusters, including *NR4A1* and *NR4A2*[258], with β1-β3 having the highest degree of overlap. β1-β3 also expressed the highest number of calcium-regulated genes, including known activity-regulated genes like *IAPP* and *NPAS4*[319,320] (Appendix A). In summary, β1-β3 are the most calcium-responsive beta cell clusters, and beta cells have an overall more homogeneous calcium-regulated profile than alpha cells, based on the number of Core calcium-regulated genes.

Next, I compared the Low and Positive conditions to determine the glucose-regulated profile for beta cells. Once again, β6 seemed to be unresponsive, with no detected glucose-regulated genes (Fig. 3.7d). In contrast, most beta cell clusters had more than 50 glucose-regulated genes, with

the majority being glucose-induced (Fig. 3.7d). In at least two clusters, activity-regulated genes such as *NR4A1*, *NR4A2*, *IER3*, and *NPAS4* were all glucose-induced and calcium-regulated (Appendix A). However, not all glucose-induced genes were calcium-regulated in the same clusters, and vice versa. For example, *FOS* was glucose-induced in β1-β5, but it was calcium-regulated in only three clusters. Conversely, genes such as *C2CD4B* and *ELL2*, which were calcium-regulated in almost all clusters, were only glucose-induced in 1 or 2 clusters. From these results, I conclude that not all glucose-regulated genes are calcium-regulated, and purely calcium-regulated genes are detectable using the method of pairwise cross-conditional comparisons.

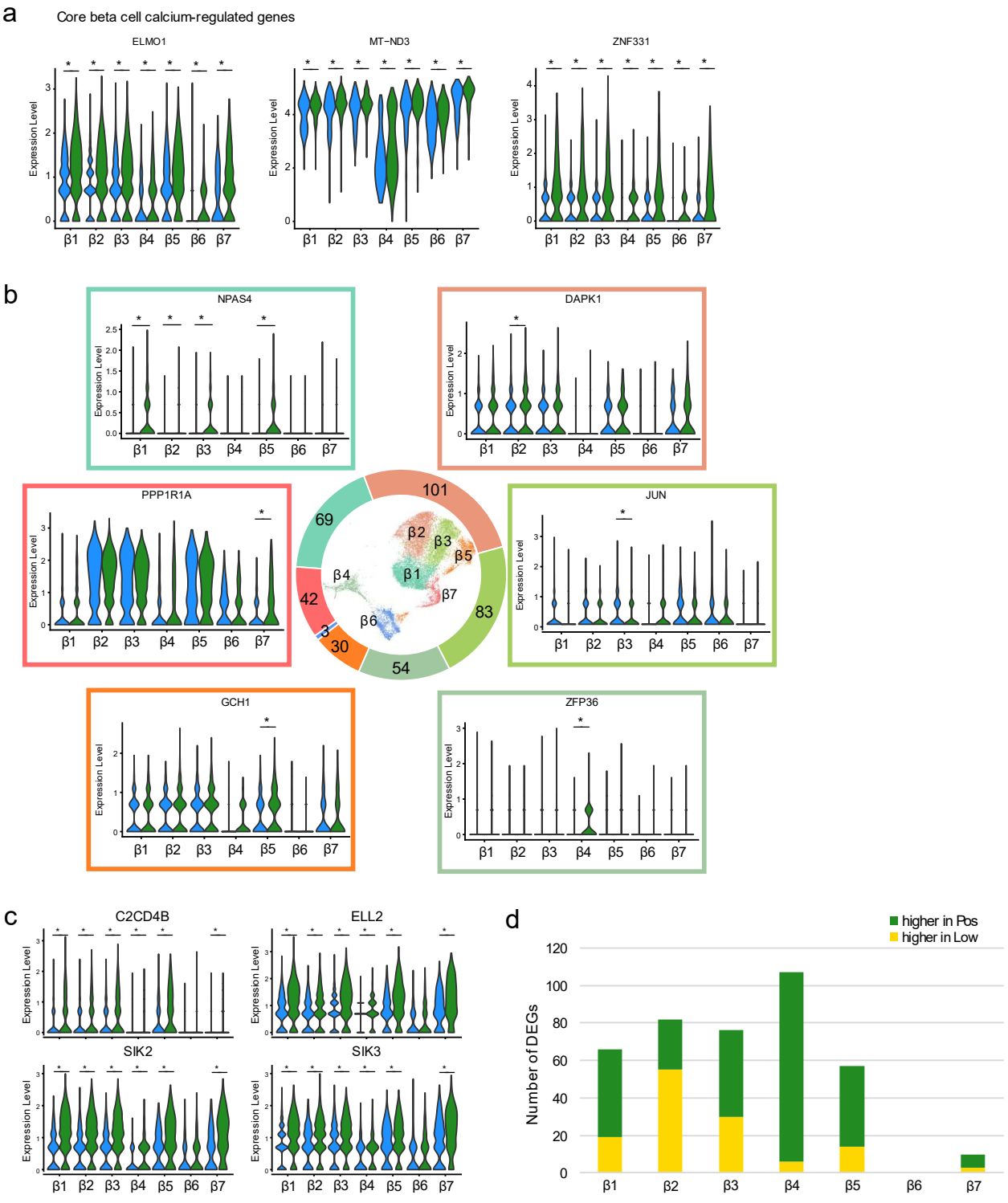

Figure 3.7 | Beta cell clusters show heterogeneity in calcium-regulated genes. a, Violin plot showing the expression of the core beta cell calcium-regulated genes in clusters β1-β7 across the Positive (green) and Negative (blue) condition. **b,** Donut pie chart showing the total number of calcium-regulated genes in beta cell clusters excluding β6, with violin plots of a representative calcium-regulated gene in the square colour-coded for each cluster. **c,** Violin plots showing the

expression of the common calcium-regulated genes in all beta cell clusters excluding β6. **d,** Stacked bar plot showing the number of glucose-regulated genes per cluster from the Positive vs Low comparison in each beta cell cluster, with genes expressed higher in the Low condition shown in yellow and genes expressed higher in the Positive condition shown in green. Non-parametric Wilcoxon rank sum test, $*P_{adjusted} < 0.05$.

3.6 Alpha, beta, and delta express unique calcium-regulated genes

Next, I carried out the same pairwise conditional comparisons in delta cells. Delta cells had less calcium-regulated genes than alpha or beta cells, with 67 calcium-regulated genes and 95 glucose-regulated genes detected. Of these, 34 calcium-regulated genes were unique to delta cells, including *C4orf48, KLF10, NPHP4,* and *TMEM51* (Fig. 3.8a-b). Likewise, 44 out of the 95 glucose-regulated genes were unique to delta cells (Fig. 3.8c). From comparing all calcium-regulated genes in alpha, beta, and delta cells, I found 17 genes that were calcium-regulated in all three cell types. One of these was *IAPP*, even though it is thought to be specific to adult beta cells (Fig. 3.8b). Similarly, *INS* was surprisingly calcium-regulated in delta cells and alpha cells, but not to any significant degree in beta cells. Comparison of glucose-regulated genes across the three cell types also showed that *IAPP* was one of the 24 genes that are commonly glucose-regulated. Again, not all calcium-regulated genes are glucose-regulated, but genes such as *CPE, HSPB1, IER3, SIK2,* and *SIK3* were calcium-regulated and glucose-regulated in alpha, beta, and delta cells (Fig. 3.8c). The majority of genes were specific to a cell type, showing that adult human islet cell types have their own unique calcium-regulated transcriptional response.

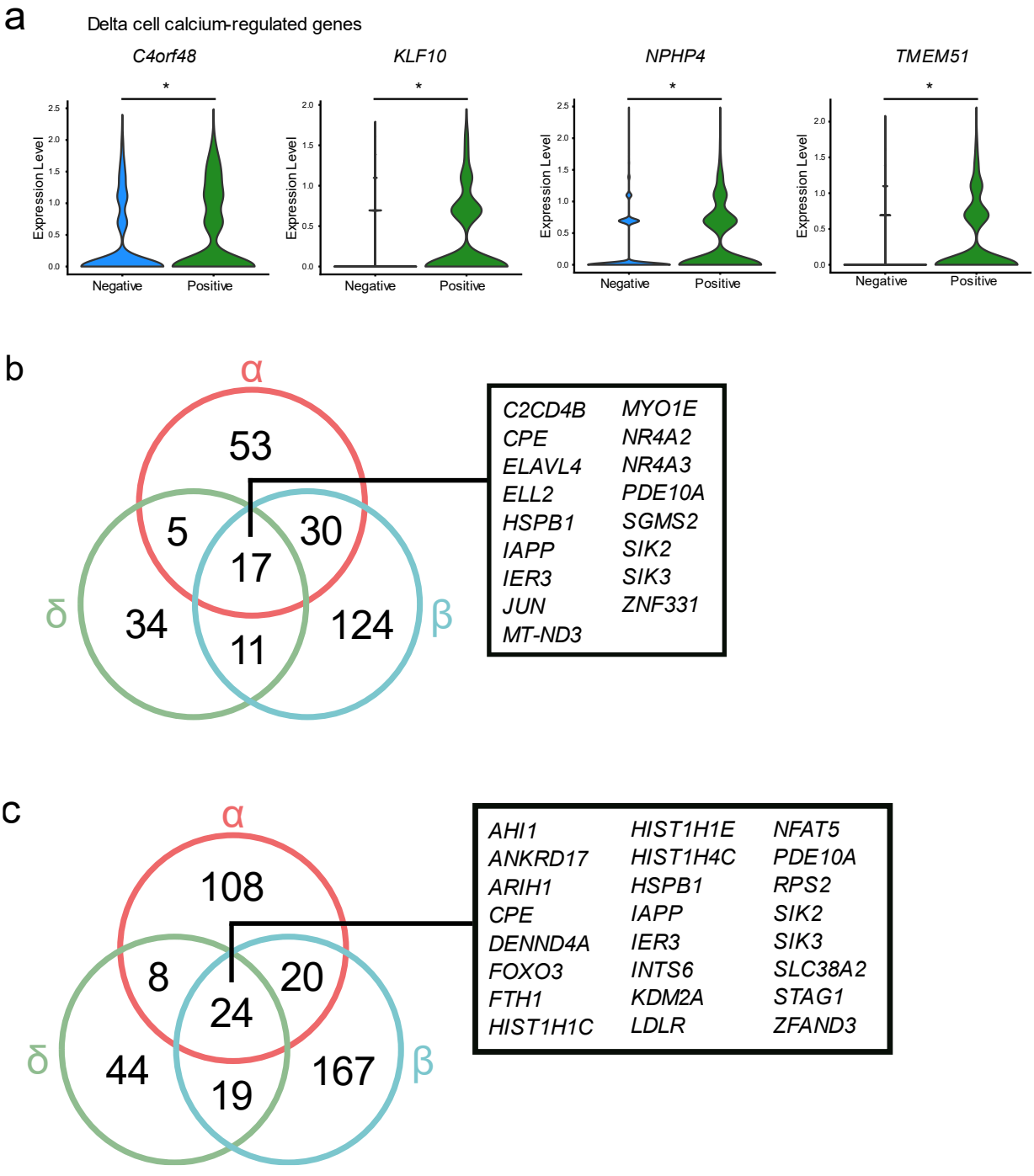

Figure 3.8 | calcium-regulated genes in alpha, beta, and delta cells. a, Violin plots showing the expression of representative calcium-regulated genes unique to delta cells across the Positive (green) and Negative (blue) conditions. Non-parametric Wilcoxon rank sum test, *$P_{adjusted} < 0.05$. **b-c,** Venn diagrams showing the number of common and unique calcium-regulated genes (b) and glucose-regulated genes (c) between alpha, beta, and delta cells. The identities of genes that are calcium-regulated (b) or glucose-regulated (c) in all three cell types are shown in the black boxes.

3.7 Polyhormonal cells in the adult human islet have a unique gene expression profile compared to alpha and beta cells

As mentioned previously in 3.2 and 3.3, one cluster in the dataset co-expressed *INS*, *GCG*, and to a lesser degree, *SST* as well (Fig. 3.2e, 3.4b). Comparing *INS*, *GCG*, and *SST* levels across all endocrine cell types shows that polyhormonal cells express lower levels of all three genes compared to alpha, beta, and delta cells, but the proportion of cells expressing *INS*, *GCG*, and *SST* is almost 100% (Fig 3.9a). This suggests that the polyhormonal cluster is not composed of distinct groups of *INS*-expressing cells and *GCG*-expressing cells, but true polyhormonal cells expressing multiple combinations of these hormone-encoding genes. I do not believe these are scRNA-seq artifacts composed of multiplets (multiple cells encased in a single droplet and barcoded as one cell), for the following reasons: First, comparing the number of genes and transcripts per cell across all endocrine cells in our dataset shows that polyhormonal cells do not express significantly higher (doubled or tripled) numbers of genes and/or transcripts, which would be likely for a multiplet. Second, levels of housekeeping genes such as *RPLP0* are comparable between polyhormonal cells and other endocrine cells (Fig. 3.9b). Third, polyhormonal cells have their own unique set of calcium-regulated and glucose-regulated genes that are not detected in cross-conditional comparisons in other cell types (Fig. 3.9c). Most importantly, I detected islet cells that expressed both *INS* and *GCG* mRNA using RNAscope fluorescent *in situ* hybridization (FISH) in sections of both *ex vivo* isolated human islets and human pancreas biopsies from multiple male donors, including the donors whose islets were used for the scRNA-seq libraries (Fig. 3.9d-e). Overall, I am confident that polyhormonal cells are a real population within the adult human islet, distinct from alpha or beta cells that make up the majority of endocrine cells.

To investigate whether polyhormonal cells could be an immature endocrine cell population, I compared the average expression of known markers of mature alpha or beta cells between polyhormonal cells, alpha cell clusters, and beta cell clusters. Compared to alpha cell clusters α1-α5, polyhormonal cells express lower levels of alpha cell markers such as *GCG, TTR,* and *IRX2,* but similar levels of *ALDH1A1, CRYBA2, TM4SF4,* and *LOXL4* as α1 or α4 (Fig. 3.5c). Compared to beta cell clusters, polyhormonal cells expressed similar levels of *INS* as β2, β3, or β7, but lower levels of almost all other mature beta cell markers such as *IAPP*, *MAFA,* and *ERO1B* (Fig. 3.5d). These results show that compared to mature alpha or beta cells, polyhormonal cells are immature at the transcriptional level, but it's uncertain whether this means that polyhormonal cells are precursors to either of these cell types.

Given the age of the sequenced donors, I thought polyhormonal cells were potentially senescent cells[347–349]. I compared the average expression of previously identified senescence markers *IGF1R, CDKN2A,* and *SERPINE2* across alpha, beta and polyhormonal clusters. None of the three senescence markers showed an elevation in the polyhormonal cells compared to alpha or beta clusters at the mRNA level (Fig 3.10a-b). Within beta cells, only less than 25% of cells in any cluster even expressed *CDKN2A* and *SERPINE2,* but most clusters except β4 and β6 expressed *IGF1R* (Fig 3.10a). Within alpha cells, less than 50% of α1-α4 clusters expressed *CDKN2A* and *SERPINE2,* while polyhormonal cells did not (Fig 3.10b). In addition to senescence markers, I found that the beta cell "disallowed" gene *LDHA*[350] was robustly expressed in the polyhormonal cells when compared with beta cells, but not alpha cells (Fig 3.10a-b).

As mentioned above, I determined the calcium- and glucose-regulated genes for the polyhormonal cluster and compared with those in alpha and beta cells. I found 485 calcium-regulated and 1,001 glucose-regulated genes in the polyhormonal cluster, which is several times the number of regulated genes in any other cell type. The majority of these genes were unique to polyhormonal cells when compared with alpha or beta cells (Fig. 3.10c-d). Only 44 out of 453 calcium-induced genes and 29 out of 32 calcium-suppressed genes were also regulated in alpha and beta cells. 39 out of 933 of the glucose-induced genes were also regulated in beta cells, and 61 out of 68 genes that had higher expression in the Low condition (vs Positive) were unique to polyhormonal cells.

From these results, I can conclude that polyhormonal cells are a distinct population in the adult human islet, but the biological role of these cells is yet unknown. They may be less mature than alpha or beta cells at the transcriptional level, but express a large number of unique calcium- and glucose-regulated genes, as well as the beta cell "disallowed" gene *LDHA*.

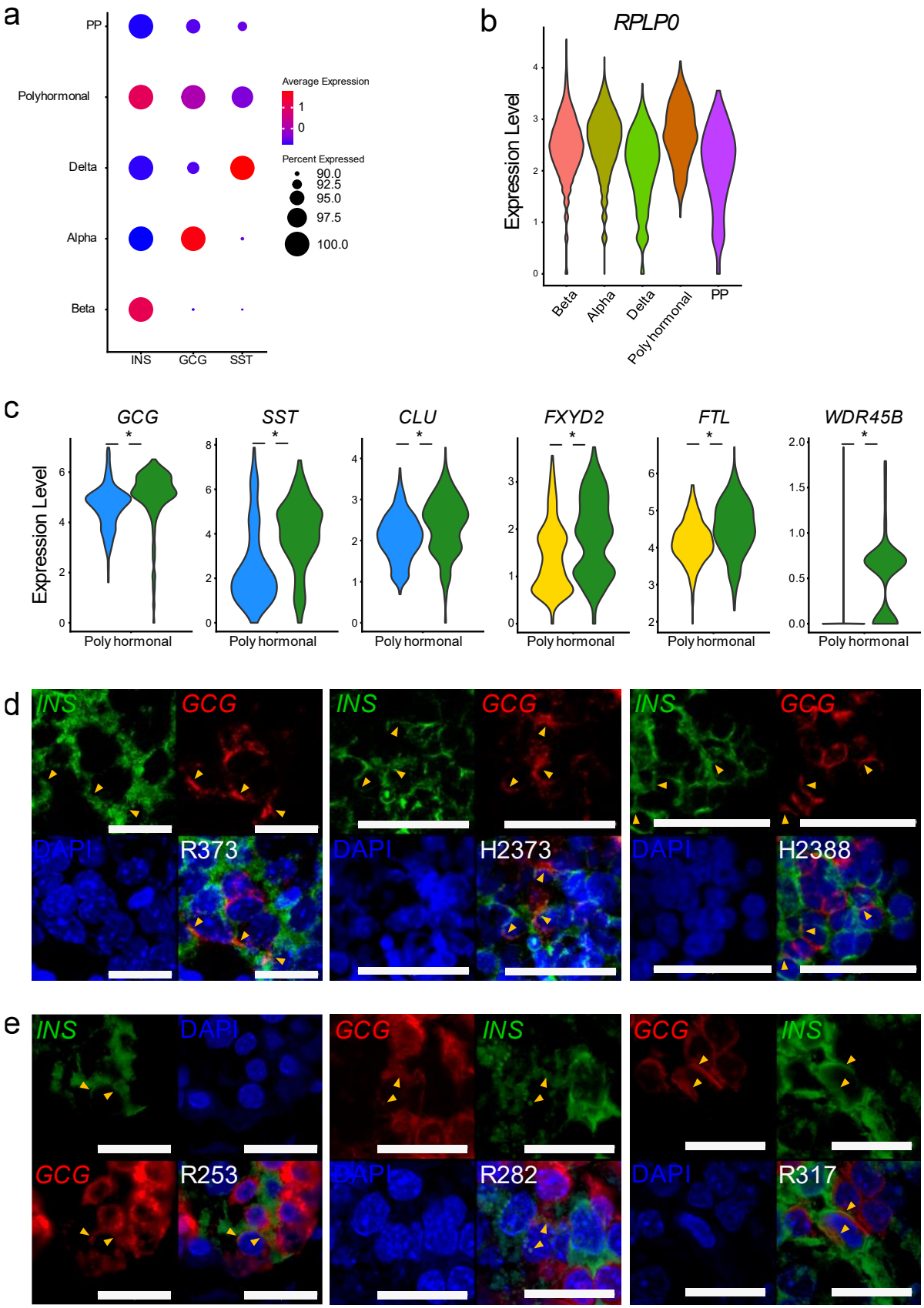
a
PP
Polyhormonal
Delta
Alpha
Beta
INS
GCG
SST
Average Expression
1
0
Percent Expressed
90.0
92.5
95.0
97.5
100.0
b
RPLP0
Expression Level
Beta
Alpha
Delta
Poly hormonal
PP
c
GCG
SST
CLU
FXYD2
FTL
WDR45B
Expression Level
Poly hormonal
d
INS
GCG
DAPI
R373
H2373
H2388
e
INS
DAPI
GCG
R253
R282
R317

Figure 3.9 | Polyhormonal cells expressing *INS, GCG,* and *SST* are detectable in human islets. a, Dot plot showing the expression of *INS, GCG,* and *SST* genes in polyhormonal cells and all other endocrine cell types. The proportion of cells in each cluster expressing a gene is represented by the size of the dot, and higher expression of a gene is shown from blue (low) to red (high). **b,** Violin plot showing the expression of housekeeping gene *RPLP0* is similar between polyhormonal cells and other endocrine cell types. **c,** Violin plots showing representative calcium-regulated genes and glucose-regulated genes unique to the polyhormonal cells across the Positive (green), Negative (blue), and Low (yellow) conditions. Non-parametric Wilcoxon rank sum test, $*P_{adjusted} < 0.05$. **d-e,** Representative RNAscope images of *INS* (green) and *GCG* (red) mRNA with DAPI nuclear stain (blue) in *ex vivo* human islet sections (d) and human pancreas biopsy sections (e). Arrowheads indicate regions of *INS* and *GCG* mRNA co-localization. Donor IDs in white text are shown on the merged image for each section. Scale bars indicate 20um in R373, R253, R282, and R317 islets; 50um in H2373 and H2388 islets.

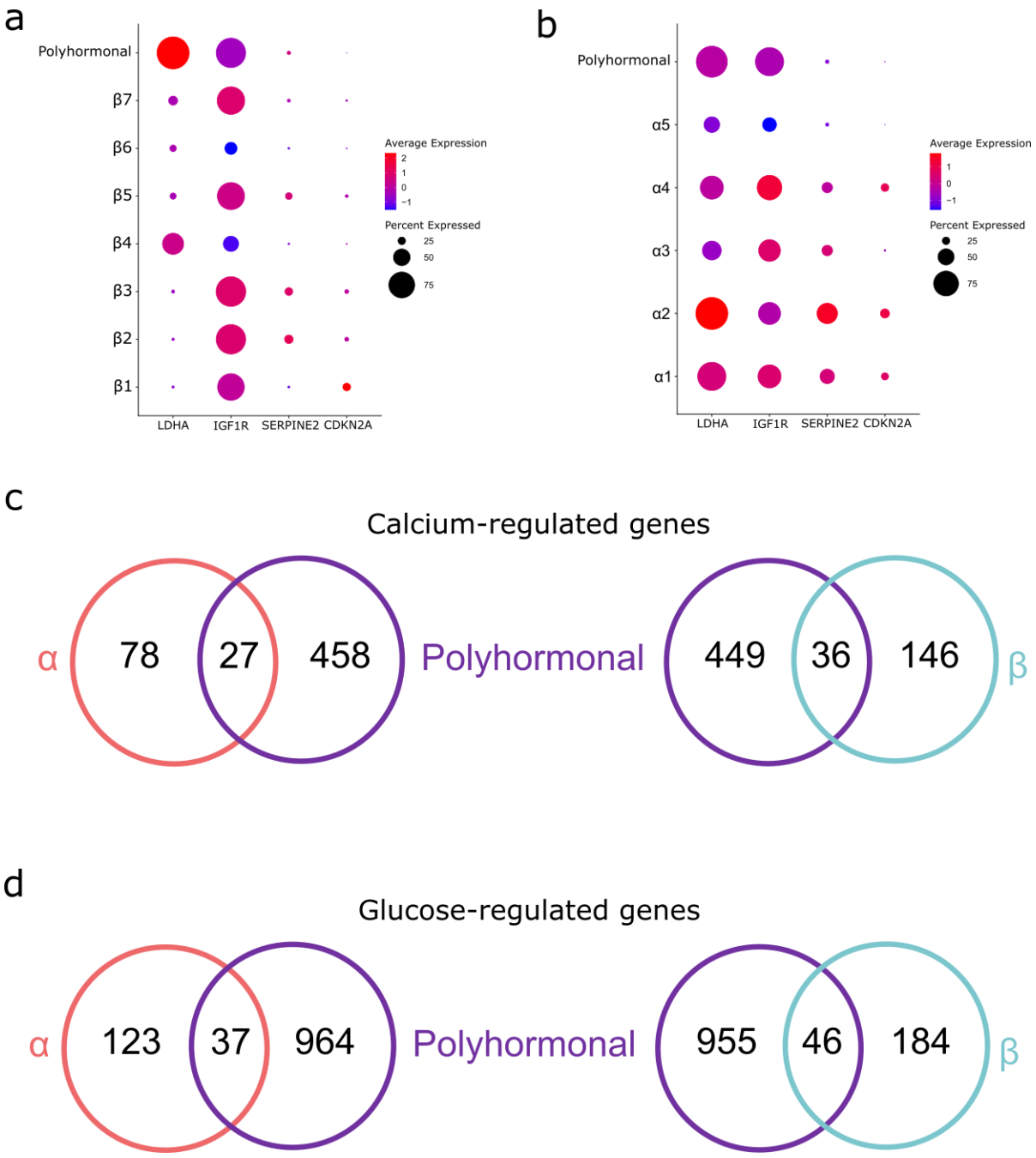

Figure 3.10 | Polyhormonal cells have a unique gene expression profile compared to alpha and beta cells. a-b, Dot plots showing expression of senescence marker genes in polyhormonal cells compared to clusters β1-β7 (c) and clusters α1- α5 (d). The proportion of cells in each cluster expressing a gene is represented by the size of the dot, and higher expression of a gene is shown from blue (low) to red (high). **c-d,** Venn diagrams showing the number of calcium-regulated genes (e) and glucose-regulated genes (f) that are common to polyhormonal cells alpha cells or beta cells.

3.8 PCDH7 is a novel marker of beta cells with enhanced insulin secretion

Given the clearly different magnitudes of response to calcium signalling between beta cell clusters, I reasoned that a method of identifying some of these clusters with higher calcium response could be useful in the future to study different beta cell subtypes. In section 3.5, I showed that β1-β3 clusters expressed the most calcium-regulated genes and activity-regulated genes. I decided to look for cell surface markers that could be used to enrich for this more calcium-responsive population. I found that protocadherin 7 (PCDH7), a transmembrane protein and member of the cadherin superfamily, was expressed in mostly beta cells (Fig 3.11a). Within the beta cell clusters, *PCDH7* expression was particularly enriched in the β1-β3 and β7 clusters, while it was absent in the β4 and β6 clusters (Fig 3.11b). In a previous study, *PCDH7* was noted as one of the many upregulated DEGs in *CD9*-negative beta cells with elevated GSIS, but was not explored further as an independent marker of this elevated function[351]. Therefore, I hypothesised that PCDH7 alone could be a marker of mature beta cells with elevated function.

Based on *PCDH7* expression levels at the transcript level, I divided all beta cells in the dataset into *PCDH7*-high and *PCDH7*-low cells. Out of the 14,949 beta cells, 4,886 (32.7%) cells were classified as *PCDH7*-high. A DEG analysis comparing *PCDH7*-high cells vs *PCDH7*-low cells revealed 311 genes that were enriched in *PCDH7*-high cells. The top 10 DEGs in *PCDH7*-high cells and *PCDH7*-low cells are listed in Table 3.2. The second-most enriched gene in *PCDH7*-high cells was *SPP1,* which was previously detected as highly expressed in the β1 cluster (Fig 3.4d). This supports the finding that *PCDH7* was highly expressed in the β1 cluster, which was one of the most calcium-responsive beta cell clusters. To validate whether *PCDH7*-high cells were functionally different, human islets were sorted using an anti-PCDH7 antibody.

Approximately 20% of PCDH7^{+} cells could be obtained from sorting human islets, which was a similar proportion to the *PCDH7*-high cells found in the scRNA-seq dataset (Fig 3.11c). The sorted PCDH7^{+} and PCDH7^{-} cells were re-aggregated into spheroids, then their function was assessed with secreted C-peptide measurements during a static GSIS. PCDH7^{+} cells showed roughly two-fold higher GSIS stimulation index compared with PCDH7^{-} cells (Fig 3.11d). From measuring transcript levels of beta cell maturity genes with qPCR, we observed no significant differences in *INS, ERO1B, NKX6-1,* or *SLC30A8,* suggesting that the differences in GSIS was not due to PCDH7^{+} cells expressing more insulin or any differences in maturity state (Fig 3.11e). To further support PCDH7 being used as a detectable marker of a beta cell subtype, immunostaining of human islets showed that PCDH7 was present on the membrane of some INS-positive beta cells, but was absent in GCG-positive alpha cells (Fig 3.11f). While it is unknown whether PCDH7 is mechanistically involved in the enhanced function, PCDH7 can serve as a marker of beta cells with enhanced function, due to being optimally located on the cell surface, specifically in beta cells. In conclusion, correlating calcium-regulated gene expression to function in islet cells is a novel method of identifying cells with functional heterogeneity using scRNA-seq data.

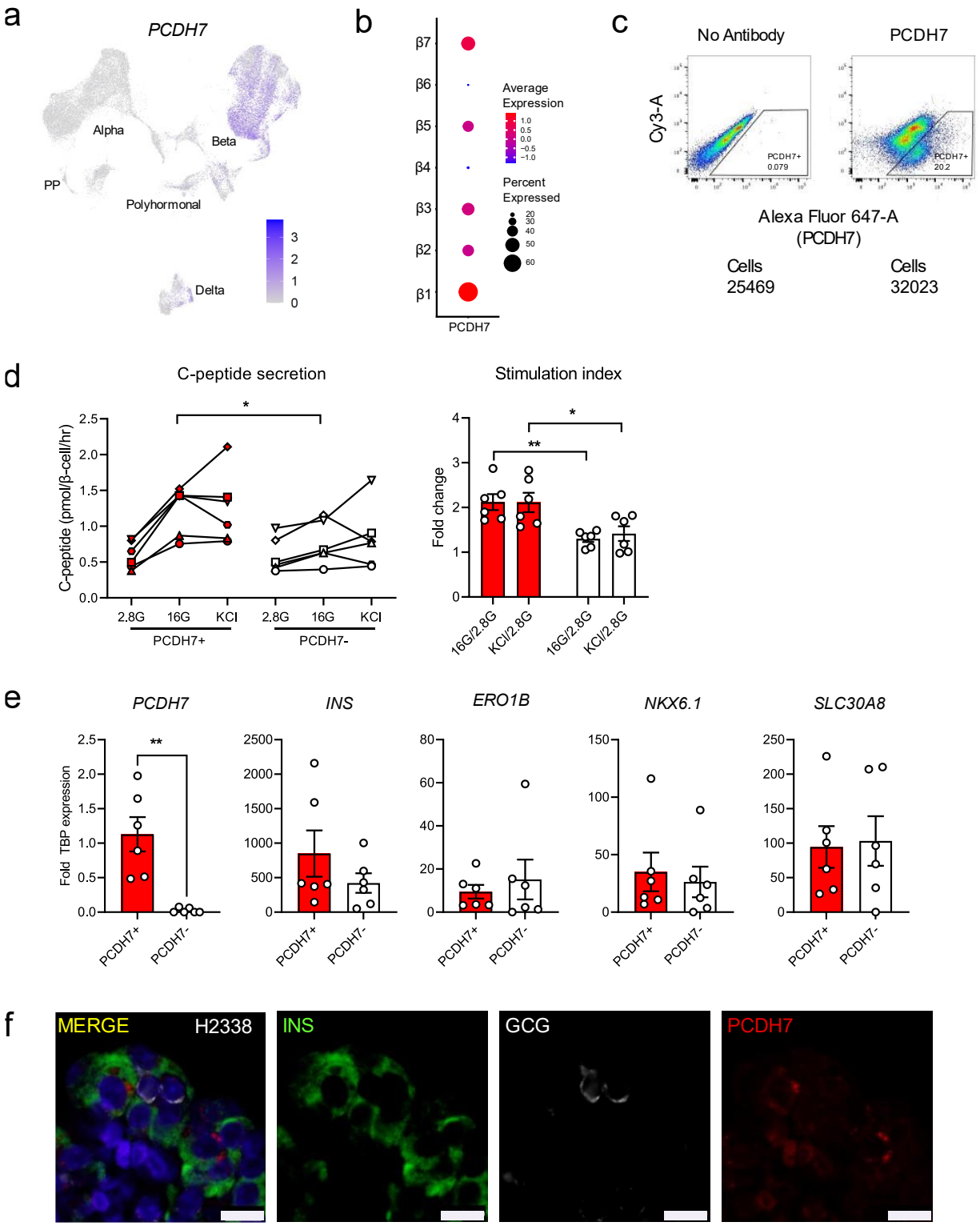

Figure 3.11 | PCDH7 is a marker of beta cells with enhanced glucose-stimulated insulin secretion. a, UMAP plot of *PCDH7* expression in endocrine cells, with higher expression shown as darker shades of blue. **b,** Dot plot showing *PCDH7* expression across beta cell clusters. The proportion of cells in each cluster expressing a gene is represented by the size of the dot, and

higher expression of a gene is shown from blue (low) to red (high). **c,** Sorting protocol used to isolate PCDH7+ beta cells from human islets. **d,** C-peptide concentrations from a static GSIS assay performed on reaggregated PCDH7+ and PCDH7− beta cells from donors R366, R367, R369, H2330, H2337 and H2338, with each donor shown as one symbol. Cells were exposed to 2.8mM glucose (2.8G), 16mM glucose (16G), and 2.8mM glucose with 40mM KCl (KCl). **e,** qPCR results for key beta cell maturity genes in PCDH7+ and PCDH7− sorted cells, with each donor shown as one circle. **f,** Representative image of an islet section from donor H2338, immunostained for INS (green), PCDH7 (red), GCG (white), and DAPI (blue) in a representative islet section of donor H2338. Scale bar =10μm. Student's t-test: *P < 0.05 and **P < 0.01.

Table 3.2 Top 10 DEGs in PCDH7-high vs PCDH7-low beta cells

Population	Gene	Average Log_2 fold change	Adjusted P-value
PCDH7-high	PCDH7	2.370570919	1.68E-298
PCDH7-high	SPP1	1.18475072	4.16E-88
PCDH7-high	LSAMP	0.97634637	3.66E-263
PCDH7-high	CNTN5	0.87173131	1.39E-249
PCDH7-high	KIRREL3	0.840837163	3.22E-242
PCDH7-high	SEMA6D	0.788115299	3.81E-242
PCDH7-high	LINC01099	0.767186614	5.56E-189
PCDH7-high	DGKB	0.75559034	5.79E-123
PCDH7-high	GRIA4	0.752331092	2.51E-236
PCDH7-low	SST	2.066242627	2.83E-155
PCDH7-low	PPY	1.200653208	8.76E-10
PCDH7-low	FXYD2	0.964483007	7.94E-235
PCDH7-low	RPL31	0.863230315	8.16E-198
PCDH7-low	RBP4	0.827754849	1.59E-184
PCDH7-low	RPL21	0.7684447	2.07E-183
PCDH7-low	GCG	0.74200527	1.58E-206
PCDH7-low	RPL34	0.728562169	4.34E-174
PCDH7-low	RPS27	0.721142464	5.54E-209
PCDH7-low	DEPP1	0.709479779	2.29E-67

3.9 Discussion

The primary goal of this scRNA-seq experiment was to identify calcium-regulated genes in adult alpha, beta, and delta cells. I also showed distinct clusters of polyhormonal cells that express their own unique calcium-regulated profile, and histologically validated these cells in human islets. Finally, I found that a proportion of beta cells with the most calcium-regulated genes is marked by *PCDH7*, and these cells have greater GSIS, establishing *PCDH7* as a novel marker of

beta cells with enhanced function. Overall, analysis of this multi-conditional human islet dataset demonstrates that the differences in calcium-regulated genes are associated with islet cell function and maturity.

A limitation of this study is the low number of donors I used to generate the single-cell dataset. I specifically used islets from healthy male donors and tried to match donor biometrics (e.g. age, BMI, sex) as much as possible to reduce biological variation within the data. However, this did limit the total number of islet preps I could include in the experiment, since even obtaining three matched donors' islets spanned over a year. Even with the matched donors, there were poorly integrated clusters that had to be removed after subsetting and reclustering the endocrine cells. Clusters that were removed all had drastically different proportions of cells from each donor compared to the total proportions of cells from each donor across the entire dataset. For example, less than 10% of cells in certain clusters were composed of cells from a single donor, but the entire dataset was composed of 17% R253 cells, 35% R282 cells, and 46% R317 cells. The removal of poorly integrated clusters ensured that the identification of calcium-regulated genes was a good representation of all biological replicates, and the identity of the genes were not disproportionately affected by a single donor.

One unexpected finding was the regulation of *INS* expression in non-beta cell populations. *INS* was detected as a calcium-regulated gene in two out of five alpha cell clusters and in delta cells, albeit at lower levels overall compared with beta cell clusters. One possibility is that the non-physiological stimulatory conditions could have led to abnormal expression and regulation of *INS* in alpha and delta cells. While alpha cells can respond to high glucose, their activation and

glucagon secretion would normally be inhibited in a hyperglycaemic environment due to paracrine signalling from beta cells and delta cells[352,196,353,354]. However, I exposed the islets to high glucose and directly depolarised all populations, which would not occur in physiological conditions but might occur in pathophysiological conditions like diabetes. It is possible that under these conditions, non-beta cells can express a low level of *INS*. Whether this is translated to the protein level is unknown.

While the goal was not to specifically study rare cell populations, I found cells that expressed *INS*, *GCG*, and *SST*. I am not the first to detect so-called "polyhormonal" cells, as others have found islet cells that express two or even three characteristic endocrine genes[328,329,334,330,355]. I did not observe any progenitor gene expression, so it is unlikely that this resulted from dedifferentiation of mature cells. In previous studies, there have been very few polyhormonal cells relative to the overall dataset. Within my dataset, I observed a distinct cluster of polyhormonal cells that clustered away from all other endocrine cell types. While the biological role of these cells within the islet is unknown, polyhormonal cells express large, unique sets of hundreds of calcium-regulated genes. It is possible that polyhormonal cells could be immature cells that have a hyperactive transcriptional response to calcium. In the future, it would be ideal to identify a marker specific for this population to isolate the cells directly from human islets for closer study. This could be difficult without a large supply of human islets, because polyhormonal cells make up less than 4% of all endocrine cells, according to the scRNA-seq. At the histological level, they seemed even more difficult to locate, and were not present in every islet section.

When I did attempt to find any rare beta cells that were previously established, such as virgin beta cells, hub beta cells and senescent beta cells[345,347,356,357], there was no single cluster that perfectly aligned with published gene expression profiles of these rare populations. While I did find the clusters β4 and β6 had lower expression of many key beta cell genes, these clusters had the highest expression levels of *INS* (Fig 3.5e). Even in alpha cells, α5 had reduced expression of alpha cell marker genes and the lowest number of calcium-regulated genes, but had the highest levels of *GCG* expression (Fig 3.5d). This could indicate a trade-off between expression of hormone-encoding genes and responsiveness to calcium.

In this chapter, I defined responsiveness to calcium by the number of calcium-regulated genes in each cluster or cell type. By this definition, the polyhormonal cells that were potentially less mature than alpha, beta, or delta cells were the most calcium-responsive. True functional characterization of these cells after isolation would help support this claim, by either conducting electrophysiological measurements or visualizing calcium oscillations with fluorescent calcium indicators in response to stimuli. While mRNA expression only provides one view of the complex biology within the islet, I hope that I have provided evidence in this chapter that shows value in using transcriptomic approaches in studying the islet cell types and their responses to calcium signalling.

Chapter 4: Characterization of the immediate early gene *Npas4* induction in AgRP and POMC neurons in response to peripheral stimuli

4.1 Rationale

The bHLH-PAS domain protein NPAS4 is an IEG, known to be upregulated specifically in response to calcium signalling in neurons[300]. The bulk of studies on NPAS4 have been in the CNS, focusing on its role in excitatory/inhibitory synaptic balance and neuroprotective roles[300,304,315,358,359]. It was only recently that the first studies of NPAS4 outside of the CNS, were published and extra-neuronal roles of NPAS4 were elucidated[310,319,320]. One of these studies of NPAS4 outside of the CNS highlighted its potential role in the ARC. In HFD-fed conditional NPAS4 KO mice, recombination was observed in both the pancreatic islet and MBH[320], and these mice displayed increased light cycle food intake. Since food intake is heavily regulated by the ARC, it was suspected that NPAS4 had a role in ARC AgRP or POMC neurons.

To date, NPAS4 has not been closely studied in a specific ARC neuronal population, has not been detected in the ARC neurons in many studies, and only has an established role in any other site of the hypothalamus in one study. In the suprachiasmatic nucleus (SCN), NPAS4 was found to have role in regulating light-activated genes important for maintaining circadian rhythm[360]. Since clock proteins that are critical for circadian rhythm are also PAS domain proteins, it seems reasonable that NPAS4 would have a role in regulating SCN neurons. In other areas of the hypothalamus, NPAS4 has not been studied in a metabolic context. Even *Npas4* expression within the hypothalamic regions are sparse. One previous study used *in situ* hybridization to detect *Npas4* expression in various regions of the adult mouse brain, and found faint traces of *Npas4* in the PVN and ARC[305]. Given the nature of NPAS4 as an IEG with low basal expression

levels, it is possible that previous studies that did not specifically activate the cells of interest could have missed or underestimated NPAS4 expression.

In order to study the potential role of NPAS4 in regulating food intake, it is important to consider which inducers would be useful for effective NPAS4 induction and detection in the ARC. Since it is currently unknown which cell types in the ARC express NPAS4, AgRP and POMC neurons were hypothesized as the most likely candidates, due to their well-characterized roles in regulating food intake. The studies in this chapter will determine whether *Npas4* mRNA is expressed in ARC AgRP and POMC neurons and explore potential metabolically relevant inducers of *Npas4*.

4.2 *Npas4* expression in the ARC neurons can be detected with RNAscope

In order to detect and quantify *Npas4* expression in the ARC neurons, I used the RNAscope FISH technology that was used in Chapter 3 to detect *INS* and *GCG* mRNA in human islets. First, I tested the probe for *Npas4* mRNA for specificity and general expression levels, and optimized the protocol to be suitable for fixed frozen adult mouse brain sections. To determine whether the *Npas4* probe was specific and robust, I sectioned brains from NPAS4$^{-/-}$ mice and littermate NPAS4$^{+/+}$ mice and compared detectable *Npas4* mRNA signals in two regions: the hippocampus, which is known as a site of high *Npas4* mRNA expression, and the ARC, where *Npas4* expression levels were less characterized. In the hippocampus CA3 region of NPAS4$^{+/+}$ mice, *Npas4* expression was clearly visible as collections of bright puncta in and around the nucleus of cells (Fig 4.1a). In stark contrast, NPAS4$^{-/-}$ mice showed no *Npas4* expression at all. Each experiment of RNAscope is run with technical positive control sections and probes to ensure the confirmation of a successful probe hybridization and amplification, which show that

the lack of *Npas4* expression seen in NPAS4$^{-/-}$ mice is not due to the technical failure of the experiment.

In the ARC, the sections were also probed with *Pomc* to mark the ARC region, since POMC neurons are located in a diffuse pattern that spans the entire ARC. *Npas4* expression in the ARC was clearly visible as individual puncta across *Pomc*+ neurons, and *Pomc*- cell in the region as well (Fig 4.1b). Again, the *Npas4* expression in NPAS4$^{-/-}$ mice was undetectable, but the *Pomc* expression remained intact (Fig 4.1b). Next, *Npas4* expression was measured in the ARC of *ad libitum* fed B6 male mice to determine whether AgRP and POMC neurons express *Npas4* under unstimulated conditions. Using the same RNAscope approach, *Npas4* expression was readily detectable in *Agrp*+ cells, located in close proximity to either side of the 3rd ventricle (Fig 4.2a). *Npas4* expression was also detectable in *Pomc*+ cells, which subjectively appeared to have more *Npas4* puncta per cell than *Agrp*+ cells (Fig 4.2b). Overall, there were less cells in the ARC that have visibly dense clusters of *Npas4* puncta, which suggest the basal level of *Npas4* expression per cell is higher in the hippocampus than in the ARC. Nevertheless, these results show that RNAscope technology is able to detect *Npas4* expression in the CNS under unstimulated conditions.

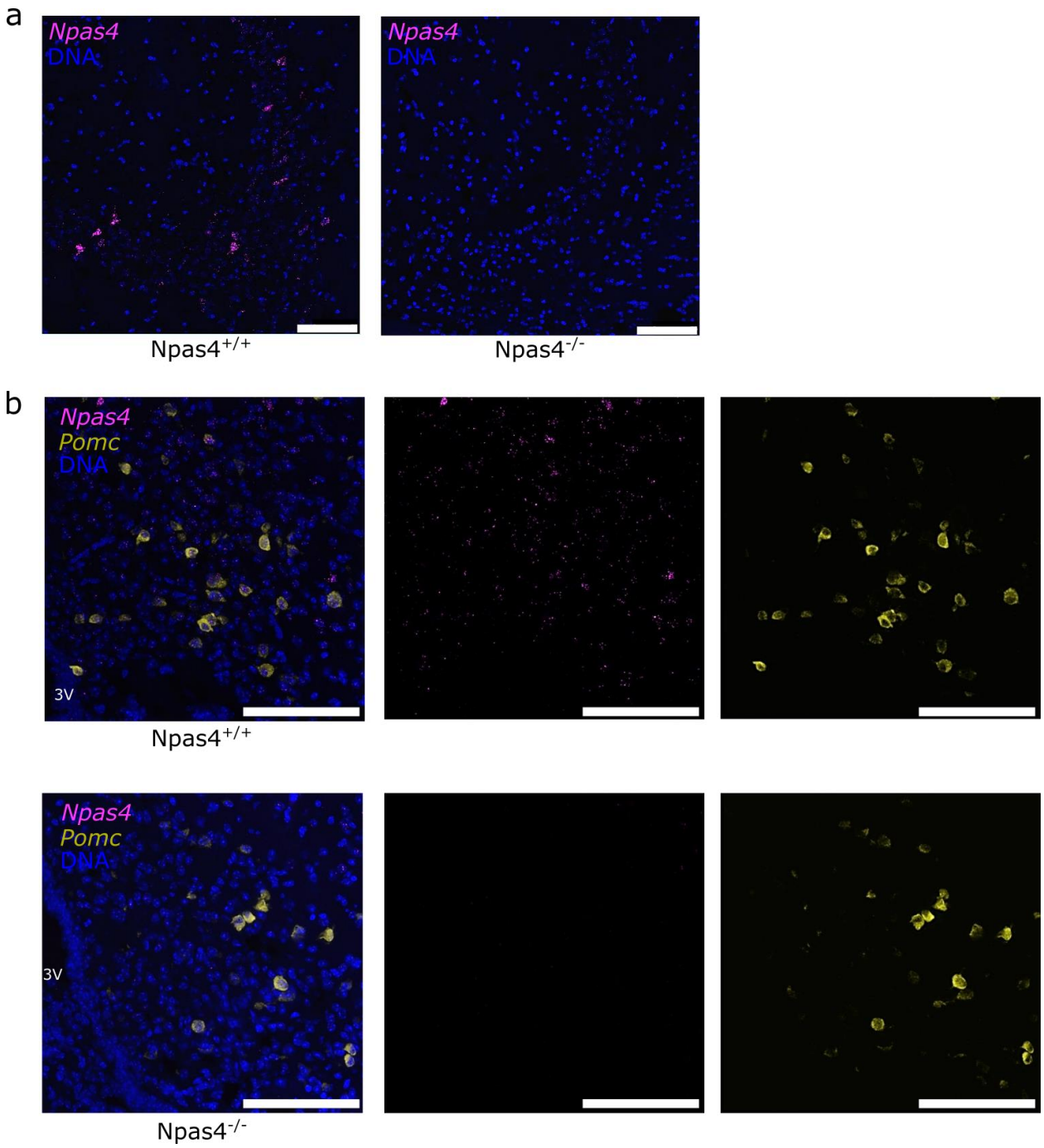

Figure 4.1 | *Npas4* expression is detectable with RNAscope in the hippocampus and arcuate nucleus. a-b, Representative RNAscope images of sectioned fixed frozen NPAS4$^{+/+}$ and NPAS4$^{-/-}$ mouse hippocampus CA3 regions (a) and hypothalamic arcuate nucleus (b), probed for *Npas4* expression (magenta), *Pomc* expression to specifically mark the arcuate nucleus (yellow), and DAPI nuclear stain (DNA; blue). 3V = 3rd ventricle. Scale bars = 100μm.

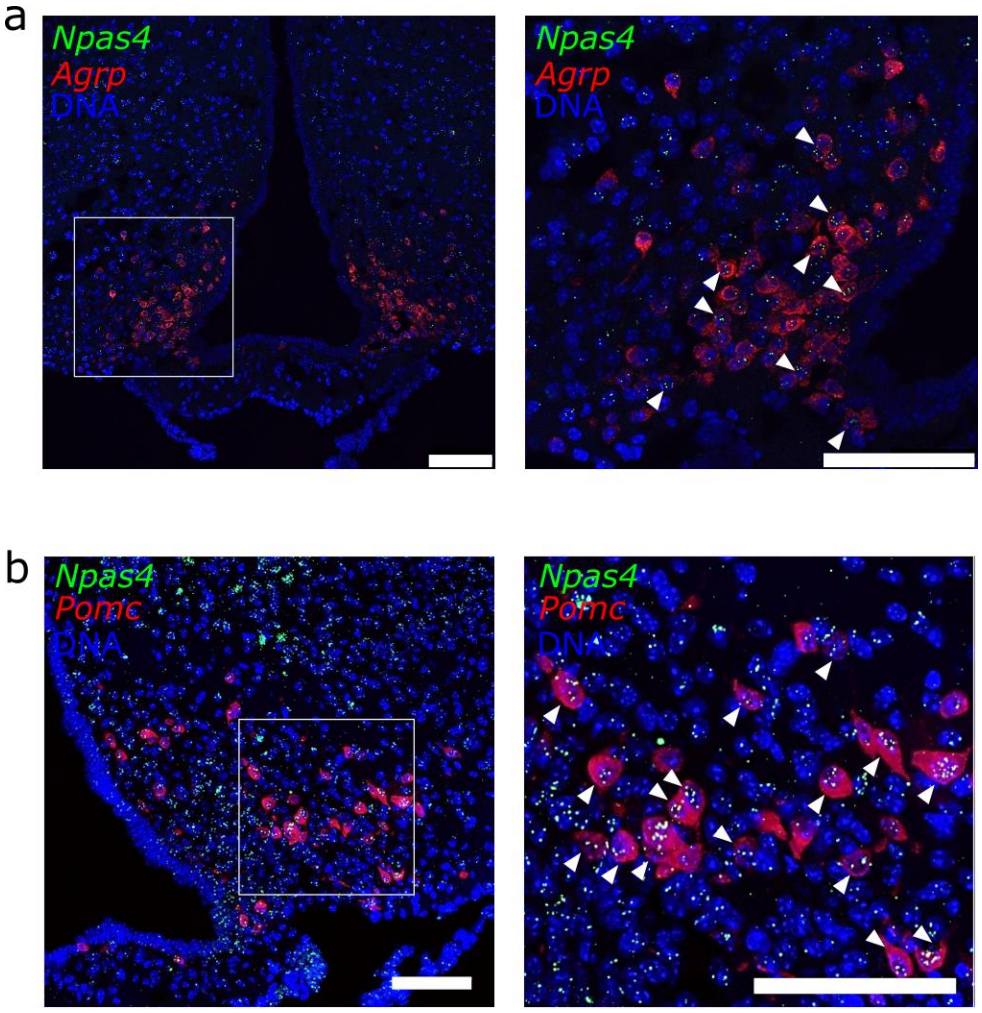

Figure 4.2 | *Npas4* is expressed in AgRP and POMC neurons of the arcuate nucleus. a-b, Representative RNAscope images of wild-type B6 mouse arcuate nucleus regions, probed for *Npas4* (green), *Agrp* (red; a) or *Pomc* (red; b), with DAPI nuclear stain (DNA; blue). White boxes on the left panels highlight the magnified region shown in the right panels (a-b). White arrowheads indicate cells with both red and green signals. Scale bars = 100μm.

4.3 Refeeding after an overnight fast induces *Npas4* in POMC neurons, but not in AgRP neurons

The next objective was to determine whether *Npas4* expression could be induced in AgRP and POMC neurons in the ARC. It is known that *Npas4* expression is induced in an activity-dependent manner in neurons, and AgRP and POMC neurons are known to be activated in fasted and fed states, respectively. Therefore, brains were harvested from adult male B6 mice after an overnight fast of 10-12 hours, or after a 1 hour refeeding period following the overnight fast (Fig 4.3a). Using the validated RNAscope approach, *Npas4* expression was quantified specifically in cells that expressed *Agrp* or *Pomc* (Fig 4.3b, e). In the fasted condition, 70-80% of *Agrp*+ cells expressed *Npas4*, and this proportion of *Npas4*+ *Agrp*+ cells did not change with 1 hour of refeeding (Fig 4.3c). When *Npas4* expression levels were quantified as number of puncta per *Agrp*+ cell, there were no differences seen in the proportion of *Npas4*- (no puncta), *Npas4*-low (1-3 puncta/cell), *Npas4*-medium (4-9 puncta/cell), or *Npas4*-high (10 or more puncta/cell) *AgRP*+ cells between the fasted and refed states (Fig 4.3d).

Similar to *Agrp*+ cells, about 70% of *Pomc*+ cells had detectable *Npas4* expression in the overnight fasted state, but this proportion was significantly increased after 1 hour refeeding, in which 80-90% of *Pomc*+ cells were *Npas4*+ (Fig 4.3f). Furthermore, quantifying *Npas4* puncta per *Pomc*+ cell showed significant decreases in the proportions of *Npas4*- and *Npas4*-low populations with corresponding significant increases in the proportions of *Npas4*-medium and *Npas4*-high populations in the 1 hour refed state (Fig 4.3g). In addition, ARC sections from fasted and 1 hour refed mice were immunostained for NPAS4 to determine if refeeding also induced NPAS4 protein in POMC neurons. In order to visualize POMC neurons, POMC-CreER

mice with a STOP-floxed tdTomato in the *Rosa26* locus were used. 1 week before the fasting and refeeding, tdT^+ POMC-CreER mice were given tamoxifen to induce CreER-mediated recombination specifically in POMC neurons, which excised the STOP cassette upstream of the tdTomato and allowed visualization of POMC neurons with red fluorescence. Immunostaining for NPAS4 protein showed a greater number of $tdTomato^+$ POMC neurons with nuclear NPAS4 protein in the 1 hour refed condition compared to the overnight fasted condition (Fig 4.4). These results show that 1 hour of refeeding after an overnight fast is sufficient to induce *Npas4* by activating POMC neurons, but refeeding does not reduce the *Npas4* levels in AgRP neurons.

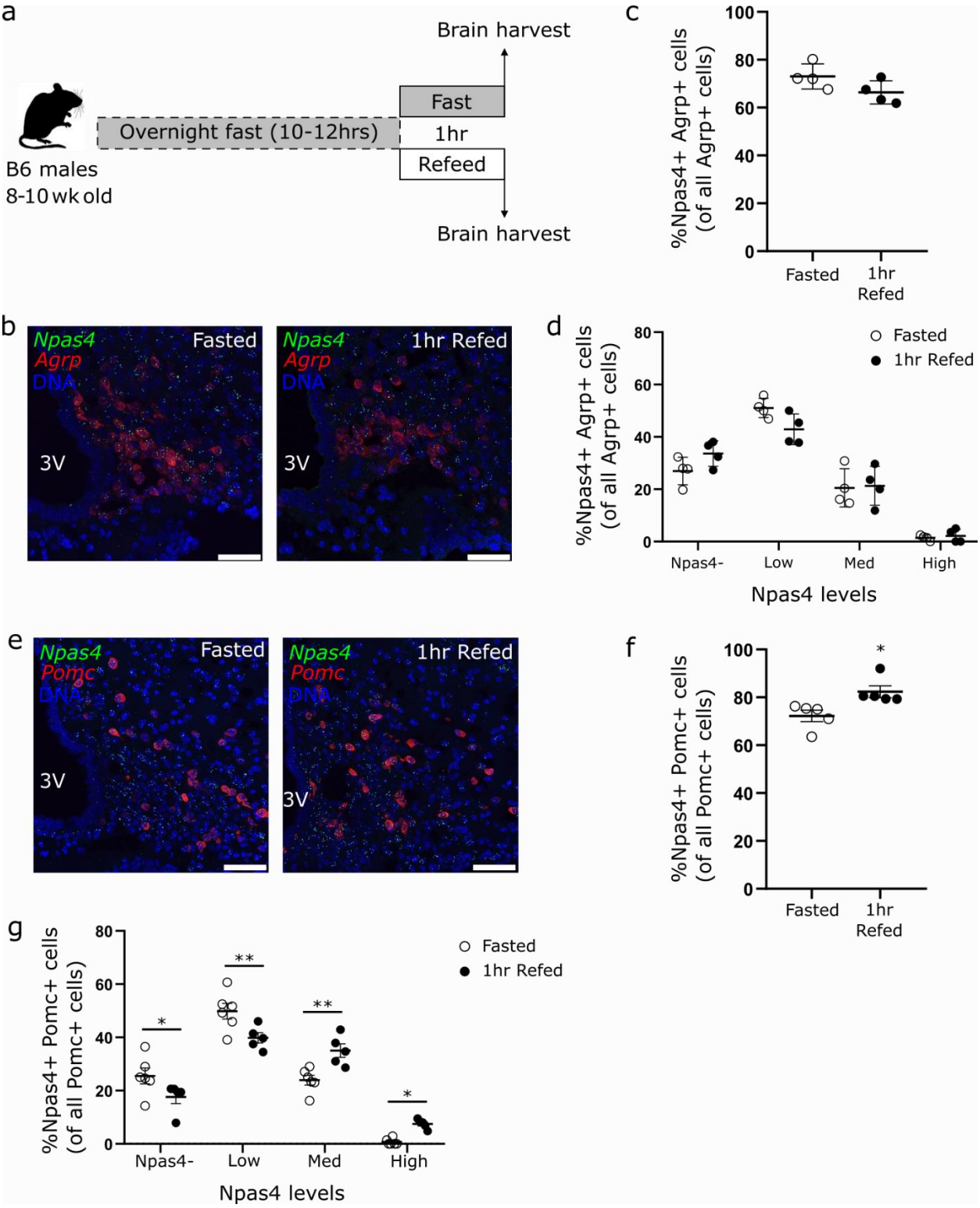

Figure 4.3 | *Npas4* expression in POMC neurons of the arcuate nucleus is induced by refeeding after a fast. a, Schematic of experimental timeline. Wild-type B6 males were fasted overnight for 10-12 hours, then fasted for an additional hour or refed for 1 hour before

euthanasia and brain harvest for histology. **b,** RNAscope images of fasted and 1 hour refed wild-type B6 mouse arcuate nucleus regions, probed for *Npas4* (green), *Agrp* (red), and DAPI nuclear stain (DNA; blue). **c,** Quantifications of *Npas4*-positive, *Agrp*-positive cells as a percentage of total *Agrp*-positive cells from RNAscope images (b), data are mean ± SD. **d,** Breakdown of quantifications (c) into bins of *Npas4* expression levels: Npas4- = no *Npas4* signal in the *Agrp*-positive cell, Low = 1-3 *Npas4* punctae/cell, Med = 4-9 *Npas4* punctae/cell, and High = 10 or more *Npas4* punctae/cell. In each category, the values are expressed as *Npas4*-positive, *Agrp*-positive cells as a percentage of total *Agrp*-positive cells, and data are mean ± SD. **e,** RNAscope images of fasted and 1 hour refed wild-type B6 mouse arcuate nucleus regions, probed for *Npas4* (green), *Pomc* (red), and DAPI nuclear stain (DNA; blue). **f,** Quantifications of *Npas4*-positive, *Pomc*-positive cells as a percentage of total *Pomc*-positive cells from RNAscope images (e). **g,** Breakdown of quantifications (c) into bins of *Npas4* expression levels. Values are expressed as *Npas4*-positive, *Pomc*-positive cells as a percentage of total *Pomc*-positive cells. Scale bars = 50μm. Student's t-test: *P < 0.05, **P < 0.01.

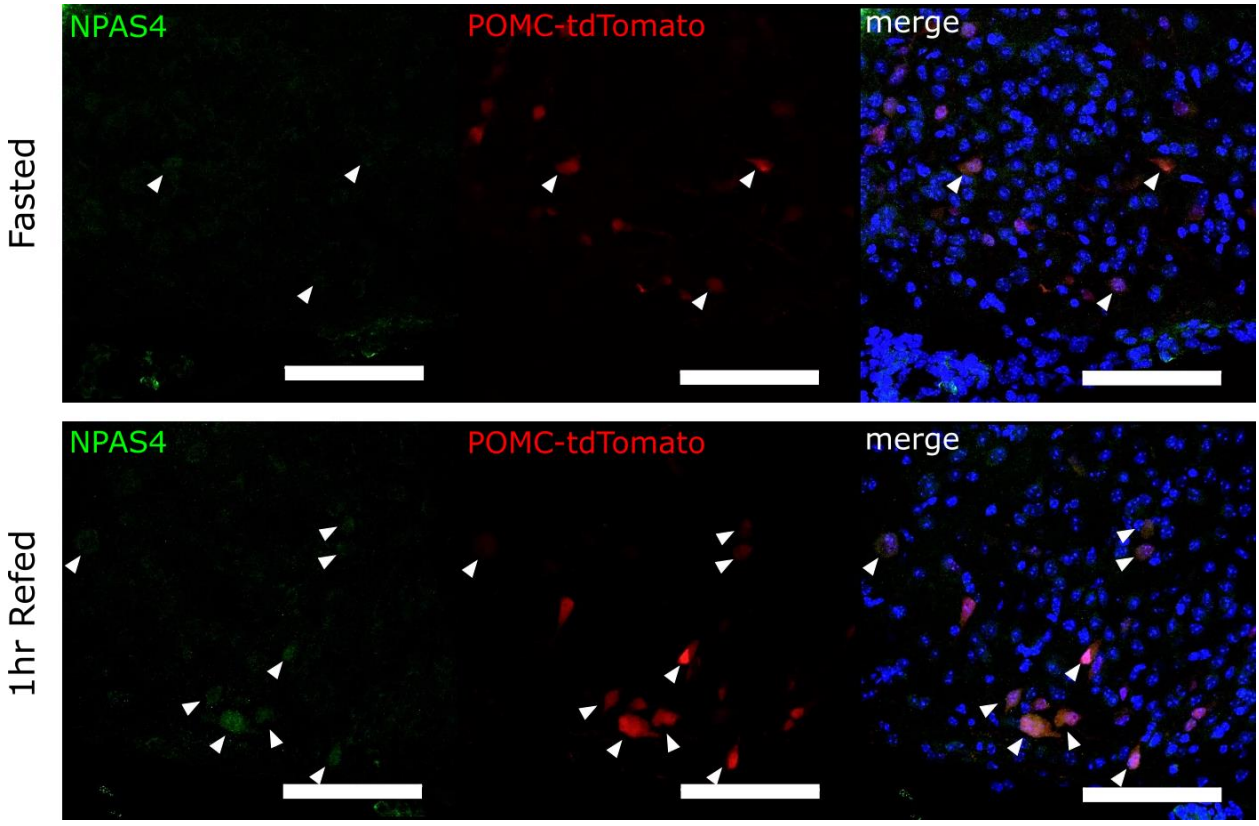

Figure 4.4 | NPAS4 protein is induced in response to refeeding in POMC neurons. Representative immunofluorescent images of ARC sections of overnight fasted POMC-CreER mice with or without a 1 hour refeed, 0 weeks after tamoxifen administration to induce tdTomato expression in POMC neurons. White arrowheads mark cells where co-localization of NPAS4 (green) and tdTomato that marks POMC neurons (red) in regions positive for DAPI (blue).

4.4 Oral glucose induces *Npas4* expression in POMC neurons

In order to further explore additional inducers of *Npas4* in the ARC, several peripheral or systemic options were chosen. While it's known that AgRP neurons are activated in states of general negative energy balance like fasting, POMC neurons are activated by positive energy balance, which can be elevated levels of nutrient or endocrine signals. As *Npas4* induction in POMC neurons was seen after refeeding, additional experimental methods of peripherally inducing or mimicking extreme conditions of positive energy balance were examined. One such method is a simple oral gavage of glucose, which can raise circulating glucose to supraphysiological levels, beyond that of typical postprandial glucose levels in a mouse. As discussed in section 1.8, some POMC neurons are known to be glucose-activated, and the similarities in glucose-coupled activation mechanisms between neurons and pancreatic beta cells supported the use of glucose as a potential POMC activator to induce *Npas4.*

To determine whether oral glucose can induce *Npas4* in POMC neurons, adult B6 mice were fasted overnight for 10-12 hours (similar to an oral glucose tolerance test protocol) and gavaged with 2g/kg of D-glucose (Fig 4.5a). Brains were collected from mice at 0 (fasted, not gavaged), 5, 15, 30, 60, and 180 minutes post-gavage and *Npas4* and *Pomc* expression in the ARC were detected with RNAscope (Fig 4.5b). Quantifications of RNAscope images showed that *Npas4* induction was detectable as early as 5-15 minutes post-gavage (Fig 4.5c). By 3 hours post-gavage, the proportion of *Npas4+ Pomc+* cells were comparable to that in fasted mice. However, quantifying the *Npas4* puncta per cell showed a significant decrease in *Npas4*-low cells and a corresponding increase in *Npas4*-high cells only at 15 minutes post-gavage (Fig 4.5d). These results show that oral glucose can activate POMC neurons and induce *Npas4* in a rapid

manner, with the peak of induction at 15 minutes after administration, which is within the possible time frame of induction of an IEG like *Npas4*.

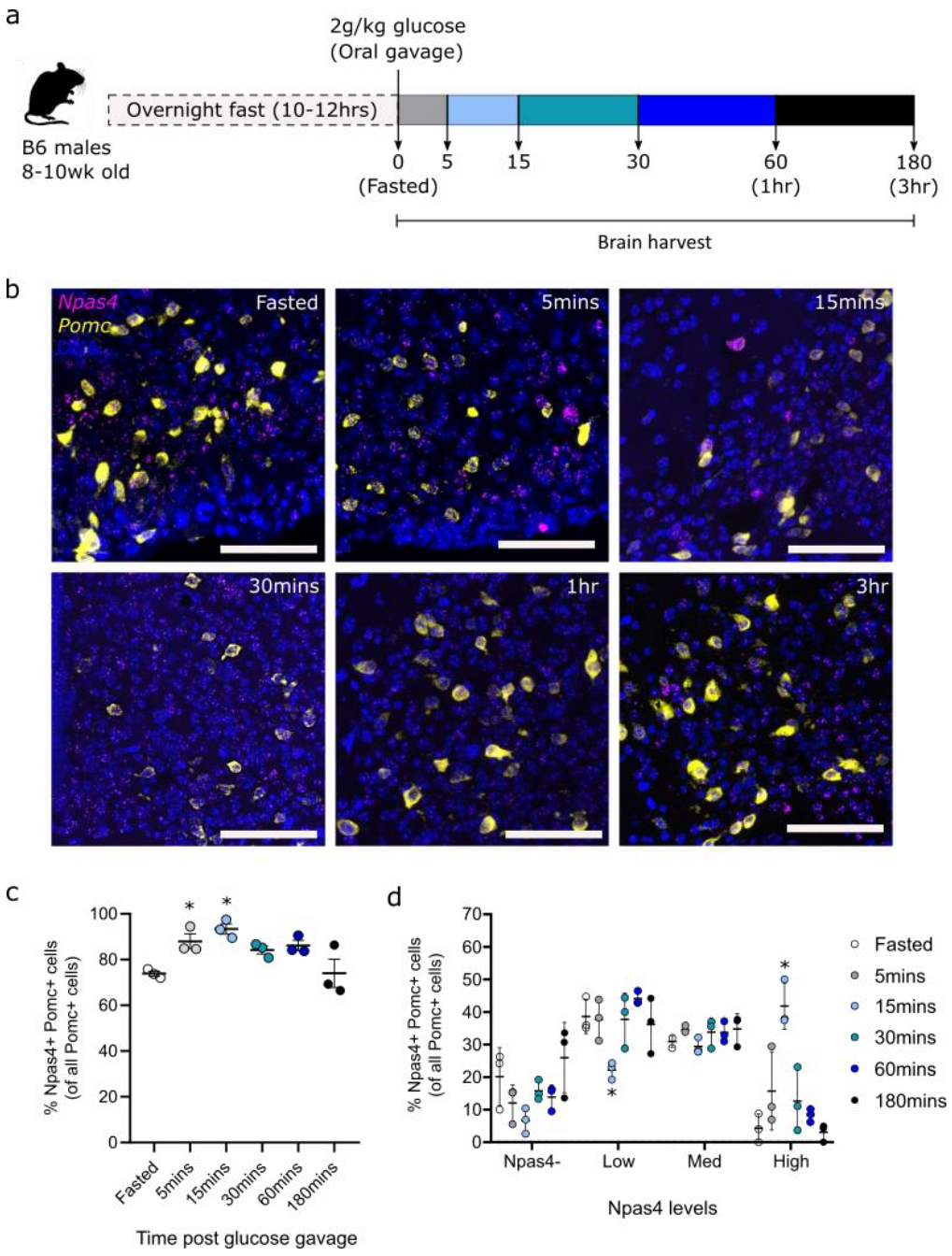

Figure 4.5 | *Npas4* expression in POMC neurons of the arcuate nucleus is induced by orally administered glucose. a, Schematic of experimental timeline. **b,** Representative RNAscope images of mice from each group, showing the arcuate nucleus region probed with *Npas4* (magenta), *Pomc* (yellow), and DAPI nuclear stain (DNA; blue). Scale bars = 50µm. **c,** Quantifications of *Npas4*-positive, *Pomc*-

positive cells as a percentage of total *Pomc*-positive cells from RNAscope images (b), shown as mean ± SD. **d,** Breakdown of quantifications (c) into bins of *Npas4* expression levels: Npas4- = no *Npas4* signal in the *Pomc*-positive cell, Low = 1-3 *Npas4* punctae/cell, Med = 4-9 *Npas4* punctae/cell, and High = 10 or more *Npas4* punctae/cell. Values are expressed as *Npas4*-positive, *Pomc*-positive cells as a percentage of total *Pomc*-positive cells, shown as mean ± SD. One-way ANOVA with Tukey's multiple comparisons: *P < 0.05 vs Fasted.

4.5 Acute administration of insulin does not affect *Npas4* expression in POMC neurons

Following a typical postprandial spike in blood glucose, circulating insulin also increases as pancreatic beta cells sense and respond to the increased blood glucose. During oral glucose tolerance tests in mice, elevated plasma insulin can be detected within the first 10 minutes following the glucose bolus. It is possible that the observed glucose-induced *Npas4* in POMC neurons was due to the increased circulating insulin levels acting on insulin-activated POMC neurons, rather than the direct action of elevated circulating glucose. However, whether POMC neurons are truly activated by insulin is a source of debate, as discussed in section 1.6.

To determine whether insulin can directly induce *Npas4* in POMC neurons, 10 week-old B6 mice were fasted for 2 hours during the light cycle and intraperitoneally injected with 0.75U/kg of insulin or PBS vehicle (Fig 4.6a). Brains from vehicle-injected mice were harvested 10 minutes after injection, and compared with insulin-injected brains harvested at 30 and 60 minutes post-injection. Insulin action was confirmed with blood glucose measurements after fasting, before injections, and before euthanasia at each time point (Fig 4.6b). Quantifications of *Npas4+ Pomc+* cells in the ARC showed that peripheral insulin administration did not affect the proportion of POMC neurons expressing *Npas4* (Fig 4.6c) within 1 hour. This was confirmed by quantifying the number of *Npas4* puncta per *Pomc+* cell, which showed no differences in any populations of *Npas4* expression levels (Fig4.6d). These results showed that peripherally administered insulin does not induce or suppress *Npas4* in POMC neurons within 1 hour.

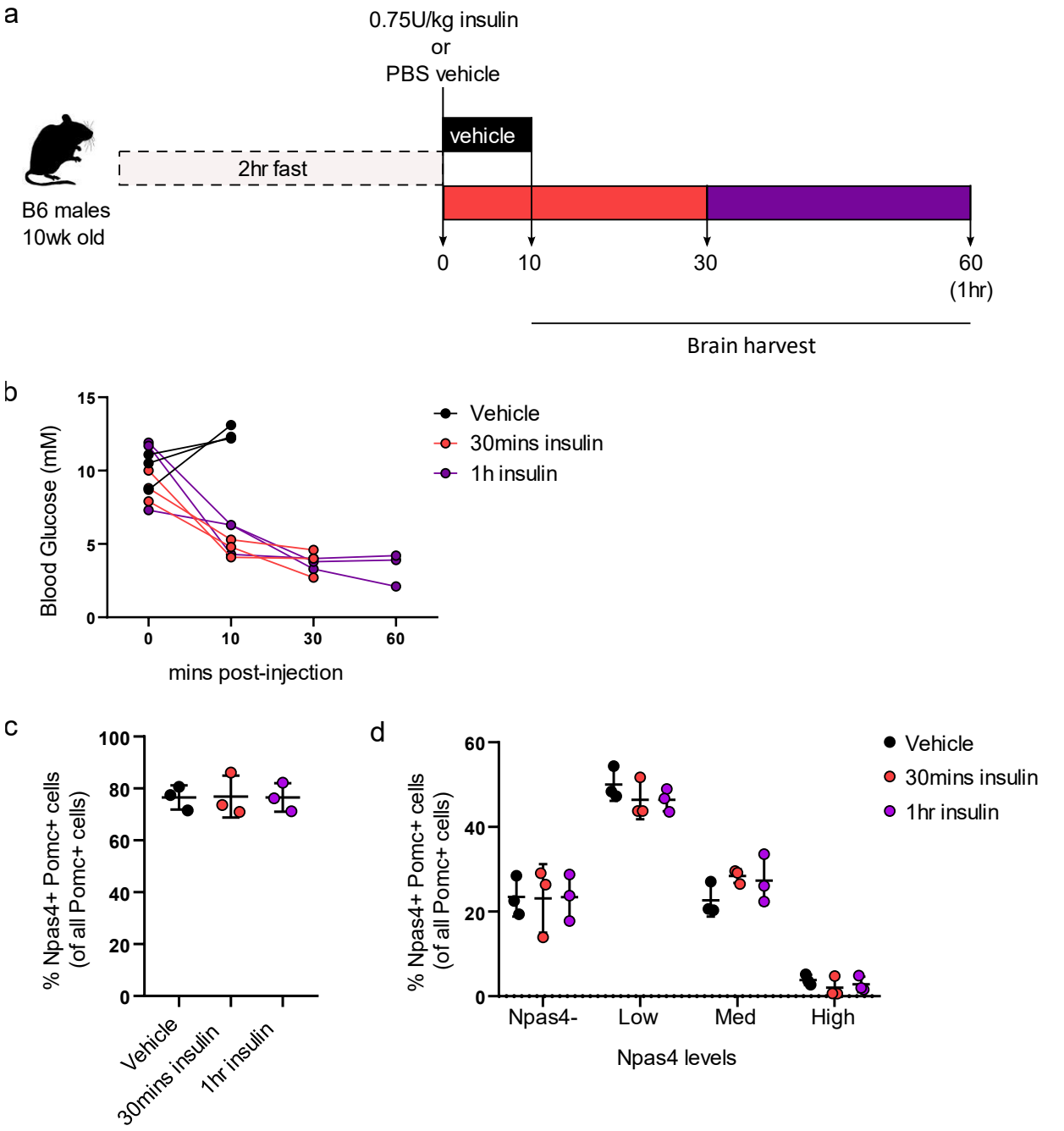

Figure 4.6 | *Npas4* expression in POMC neurons of the arcuate nucleus is not affected by peripherally injected insulin. a, Schematic of experimental timeline. **b,** Blood glucose measurements of mice that underwent the experiment at 0mins, 10mins, 30mins, and 60mins post-injection. Vehicle group mice were euthanized for brain harvest at 10mins post-injection. **c,** Quantifications of *Npas4*-positive, *Pomc*-positive cells as a percentage of total *Pomc*-positive cells from RNAscope images, shown as mean ± SD. **d,** Breakdown of quantifications (c) into bins of *Npas4* expression levels: Npas4- = no *Npas4* signal in the *Pomc*-positive cell, Low = 1-3 *Npas4* punctae/cell, Med = 4-9 *Npas4* punctae/cell, and High = 10 or more *Npas4* punctae/cell. Values are expressed as *Npas4*-positive, *Pomc*-positive cells as a percentage of total *Pomc*-positive cells. Data shown as mean ± SD.

4.6 HFD feeding induces *Npas4* expression in POMC neurons

While it is known that POMC neuronal activity is decreased in rodent models of chronic diet-induced obesity, short-term increases in FFA availability has been shown to initially increase POMC excitability[157]. To investigate the effects of acute and chronic HFD feeding on *Npas4* induction in POMC neurons, 6 week old B6 mice were fed Chow for 1 more week or fed HFD for 3 days, 1 week, or 6 weeks (Fig 4.7a). At the end of these time points, all mice were overnight fasted, refed with their respective diets for 1 hour, and brains were harvested for RNAscope. The refeeding was performed on all mice because it is now known that refeeding induces *Npas4* (Fig 4.3f-g). Compared to Chow-fed 7 week old mice, mice that were fed HFD for 3 days did not show differences in *Npas4* induction in POMC neurons. After 1 week of HFD, there was a significant increase in the proportion of *Npas4*-expressing POMC neurons compared to the Chow and 3 days of HFD groups. (Fig 4.7b). Initially, this increase seemed to be maintained at 6 weeks of HFD, but quantifying *Npas4* puncta per *Pomc*+ cell showed that only the 1 week of HFD led to a significant decrease in *Npas4*- and *Npas4*-low populations with a corresponding significant increase in *Npas4*-medium and *Npas4*-high populations (Fig 4.7c). Taken together, this shows that 1 week of HFD sensitizes POMC neurons to *Npas4* induction, but the overall *Npas4* levels per cell is decreased over time with longer exposure to HFD, even though the total proportion of *Npas4*-expressing POMC neurons may remain elevated.

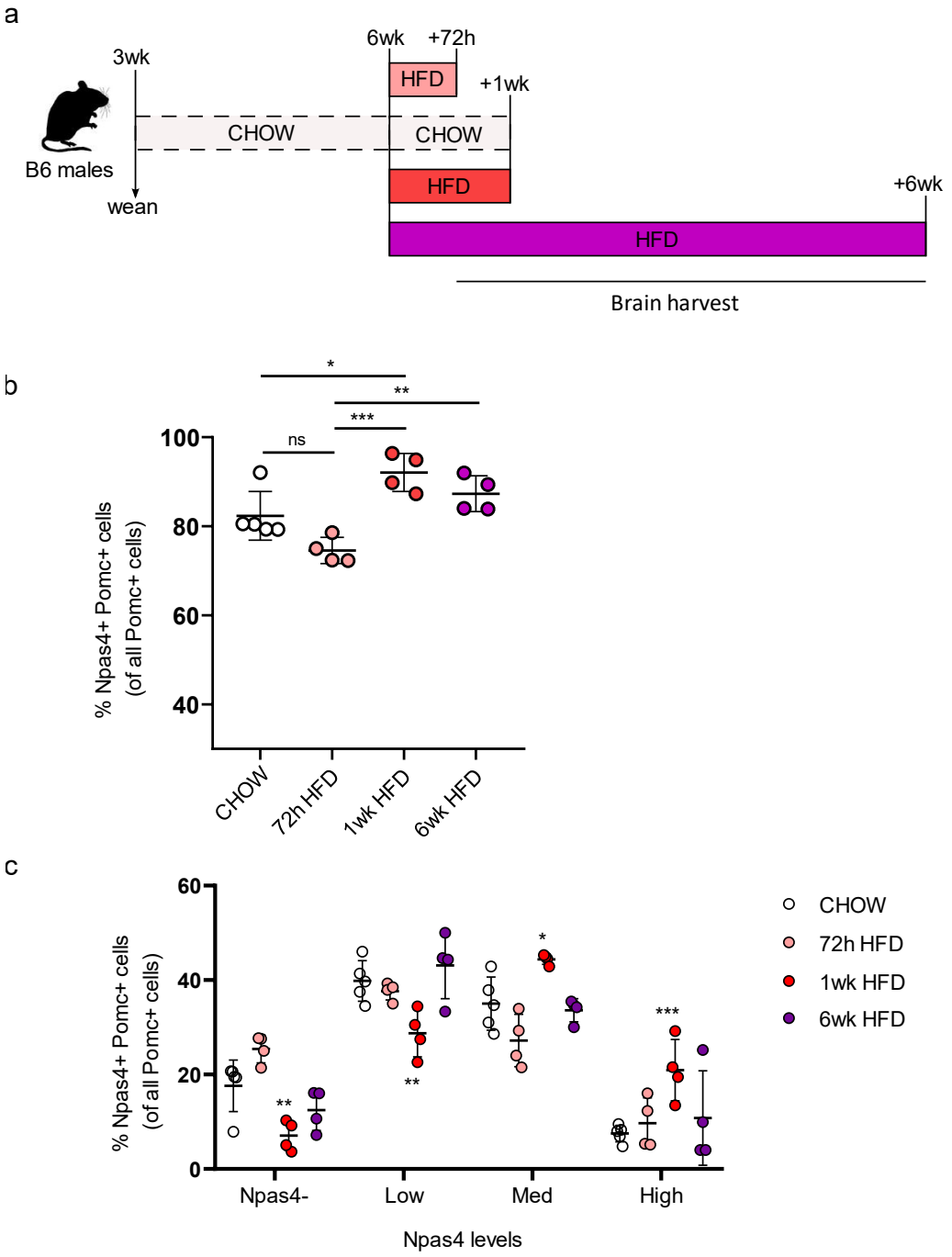

Figure 4.7 | 1 week to 6 weeks of HFD feeding increases the refeed-induced *Npas4* expression in POMC neurons of the arcuate nucleus. a, Schematic of experimental timeline. **b,** Quantifications of *Npas4*-positive, *Pomc*-positive cells as a percentage of total *Pomc*-positive cells from RNAscope images. *P < 0.05, **P < 0.01, ***P < 0.001. **c,** Breakdown of quantifications (b) into bins of *Npas4* expression levels: Npas4- = no *Npas4* signal in the *Pomc*-positive cell, Low = 1-3 *Npas4* punctae/cell, Med = 4-9 *Npas4* punctae/cell, and High = 10 or more *Npas4* punctae/cell. Values are expressed as *Npas4*-positive, *Pomc*-positive cells as a percentage of total *Pomc*-positive cells. Data shown as mean ± SD. One-way ANOVA with Tukey's multiple comparisons: *P < 0.05, **P < 0.01, ***P < 0.001 vs Chow.

4.7 Discussion

The experiments in Chapter 3 confirmed the expression of *Npas4* at the mRNA level in ARC AgRP and POMC neurons, and examined how peripheral or systemic changes in indicators of energy availability affected *Npas4* expression in these neurons. It was found that *Npas4* expression was induced in POMC neurons by refeeding after an overnight fast, oral glucose, and HFD feeding in wild-type B6 male mice.

A common finding in these experiments was that the percentage of *Npas4*+ POMC neurons was unexpectedly high in the fasted state. Even after an overnight fast in Chow-fed animals, 70-80% of POMC neurons were *Npas4*+ (Fig 4.3f, 4.5c). This was due to the strategy used to quantify *Npas4*+ POMC neurons. The quantification approach used here for RNAscope images first obtains the overall percentage of POMC neurons that express any level of *Npas4*, then categorizes each cell into different populations based on its *Npas4* puncta counts. This meant that even if only 1 *Npas4* signal was observed in the *Pomc*+ cell, it would be included as a *Npas4*+ POMC neuron. This was intentionally done in order to include as many cells as possible in the quantifications, and because the background expression of the *Npas4* probe was negligible (Fig 4.1b). If there had been a threshold set for the minimum expression level of *Npas4*, the proportion of *Npas4*+ POMC neurons would have been much lower, as the majority of the cells in most experiments only had 1-3 *Npas4* puncta (Fig 4.3g, 4.6d). An additional drawback of the method of quantification used here is that it does not account for entirety of the upper range of the number of *Npas4* signals. A cell with 10 or more *Npas4* puncta was classified as *Npas4*-high, but a cell in this category could have 11 puncta or 43 puncta. While this is a shortcoming of this quantification approach, the method of categorizing each cell based on *Npas4* puncta counts

yielded useful insights. This was seen in the HFD experiment, where both 1 week and 6 weeks of HFD feeding resulted in comparable proportions of *Npas4+ Pomc+* cells (Fig 4.7b). However, it was determined that significant changes in *Npas4* expression levels in POMC neuronal populations only occurred at 1 week, and not 6 weeks, of HFD feeding (Fig 4.7c). The most likely explanation of this is that by 6 weeks of HFD, the POMC neurons are already dysregulated and their activity is decreased as previously noted[176,361,362], resulting in more POMC neurons that have lower *Npas4* expression. In contrast, POMC neurons at 1 week of HFD could still be adjusting to the caloric overload and trying to compensate for this by increasing their activity, which would result in increased *Npas4* levels. As *Npas4* has also been studied as neuroprotective factor in stressful conditions, it would be interesting to determine if a chronic HFD exposure in addition to removal of NPAS4 would exacerbate the dysfunctional POMC activity. If so, it would implicate NPAS4 as having a potential role in the compensatory activity of POMC neurons during development of diet-induced obesity.

While *Npas4* induction was seen in multiple conditions in POMC neurons, the same changes in the proportion of *Npas4+* AgRP neurons were not observed. AgRP neurons are canonically known to be activated during fasting conditions, and *Npas4* has been identified as a "fasting-induced gene" in a previous scRNA-seq study of the MBH [363]. In this study, the mice were fasted for 18-20 hours overnight, which is almost double the fasting period used in this chapter. More importantly, the fasted animals in the scRNA-seq study were compared to *ad libitum* fed animals, which was not done here. If the fasted animals in Figure 4.3 were compared to *ad libitum* fed animals, *Npas4* induction may have been observed.

Finally, an overarching caveat in this chapter is that only mRNA levels of *Npas4* was studied without protein detection in most of the experiments. The unfortunate reason behind this is that my attempts to detect NPAS4 protein in the ARC using fixed frozen sections and available NPAS4 antibodies were not successful until very recently, and not without a great degree of troubleshooting. In this chapter, I only showed NPAS4 immunostaining results for the POMC neurons in fasted and 1 hour refed conditions in which an induction of NPAS4 protein was seen in response to refeeding, in line with the RNAscope results. However, I hope to apply this protocol to other experimental samples in the future to confirm the other RNAscope results. Given that mRNA detection in this chapter dealt with small numbers of *Npas4* mRNA being observed as puncta, it is possible that the absolute levels of NPAS4 protein are quite low in abundance within ARC neurons, or the right time frame was not examined. Since NPAS4 is a dynamically regulated transcription factor, high protein and mRNA levels may not be easily detectable, or even necessary for its function[364,365]. While the levels of any gene or protein is commonly used as an indicator of importance within a cell type, the mRNA and protein levels are not always proportional to each other, and the RNAscope method used here may not be able to capture the full range of *Npas4* expression dynamics[364].

In summary, the data in this chapter are the first to specifically determine expression levels and dynamics of the immediate early gene *Npas4* in AgRP and POMC neurons of the ARC. While low levels of *Npas4* are quite ubiquitously seen throughout cells of the ARC based on RNAscope images, it is specifically induced in POMC neurons by systemic increases in energy availability such as refeeding or HFD. Acute changes to energy availability in the form of oral glucose can also induce *Npas4*, but for a relatively short period of time. In general, indicators of positive

energy balance that can activate POMC neurons induce *Npas4.* As both AgRP and POMC neurons are important for regulation of energy homeostasis by responding to peripheral signals, it will be important to characterize the role of NPAS4 in the presence of nutrient stresses. In order to study the role of NPAS4 specific to AgRP and POMC neurons, a model of NPAS4 depletion in these cell types and a robust method of inducing nutrient stress is required.

Chapter 5: Characterization of mice with conditional NPAS4 knockout in adult AgRP and POMC neurons of the ARC

5.1 Rationale

Previous *in vivo* knockout studies of NPAS4 have been largely in the CNS, but none have been in the ARC. A previous study in which the Pdx1-CreER line was used showed visible recombination with a lineage marker in the ARC region, and those knockouts displayed altered feeding behaviour when fed HFD[320]. This suggested that NPAS4 in the ARC had a role in regulating food intake that was particularly important in conditions of high energy availability. As data from chapter 4 showed, Npas4 is expressed in AgRP and POMC neurons and its expression is elevated in HFD-fed mice. Therefore, new NPAS4 KO mouse lines were generated in order to specifically study the role of NPAS4 in either the AgRP neurons or POMC neurons in a diet-induced obesity model using HFD.

The simplest approach in generating these new NPAS4 KO mouse lines was to use a mouse line that expressed Cre recombinase specifically in AgRP or POMC neurons. While the AgRP-IRES-Cre line[366] and POMC-Cre[100] lines have been widely used in the field of ARC study, the caveat of these lines is that they are activated before mice reach adulthood. In mouse hypothalamus development, *Agrp* and *Pomc* expression have been detected as early as embryonic days 10 to 14[367]. There have been previous reports that NPAS4 may have a role in developmental stages[314], so the use of the traditional Cre mouse lines could result in knocking out of NPAS4 at the embryonic stage. To avoid this and to control the timing of NPAS4 KO, conditional Cre recombinase lines where a portion of the estrogen receptor (ER) containing the ligand-binding site is fused to the Cre recombinase were selected instead. The breeding of AgRP-CreER or

POMC-CreER lines with the Npas4 flox line would both allow the generation of a conditional NPAS4 KO line, where upon administration of tamoxifen, the CreER fusion recombinase would translocate to the nucleus to induce recombination.

5.2 Recombination assessment of AgRP-CreER transgenic mice

CreER-mediated recombination was induced by administrating three doses of 8mg tamoxifen to male AgRP-CreER^{+}; Npas4$^{wt/wt}$ (AgRP-CreER), AgRP-CreER^{-}; Npas4$^{flox/flox}$ (Npas4 flox), and AgRP-CreER^{+}; Npas4$^{flox/flox}$ (AgRP-NPAS4 KO) mice at 6 weeks of age. The tamoxifen doses have been previously shown to induce Pdx1-CreER-mediated recombination in the ARC[320]. When the mice were 7 weeks old (0 weeks post-tamoxifen), brains were collected from AgRP-CreER and AgRP-NPAS4 KO mice after an overnight fast.

Recombination efficiency was assessed by directly measuring *Npas4* mRNA levels with RNAscope in the same manner as chapter 4 experiments. The right and left sides of the ARC showed strong *Agrp* signals clustered closely around the ventral and ventromedial sides of the 3rd ventricle (3V) in the expected pattern of expression for AgRP neurons in both AgRP-CreER and AgRP-NPAS4 KO mice (Fig 5.1a). Qualitatively, *Npas4* signals in the AgRP-NPAS4 KO appeared dimmer, and quantification of the proportion of *Npas4+ Agrp+* cells showed a 20-30% decrease in the AgRP-NPAS4 KO (Fig 5.1b). This decrease was due to the significant increase in *Npas4- Agrp+* cells in the KO mice (Fig 5.1c). These results show that the oral method of tamoxifen is sufficient to induce recombination mediated by AgRP-CreER, and the resulting NPAS4 KO is confirmed by an increase in *Npas4-* cells in the ARC neurons.

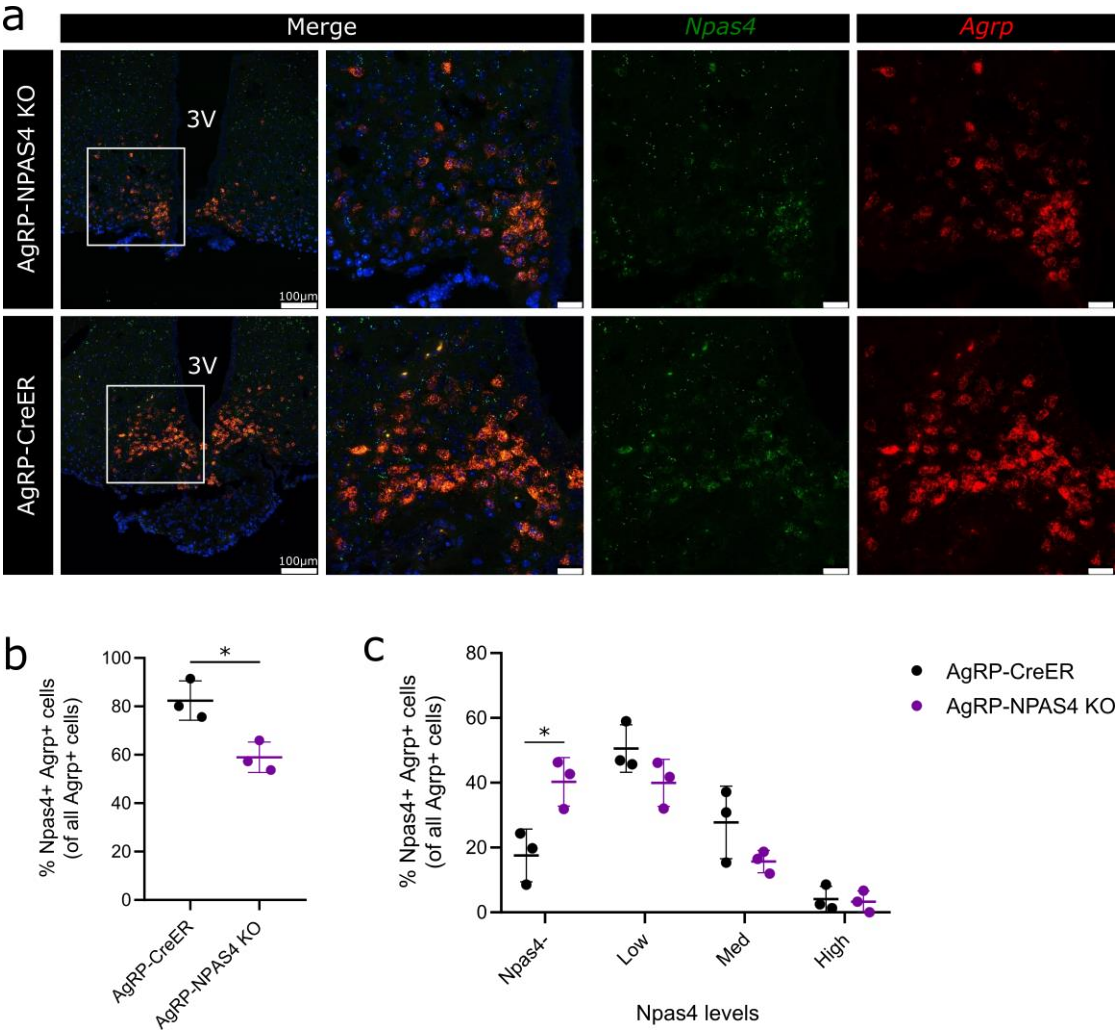

Figure 5.1 | Recombination assessment of AgRP-CreER mice. a, Representative RNAscope images of the arcuate nucleus from AgRP-CreER and AgRP-NPAS4 KO mice 7 weeks of age, 0 days after tamoxifen administration, probed with *Npas4* (green), *Pomc* (red), and DAPI nuclear stain (blue). Scale bars = 25μm unless otherwise indicated. **b,** Quantifications of *Npas4*-positive, *Agrp*-positive cells in each genotype as a percentage of total *Agrp*-positive cells from RNAscope images (a). **c,** Breakdown of quantifications (b) into bins of *Npas4* expression levels: Npas4- = no *Npas4* signal in the *Agrp*-positive cell, Low = 1-3 *Npas4* punctae/cell, Med = 4-9 *Npas4* punctae/cell, and High = 10 or more *Npas4* punctae/cell. Data shown as mean ± SD. Student's t-test: *P < 0.05.

5.3 Characterization of the AgRP-NPAS4 KO mouse phenotype on Chow and HFD

To characterize the effects of specific NPAS4 KO in AgRP neurons, AgRP-CreER, Npas4 flox, and AgRP-NPAS4 KO mice were given tamoxifen at 6 weeks of age and maintained on Chow or

switched to 58% HFD for 30 weeks starting at 7 weeks of age (Fig 5.2a). Body weights of all mice were measured during the week of tamoxifen administration, before division of Chow and HFD groups (week 0), and every week during the 30 weeks of diet. Random-fed blood glucose and overnight fasted blood glucose were measured on alternating weeks. At 30 weeks of diet, mice of all genotypes were fasted overnight and whole brain, liver, and pancreas were harvested for future histology if necessary.

In both Chow and HFD groups, an immediate and significant body weight difference was observed between Npas4 flox mice and AgRP-CreER and AgRP-NPAS4 KO mice. In the Chow group, AgRP-CreER and AgRP-NPAS4 KO mice were approximately 3-4g lighter at 0 weeks, and this difference grew larger over time until AgRP-CreER mice were 13g lighter than Npas4 flox (Fig 5.2b). Relative to the original body weight at 0 weeks, Chow group Npas4 flox controls gained 70.6% body weight while AgRP-NPAS4 KO mice gained 53.3% and AgRP-CreER controls gained 33.2%. Unexpectedly, AgRP-NPAS4 KO mice gained enough weight over time to become significantly heavier than AgRP-CreER mice by study endpoint, despite still being significantly lighter than the Npas4 flox littermates. This difference in body weight between the two control groups was almost certainly due to the presence of the AgRP-CreER transgene, since the KO mice were also affected. The body weight difference between control groups was observed even before (day -7) and during (days -5, -3) tamoxifen administration, although the AgRP-NPAS4 KO were moderately but significantly heavier than AgRP-CreER controls and lighter than Npas4 flox controls (Fig 5.2d). In the HFD group, AgRP-NPAS4 KO were again significantly lighter than Npas4 flox animals but not AgRP-CreER mice, possibly due to the higher variability in the AgRP-CreER mice (Fig 5.2c). HFD-fed Npas4 flox mice gained 95.8%

body weight, AgRP-NPAS4 KO mice gained 80.1% body weight, and AgRP-CreER mice gained 107.8% body weight relative to their original body weight at 0 weeks. The same differences as the Chow-fed group were observed from body weights before and during tamoxifen administration (Fig 5.2e).

In glycemia assessments for the Chow group, neither random-fed nor overnight fasted blood glucose were initially different between genotypes despite the difference in body weights. During 30 weeks of Chow, random-fed blood glucose was generally not different between the genotypes, whereas AgRP-NPAS4 KO displayed significantly lower fasting glycemia compared to Npas4 flox controls only starting at 7 weeks of Chow (Fig 5.2f). For the HFD group, random-fed blood glucose was generally not different between the genotypes, and the persistent difference in fasting blood glucose between AgRP-NPAS4 KO and Npas4 flox seen in the Chow group in the later study weeks was not observed (Fig 5.2g).

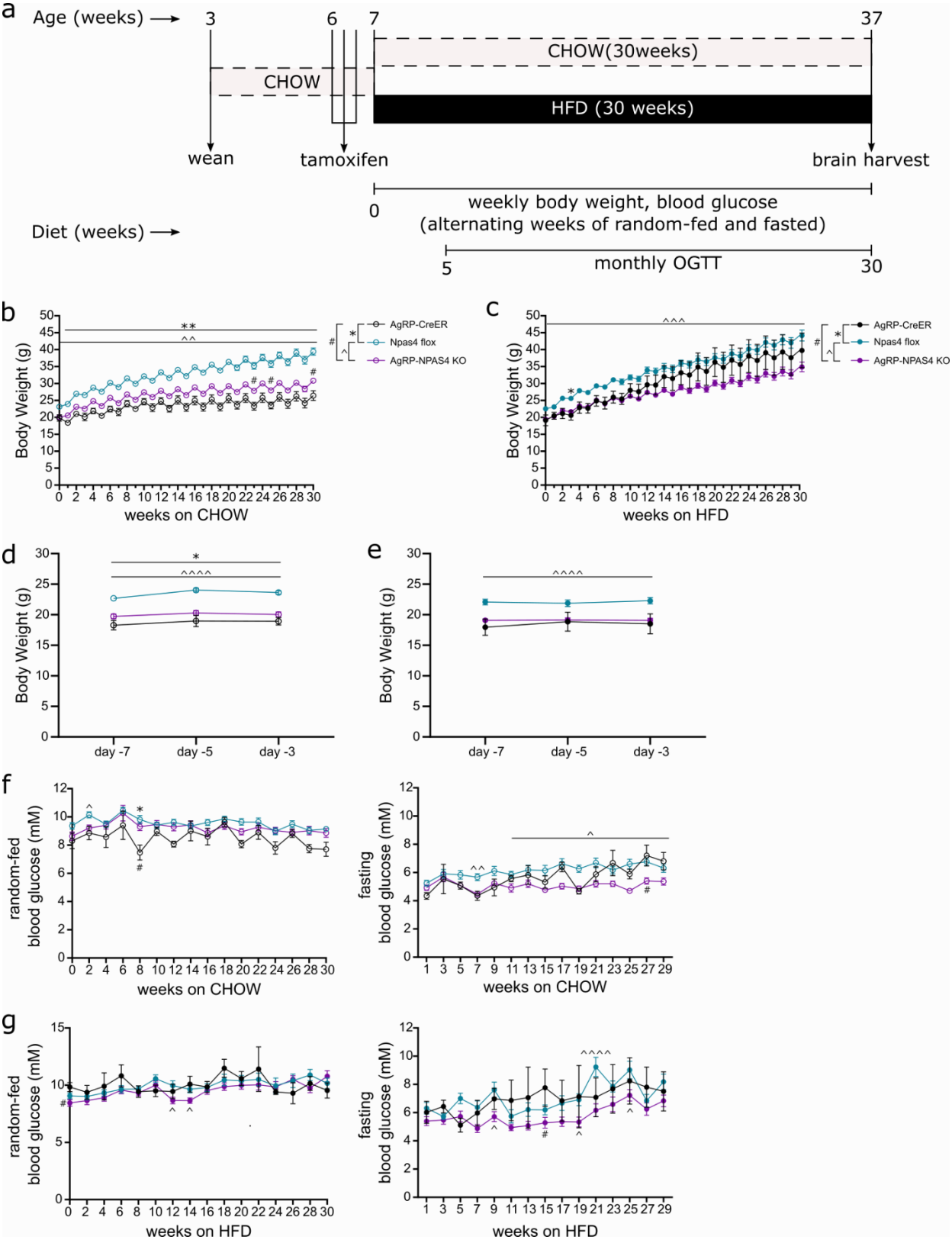

Figure 5.2 | AgRP-CreER and AgRP-NPAS4 KO mice show lower body weight on Chow and HFD. a, Initial timeline of diet and experiments to characterize AgRP-NPAS4 KO and

POMC-NPAS4 KO mice. **b,** Weekly body weights of AgRP-CreER (n=4), Npas4 flox (n=28), and AgRP-NPAS4 KO (n=23) mice in the CHOW group. **c,** Weekly body weights of AgRP-CreER (n=5), Npas4 flox (n=17), and AgRP-NPAS4 KO (n=19) mice in the HFD group. **d-e,** Body weights of all genotypes measured during the week of tamoxifen administration for the CHOW (d) and HFD (e) groups. **f-g,** Biweekly random-fed and fasting blood glucose measurements for all genotypes in the CHOW (f) and HFD (g) groups. 2-way ANOVA with Tukey's multiple comparisons: *P < 0.05, **P < 0.01 (AgRP-CreER vs Npas4 flox); ^P < 0.05, ^^P <0.01, ^^^^P <0.0001 (Npas4 flox vs AgRP-NPAS4 KO); #P < 0.05 (AgRP-CreER vs AgRP-NPAS4 KO).

To further characterize differences in glucose homeostasis, monthly oral glucose tolerance tests (OGTT) were performed starting at 5 weeks of diet in the Chow and HFD groups (Fig 5.3a). At every OGTT from 5 weeks to 29 weeks of Chow, only the AgRP-CreER mice showed abnormal glucose curves where the blood glucose greatly spiked at 30-60 minutes compared to the other two genotypes (Fig 5.3a, c) Despite these significant differences in the blood glucose measurements, the area under the curve (AUC) was not different between genotypes (Fig 5.3b, d). However, this difference was partially explained by the AgRP-CreER mice having lower plasma glucose-stimulated insulin compared to Npas4 flox mice from 5 weeks to 29 weeks of diet (Fig 5.3e, f). In contrast, AgRP-NPAS4 KO in the Chow group showed blood glucose levels comparable to those of Npas4 flox mice, but their plasma insulin was similar to that of AgRP-CreER mice. This implies that while part of the unexpected phenotypes most likely caused by the AgRP-CreER transgene includes lower glucose-stimulated insulin secretion, the AgRP-NPAS4 KO mice are somehow able to tolerate the spike of blood glucose with the same low level of insulin. This difference was not observed in the HFD group. At 5 weeks to 29 weeks of HFD, no genotypes showed a difference in blood glucose measurements during the OGTT or in the AUC (Fig 5.3g-j). At 5 weeks of HFD, the HFD-fed AgRP-CreER and AgRP-NPAS4 KO mice both showed significantly lower glucose-stimulated plasma insulin compared to Npas4 flox controls,

similar to the Chow group (Fig 5.3k). Unliked the Chow group, these differences were not present by 29 weeks of HFD (Fig 5.3k-l).

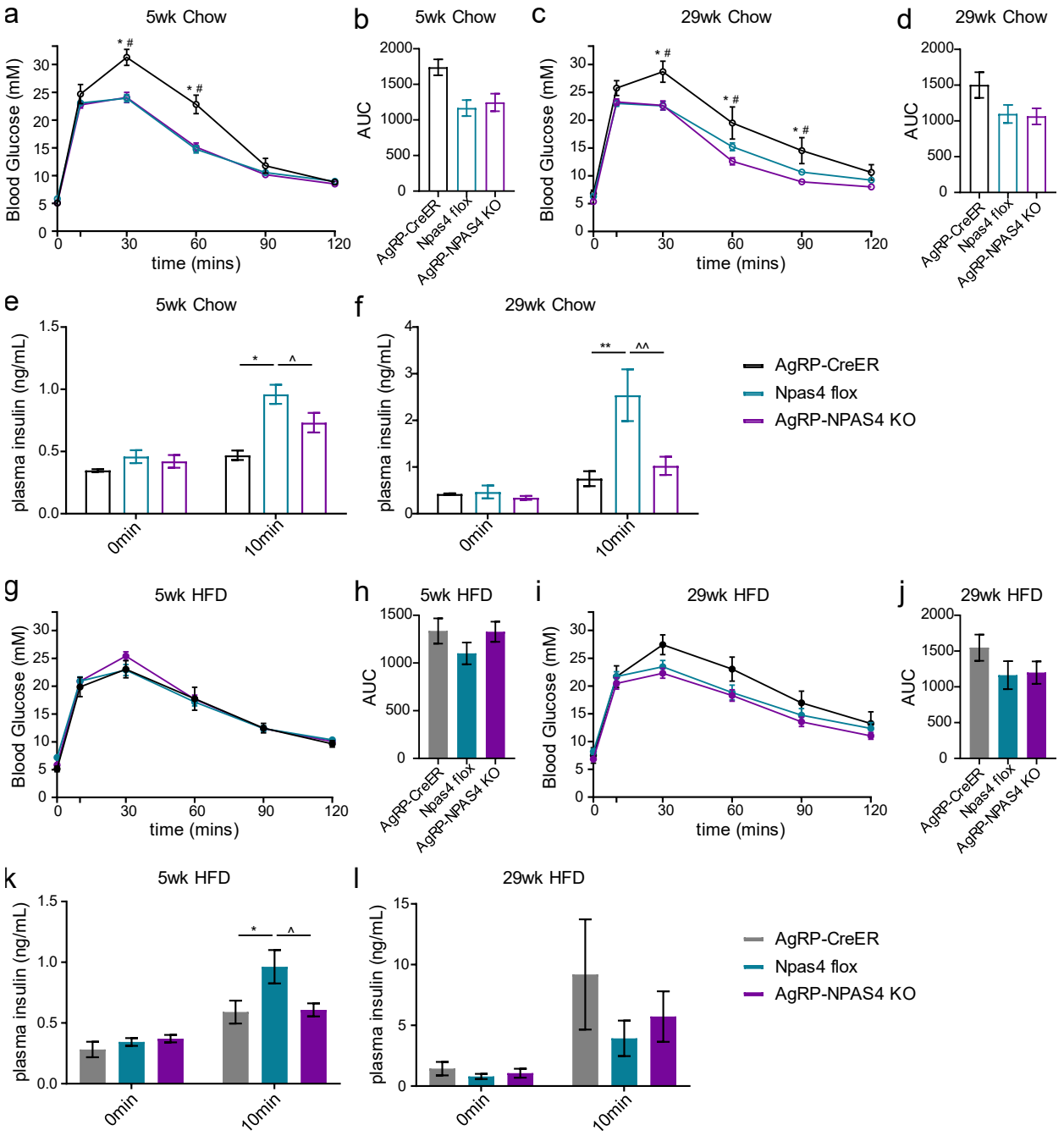

Figure 5.3 | AgRP-NPAS4 KO mice show normal oral glucose tolerance but lower plasma glucose-stimulated insulin on a Chow diet. a-d, Blood glucose measurements (a, c) and

calculated AUC (b, d) from oral glucose tolerance tests performed on AgRP-CreER (n=4), Npas4 flox (n=28), and AgRP-NPAS4 KO (n=23) mice at 5 weeks (a, b) and 29 weeks (c, d) of CHOW. **e-f,** Plasma insulin measured at 0 minutes and 10 minutes of oral glucose tolerance tests at 5 weeks (e) and 29 weeks (f) of CHOW. **g-j,** Blood glucose measurements (g, i) and calculated AUC (h, j) from oral glucose tolerance tests performed on AgRP-CreER (n=5), Npas4 flox (n=17), and AgRP-NPAS4 KO (n=19) mice at 5 weeks (g, h) and 29 weeks (i, j) of HFD. **k-l,** Plasma insulin measured at 0 minutes and 10 minutes of oral glucose tolerance tests at 5 weeks (k) and 29 weeks (l) of HFD. 2-way ANOVA with Tukey's multiple comparisons: *P < 0.05, **P < 0.01 (AgRP-CreER vs Npas4 flox); ^P < 0.05, ^^P <0.01 (Npas4 flox vs AgRP-NPAS4 KO); #P < 0.05 (AgRP-CreER vs AgRP-NPAS4 KO).

AgRP neurons are known to regulate hepatic gluconeogenesis. Glycerol tolerance tests were performed to assess whether NPAS4 KO in AgRP neurons affects gluconeogenesis, a process that uses glycerol as a substrate. In the Chow group, there were no differences in blood glucose levels in response to a 2g/kg glycerol bolus at 9 weeks of Chow (Fig 5.4a-b). At 15, 19, and 23 weeks of Chow when the fasting blood glucose between the two genotypes were significantly different, the blood glucose levels appeared lower in the AgRP-NPAS4 KO mice, but the AUC were not different (Fig 5.4c-h). This suggested that accounting for the differences in basal blood glucose, the actual magnitude of the response to glycerol as a hepatic gluconeogenic substrate was the same in Npas4 flox and AgRP-NPAS4 KO mice. The same pattern was observed in the HFD group (Fig 5.4 i-p).

The presence of a strong and unexpected body weight and blood glucose phenotype present in animals with the AgRP-CreER transgene make the interpretation of the physiological data very challenging. Despite the two control groups showing differences in most measured parameters, the effects of NPAS4 KO in AgRP neurons were more pronounced in the Chow group. The observation that AgRP-NPAS4 KO mice can maintain normal glucose tolerance with lower plasma insulin levels comparable to AgRP-CreER controls is interesting, and this is only seen in

the Chow group as well. Overall, it seems that the specific NPAS4 KO effects are minimal at best or shadowed by the effects of the AgRP-CreER transgene.

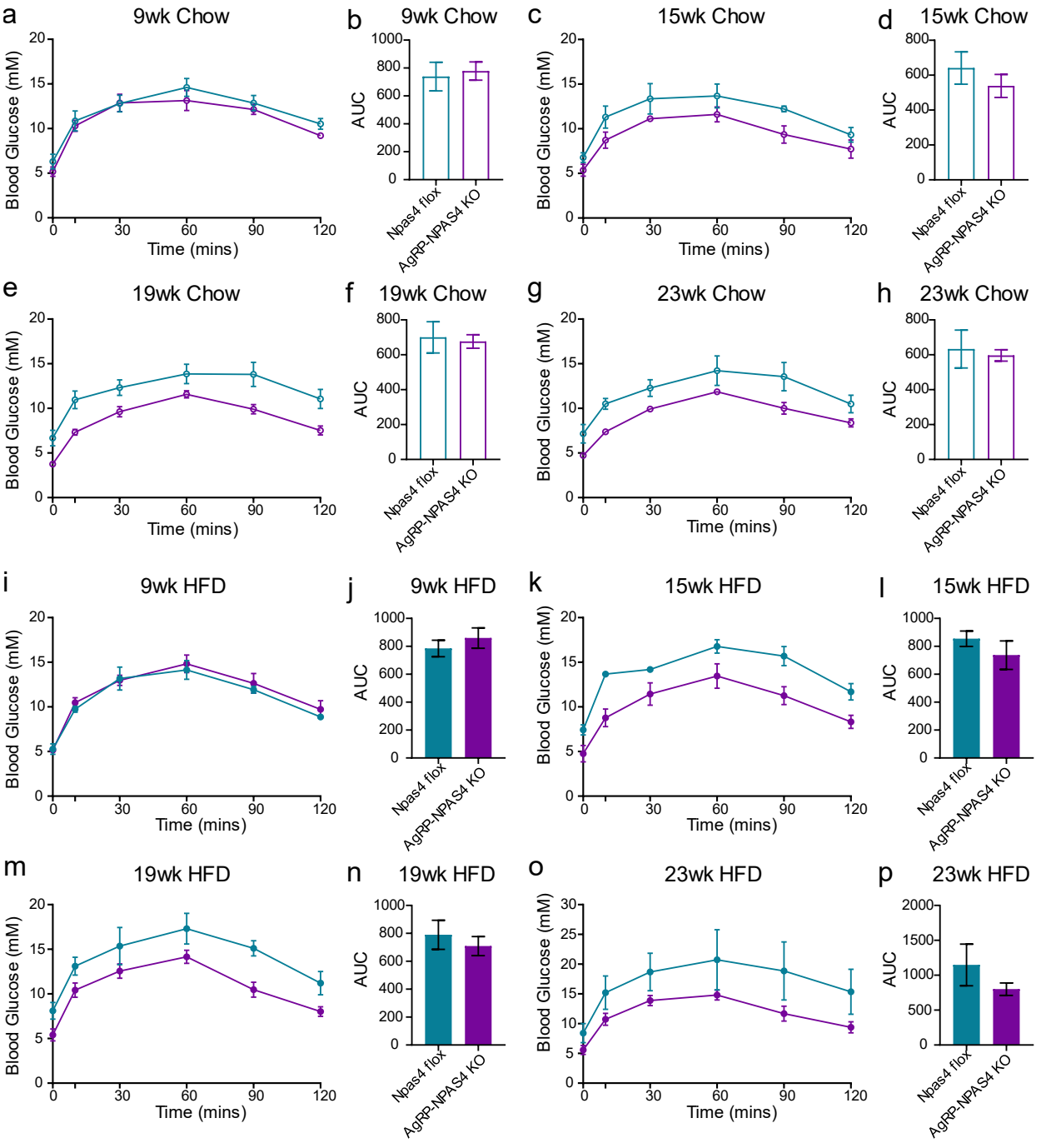

Figure 5.4 | AgRP-NPAS4 KO mice show similar magnitudes of response to glycerol as Npas4 flox controls on Chow and HFD. a-h, Blood glucose measurements and calculated AUC from intraperitoneal glycerol tolerance tests performed on Npas4 flox (n=4) and AgRP-NPAS4

KO (n=4) mice at 9 weeks (a, b), 15 weeks (c, d), 19 weeks (e, f), and 23 weeks (g, h) of CHOW. **i-p,** Blood glucose measurements and calculated AUC from intraperitoneal glycerol tolerance tests performed on Npas4 flox (n=3) and AgRP-NPAS4 KO (n=4) mice at 9 weeks (i, j), 15 weeks (k, l), 19 weeks (m, n), and 23 weeks (o, p) of HFD.

5.4 Recombination assessment of POMC-CreER transgenic mice

In parallel to the characterization of AgRP-NPAS4 KO mice, POMC-NPAS4 KO mice were also characterized. Before physiological parameters were measured, recombination assessment of the POMC-CreER and POMC-NPAS4 KO mice was performed in a similar manner to AgRP-CreER and AgRP-NPAS4 KO mice. CreER-mediated recombination was induced by administrating three doses of 8mg tamoxifen to male POMC-CreER^{+}; Npas4$^{wt/wt}$ (POMC-CreER), POMC-CreER^{-}; Npas4$^{flox/flox}$ (Npas4 flox), and POMC-CreER^{+}; Npas4$^{flox/flox}$ (POMC-NPAS4 KO) mice at 6 weeks of age. At 0 weeks post-tamoxifen (7 weeks of age), brains were harvested from POMC-CreER, and POMC-NPAS4 KO mice after an overnight fast and 1 hour of refeeding. In both POMC-CreER and POMC-NPAS4 KO mice, robust *Pomc*+ signals were detected scattered across the entire ARC area in the expected pattern of expression for POMC neurons (Fig 5.5a). Quantification of images showed a 20-30% decrease in the *Npas4*+ *Pomc*+ cells in the POMC-NPAS4 KO mice (Fig 5.5b). Similar to AgRP-NPAS4 KO mice, this decrease was due to the significant 20-30% increase in *Npas4*- *Pomc*+ cells in POMC-NPAS4 KO mice (Fig 5.5c). Additional confirmation on recombination was performed by visualization of the red fluorescent tdTomato (tdT) protein in cells with CreER activity. This was possible because some mice had a tdT-encoding sequence downstream of a STOP cassette flanked by loxP sites in the *Rosa26* locus. Upon CreER-mediated recombination, the excision of the STOP cassette allowed for the expression of tdT, which was detectable without immunostaining in fixed frozen sections of the brain. In tdT^{+} POMC-CreER mice and tdT^{+} POMC-NPAS4 KO mice two weeks after tamoxifen

administration, tdT^+ cells were visible throughout the ARC in a pattern similar to that of POMC neurons, indicating successful CreER-mediated recombination in those cells (Fig 5.6a). As expected, no tdT fluorescence was visible in the tdT^- POMC-CreER mice used as a control. Since POMC neurons are known to be present in the nucleus of the solitary tract (NTS) of the hindbrain in addition to the ARC, the hindbrain was also sectioned and checked for tdT positivity. tdT expression was not visible in the NTS of tdT^+ POMC-CreER, tdT^+ POMC-NPAS4 KO, and tdT^- POMC-CreER mice (Fig 5.6b). In addition to assessing expression of tdT protein, *tdtomato* mRNA expression in *Pomc+* cells was also visualized with RNAscope (Fig 5.6c). In tdT^+ POMC-CreER mice, *tdtomato* expression was detected in 50% of *Pomc+* cells (Fig 5.6d). This additional assessment of CreER activity showed that the POMC-CreER transgene allowed for NPAS4 KO in roughly half of ARC POMC neurons but not NTS POMC neurons.

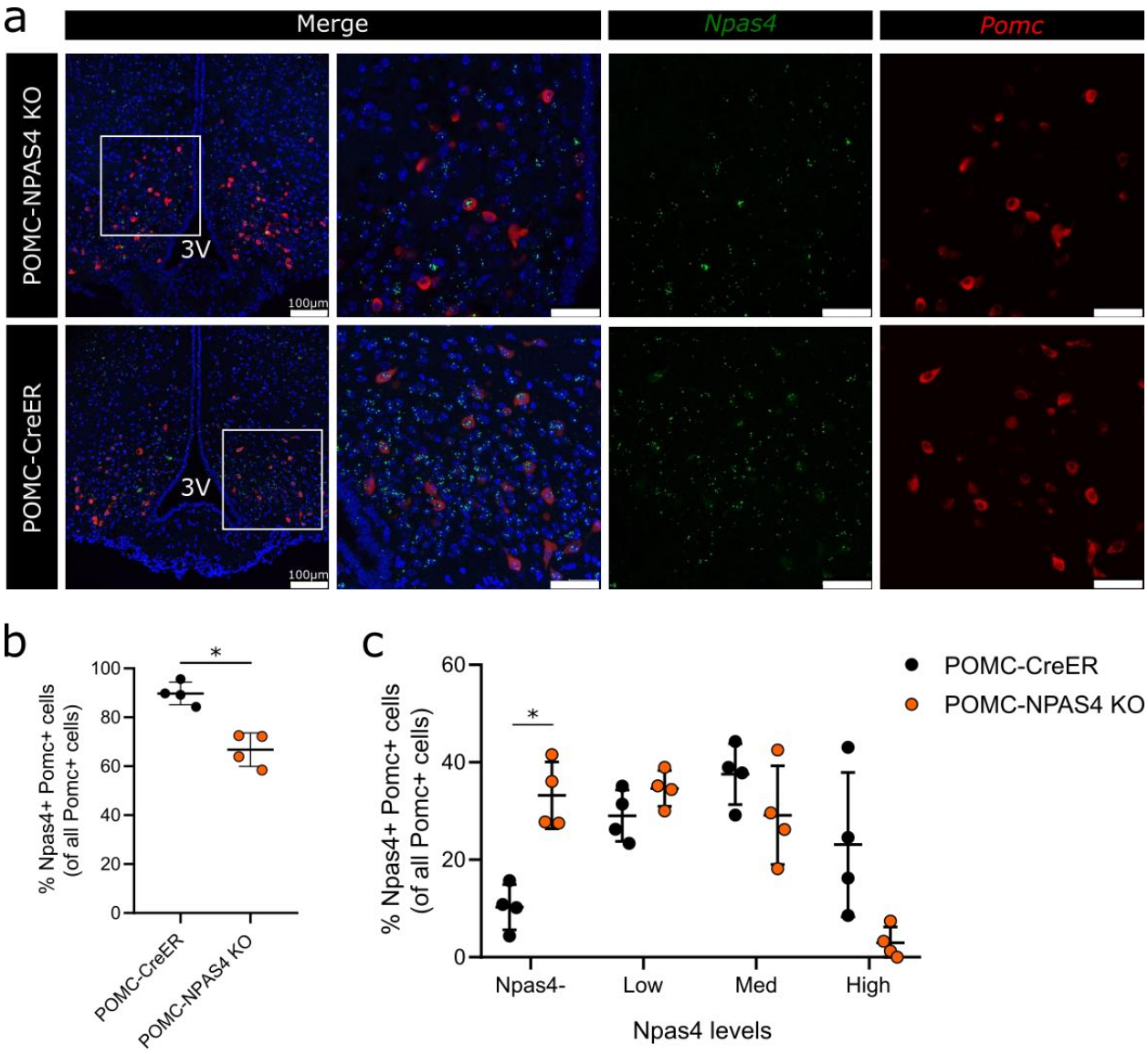

Figure 5.5 | Recombination assessment of POMC-CreER mice. a, Representative RNAscope images of the arcuate nucleus from POMC-CreER and POMC-NPAS4 KO mice 7 weeks of age, 0 days after tamoxifen administration, probed with *Npas4* (green), *Pomc* (red), and DAPI nuclear stain (blue). **b,** Quantifications of *Npas4*-positive, *Pomc*-positive cells in each genotype as a percentage of total *Pomc*-positive cells from RNAscope images (a). **c,** Breakdown of quantifications (b) into bins of *Npas4* expression levels: Npas4- = no *Npas4* signal in the *Pomc*-positive cell, Low = 1-3 *Npas4* punctae/cell, Med = 4-9 *Npas4* punctae/cell, and High = 10 or more *Npas4* punctae/cell. 3V = 3rd ventricle. Scale bars = 100µm. Data shown as mean ± SD. Student's t-test: *P < 0.05.

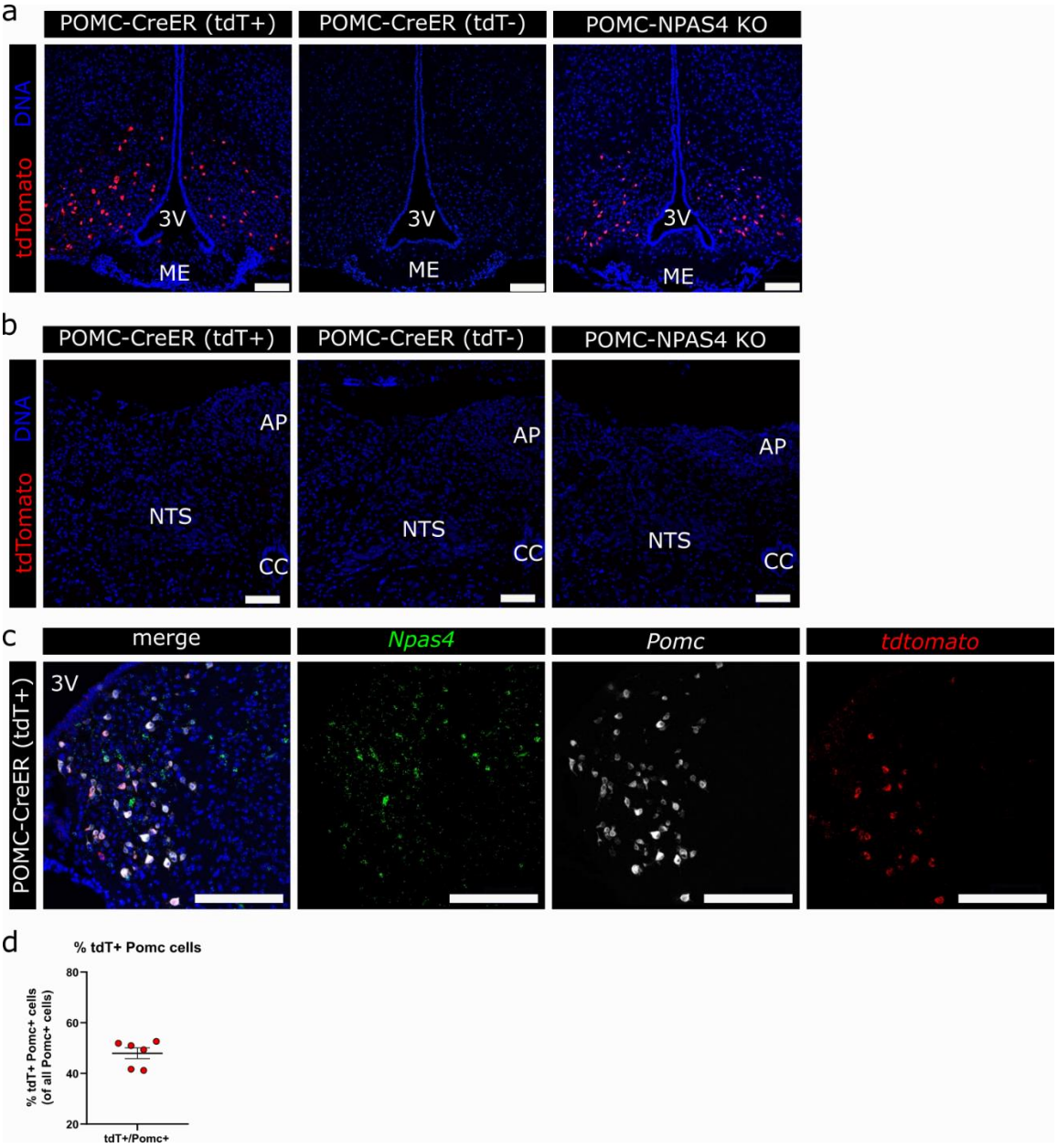

Figure 5.6 | Assessment of POMC-CreER recombination by tdTomato expression. a, Representative immunofluorescence images of arcuate nucleus sections from tdTomato+ POMC-CreER mice, tdTomato- POMC-CreER mice, and POMC-NPAS4 KO mice 2 weeks after tamoxifen administration, showing tdTomato (red) and nuclear stain DAPI (DNA; blue). **b,** Representative immunofluorescence images of hindbrain NTS sections from tdTomato-positive (tdT+) POMC-CreER mice, tdTomato-negative (tdT-) POMC-CreER mice, and POMC-NPAS4 KO mice. **c,** Representative RNAscope images of arcuate nucleus sections from tdTomato+ POMC-CreER mice two weeks after tamoxifen, probed with *Npas4* (green), *Pomc* (white), *tdtomato* (red), and nuclear stain DAPI (blue). **d,** Quantification of *tdtomato*-positive, *Pomc*-positive cells as a percentage of all *Pomc*-positive cells. 3V = 3rd ventricle, ME = median eminence, AP = area postrema, NTS = nucleus of the solitary tract, cc = central canal. Scale bars = 100μm.

5.5 Characterization of the POMC-NPAS4 KO mouse on Chow

The characterization of the POMC-NPAS4 KO mice was performed in a similar manner to the AgRP-NPAS4 KO mice, following the same diets and experimental timeline discussed in 5.3 (Fig 5.2a). Unlike the AgRP-CreER mice, the POMC-CreER control mice did not show any differences in body weight compared to Npas4 flox controls and POMC-NPAS4 KO mice before, during, and after tamoxifen administration (Fig 5.7a). During 30 weeks of Chow, weekly body weights were not different between the three genotypes (Fig 5.7b). Random-fed and overnight fasted blood glucose measurements also showed no differences between genotypes (Fig 5.7c-d). In additional assessment of glucose homeostasis, OGTT performed from 5 weeks of Chow to 29 weeks of Chow did not show any differences between genotypes (Fig 5.8a-d). Plasma collected from 0 minutes and 10 minutes during the OGTT at any point of the 30 weeks of Chow did not show differences between genotypes, and all genotypes showed the expected higher plasma insulin at 10 minutes. (Fig 5.8e-f). During glycerol tolerance tests at 15 weeks and 19 weeks of Chow, blood glucose measurements were not different between Npas4 flox and POMC-NPAS4 KO mice (Fig 5.8g-j). Finally, insulin sensitivity was assessed with monthly 0.75U/kg insulin tolerance tests starting at 10 weeks of Chow to 26 weeks of Chow. Representative blood glucose measurements during the insulin tolerance tests at 15 and 19 weeks of Chow are shown, but there were no differences in response to insulin at any time point (Fig 5.8k-l). These results show that NPAS4 KO specifically in ARC POMC neurons has no effects on overall mouse body weight or glucose homeostasis when animals are maintained on a standard Chow diet.

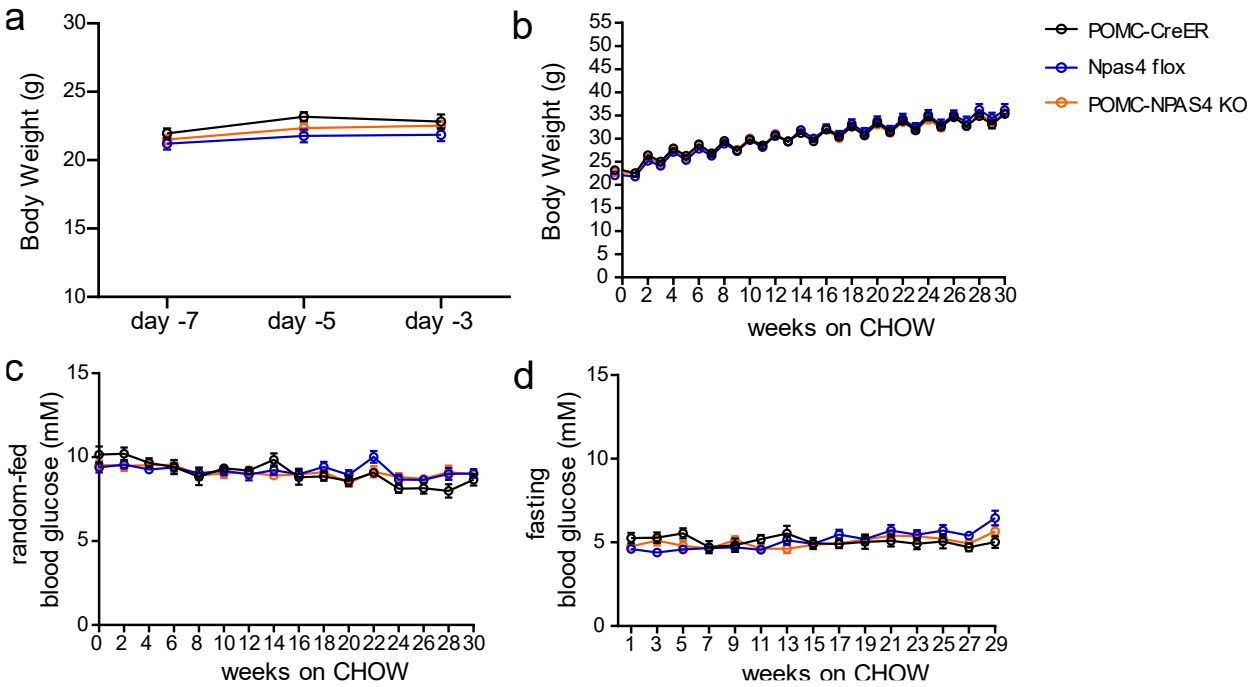

Figure 5.7 | POMC-NPAS4 KO mice show normal body weight and glycemia on Chow. a, Body weights measured during tamoxifen administration to POMC-CreER (n=10), Npas4 flox (n=22), and POMC-NPAS4 KO (n=19) mice. **b,** Weekly body weights measured during 30 weeks of CHOW for all genotypes. **c-d,** Biweekly random-fed (c) and 10 hour overnight fasted (d) blood glucose measurements for all genotypes.

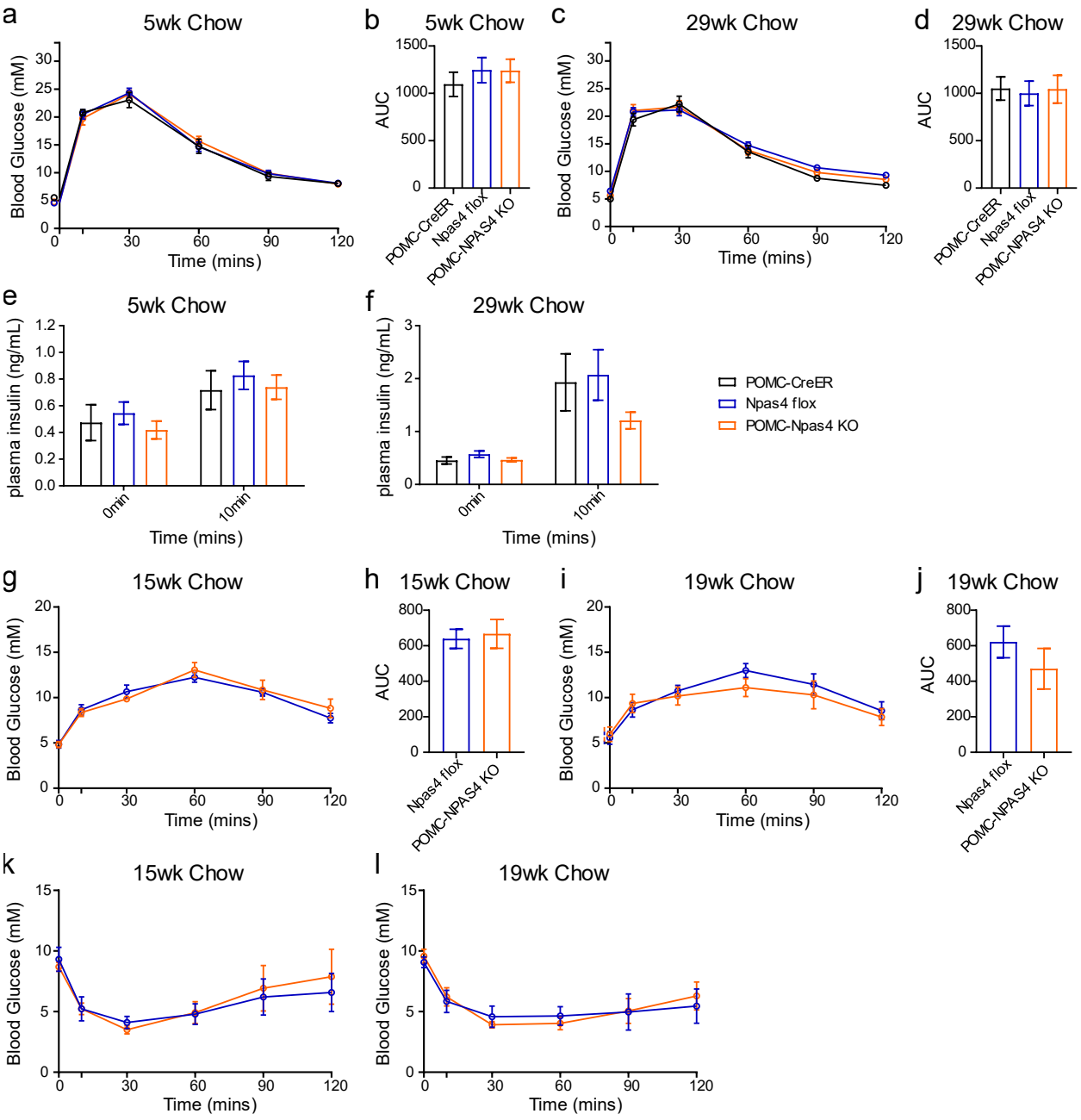

Figure 5.8 | POMC-NPAS4 KO mice show normal glucose tolerance, glycerol tolerance, and insulin tolerance on Chow. a-d, Blood glucose measurements (a, c) and calculated AUC (b, d) from oral glucose tolerance tests performed on POMC-CreER (n=10), Npas4 flox (n=22), and POMC-NPAS4 KO (n=19) mice at 5 weeks (a, b) and 29 weeks (c, d) of CHOW. **e-f,** Plasma insulin measured at 0 minutes and 10 minutes of oral glucose tolerance tests at 5 weeks (e) and 29 weeks (f) of CHOW. **g-j,** Blood glucose measurements (g, i) and calculated AUC (h, j) from intraperitoneal glycerol tolerance tests performed on Npas4 flox (n=6) and POMC-NPAS4 KO (n=6) mice at 15 weeks (g, h) and 19 weeks (i, j) of CHOW. **k-l,** Blood glucose measurements from intraperitoneal insulin tolerance tests performed on Npas4 flox (n=4) and POMC-NPAS4 KO (n=4) mice at 15 weeks (k) and 19 weeks (l) of CHOW.

5.6 Characterization of the POMC-NPAS4 KO mouse on HFD

The POMC-CreER mice used for the HFD cohorts also did not show differences in body weight before and during tamoxifen administration (Fig 5.9a). On week 0, prior to HFD feeding but after tamoxifen administration, POMC-CreER did show a moderate body weight difference of 1-2g over Npas4 flox and POMC-NPAS4 KO mice (Fig 5.9b). However, the most striking body weight difference was observed in the POMC-NPAS4 KO mice that displayed a consistent significantly lower body weight compared to POMC-CreER mice starting at 9 weeks of HFD, and compared to Npas4 flox mice starting at 13 weeks of HFD in a less consistent but still significant manner (Fig 5.9b). By study endpoint, POMC-NPAS4 KO mice were 7-8g lighter than POMC-CreER controls and Npas4 flox controls. Even if the slight body weight difference at week 0 is taken into account, POMC-CreER mice still gained roughly 6g more over the course of 30 weeks of HFD than POMC-NPAS4 KO mice. Relative to their original body weights at 0 weeks of HFD, this meant that Npas4 flox controls gained 137.9% body weight and POMC-CreER controls gained 116.1%, while POMC-NPAS4 KO mice only gained 102.6% over 30 weeks of HFD feeding. Among the POMC-NPAS4 KO group, some mice still became obese. While most POMC-NPAS4 KO mice weighed between 31.3g and 41.7g by 30 weeks of HFD, two mice became heavier than 60g, similar to obese mice in the control groups, and six mice were between 46.8g and 54.4g.

Despite a clear difference in body weight gain, glycemia was barely altered. Neither random-fed nor overnight fasted blood glucose measurements showed a consistent difference between the genotypes (Fig 5.9c-d). Fasting blood glucose in all genotypes steadily increased over time with chronic HFD feeding, which was expected as most mice became more and more obese (Fig

5.9d). At 30 weeks of HFD, it was observed that POMC-CreER mice displayed higher fasting blood glucose compared to POMC-NPAS4 KO mice. To further assess whether glucose homeostasis was altered by NPAS4 KO and HFD, monthly OGTTs were performed. In line with the biweekly blood glucose measurements, glucose tolerance was not different between the three genotypes before (5 weeks), at (9 weeks), and after (29 weeks) the body weight separation occurred (Fig 5.10a-f). Plasma insulin measured at 0 and 10 minutes during OGTTs were also not different between genotypes at any point during the 30 weeks of HFD (Fig 5.10g-i). Finally, the response to glycerol and insulin sensitivity was assessed with 2g/kg glycerol tolerance tests and insulin tolerance tests. The response to glycerol was not different between Npas4 flox and POMC-NPAS4 KO mice at 15 and 19 weeks of HFD (Fig 5.11a-d). Insulin tolerance tests also showed no differences at 10, 18, and 26 weeks of HFD (Fig 5.11e-g). These results show that NPAS4 KO specifically in ARC POMC neurons protects male mice from HFD-induced body weight gain over time, without affecting glucose homeostasis.

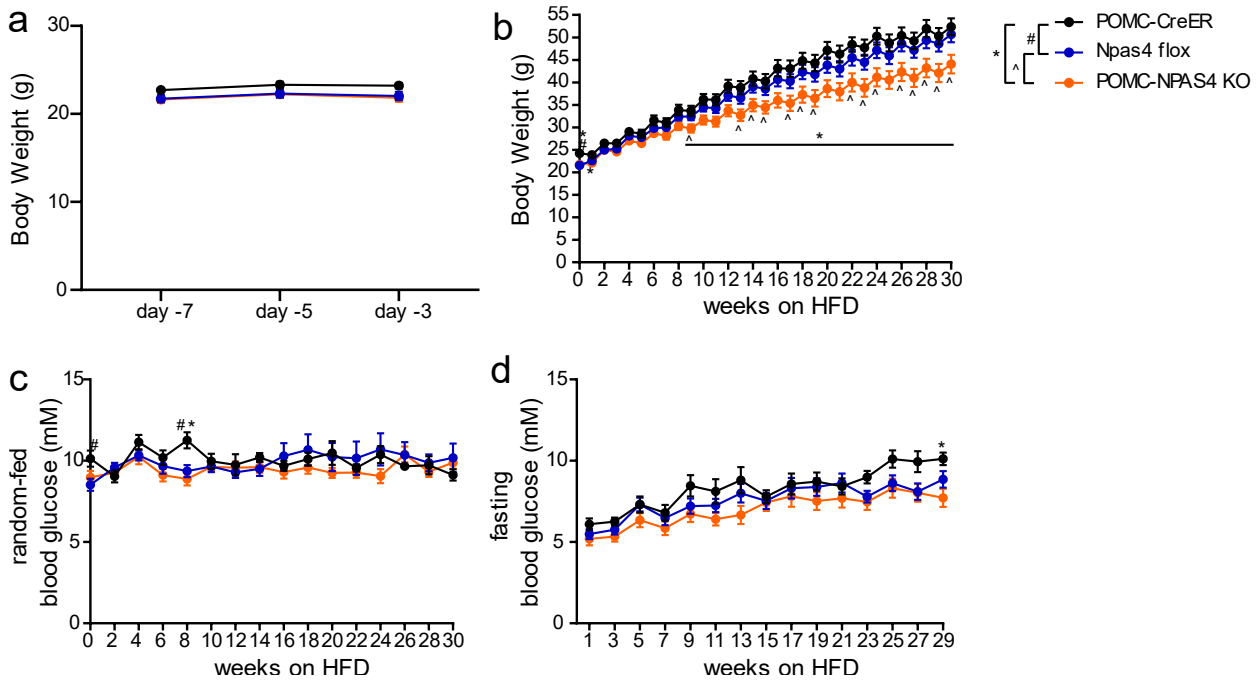

Figure 5.9 | POMC-NPAS4 KO mice gain less body weight over time on HFD without differences in glycemia. a, Body weights measured during tamoxifen administration to POMC-CreER (n=9), Npas4 flox (n=20), and POMC-NPAS4 KO (n=19) mice. **b,** Weekly body weight measurements of all genotypes during 30 weeks of HFD. **c-d,** Biweekly blood glucose measurements on random-fed (c) and 10 hour overnight fasted (d) mice from all genotypes on HFD. 2-way ANOVA with Tukey's multiple comparisons: *P < 0.05, (POMC-CreER vs POMC-NPAS4 KO); ^P < 0.05 (Npas4 flox vs POMC-NPAS4 KO); #P < 0.05 (POMC-CreER vs POMC-NPAS4 KO).

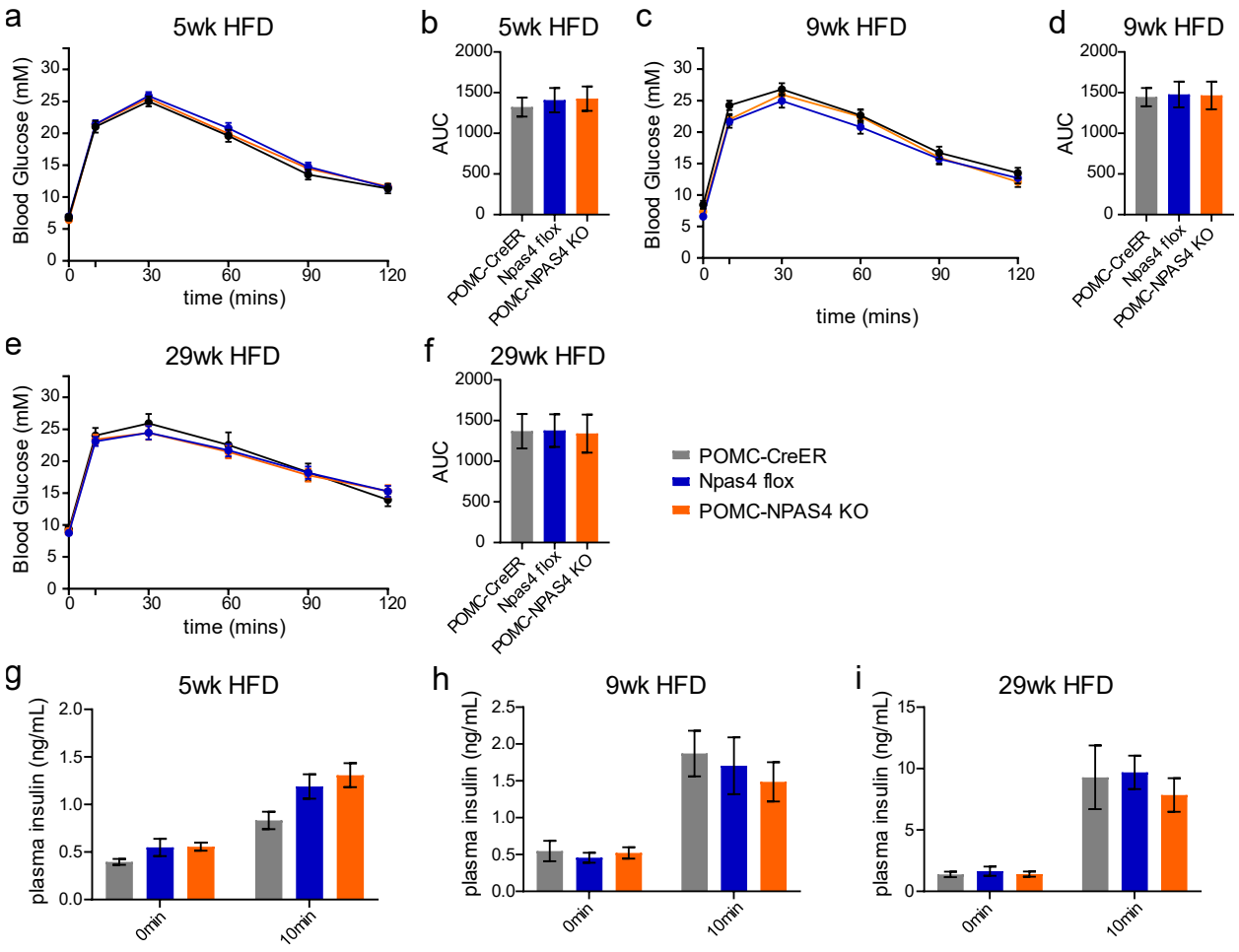

Figure 5.10 | POMC-NPAS4 KO mice show normal oral glucose tolerance and plasma insulin on HFD. a-f, Blood glucose measurements (a, c, e) and calculated AUC (b, d, f) from oral glucose tolerance tests performed on POMC-CreER (n=9), Npas4 flox (n=20), and POMC-NPAS4 KO (n=19) mice at 5 weeks (a, b), 9 weeks (c, d), and 29 weeks (e, f) of HFD. **g-i,** Plasma insulin measured at 0 minutes and 10 minutes of oral glucose tolerance tests at 5 weeks (g), 9 weeks (h), and 29 weeks (i) of HFD.

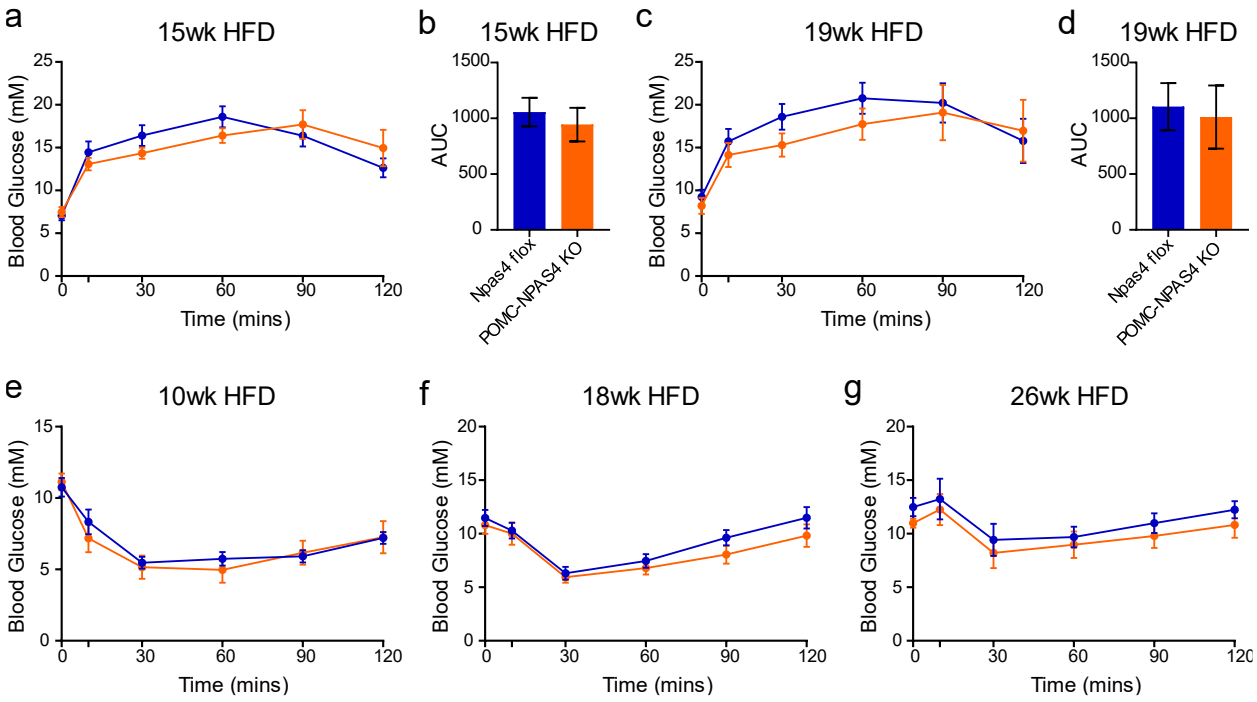

Figure 5.11 | POMC-NPAS4 KO mice show normal glycerol tolerance and insulin tolerance on HFD. a, Blood glucose measurements (a, c) and calculated AUC (b, d) from intraperitoneal glycerol tolerance tests performed on Npas4 flox (n=7) and POMC-NPAS4 KO (n=8) mice at 15 weeks (a, b) and 19 weeks (b, d) of HFD. **e-g,** Blood glucose measurements from intraperitoneal insulin tolerance tests performed on Npas4 flox (n=7) and POMC-NPAS4 KO (n=7) mice at 10 weeks (e), 18 weeks (f), and 26 weeks (g) of HFD.

5.7 Metabolic cage analyses in 6 week HFD POMC-NPAS4 KO mice

The data so far have shown that NPAS4 KO in POMC neurons only alters body weight during the development of diet-induced obesity. Due to the known role of ARC POMC neurons regulating food intake, I hypothesized that POMC-NPAS4 KO mice are protected from severe weight gain on HFD due to reduced food intake. A secondary possibility is that energy expenditure was increased in the KO mice regardless of food intake changes, as POMC neurons have been shown to affect activity and energy expenditure upon deletion of key genes for its function[368,369]. Either scenario would be a reasonable explanation behind why POMC-NPAS4 KO mice gain less weight on HFD.

To examine the effects of NPAS4 KO on food intake, activity, and energy expenditure, three POMC-NPAS4 KO mice, three POMC-CreER mice, and two Npas4 flox mice were placed in metabolic cages after 6 weeks of HFD. The mice were allowed to acclimate to the metabolic cages where they were singly-housed for 24 hours, then metabolic parameters were recorded for the following 72 hours. There were no differences observed in oxygen consumption (VO_2), carbon dioxide production (VCO_2), energy expenditure in estimated heat production or respiratory exchange ratio (RER) between the three genotypes (Fig 5.12a-d). Activity was measured as counts of infrared beam breakage as mice moved around within the cage, and while POMC-NPAS4 KO mice showed the most variability in activity, there were no significant differences seen between genotypes (Fig 5.12e-f).

Cumulative food intake over the 72 hours of metabolic cage analyses showed that POMC-NPAS4 KO may have reduced food intake compared to Npas4 flox mice ($P = 0.0508$), but not compared to POMC-CreER mice (Fig 5.13a-b). Water intake was not affected by NPAS4 KO (Fig 5.13c). Finally, none of the metabolic cage analyses were affected by differences in fat mass, lean mass, or total body weight, as body composition measurements before metabolic cages showed no differences between genotypes (Fig 5.13d).

The results of the metabolic cages suggest that there may be a slight reduction in food intake in the POMC-NPAS4 KO mice. The lack of statistical significance in the results was disappointing but expected from a small sample size. Unfortunately, this experiment could not be replicated due to persistent equipment failure, preventing further data acquisition from additional cohorts.

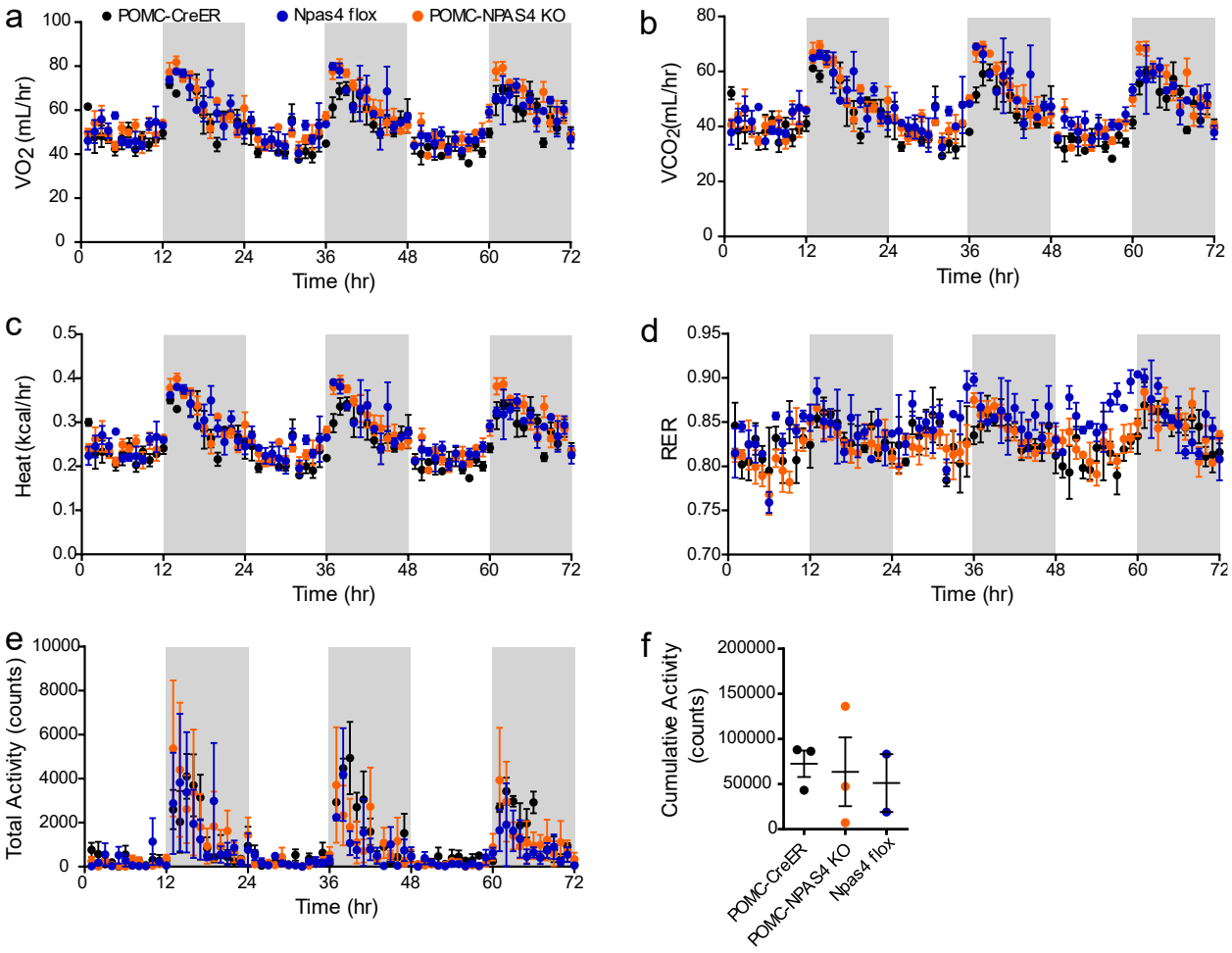

Figure 5.12 | POMC-NPAS4 KO mice show normal indirect calorimetry readouts and activity at 6 weeks of HFD. a, Oxygen consumption (VO_2) measurements (mL/hr) for POMC-CreER (n=3), Npas4 flox (n=2), and POMC-NPAS4 KO (n=3) mice. **b,** Carbon dioxide production (VCO_2) measurements (mL/hr) for all genotypes. **c,** Energy expenditure as heat production estimated from VO_2 (kCal/hr) for all genotypes. **d,** Respiratory exchange ratio (RER) for all genotypes. **e,** Locomotor activity over time in counts for all genotypes. **f,** Calculated cumulative locomotor activity in counts for each mouse in all genotypes.

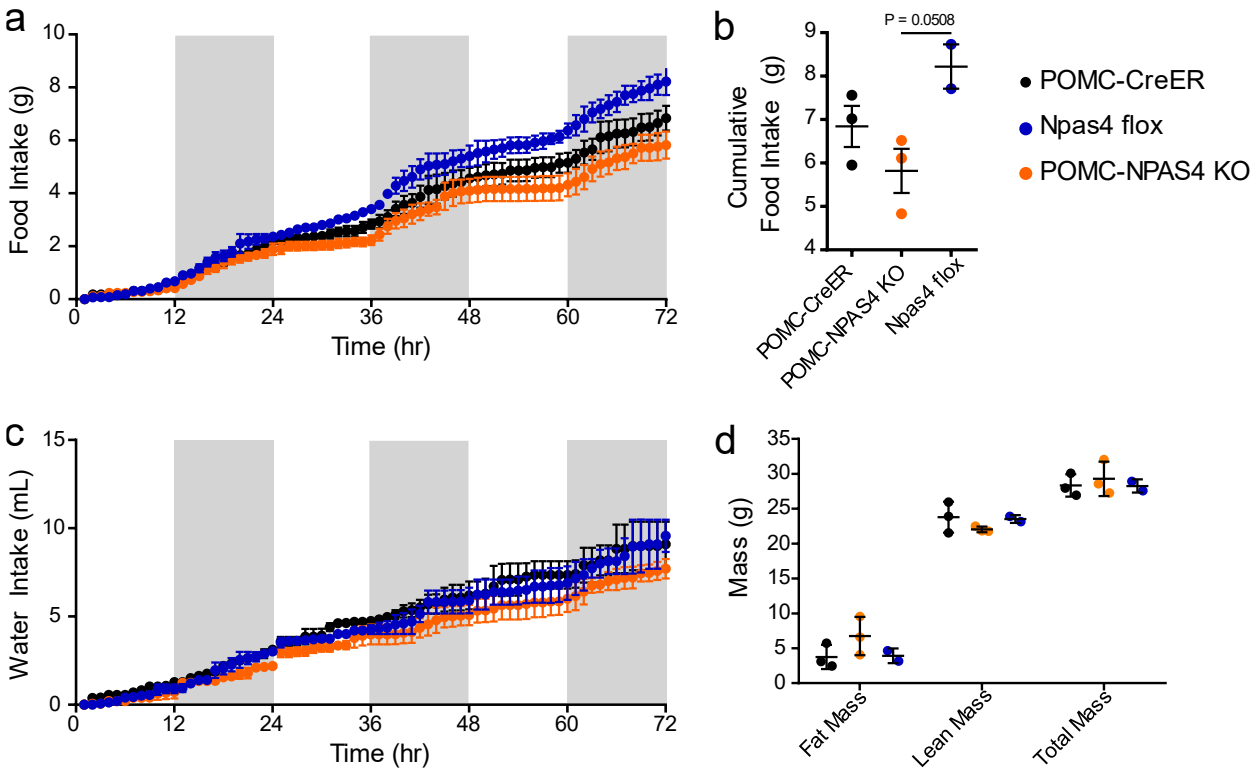

Figure 5.13 | POMC-NPAS4 KO mice show a trend of reduced food intake at 6 weeks of HFD. a, Food intake in grams over 72 hours for POMC-CreER (n=3), Npas4 flox (n=2), and POMC-NPAS4 KO (n=3) mice. **b,** Calculated cumulative food intake in grams over 72 hours for each mouse in all genotypes. **c,** Water intake in mL over 72 hours for all genotypes. **d,** Body composition showing fat mass, lean mass, and total mass in grams for each mouse before the 72 hours of metabolic cage analyses.

5.8 Reassessment of food intake in HFD-fed POMC-NPAS4 KO mice

Due to the unavailability of the metabolic cages for additional cohorts, an alternative method to perform follow-up assessments of food intake became necessary. I decided to measure food intake in control and NPAS4 KO mice manually and reassess the difference in food intake in a larger cohort than the one used for metabolic cages, and at an earlier time point of HFD feeding. Six POMC-CreER controls and six POMC-NPAS4 KO mice were singly housed after tamoxifen and body weight and food intake were measured weekly. Each week, 10 new pellets of HFD were given to the mice and the food remaining in the hoppers from the previous week was weighed, along with the uneaten crumbs from the cage floor. No body weight differences were

observed between controls and KO mice before or during the first 2 weeks of HFD feeding (Fig 5.14a). POMC-NPAS4 KO mice showed reduced food intake compared to POMC-CreER mice as early as 2 weeks of HFD (Fig 5.14b). Body composition assessment for four POMC-CreER and four POMC-NPAS4 KO mice at 2 weeks of HFD showed no differences in fat mass or lean mass in these animals (Fig 5.14c). When mice were fasted overnight and refed for 1 hour, there were no differences in their body weights before and after refeeding, their blood glucose levels before and after refeeding, and the amount of food eaten during the 1 hour. NPAS4 KO was also assessed at both 1 week and 2 weeks of HFD, to confirm that the difference in food intake was observed in mice with detectable NPAS4 KO. At 1 week of HFD, three additional POMC-CreER and POMC-NPAS4 KO mice were assessed, and the presence of fewer *Npas4*- *Pomc*+ cells was confirmed in KO mice (Fig 5.14g). In addition to the increased *Npas4*- *Pomc*+ cells seen at 0 weeks post-tamoxifen previously, *Npas4*-medium and *Npas4*-high populations were decreased at 1 week of HFD compared to POMC-CreER mice (Fig 5.14h). Similar results were seen at 2 weeks of HFD, although *Npas4*-low *Pomc*+ cells were also significantly decreased compared to POMC-CreER mice (Fig 5.14i-j).

Overall, these additional studies during the first two weeks of HFD show that in addition to what the metabolic cage data showed, POMC-NPAS4 KO mice display a reduction in food intake much earlier than expected during the first few weeks of HFD. This difference in food intake seems to be limited to *ad libitum* feeding behaviour, as refeeding dynamics did not show the same difference.

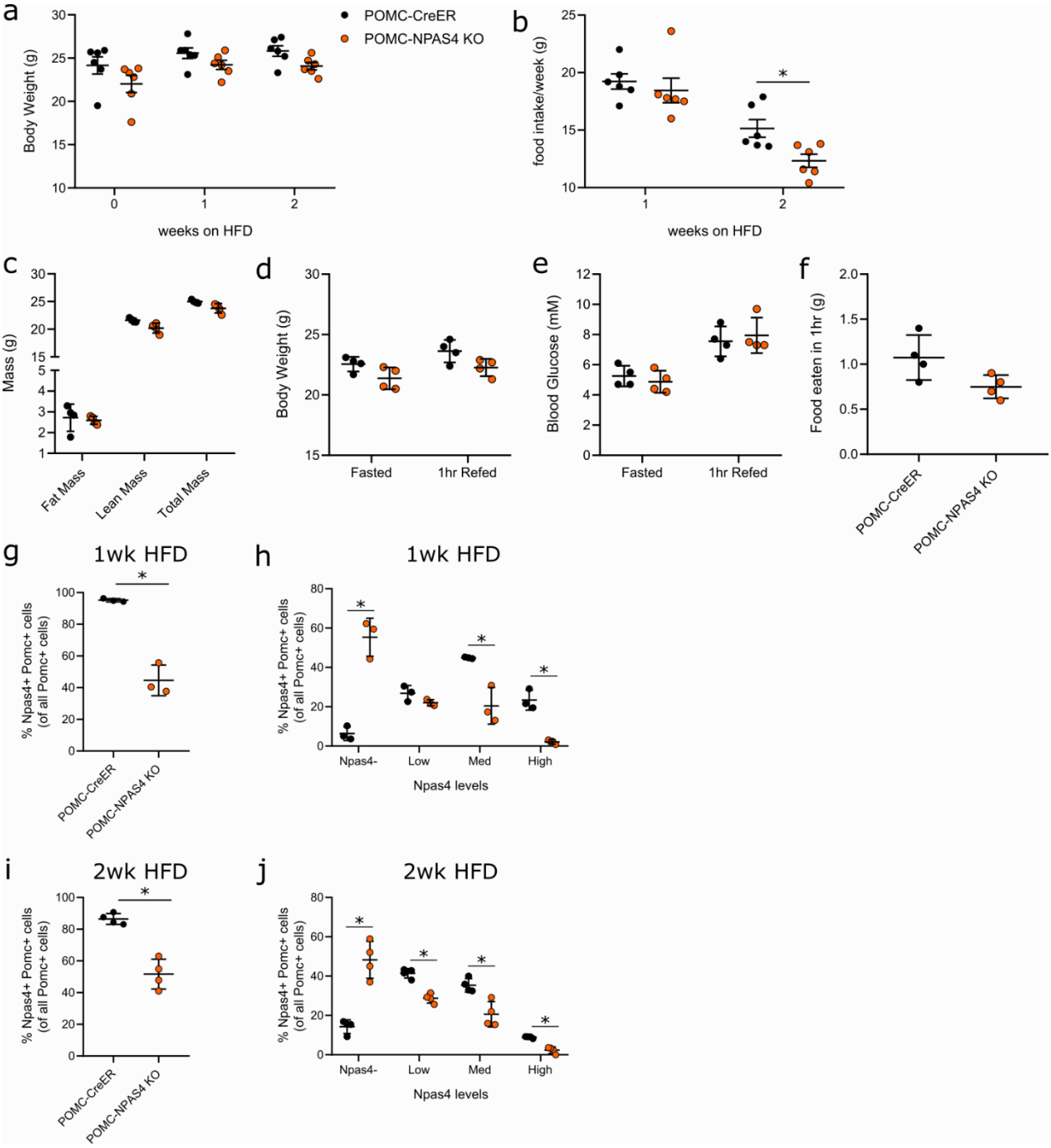

Figure 5.14 | POMC-NPAS4 KO mice show reduced food intake at 2 weeks of HFD, independent of body composition or body weight. a, Weekly body weight measurements for POMC-CreER (n=6) and POMC-NPAS4 KO (n=6) mice during 2 weeks of HFD. **b,** Manually measured food intake over a week for 2 weeks of HFD. Measurement at week 2 was before the mice were fasted overnight and refed for 1 hour. **c,** Body composition showing fat mass, lean mass, and total mass in grams for POMC-CreER (n=4) and POMC-NPAS4 KO (n=4) mice at 2 weeks of HFD. **d-f,** Body weight gained (d), blood glucose measurements (e), and food eaten (f) during 1 hour of refeeding after an overnight fast at 2 weeks of HFD for mice shown in c. **g,** Quantifications of *Npas4*-positive, *Pomc*-positive cells from arcuate nucleus sections as a

percentage of total *Pomc*-positive cells from RNAscope images. Brains were harvested after overnight fasting and 1 hour refeeding after 1 week of HFD. **h,** Breakdown of quantifications (g) into bins of *Npas4* expression levels: Npas4- = no *Npas4* signal in the *Pomc*-positive cell, Low = 1-3 *Npas4* punctae/cell, Med = 4-9 *Npas4* punctae/cell, and High = 10 or more *Npas4* punctae/cell. **i,** Quantifications of *Npas4*-positive, *Pomc*-positive cells from arcuate nucleus sections as a percentage of total *Pomc*-positive cells from RNAscope images. Brains were harvested after overnight fasting and 1 hour refeeding after 2 weeks of HFD. **l,** Breakdown of quantifications (i) into bins of *Npas4* expression levels as described in h. Data in c-j shown as mean $\pm$ SD. Student's t-test: *P <0.05.

5.9 Discussion

In this chapter, mice with NPAS4 KO specifically in ARC AgRP or POMC neurons were generated and characterized. A priority with studying these novel NPAS4 KO mouse lines was assessing recombination in both lines to ensure that CreER activity was occurring in the cells of interest. As with experiments in chapter 4, RNAscope was used to directly quantify the *Npas4* mRNA levels to confirm genetic knockout of *Npas4.* In both AgRP-CreER and POMC-CreER lines, only a 20% reduction in *Npas4+* cells was seen in brains harvested immediately after tamoxifen administration (0 weeks). The highest recombination efficiency observed with this method was 50% at 1 week and 2 weeks post-tamoxifen. This suggests that either the knockout process takes 1 week to 2 weeks to reduce the *Npas4* levels, or a wide range of variability in recombination efficiency from mouse to mouse. The latter seems quite plausible, as seen from the POMC-NPAS4 KO mice in the HFD group that became obese despite the majority of mice being protected from body weight gain. The KO mice that became obese at levels comparable to control groups could have been due to lower recombination efficiency in those animals. The tamoxifen used to induce recombination was administered orally, but it was confirmed by visualizing tdT expression in the ARC neurons that at least 50% of the POMC neurons are undergoing CreER-mediated recombination, so the method of inducing recombination is not problematic. However, the amount of tamoxifen that reaches the ARC could be slightly different

from animal to animal, resulting in recombination variability.

The results of the AgRP-NPAS4 KO mice were difficult to interpret due to the presence of a strong phenotype caused by the AgRP-CreER transgene. AgRP-CreER^{+} animals, whether they were controls or AgRP-NPAS4 KO mice, were much lighter than Npas4 flox controls even before tamoxifen was administered when mice were 6 weeks old. In fact, the difference in body weight was seen much earlier during weaning, to the point where AgRP-NPAS4 KO mice were identifiable from their littermate Npas4 flox controls before genotyping. With such an early difference in body weight, it could suggest a developmental problem in embryonic stages. If the addition of the *CreER* transgene disrupted *Agrp* expression levels or other genes important for body size, it's possible that pups at postnatal ages could have nursed less from the dam and were therefore smaller than their littermates. This resulted in the Npas4 flox controls and AgRP-CreER controls showing vastly different values, making the actual effect of NPAS4 KO difficult to interpret. In the future, this study could be repeated if a method of specifically knocking out *Npas4* in postnatal AgRP neurons without causing transgenic effects is available.

A key finding in chapter 5 was that HFD-fed POMC-NPAS4 KO mice gained less weight over time and ate less HFD in the first few weeks of switching from Chow to HFD. Across the cohorts used in this chapter, body weights were generally not different in the early weeks of HFD, but a food intake difference at two weeks of HFD was seen. In addition, the metabolic cages suggested a food intake difference at six weeks of HFD, but this was not statistically significant. Nevertheless, with no other measured metabolic parameters showing differences between controls and POMC-NPAS4 KO groups, it is almost certain that the difference in body

weight was caused by a difference in food intake.

A resulting question from the findings, however, is how an early difference in food intake leads to a significant body weight difference eight weeks later. Assuming the food intake per week continues to be lower in the POMC-NPAS4 KO mice from two weeks to ten weeks when the body weight difference is seen, there was most likely a change of POMC neuronal function in POMC-NPAS4 KO mice with the reduction in NPAS4. The data suggest that NPAS4 is normally important for decreasing POMC tone somehow, and the knockout of NPAS4 results in increased POMC neuronal output, which results in decreased food intake over time. A possible explanation draws from known roles of NPAS4 in other neuronal populations. In hippocampal neurons, NPAS4 is required for the formation and maintenance of inhibitory GABAergic synapses in the postsynaptic cell [300]. In the ARC, AgRP neurons are known to directly inhibit POMC neurons by GABAergic signalling [370]. If loss of NPAS4 in POMC neurons led to degradation of GABAergic synapses on the POMC neuron, it could lead to decreased POMC suppression over time. In a HFD setting where POMC neurons are stimulated and activity is increased early on, POMC neurons that had fewer GABAergic synapses would be activated more frequently, and this could lead to decreased food intake and body weight gain over time. Another possible explanation is that the food intake and body weight difference was a result of overcompensation by the 50% of POMC neurons that did not undergo recombination. In figure 5.5a, a few *Pomc+* cells with very high *Npas4* expression (dense clusters of bright green signal) are visible, and in all quantifications of KO mice, there is a small percentage of *Npas4*-high cells.

In conclusion, POMC-CreER mediated deletion of NPAS4 in ARC POMC neurons leads to

reduced weight gain in an obesogenic environment, potentially due to reduced food intake. At the very least, the data shown in this chapter show for the first time that NPAS4 in POMC neurons has a role in regulating food intake and by extension, body weight. In the future, the excitability or electrophysiological activity of POMC neurons lacking NPAS4 could be measured to uncover the electrophysiological consequences of NPAS4 knockout in these cells. In addition to measuring functional activity, another future direction to consider is investigating the molecular mechanism behind the phenotype of the POMC-NPAS4 KO mice. Since NPAS4 is a transcription factor, additional experiments to examine the transcriptional changes that have occurred in response to NPAS4 KO in POMC neurons exposed to HFD would be useful to determine how NPAS4 KO alters POMC neuronal function.

Chapter 6: Investigating the feeding-regulated and NPAS4-regulated transcriptomic changes in POMC neurons during obesity development

6.1 Rationale

Even before scRNA-seq technology, the ARC was already known to be heterogeneous. Aside from documented neuronal subtypes based on their primary neuropeptides, neurons can also be classified as excitatory or inhibitory based on whether they are glutamatergic or GABAergic. In addition to neurons, the bulk of the CNS is actually composed of glial cells. Just within the ARC and ME alone, there are tanycytes, ependymocytes, astrocytes, microglia, oligodendrocytes, and endothelial cells making up fenestrated capillaries at the ME. Even POMC neuron heterogeneity has already been reported without the use of scRNA-seq. For example, there are populations of neurons that are differentially activated by insulin that were discussed in chapter 4[106,107]. There are also reports of leptin-sensitive and leptin-insensitive POMC neurons[371]. Now with recent advances in single cell technology, multiple groups have already performed transcriptomic profiling of the complex MBH region. Most have focused on comparing fasting conditions to *ad libitum* fed conditions, and utilized a fluorescent reporter protein whose expression is driven by a gene of interest that marks the region[322,372,373]. These approaches make it infinitely easier to isolate the precious few neuronal populations of interest from the adult mouse brain, since the ARC is a small region, and the POMC neurons are estimated to be relatively rare.

Data in chapter 5 showed that POMC-NPAS4 KO mice ate less food during early weeks of HFD and eventually were protected from HFD-induced weight gain. It was hypothesized that the reduction in food intake could have been caused by altered POMC neuronal function as a result of the NPAS4 KO, but the molecular mechanism behind such changes were not addressed in

chapter 5. Therefore, these molecular changes will be explored in chapter 6 using scRNA-seq on cells from the MBH of POMC-CreER controls and POMC-NPAS4 KO mice that have been fed HFD. The body weight difference became significant at 9-10 weeks of HFD, but this was not chosen as the time point for scRNA-seq, because the difference in body weight was expected to cause secondary effects in the mice. It's been shown in chapter 4 that *Npas4* expression is elevated in ARC POMC neurons at 6 weeks compared to Chow-fed animals, and it was shown in chapter 5 that POMC-NPAS4 KO mice may have reduced food intake at 6 weeks of HFD. Therefore, 6 weeks of HFD was chosen as the time point to perform scRNA-seq on POMC-CreER controls and POMC-NPAS4 KO mice in order to identify potentially NPAS4-regulated genes in POMC neurons that may explain the mechanism behind the reduced food intake. In addition, the two genotypes of mice would be fasted or refed for 1 hour following the fast, in order to identify ARGs that were specifically regulated by acute refeeding in POMC neurons.

6.2 scRNA-seq of ARC from fasted and refed 6 week HFD mice

The primary aim of this experiment was to identify genes in the ARC POMC neurons that are regulated by an acute refeeding period following a fast, and genes that potentially regulated by NPAS4. The scRNA-seq libraries were generated from the ARC of mice from four different groups fed HFD for 6 weeks after tamoxifen: 1) fasted and 1 hour refed POMC-CreER, 2) fasted POMC-CreER, 3) fasted and 1 hour refed POMC-NPAS4 KO, and 4) fasted POMC-NPAS4 KO. To isolate the ARC, mice were fasted overnight, refed with HFD for 1 hour if in the refeeding group, then euthanized for brain harvests immediately. A schematic of the experimental groups and protocol is found in figure 6.1a. 2 thick coronal sections (~0.5mm) were shaved from the brains to contain the bulk of the MBH, then pie-shaped sections were dissected out from the

regions surrounding the ventral regions of the 3rd ventricle. The neural tissue was then dissociated with papain and trituration, and the resulting cell solution was filtered, counted, and used immediately for droplet-based single cell library generation.

Following sequencing of pooled libraries, data processing and analysis was performed with publicly available software (Fig 6.1b). Processing of the raw sequencing files was performed with the Cell Ranger software, version 7.0.0 (10x Genomics). BCL files from sequencing outputs were used to generate FASTQ files that were demultiplexed into individual samples. The demultiplexed sample FASTQ files were combined per sample from multiple sequencing runs if necessary, and aligned to a reference genome that was custom-generated by adding the *tdtomato* sequence onto the existing GRCm38 genome. Counts of genes, cells, and UMIs were generated by the software and the outputs were moved to Rstudio for further analysis with Seurat version 4.0.4. First, Cell Ranger outputs were converted to Seurat objects, and the number of genes, number of counts, and percentage of mitochondrial genes (any gene beginning with "*Mt*-") per cell were visualized in each sample to determine library quality and filtering thresholds. Since it is known that cells with high percentage of mitochondrial genes were most likely dying or under great stress during sample preparation, and should not be included in further analysis, the threshold for mitochondrial genes was set at 20%/cell. All cells that expressed greater than 7500 genes or greater than 20% mitochondrial genes/cell were filtered and removed from further analysis (Fig 6.2a). This filtering process did not remove a large number of cells overall (Table 6.1). Post-filtering, samples were normalized by SCTransform and integrated to form one Seurat object containing 41883 cells. The success of the filtering was confirmed by visualizing the same QC parameters across the two genotypes and two conditions. Going forward, cells from POMC-CreER controls will be called CT and cells from POMC-NPAS4 KO mice will be called KO.

There were no differences between the number of genes, number of counts, or the percentage of mitochondrial genes/cell between refed and fasted or between CT and KO (Fig 6.2b).

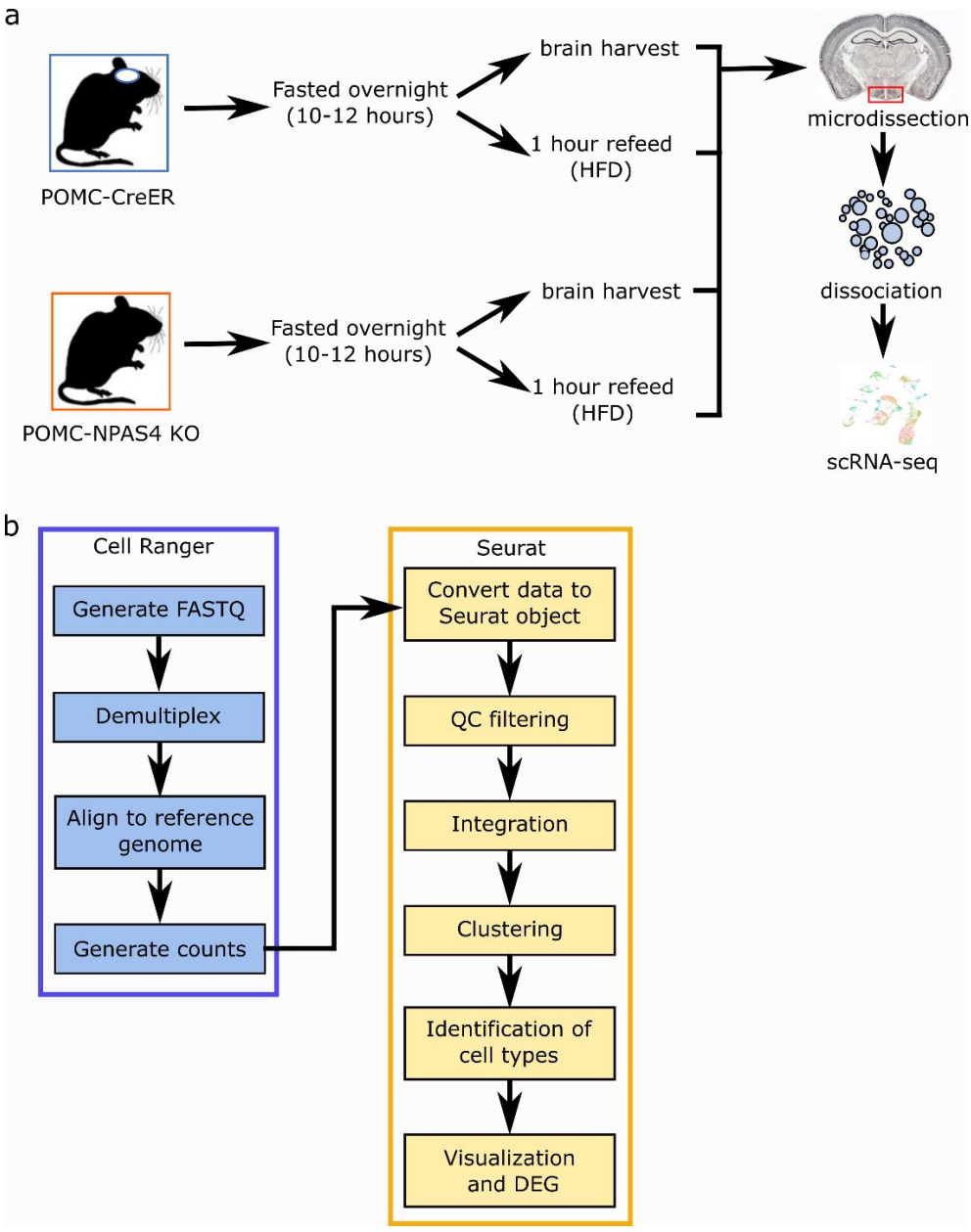

Figure 6.1 | Strategy of using scRNA-seq to investigate feeding-regulated and NPAS4-regulated genes in POMC neurons. a, Overview of experimental groups used for mouse ARC scRNA-seq and key steps in sample preparation. **b,** Pipeline of data analysis after sequencing. Steps in blue boxes indicate data processing stages performed with the Cell Ranger v7 software (10x Genomics). Steps in yellow boxes indicate downstream QC and data analysis steps performed in Seurat, a publicly available Rstudio package.

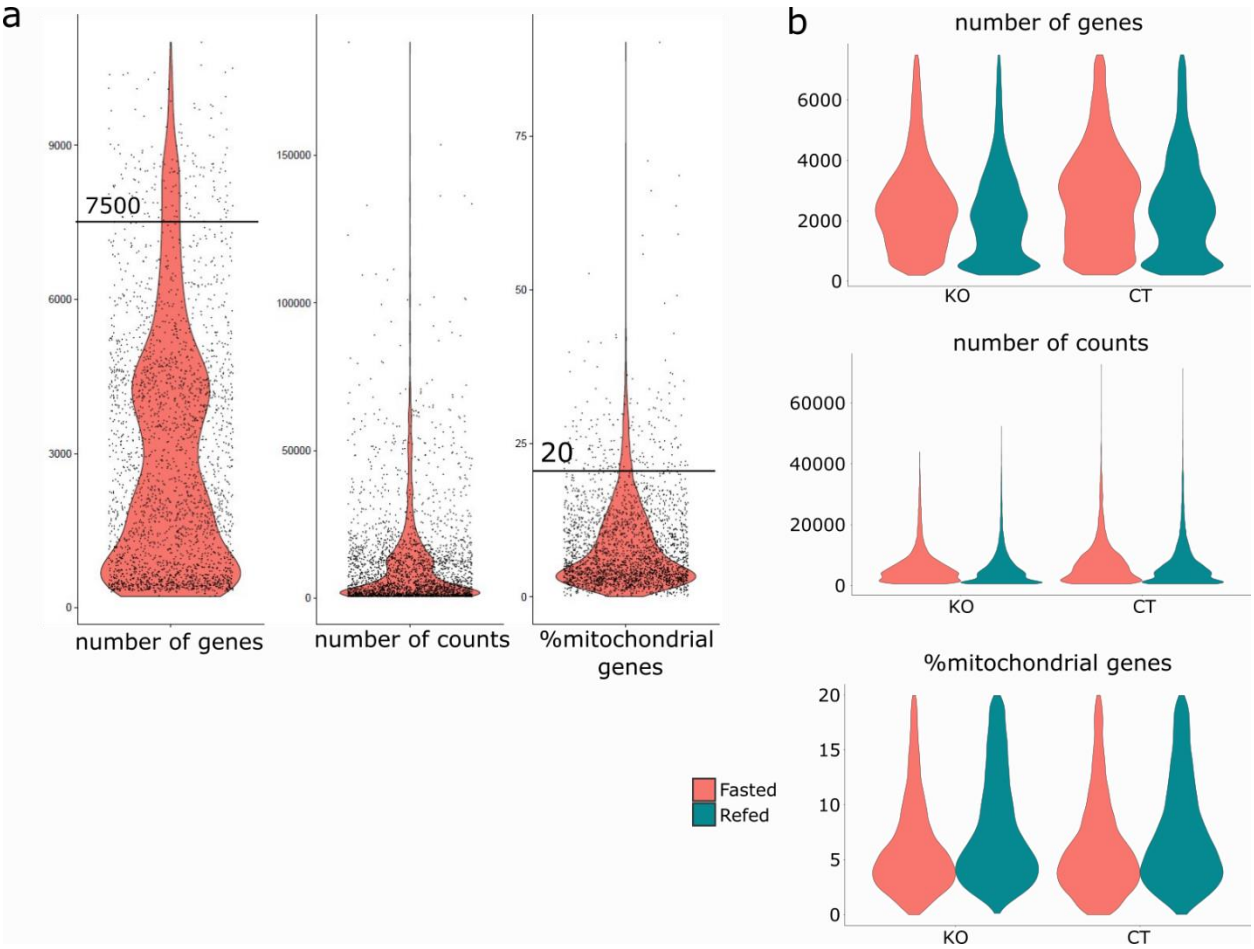

Figure 6.2 | Quality assessment and filtering of scRNA-seq data. a, Violin plots showing the number of genes/cell, number of counts (UMI; number of mRNA molecules), and the percentage of mitochondrial genes/cell for a representative sample, Control 3. Black lines at 7500 genes/cell and 20% mitochondrial genes/cell indicate thresholds used for filtering cells. **b,** Violin plots showing the number of genes/cell, number of counts, and the percentage of mitochondrial genes/cell in all samples after filtering and integration, split into genotypes and conditions. KO = POMC-NPAS4 KO, CT = POMC-CreER controls.

Table 6.1 Sample information and cell numbers at key steps for mouse ARC scRNA-seq

ID	Genotype	Group	Body weight (g)	Sequenced cells (Cell Ranger)	Mean reads/cell (Cell Ranger)	After creating Seurat object	After QC filtering
1	Control	Refed	36.5	5360	36548	5353	4698
2	Control	Refed	32.9	3478	50763	3471	3094
3	Control	Refed	30.8	2645	98267	2640	2261
4	Control	Refed	29.7	1865	140861	1860	1613
5	Control	Fasted	25.7	1954	38781	1952	1769
6	Control	Fasted	26	1958	41760	1948	1816
7	Control	Fasted	31.7	2567	80678	2559	2233
8	Knockout	Refed	36.2	5073	35498	5065	4143
9	Knockout	Refed	32.1	4319	41281	4310	3932
10	Knockout	Refed	26.4	6529	46033	6524	5765
11	Knockout	Fasted	29.7	2008	39908	1999	1831
12	Knockout	Fasted	27.6	4133	23017	4125	3969
13	Knockout	Fasted	26.3	5270	37615	5249	4759

6.3 Clustering and identification of biological cell types

At this point, the dataset was composed of 41883 mouse ARC cells, integrated from all genotypes and conditions. This was the sum of 24399 (58%) KO cells and 17484 (42%) CT cells, or 16377 (39%) fasted cells and 25506 (61%) refed cells. The 41883 cells were clustered at a resolution of 0.6 and visualized in UMAP space as 32 different clusters (Fig 6.3a). As with data in chapter 3, it was important to check whether this clustering was overly influenced by any

genotypes or conditions; this was of particular concern, as data from 13 different biological replicates from two genotypes and two conditions were integrated into a single object for analysis. If any single cluster greatly differed from the overall composition of cells from either genotype or condition, it would be a cluster with a skewed proportion.

The percentage of cells from both genotypes were calculated from raw cell numbers in each cluster, and it became apparent that while there were more KO cells than CT cells overall, no clusters showed a skewed proportion (Fig 6.3b-c). In the same manner, the percentage of cells from both conditions were calculated, and it was determined that certain clusters did show slightly skewed proportions of fasted vs refed cells compared to the bulk of the clusters (Fig 6.4a). Clusters 7, 14, and 29 were all composed of slightly more refed cells than the bulk of clusters, and cluster 22 showed the opposite composition where more fasted cells than refed were found (Fig 6.4a-b). The most severe was cluster 7, which only had about 10% of fasted cells. However, for the great majority of the data, clustering was not influenced by genotype or condition.

Next, the biological identity of each of the 32 clusters was determined through examining expression plots of known marker genes for each cell type. The marker genes used were as follows: *Syt1* to mark neurons, *Olig1* to mark oligodendrocytes, *Agt* to mark astrocytes, *Ccdc153* to mark ependymocytes, *Gpr50* to mark tanycytes, *Cldn5* and *Myh11* to mark endothelial cells, and *C1qa* and *Mrc1* to mark microglia (Fig 6.5). It became apparent after examining marker genes that the separation of clusters were largely based on cell type, similar to the human islet dataset in chapter 3. Each cluster was assigned a unique name, based on an abbreviated form of

their biological cell type followed by a number based on the size of the cluster. Cluster names and cell types were added into the metadata to permanently label each cell with this information (Fig 6.6a-b). From this process, 7 neuron clusters (Neuron1-Neuron7), 7 astrocyte clusters (Astro1-Astro3), 3 ependymocyte clusters (Ependy1-Ependy3), 4 tanycyte clusters (Tany1-Tany4), 3 microglia clusters (Micro1-Micro3), 5 endothelial clusters (Endo1-Endo5), 3 oligodendrocyte clusters (Oligo1-Oligo3), and one mystery cluster that did not express any of the examined marker genes were identified. A complete list of the cell numbers from each genotype and condition, along with the cluster name and cell type for each cluster is found in Table 6.2.

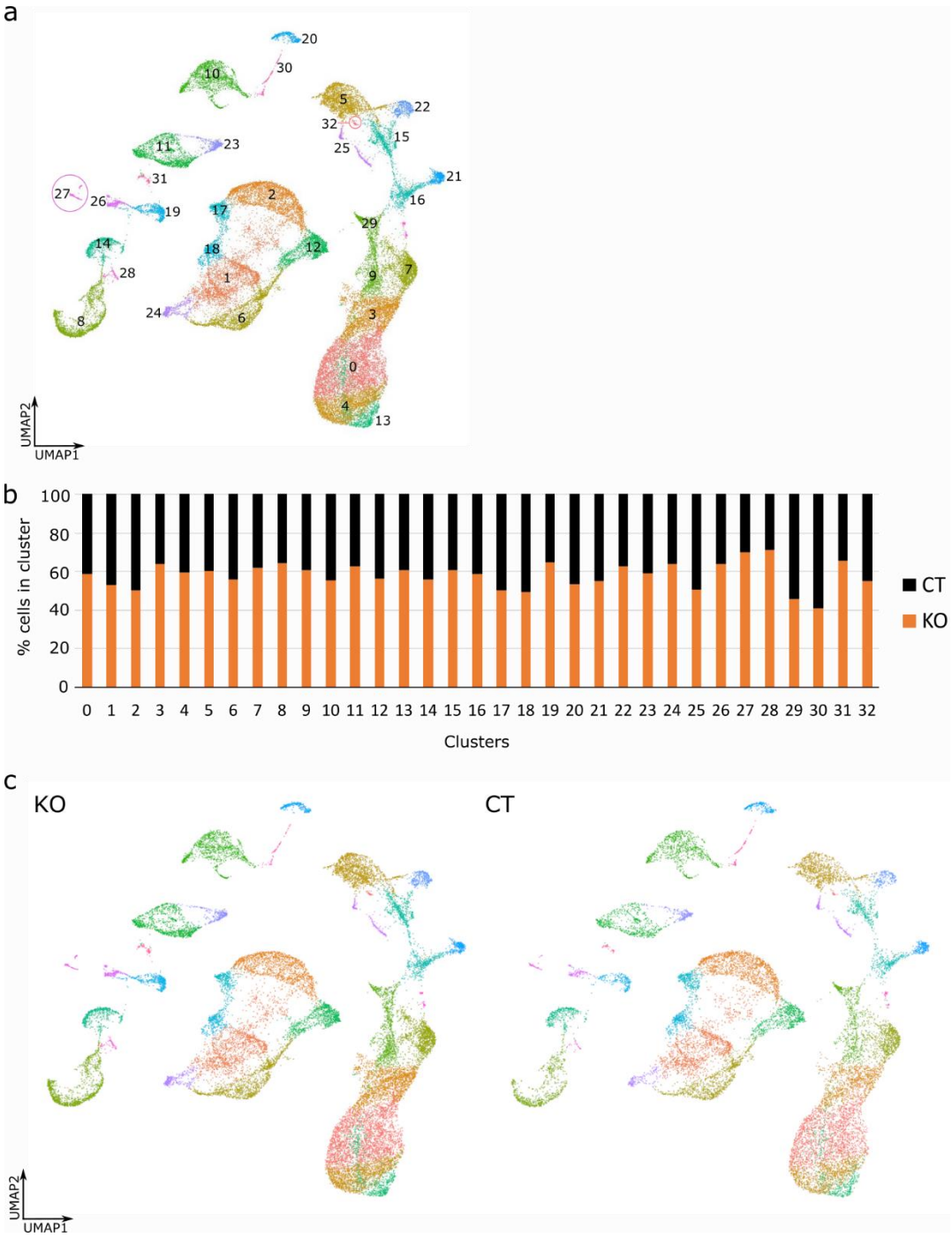

Figure 6.3 | Clustering of mouse ARC scRNA-seq data is not influenced by genotypes of mice. a, All samples integrated and shown as 32 clusters projected in UMAP space. Clusters are labelled with their original Seurat-assigned cluster numbers, based on the number of cells in each cluster, with cluster 0 being the largest. Clusters 27 and 32 have been placed in circles for ease of identification. **b,** Proportion bar graphs showing the % of cells from each genotype in each cluster. No cluster is composed of abnormally large %KO or %CT cells. **c,** All 32 clusters shown projected in UMAP space, split by genotype, to show all clusters contain KO and CT cells. KO = POMC-NPAS4 KO, CT = POMC-CreER controls.

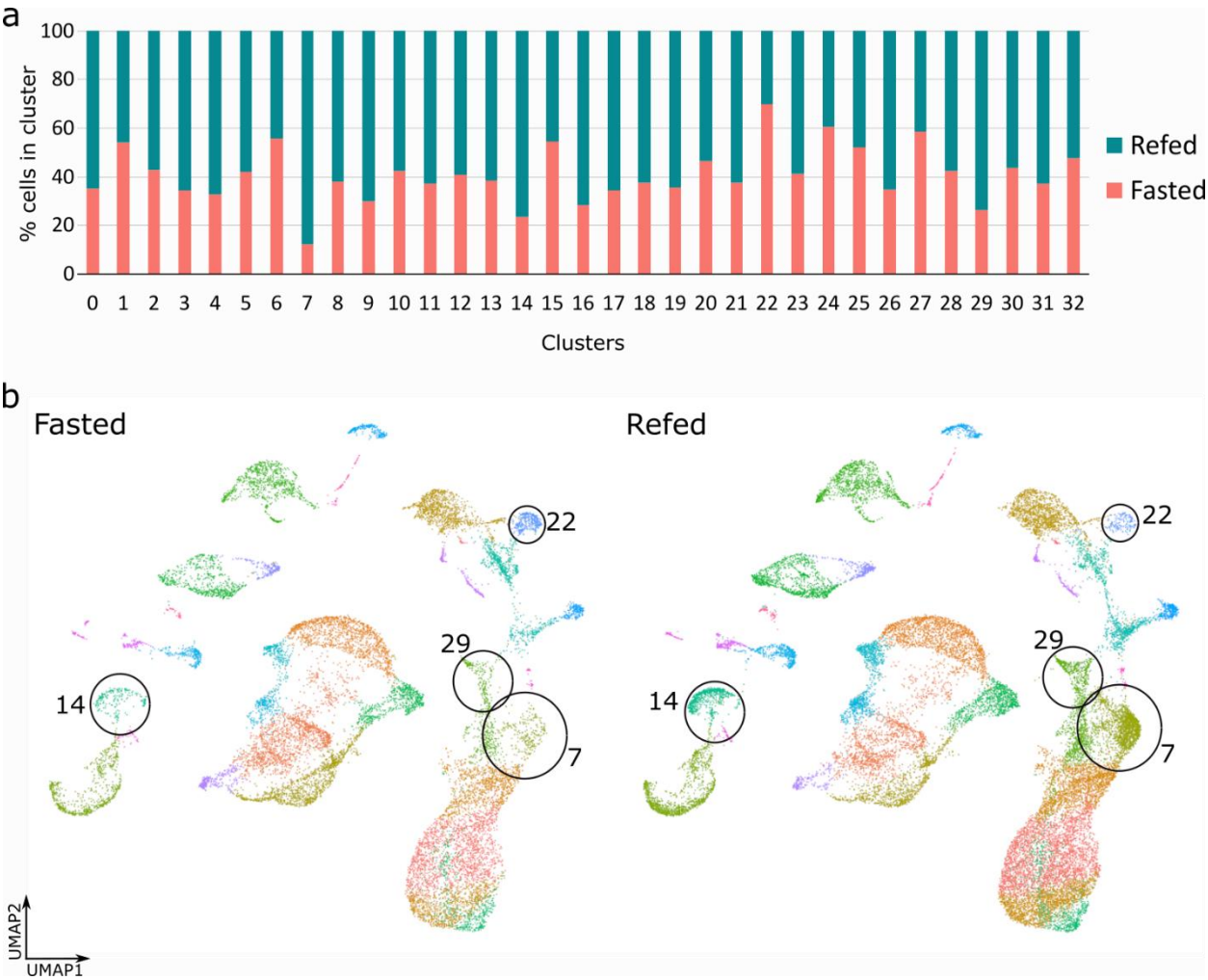

Figure 6.4 | Clustering of mouse ARC scRNA-seq data is not influenced by the feeding states of mice. a, Proportion bar graphs showing the % of cells from either fasted or refed conditions in each cluster. **b,** All 32 clusters shown projected in UMAP space, split by the feeding states, to show all clusters contain fasted and refed cells. Clusters 7, 14, 22, and 29 are located in black circles to highlight their skewed composition of fasted and refed cells from the average.

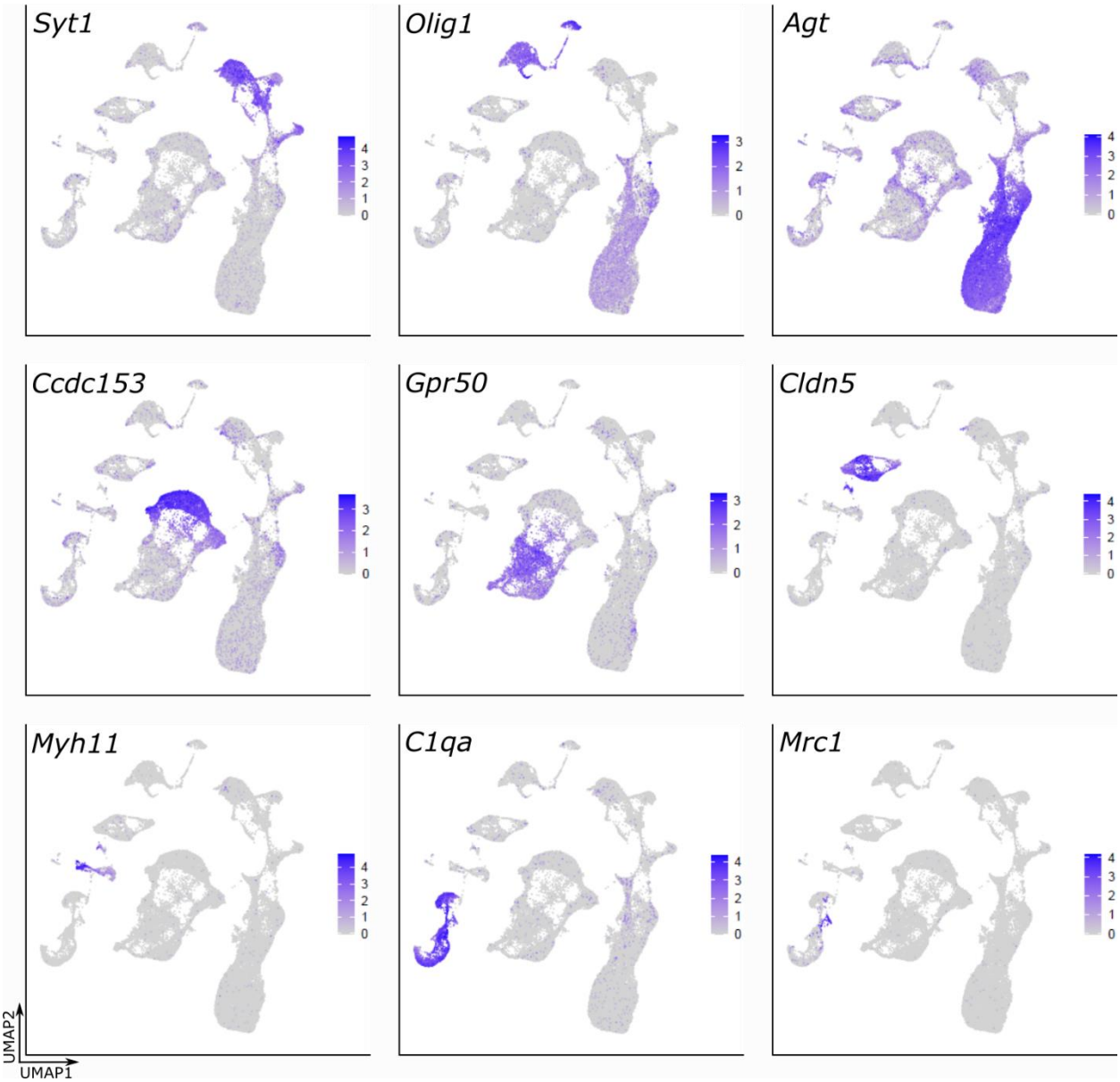

Figure 6.5 | Known marker genes for expected cell types in the mouse ARC for biological annotation of clusters. Expression plots of individual genes projected in UMAP space to identify the biological cell types for each cluster. Expression is shown for *Syt1* to mark neurons, *Olig1* to mark oligodendrocytes, *Agt* to mark astrocytes, *Ccdc153* to mark ependymocytes, *Gpr50* to mark tanycytes, *Cldn5* and *Myh11* to mark endothelial cells, and *C1qa* and *Mrc1* to mark microglia.

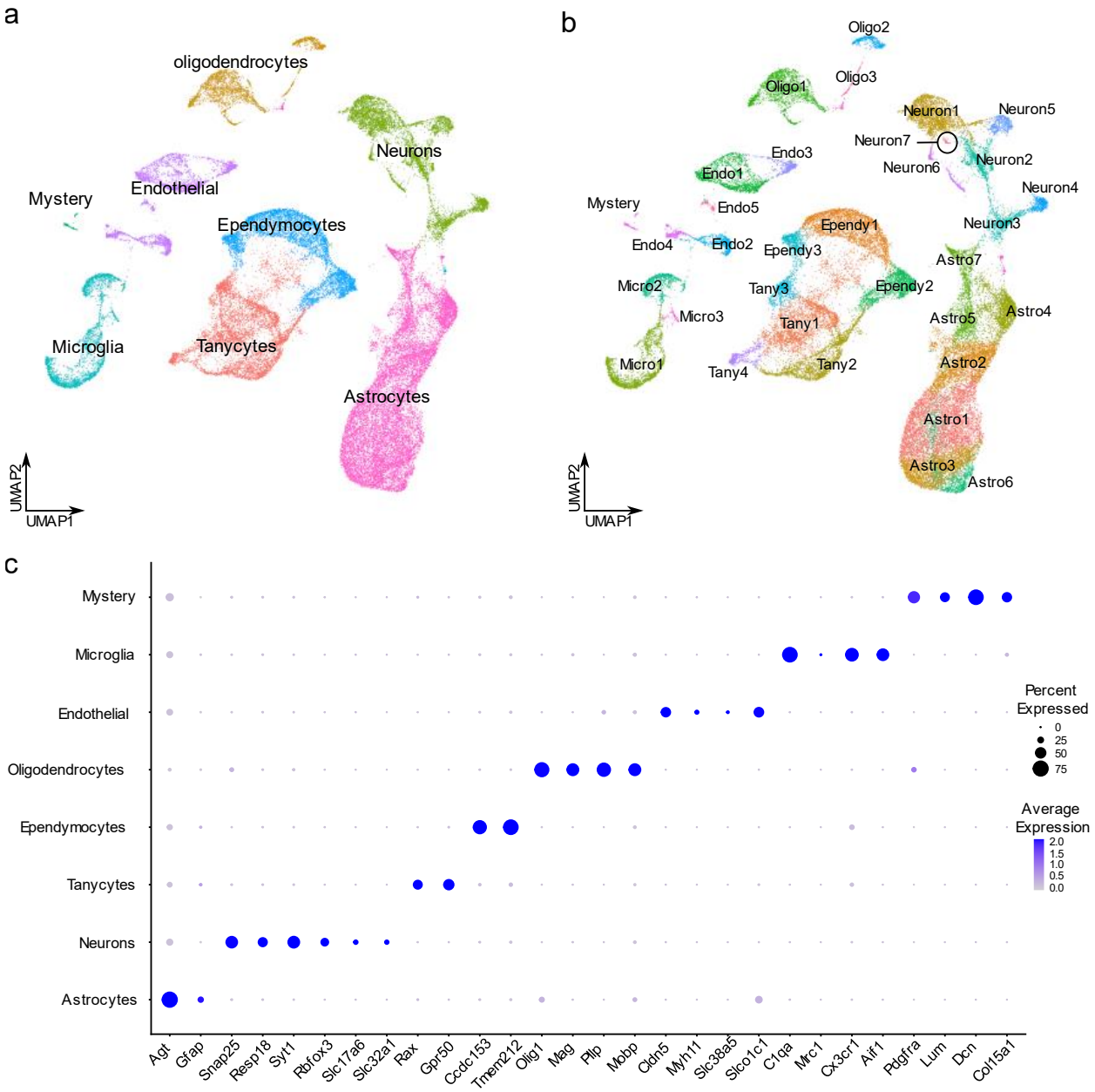

Figure 6.6 | Eight cell types are identified within the mouse ARC scRNA-seq dataset. a, All cells projected in UMAP space, identified by their biological cell types. **b,** All cells projected in UMAP space, identified by their biological cluster names, assigned based on cell type and cluster size. Cluster names are based on an abbreviated form of their biological cell type, followed by a number that is assigned based on cluster size within the cell type. Neuron1-Neuron7 are neurons, Astro1-Astro7 are astrocytes, Ependy1-Ependy3 are ependymocytes, Tany1-Tany4 are tanycytes, Micro1-Micro3 are microglia, Endo1-Endo5 are endothelial cells, Oligo1-Oligo3 are oligodendrocytes, and there is one Mystery cluster that did not express any of the known cell type markers. **c,** dotplot of the top DEGs expressed per cell type. Dot sizes represent percent of cells expressing a gene on the x-axis ("Percent Expressed") and shade of blue represents expression levels in the cell type ("Average Expression"), with darker blue being higher average expression.

6.4 Detection of ARC neurons and immediate early genes

At this point, cell types and cluster identification had been completed. It was now possible to perform a series of checks into the neurons in the dataset before moving forward with more detailed analyses. The dissection method used to procure samples was overall limited in its specificity due to the lack of the tdTomato lineage marker in almost all POMC-NPAS4 KO mice used for the experiment. The tiny region that comprises the mouse ARC was a further barrier to perfect microdissection, so most samples were comprised of cells from the general MBH, rather than the ARC specifically. Therefore, it was important to confirm that the neuronal populations of interest had been correctly included in the dissected tissue. Expression plots of *Agrp* and *Npy* to mark AgRP/NPY neurons showed a very clear segregation of the expression in cluster 25, or Neuron6 (6.7a). Meanwhile, *Pomc* and *Cartpt* expression that marked POMC/CART neurons were more diffused throughout several neuronal clusters, but the expression of the two genes did appear to overlap in the same cells. *Npas4,* the gene of interest in this study, was also confirmed to be expressed throughout neurons, albeit at a low absolute level, which was already shown through the previous RNAscope experiments in chapters 4 and 5 (Fig 6.7b). Aside from *Npas4,* several other immediate early genes were also visualized in the dataset. *Fos*, *Egr1,* and *Arc* are all well-known immediate early genes in the CNS, and they showed varying degrees of expression in multiple cell types (Fig 6.7c). In comparison to these three other immediate early genes, the neuronal specificity of *Npas4* across the cell types was clearly shown.

Table 6.2 Number of cells from each genotype and condition for each unique cluster

Seurat cluster #	Cluster name	Cell type	KO cells (% of total)	CT cells (% of total)	Fasted cells (% of total)	Refed cells (% of total)
0	Astro1	Astrocytes	58.7	41.3	35.1	64.9
1	Tany1	Tanycytes	52.9	47.1	54.1	45.9
2	Ependy1	Ependymocytes	50.2	49.8	42.7	57.3
3	Astro2	Astrocytes	63.8	36.2	34.4	65.6
4	Astro3	Astrocytes	59.6	40.4	33.0	67.0
5	Neuron1	Neurons	60.1	39.9	42.1	57.9
6	Tany2	Tanycytes	56.0	44.0	55.9	44.1
7	Astro4	Astrocytes	62.1	37.9	12.3	87.7
8	Micro1	Microglia	64.1	35.9	38.0	62.0
9	Astro5	Astrocytes	60.5	39.5	30.1	69.9
10	Oligo1	Oligodendrocytes	55.4	44.6	42.4	57.6
11	Endo1	Endothelial	62.8	37.2	37.4	62.6
12	Ependy2	Ependymocytes	56.3	43.7	40.9	59.1
13	Astro6	Astrocytes	60.7	39.3	38.2	61.8
14	Micro2	Microglia	56.0	44.0	23.6	76.4
15	Neuron2	Neurons	60.7	39.3	54.7	45.3
16	Neuron3	Neurons	58.8	41.2	28.3	71.7
17	Ependy3	Ependymocytes	50.1	49.9	34.2	65.8
18	Tany3	Tanycytes	49.5	50.5	37.6	62.4
19	Endo2	Endothelial	64.6	35.4	35.5	64.5
20	Oligo2	Oligodendrocytes	53.5	46.5	46.3	53.7
21	Neuron4	Neurons	54.9	45.1	37.7	62.3
22	Neuron5	Neurons	62.6	37.4	69.9	30.1
23	Endo3	Endothelial	59.0	41.0	41.2	58.8
24	Tany4	Tanycytes	64.0	36.0	60.5	39.5
25	Neuron6	Neurons	50.8	49.2	52.0	48.0
26	Endo4	Endothelial	64.0	36.0	34.7	65.3
27	Mystery	Mystery	69.8	30.2	58.6	41.4
28	Micro3	Microglia	71.2	28.8	42.5	57.5
29	Astro7	Astrocytes	45.6	54.4	26.5	73.5
30	Oligo3	Oligodendrocytes	40.9	59.1	43.6	56.4
31	Endo5	Endothelial	65.7	34.3	37.4	62.6
32	Neuron7	Neurons	55.0	45.0	47.5	52.5

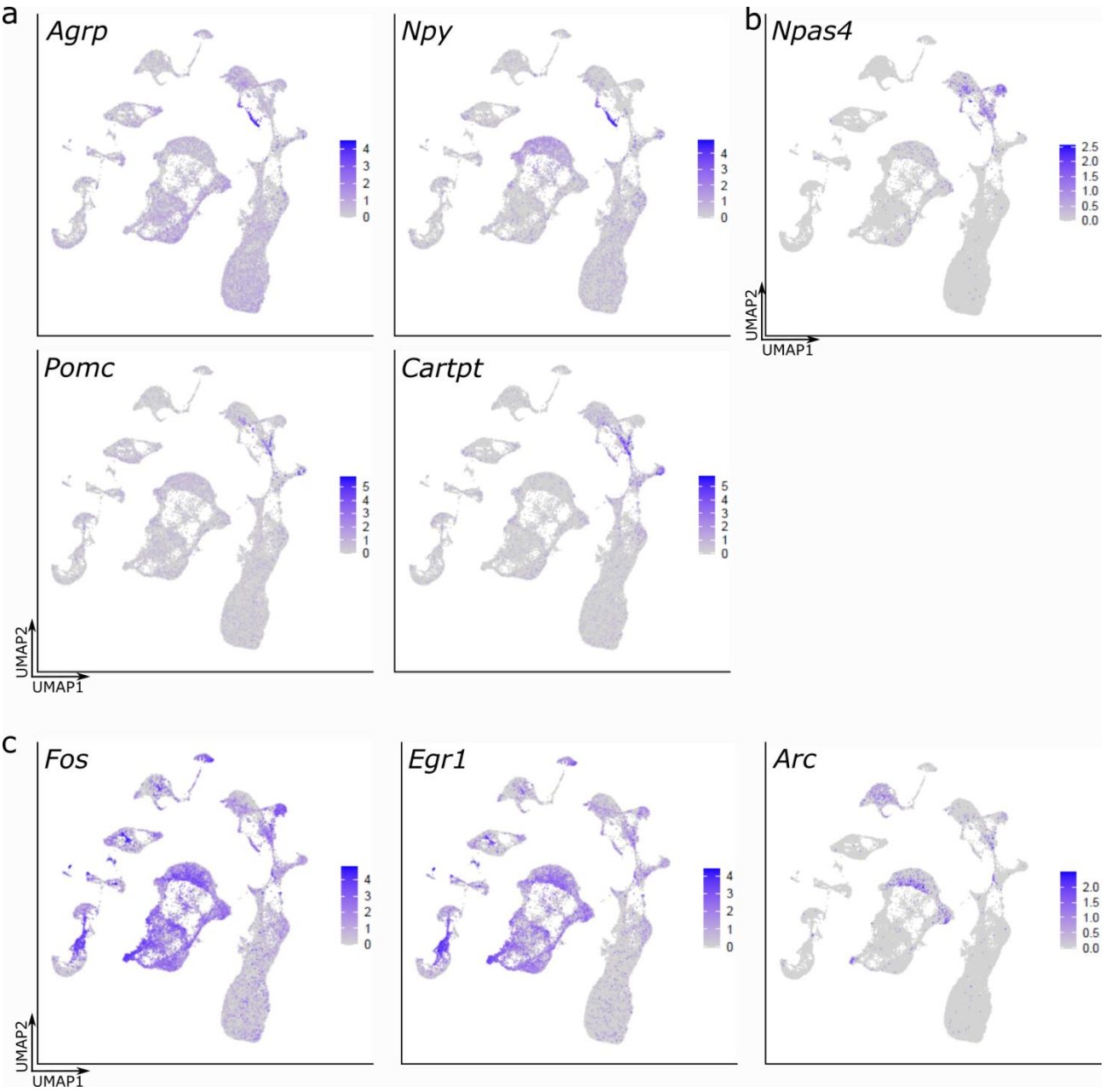

Figure 6.7 | ARC neurons and immediate early genes in the mouse ARC scRNA-seq dataset. a, Expression plots of individual genes projected in UMAP space to show location of ARC neurons. *Agrp* and *Npy* expression marks AgRP/NPY neurons. *Pomc* and *Cartpt* expression marks POMC/CART neurons. **b,** Expression plot of *Npas4*. **c,** Expression plots of immediate early genes *Fos*, *Egr1*, and *Arc* shown for all cells.

6.5 Comparing the general effects of NPAS4 KO in 6 week HFD POMC neurons

The primary goal of this mouse ARC scRNA-seq experiment was to isolate the POMC neurons for closer study in the computational space, since this was not easily feasible by sorting out recombined neurons from live neural tissue. This was performed by forming a subset of the dataset that was composed only of cells classified as neurons and expressing *Pomc*. Of the 5669 cells classified as neurons (14%), 1452 cells expressed any level of *Pomc* and were subsetted into its own object. Since the metadata had already been labelled with genotype and condition information, it was possible to form pairs of different combinations of cells for performing DEG analysis, akin to the approach undertaken in chapter 3. Initially, a general comparison of KO and CT POMC neurons was performed to identify any major transcriptomic changes that resulted from NPAS4 KO and 6 weeks of HFD. Then, fasted and refed POMC neurons were compared within each genotype to identify genes that were induced by refeeding. Finally, the KO and CT POMC neurons in the refed condition were compared to observe any changes in gene expression that occurred due to NPAS4 KO. A general schematic of this approach is shown in Fig 6.8a.

One unexpected finding was that there was a general reduction in the *Pomc* expression of KO POMC neurons compared to CT POMC neurons (Fig 6.8b). Among the DEG list obtained from the CT vs KO comparison, *Pomc* showed the greatest difference in average $\log_2$ fold change of expression (avgLog_2FC), showing roughly 3-fold higher expression in the CT cells than KO cells. 605 genes were downregulated in KO cells, but only four genes were upregulated in KO cells: *Cwc22, Mt2, Agt,* and *Slc6a11*. While it has no known role specifically in the hypothalamus or arcuate nucleus neurons, *Cwc22* encodes a splicing factor[374]. Metallotheionin 2, or *Mt2*, has been previously shown to be upregulated in the MBH neurons in response to

systemic cachexia-induced stress in a mouse model of pancreatic cancer[375], and *Mt1*- and *Mt2*-null mice have been reported to be obese with increased food intake, implying *Mt2* could have roles in regulating energy balance[376]. Angiotensinogen, or *Agt,* is commonly used in mouse neural studies as a marker gene for astrocytes (Fig 6.5). Interestingly, *Slc6a11* encodes for Gat3, the primary GABA transporter in astrocytes[377]. In contrast to these four genes, there were considerably more genes that were downregulated in KO POMC cells, which made the process of looking up individual gene identities time-consuming and inefficient. All 605 genes downregulated in KO POMC cells were used for a gene ontology (GO) analysis through the EnrichR gene list enrichment analysis program, for the GO Biological Process 2021 and Molecular Function 2021 libraries[325–327]. The top 20 results from the Biological Process library showed several terms related to neurotransmitter signalling activity, including "chemical synaptic transmission", "regulation of cation channel activity", "modulation of chemical synaptic transmission", "regulation of neurotransmitter signalling activity", and "regulation of NMDA receptor activity" (Fig 6.9a). The top 20 results from the Molecular Function library included terms that also related to neurotransmitter signalling and ion channel activity such as "transmitter-gated ion channel activity", "neurotransmitter receptor activity involved in postsynaptic membrane potential", and "ligand-gated anion channel activity" (Fig 6.9b). Furthermore, there were several terms that specifically related to GABA signalling: "GABA-gated chloride ion channel activity", "GABA-A receptor activity", and "GABA receptor activity" (Fig 6.9b). In line with the GO results, seven genes out of the 605 downregulated genes in KO encoded for GABA-A receptor subunits: *Gabrb3, Gabrb1, Gabrg3, Gabra2, Gabrg1, Gabrg2,* and *Gabra3* (Fig 6.9c). Taken together, the comparison of KO and CT POMC neurons' transcriptomes regardless of feeding state showed that the KO POMC neurons displayed

reductions in *Pomc* and GABA-A receptor genes, and GO analysis suggested there were reduced neurotransmitter and ion channel activities.

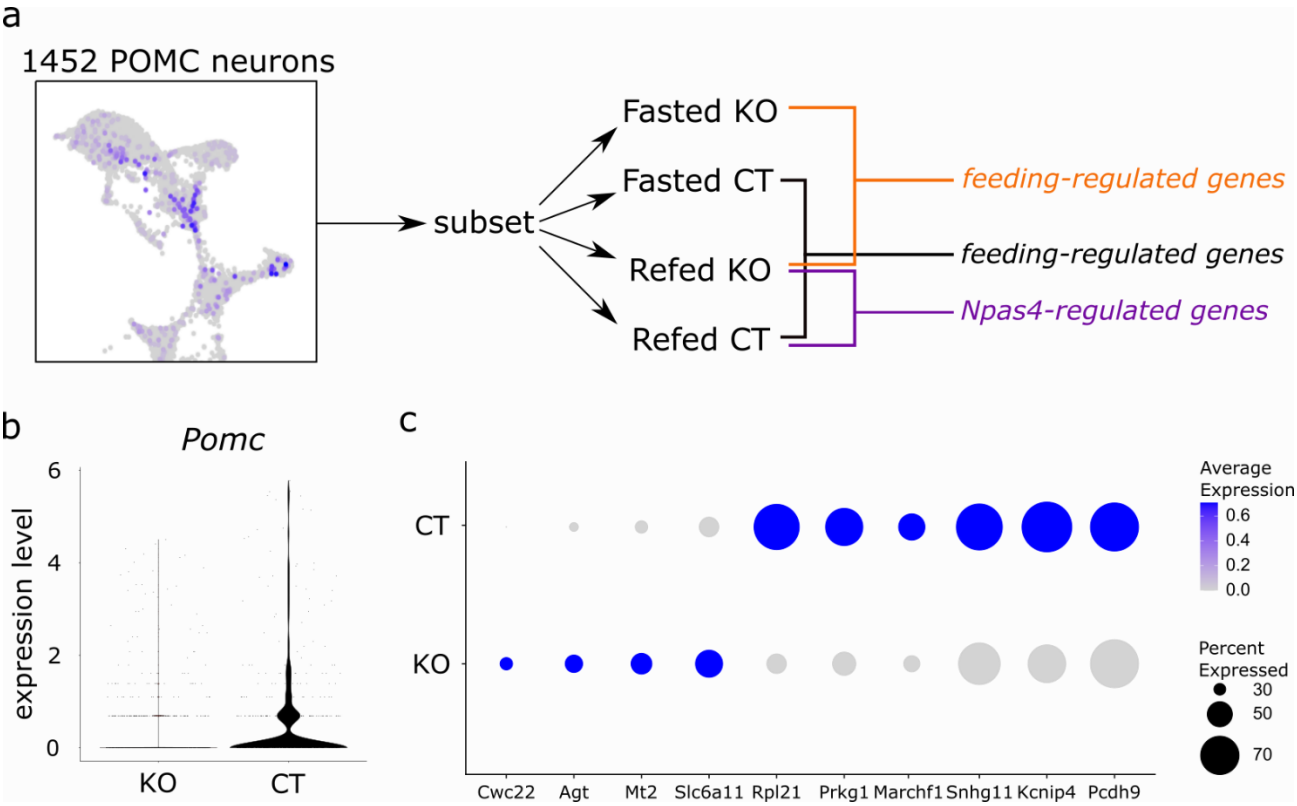

Figure 6.8 | POMC neurons from POMC-NPAS4 KO mice show reduced expression of *Pomc* and elevated expression of four genes. a, Schematic showing the analysis strategy used to identify DEGs between genotypes and conditions specifically in POMC neurons. 1452 *Pomc*+ cells classified as neurons were subsetted from the mouse ARC dataset containing all cells, and metadata was edited to include both the genotype and condition information for each cell. DEG analysis was performed for pairs of different genotype and condition combinations to identify genes regulated by feeding or fasting, and DEG between KO and CT. **b,** Violin plot of *Pomc* expression in KO and CT *Pomc*+ neurons. **c,** Dot plot of significant DEGs with the highest average $\log_2$ fold change in expression in CT vs KO *Pomc*+ neurons. The size of dots represents the percent of cells in the genotype that express the gene ("Percent Expressed") and the shade of blue represent the average expression of the gene on a normalized relative scale, with darker shades of blue representing higher expression levels. KO = POMC-NPAS4 KO, CT = POMC-CreER controls.

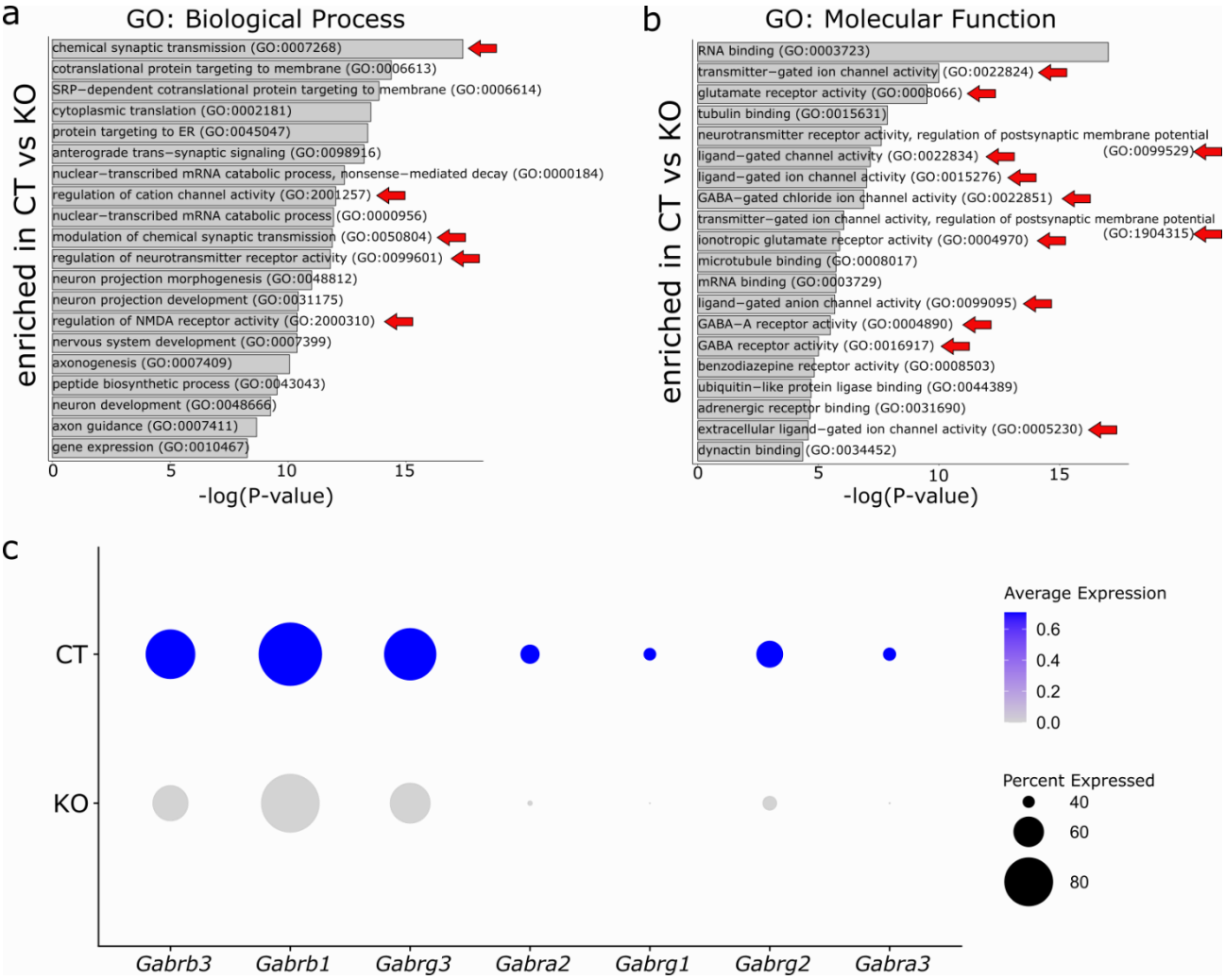

Figure 6.9 | KO POMC neurons express lower levels of GABA-A receptor subunit-encoding genes. **a-b,** Bar plots of the top 20 GO terms associated with genes enriched in CT compared to KO POMC neurons, in order of -$\log_{10}$ P-value of each GO term. GO terms were obtained from gene set libraries GO: Biological Process 2021 (a) and GO: Molecular Function 2021 (b) using EnrichR gene list enrichment analysis. Arrows indicate terms of interest that suggest higher neurotransmitter signalling activity. **c,** Dot plot of significant DEGs enriched in CT vs KO *Pomc*+ neurons encoding for GABA-A receptor subunits. The size of dots represents the percent of cells in the genotype that express the gene ("Percent Expressed") and the shade of blue represent the average expression of the gene on a normalized relative scale, with darker shades of blue representing higher expression levels. KO = POMC-NPAS4 KO, CT = POMC-CreER controls.

6.6 Identifying the effects of NPAS4 KO on feeding-induced genes in POMC neurons

Next, the fasted and refed POMC neurons were compared within each genotype to identify genes that were induced by refeeding. DEG analysis was performed across conditions in CT and KO POMC neurons separately, to generate a list of upregulated genes in the refed condition and in the fasted condition. Given that refeeding after a fast is known to be an activating condition of POMC neurons, the majority of the DEGs in each genotype was expected to show higher expression in the refed condition. Surprisingly, only seven genes were feeding-induced and 88 genes were expressed higher in the fasted condition in the CT POMC neurons (Fig 6.10a). KO POMC neurons, on the other hand, showed a much greater transcriptional response to the refeeding with 84 feeding-induced and 357 feeding-inhibited genes (Fig 6.10a). All seven of the feeding-induced genes in the CT were also feeding-induced in the KO (Fig 6.10b-c). *Cdk8, Camk1d, Gm20594, Lars2, mt-Nd3, Luzp2,* and *Prex2* were expressed and regulated at similar levels in both the CT and KO cells (Fig 6.10c). Several of the 84 refeeding-induced genes unique to the KO cells were genes that are typically enriched in glial populations. *Slc4a4, Slc1a3,* and *Slc6a11* were all confirmed within this dataset to be highly expressed in astrocytes compared to other cell types (Fig 6.10d). *Mobp*, a marker of myelinating oligodendrocytes, was confirmed to be highly expressed in a proportion of the oligodendrocyte population (Fig 6.10d). *Slc6a11* was also one of the four genes that were significantly upregulated in KO vs CT cells when DEG analysis was performed regardless of fasting or feeding conditions (Fig 6.8c).

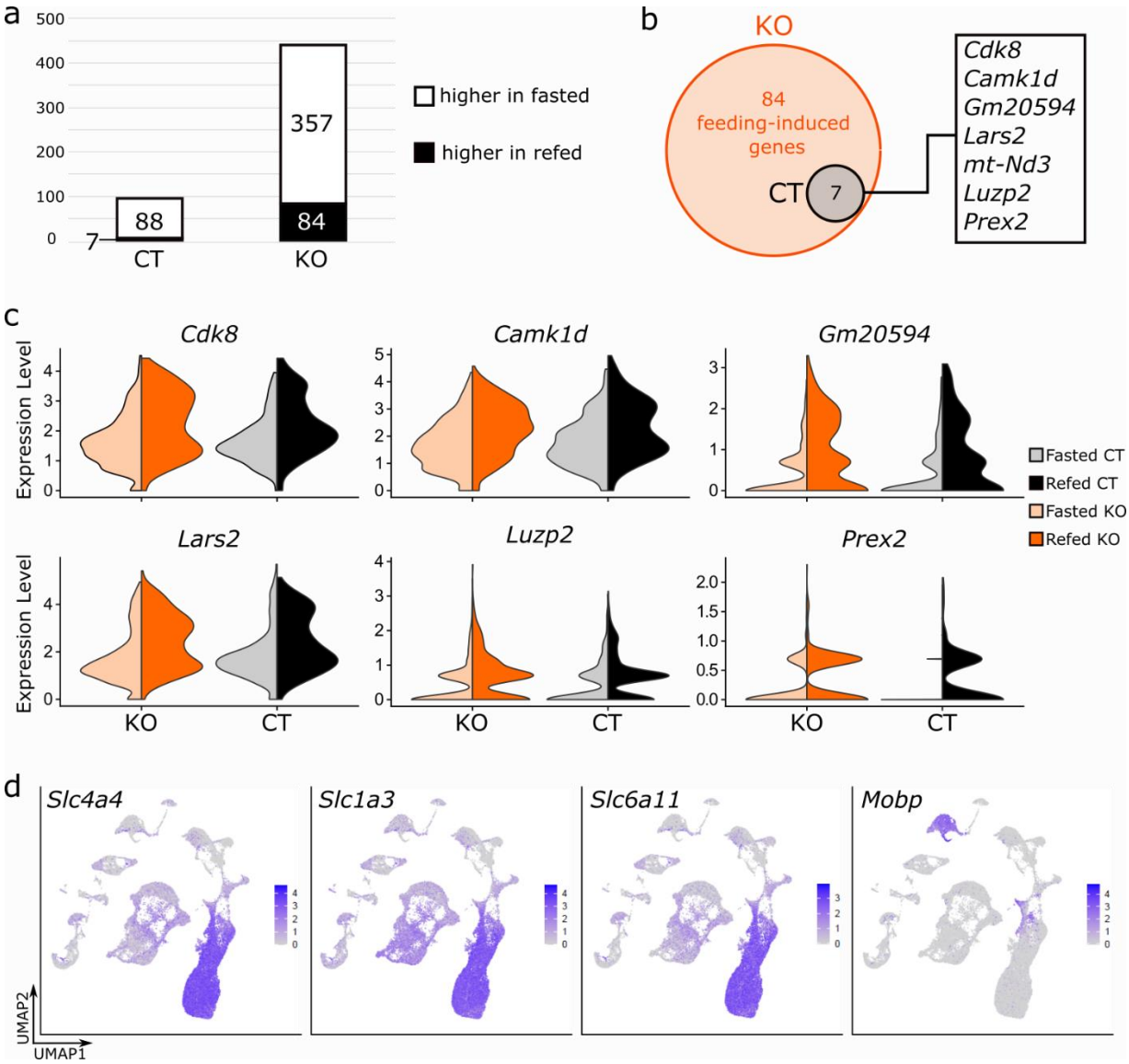

Figure 6.10 | KO POMC neurons have a greater number of refeeding-regulated genes than CT POMC neurons. a, Stacked bar graph showing the number of feeding-regulated genes that are expressed higher in the fasted condition (white bars) or higher in the refed condition (black bars) in CT vs KO. Numbers of genes in each group are shown in the bars. **b,** Venn diagram showing all seven genes that are induced by refeeding in the CT POMC neurons are also induced by feeding in the KO POMC neurons. The identities of the seven genes are shown in the black box to the right. **c,** Split violin plots showing expressions of six out of the seven genes that are significantly feeding-induced in both CT and KO. Darker shades in each group indicate the refed condition and the paler shades indicate the fasted condition. **d,** Featureplots showing the expression of significantly feeding-induced genes in KO POMC neurons across all cell types. The areas of highest gene expression are seen in the astrocytes for *Slc4a4*, *Slc1a3*, and *Slc6a11*. *Mobp* expression is highest in oligodendrocytes. KO = POMC-NPAS4 KO, CT = POMC-CreER controls.

The final comparison was performed for the KO and CT POMC neurons in the refed condition only. Since it was established that refeeding after a fast induces *Npas4* and activates POMC neurons in chapter 4, refeeding leads to hundreds of transcriptional changes in the KO but not in the CT (Fig 6.10a), the differences in gene expression in the refed condition was expected to reveal the greatest number of potentially NPAS4-regulated transcriptional changes. The pairwise comparison revealed 530 genes that were downregulated in KO cells, and only 19 genes that were upregulated in KO cells. As expected, the majority (16 out of 19) of these upregulated genes were also detected as refeeding-induced previously. All 549 significantly downregulated genes from this comparison were used for GO analysis using the GO Biological Process 2021 and Molecular Function 2021 libraries. Much like the results from the general CT vs KO comparison, the biological process results for genes downregulated in refed KO POMC cells contained terms that suggested higher neurotransmitter activity at the synapse such as "chemical synaptic transmission", "glutamate receptor signalling pathway", and "regulation of neurotransmitter receptor activity" (Fig 6.11a). Meanwhile, the biological process results for genes upregulated in KO cells mostly focused on the transmembrane transport of amino acids, such as "acidic amino acid transport", "L-alpha-amino acid transmembrane transport", and "L-aspartate transmembrane transport" (Fig 6.11a). These were further supported by the molecular function results, which again showed terms related to GABA signalling for genes downregulated in refed KO POMC cells ("GABA-gated chloride ion channel activity", "GABA-A receptor activity", and "GABA receptor activity") and terms related to amino acid transport in the KO cells ("amino acid: sodium symporter activity", "L-glutamate transmembrane transporter activity", and "acidic amino acid transmembrane transporter activity") (Fig 6.11b). Similar to figure 6.9, the GO analysis suggested KO POMC neurons may have neurotransmitter signalling,

and GABA signalling may be affected in particular. Several of the GABA-A receptor subunit genes were once again found to be downregulated in refed KO cells: *Gabrb3, Gabrg2, Gabrb1, Gabrg3,* and *Gabra3.* In addition to GABA-A receptor genes, several well-known IEGs were also downregulated in the KO cells. *Fos*, a general IEG expressed in multiple cell types, was not a refeeding-regulated gene in CT cells, but was significantly refeeding-inhibited in KO cells (Fig 6.12a). *Fosb*, which encodes for another FOS family protein, was also dysregulated in the KO in a similar pattern (Fig 6.12d). *Egr1* and *Junb* were also normally not significantly feeding-regulated, but were downregulated with feeding in KO cells only (Fig 6.12b, e). This pattern was also seen with *Jund* and *Jun* expression in KO cells, but the difference was more moderate (Fig 6.12c, f).

Taken together, the results to date imply that after NPAS4 KO followed by 6 weeks of HFD, POMC neurons regulate a greater range of genes in response to an acute fast-refeed, and some of these genes are primarily expressed in glial populations such as astrocytes and oligodendrocytes. They could also be capable of less GABAergic signalling compared to CT cells, and show a strong reduction in expression of IEGs in response to feeding. Overall, the results of the scRNA-seq show that NPAS4 KO worsens the dysregulation in POMC neurons of HFD-fed mice and alters the refeeding-regulated transcriptional profile.

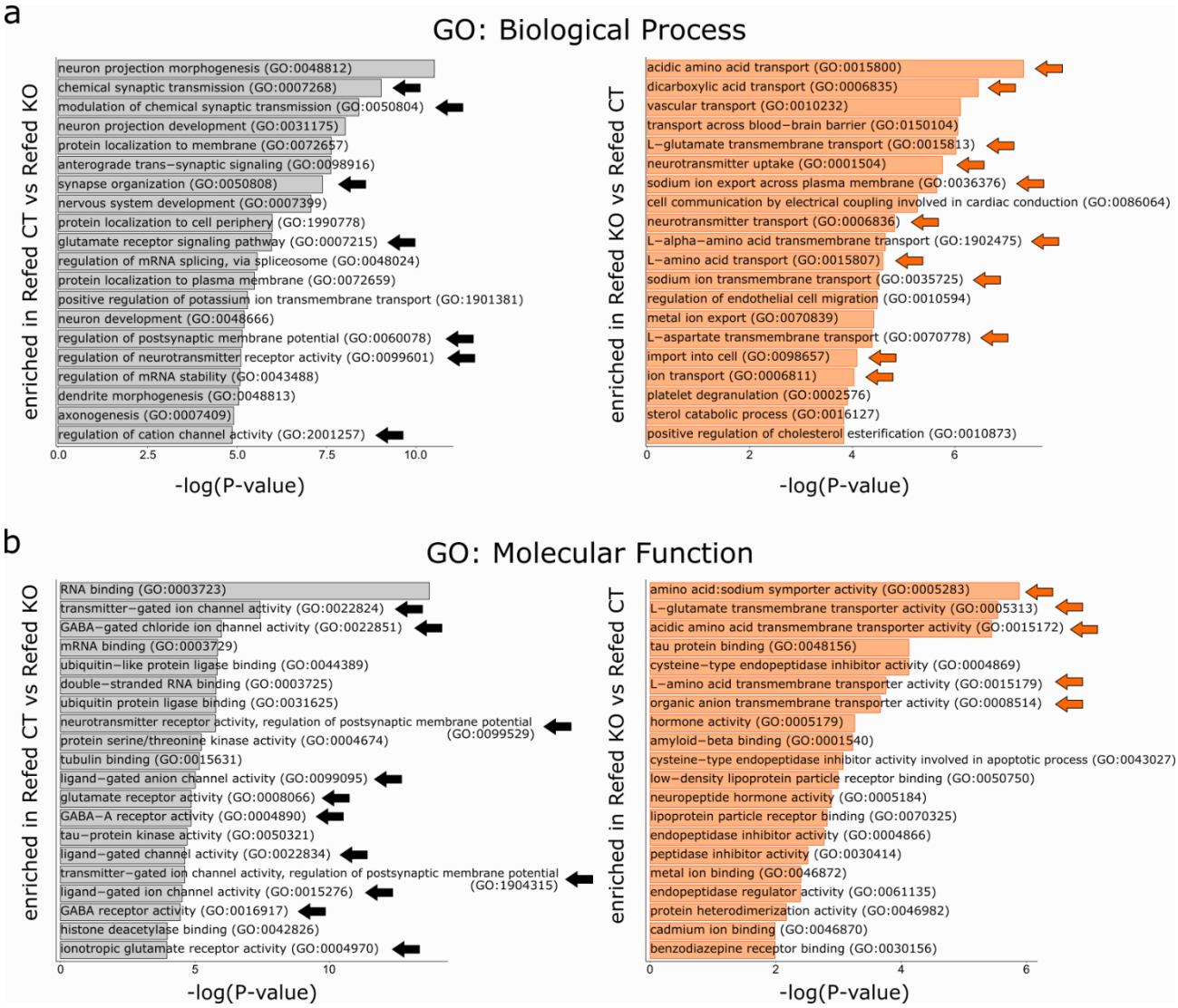

Figure 6.11 | Gene ontology results for significantly DEGs in the Refed CT vs Refed KO POMC neurons. a, Bar plots of the top 20 GO terms associated with genes enriched in Refed CT compared to Refed KO POMC neurons, in order of -$\log_{10}$ P-value of each GO term. GO terms were obtained from gene set libraries GO: Biological Process 2021 (a) and GO: Molecular Function 2021 (b) using the EnrichR gene list enrichment analysis. Black arrows indicate terms of interest that suggest higher neurotransmitter and GABA-A receptor signalling activity at the synapse in CT POMC neurons. Orange arrows indicate terms of interest that suggest higher amino acid and ion transport in KO POMC neurons.

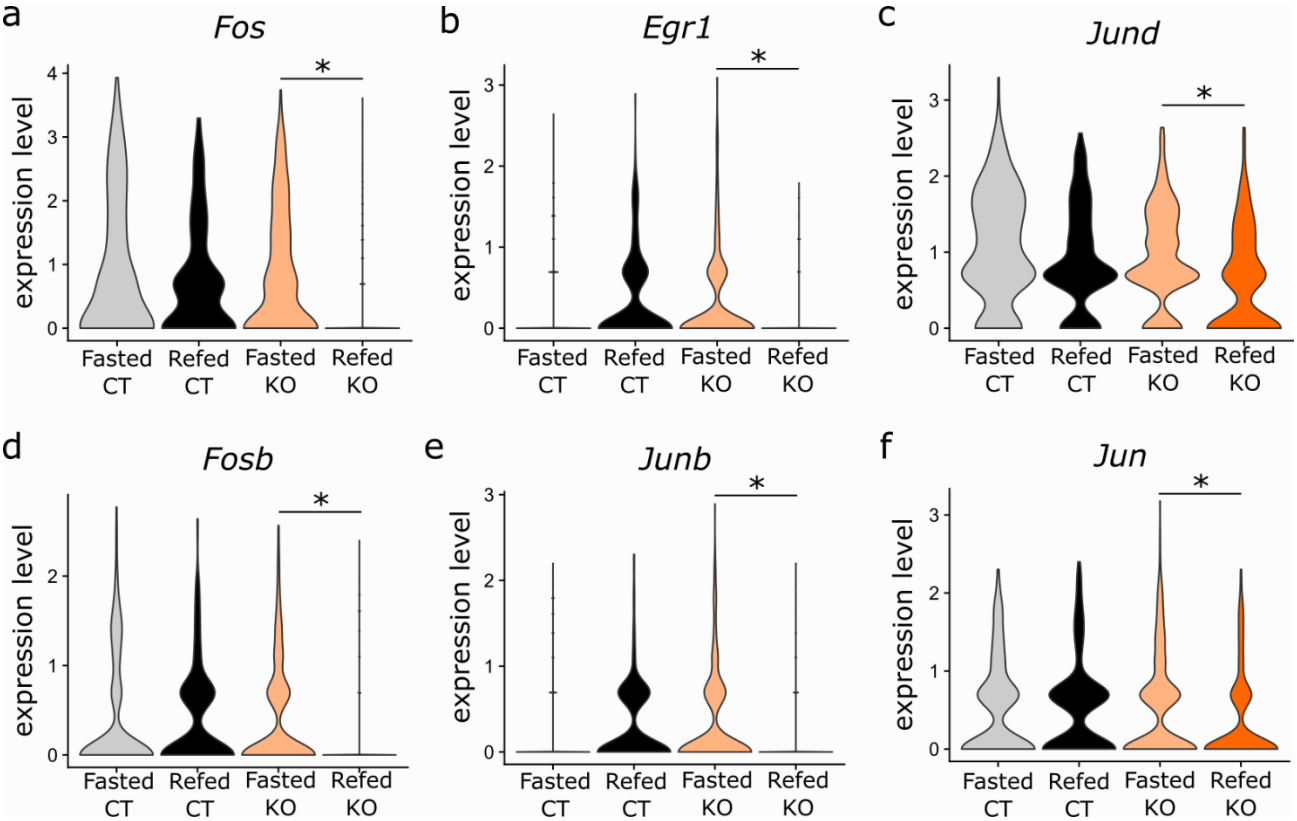

Figure 6.12 | Immediate early gene expression is dysregulated in KO POMC neurons in response to refeeding. Violin plots of established immediate early genes that are significantly feeding-regulated in KO POMC neurons but not in CT POMC neurons. Expression levels are shown for POMC neurons in the Fasted CT, Refed CT, Fasted KO, and Refed KO groups for: **a,** *Fos*, **b,** *Egr1*, **c,** *Jund*, **d,** *Fosb*, **e,** *Junb*, and **f,** *Jun*. Wilcoxon rank sum test: $*P_{adjusted} < 0.05$.

6.7 Discussion

In this final chapter, scRNA-seq was performed on mouse ARC cells to isolate the effects of NPAS4 KO on refeeding-regulated transcriptional changes in POMC neurons after 6 weeks of HFD. The justification for using scRNA-seq instead of bulk RNA-seq, despite the more complex and lengthy library preparation and analysis methods, was a lack of feasibility in specifically isolating enough POMC neurons from POMC-CreER and POMC-NPAS4 KO mouse brains. Protocols for isolating POMC neurons from adult neural tissue, especially if mice have a fluorescent lineage marker to specifically mark POMC neurons, typically involved fluorescent-

activated cell sorting methods[373]. The main problem with using this method to isolate POMC neurons and perform bulk RNA-seq instead of scRNA-seq was due to cell numbers. My previous attempts at estimating the proportion of tdTomato+ cells in POMC-CreER^{+} mice have shown that the experiment was only possible when the ARC tissue from at least four mice were pooled (data not shown). In addition, only 5% of viable, well-dissociated single cells displayed tdTomato fluorescence, which only marks 50% of POMC neurons according to data in chapter 5 (Fig 5.5d). On average, 38000 cells were counted per mouse at the end of the dissociation protocol, so a single mouse would only have been able to yield less than 2000 tdTomato+ POMC neurons. Therefore, scRNA-seq was the approach used to pool all dissociated cells from an initial crudely dissected region, despite the abundance of glial cells in the dataset due to lack of sorting. The analysis was selectively performed in POMC neurons detected in the dataset in downstream analysis for this reason. Even with this method, multiple mice per experimental and genotype groups were used, for a total of 13 mice.

As briefly discussed in section 6.1, POMC-CreER and POMC-NPAS4 KO mice that were fed HFD for 6 weeks following tamoxifen were chosen for this experiment. An advantage of using mice at this time point was that the mice had already been characterized for matched body weights and confirmed to have an early difference in food intake at 2 weeks of HFD (Fig 5.13b-c). This meant that any changes observed would not be caused as secondary effects of having a lighter body weight. Six weeks of HFD was also a time point at which recombination and NPAS4 KO had already been confirmed (Fig 5.13g-h) and *Npas4* expression was elevated in comparison to Chow-fed mice (Fig 4.6b). It was also rationalized that by 6 weeks of HFD post-tamoxifen, any long-term changes at the molecular level in POMC neurons due to NPAS4 KO or

HFD feeding would have already occurred, such as changes in activity, identity, or synaptic organization.

As expected, neurons in general were a minority population in the dataset relative to glial cell types, and less than 1500 POMC neurons were present in the dataset. This meant that approximately 111 POMC neurons were isolated from each mouse. Due to these low cell numbers, secondary clustering was not performed on all POMC neurons that were subsetted from the main dataset containing all cell types. This was not considered as a problem as studying POMC neuron heterogeneity or subpopulations was not the goal of this experiment. However, it should be noted that heterogeneous POMC subpopulations were previously reported[322,372,373], but analysis in this dataset used all pooled POMC neurons in each group, which was a caveat in this experiment.

From a general CT vs KO comparison, regardless of fasted or refed conditions, it was revealed that KO neurons unexpectedly showed a reduction in *Pomc* transcript (Fig 6.8b). In addition, half of the few upregulated genes in KO over CT were genes primarily expressed in astrocytes, and several refeeding-induced genes in KO POMC neurons were also noted to be glial-specific genes (Fig 6.8c, 6.10d). This could imply that the loss of NPAS4 leads to a potential loss of identity in POMC neurons, or even a change of identity. It has been previously reported that certain POMC neurons from HFD-fed mice express *Agrp*, which has led to hypotheses about "confused" POMC neurons that have difficulty maintaining identity which leads to dysregulation[322,373]. While astrocyte-to-neuron conversion has been heavily studied in the field of neurodegeneration therapies[378], neuron-to-astrocyte conversion has been less studied. Such a change of cell identity

seems unlikely to occur in an adult animal and should not be determined based on the expression of a few genes. A more likely possibility is that NPAS4 KO during the development of diet-induced obesity leads to POMC neurons aberrantly expressing and regulating more genes upon activation, and some of these happen to be glial lineage genes.

An alternate goal of the scRNA-seq experiment was to explore potential mechanisms by which POMC-NPAS4 KO mice are protected from diet-induced obesity. Due to their phenotype, whatever changes occurred due to NPAS4 KO must be leading to a net increase in POMC neuron activity. Much like the general KO vs CT comparisons, GO analysis on specifically the refed CT vs KO cells revealed reduced GABA receptor expression and potential reductions in GABA signalling in the KO POMC neurons. It is known that AgRP neurons can inhibit POMC neurons directly through GABA release and it has been shown that NPAS4 KO leads to decreased numbers of inhibitory synapses[300]. It seems possible that NPAS4 KO leads to decreased inhibitory GABAergic synapses on POMC neurons over time, decreasing the inhibition of POMC neuronal activity by AgRP neurons, and leading to an increase in POMC neuron firing and eventual decreased body weight gain through decreased food intake. Experiments in the future to investigate whether this change actually occurs would involve validating the decrease in GABA receptor gene expression in POMC-NPAS4 KO mice, immunostaining inhibitory postsynaptic markers such as gephyrin to determine if there is a reduction in numbers of inhibitory synapses on KO POMC neurons, and ideally using electrophysiological approaches to directly measure POMC neuron activity during HFD after NPAS4 KO.

In summary, the scRNA-seq data shown in chapter 6 reveal several key differences between CT and KO POMC neurons and potential mechanisms by which KO POMC neurons could have net increases in activity. NPAS4 KO in POMC neurons followed by 6 weeks of HFD seems to lead to increased activity due to decreased inhibitory GABAergic signalling on these neurons, and this is reflected in the increases in the magnitude of transcriptional changes regulated by refeeding after a fast.

Chapter 7: Conclusions

7.1 Research Summary

In cell types that constantly detect and respond to the environment, activity-regulated genes are essential for coupling the stimuli to long-term changes. Pancreatic islets and ARC neurons are very similar cell types that sense nutrient and endocrine signals and secrete their characteristic hormone to regulate glucose homeostasis or energy homeostasis, respectively. In both healthy states and states of impaired energy homeostasis like obesity, there is value in understanding how the transcriptional response of these cells may help them function properly and adapt to challenges.

The calcium-dependent IEG, NPAS4, has been implicated in a wide range of functions in both neurons and pancreatic beta cells. In neurons, NPAS4 has been shown to induce distinct sets of genes to regulate excitatory-inhibitory synaptic balance in neuronal circuits[256,300]. In beta cells, NPAS4 optimizes metabolism during conditions of high glucose by suppressing the action of HIF1α[320]. In both cell types, NPAS4 has been shown to have a protective role against cellular stresses specific for each cell type[317,319].

In islets, previous studies have established a role of NPAS4 in beta cells, and many studies have studied IEGs in general, but the studies have mainly been focused on beta cells and not the other islet cell types. The islet is composed of multiple different cell types, and it is known from studies in the brain that distinct sets of IEGs can be expressed in different populations, but differentially regulated IEGs in each islet cell type are unknown. In neurons, the roles of NPAS4 have been established in other regions of the brain, and many studies have identified IEGs in

neuronal populations, but the role of NPAS4 in a metabolically critical center of the brain is unknown. In the hypothalamus, the homeostatic nexus of the mammalian brain, the only other study of NPAS4 was performed in the SCN[360], which is not a site directly involved in regulation of energy homeostasis. Based on these gaps in knowledge, the experiments in this thesis were designed to answer the following questions:

1) In islets, what is the profile of calcium-dependent activity-regulated genes in healthy human alpha, beta, and delta cells?
2) In the ARC neurons of the hypothalamus, is NPAS4 expressed, and what stimuli can induce NPAS4 expression?
3) What are the effects of genetic knockout of NPAS4 specifically in AgRP and POMC neurons of the ARC that regulate energy homeostasis?
4) What activity-regulated genes in ARC neurons can be induced by acute feeding, and what genes are affected by knockout of NPAS4?

The first question was answered in chapter 3 by performing scRNA-seq on healthy human islets that had been stimulated with high glucose and islets that had the same stimulus but inhibited calcium influx with the administration of calcium chelator EGTA. Calcium-regulated genes were identified in downstream analysis by comparing transcriptomes within each cell type between the stimulated and calcium-inhibited conditions. There was a certain degree of heterogeneity found in alpha and beta cells that displayed multiple clusters within each cell type. In both cell types, different numbers of calcium-dependent genes were identified in different clusters, which was interpreted as varying degrees of response to calcium. As a general trend, both alpha and beta cells showed clusters that were more responsive to calcium, and a proportion of beta cell clusters

showed dampened calcium response. From the beta cell clusters that were more responsive to calcium, the cell surface marker PCDH7 was identified. Performing GSIS assays on reaggregates of PCDH7+ and PCDH7- cells sorted from additional human islets showed that PCDH7+ reaggregates had enhanced GSIS over PCDH7-. In addition, an unexpected cluster of polyhormonal cells that expressed insulin, glucagon, and somatostatin were found in the dataset. These cells expressed the highest number of calcium-responsive genes while showing a somewhat immature transcriptional profile compared to alpha and beta cells, and were identified in additional islet and pancreas sections by visualizing insulin and glucagon mRNA directly.

The second question was answered in chapter 4 with a series of fluorescent in situ hybridization assays on ARC sections from mice exposed to a number of conditions predicted to induce *Npas4*. After validating the specificity of the *Npas4* probe, ARC AgRP and POMC neurons were confirmed to express *Npas4*. As expected of neurons that respond to energy state, there was a clear induction of *Npas4* seen in POMC neurons in response to refeeding after an overnight fast, but refeeding did not affect *Npas4* levels in AgRP neurons. Within POMC neurons only, oral glucose administration was found to induce *Npas4*, peaking around 15 minutes, but intraperitoneal injections of insulin did not affect *Npas4* levels in POMC neurons. A systemic increase in energy availability with HFD feeding only showed an induction of *Npas4* in POMC neurons at 1 week and 6 weeks of HFD, but not at 3 days.

The third question was answered in chapter 5 by characterizing novel mouse lines with a conditional deletion of NPAS4 specifically in either the AgRP neurons or POMC neurons, with or without HFD to promote diet-induced obesity. Knockout of NPAS4 in AgRP neurons was

difficult to assess due to the strong phenotype of reduced body weight caused by the presence of the AgRP-CreER transgene in the knockout group and one of the control groups. Body weights of any mouse that had the AgRP-CreER transgene were lower even before recombination was induced. In Chow or HFD groups, the knockout of NPAS4 in AgRP neurons seemed to have minimal effects that were not influenced by the CreER. Knockout of NPAS4 in POMC neurons of mice fed Chow had no effects. However, knockout of NPAS4 in POMC neurons of mice fed HFD caused reduced body weight starting at 9-10 weeks of HFD without changes in glucose homeostasis. This difference in body weight was potentially due to a trend towards lower food intake at 6 weeks of HFD and a definite decrease in food intake at 2 weeks of HFD.

The final question was answered in chapter 6 by performing scRNA-seq on ARC cells from fasted and refed mice with or without knockout of NPAS4 in POMC neurons after 6 weeks of HFD. This experiment was done only to study the transcriptomic changes in POMC neurons, which was too rare of a population to isolate in large enough quantities for alternate methods. Generally reduced genes in the knockout mice included *Pomc* and genes encoding for various GABA-A receptor subunits. GO analysis suggested that there was a reduction of inhibitory synapses and GABAergic signalling in the knockout mice compared to controls. Similar to the approach in chapter 3, transcriptomes from the different conditions were compared to identify feeding-regulated genes in controls and knockouts. Surprisingly, the number of genes induced by feeding in knockout mice were far greater than controls, although the identity of some of these genes were ones known to be primarily glial-specific. Again, GO analysis for DEGs between refed control and refed knockout transcriptomes suggested reduced GABAergic signalling in the knockouts.

Collectively, the experiments presented in this thesis have contributed to the understanding of ARGs in islets and ARC neurons. In islets, where NPAS4 roles were already known, the study of ARGs was expanded by profiling calcium-regulated genes in human islet cell types and demonstrating that the identified marker of beta cells with higher calcium responsiveness can also act as a marker for functionally enhanced beta cells. In ARC neurons, where the roles of NPAS4 were unknown, the inducing conditions of NPAS4, the effects of NPAS4 knockout, the potential molecular mechanism behind the effects of NPAS4 KO, and ARGs regulated by feeding were examined.

7.2 Limitations of research and future directions

The data in this thesis show a number of potential avenues of research that could be pursued in the future based on these results, but they also bring to light a number of caveats that must be discussed. In chapter 3, scRNA-seq was used to identify differences in calcium-regulated transcriptional changes. scRNA-seq itself will always be accompanied by several caveats and limitations. One of them is the fact that scRNA-seq is always a snapshot in time and cannot indicate which clusters or populations are permanent or transient. Different clusters achieved by clustering methods will always be arbitrary to some degree, as adjustment of clustering resolution will result in more or less clusters, and can be easily altered during analysis. Therefore, even though different clusters within a cell type are discussed, the important takeaway is that none of these clusters may be a fixed, permanent population in human islets. The differences in calcium-regulated gene numbers in each cluster may again, reflect different states that the cells happened to be in upon time of stimulation and capture. Clustering is not an

absolute art, and should not be treated as such until clusters have been validated outside of the dataset or studied for a biological role. For example, the PCDH7+ cells having a greater response to calcium was validated by sorting them from additional islets and assessed for enhanced function. There were also clusters that were not validated but seem interesting to pursue in the future. The polyhormonal cluster was validated at the level of mRNA, but the long-standing question is if these cells also produce proteins for multiple hormone genes. In order to study this cluster, candidate markers genes could be identified within the dataset, ideally for proteins expressed on the cell surface to facilitate sorting methods. Once isolation of the cells was feasible, then additional functional assays could be performed, such as measuring calcium oscillations in response to stimuli, or investigating their potential as a stem cell niche.

In chapters 4 and 5, in situ hybridization was used to assess *Npas4* levels within the ARC neurons. In the time scale following stimuli for these experiments, it makes sense to detect mRNA levels, as *Npas4* induction is rapid and detectable within the hour. An obvious limitation of this approach is, of course, the lack of information about the NPAS4 protein levels to the same stimuli. As mentioned in chapter 4, the reason why protein levels were not assessed in every experiment was because there were significant difficulties in the NPAS4 immunostaining protocol with the existing antibody. After many rounds of troubleshooting, I was able to show a refeeding-induced upregulation in NPAS4 protein in POMC neurons, and plan to carry out the same protocol on additional samples in future experiments. While there is a different NPAS4 antibody than the one used for immunostaining in chapter 4 that can be used for western blots, it would be extremely difficult to obtain an enriched sample of POMC neurons from mouse ARC tissue for western blotting purposes. The population is relatively rare, so it would require a lot of

mice to obtain enough POMC cells to perform a western blot. It may be possible to perform western blotting on whole ARC tissue samples without enriching for POMC neurons, but it would still require multiple mice per sample and the difference may be too slight to detect confidently when all cells in the heterogeneous ARC get pooled into one sample.

Data in chapter 5 also showed variability in recombination rates of POMC-CreER, which is another caveat when working with knockout mouse lines. The highest recombination rate observed was around 50%, meaning that 50% of POMC neurons had successful knockout of NPAS4, and this was supported by the tdTomato detection. Even though the knockout mice showed reduced body weight gain on HFD over time, it was a moderate difference compared to the obese controls, and occurred weeks into the HFD regime. Part of this could have been due to the low recombination efficiency, and remaining POMC neurons with intact NPAS4 could have compensated for the neurons with NPAS4 knockout, causing a delay in the appearance of phenotype. It's possible that if recombination rates were higher, the mice would have exhibited even less weight gain on HFD, or a sustained early reduction in food intake. Instead, there was a discrepancy between the food intake reduction at 2 weeks and the potential reduction at 6 weeks. This may have been due to the low sample sizes used for the metabolic cage studies at 6 weeks of HFD, as statistical differences were difficult to assess with a slight difference in a few mice. In this case, a very obvious future direction would be to repeat this experiment with more mice, and observe if the knockout mice do display a reduction in food intake at 6 weeks of HFD. Another interesting research avenue is characterizing the female POMC-NPAS4 KO mice, because only male mice were used in this thesis. Sex differences in energy homeostasis and general and in POMC neurons specifically have already been reported[379,380]. For example, it has

been found that female mice have more POMC neurons than male mice in their ARC[381], and there have also been several reports of specific molecular drivers of sex differences in POMC neurons[369,380,381]. Future studies of female POMC-NPAS4 KO mice would provide useful information on the role of NPAS4 in males and females that is relevant to human health, regardless of whether the females showed a food intake phenotype that was similar to or different from the males.

Finally, the most important future experiment to address the limitations of this thesis is the direct functional characterization of the POMC neurons with NPAS4 knockout. The phenotype shown by the POMC-NPAS4 KO mice is interesting, but unfortunately it remains unclear whether the activity of POMC neurons with NPAS4 knockout is ultimately increased or decreased in the HFD setting. Given the reductions in food intake and the reduced body weight, it is almost certain that the activity of POMC neurons would be increased in knockout mice, but this has yet to be confirmed by electrophysiological approaches. The results from the ARC scRNA-seq also show results that would support increased activity, because of the reduced GABA receptor subunit gene expression in POMC neurons. This is another finding that could be additionally confirmed. Since NPAS4 is already known to regulate inhibitory synapses and be important for maintenance of these synapses, immunofluorescent staining for GABAergic synapses on POMC neurons would be the easiest way to confirm the results of the scRNA-seq. A quantified decrease in the number of inhibitory synapses on POMC neurons, along with increased POMC neuronal activity or excitability, would fully explain NPAS4's roles in POMC neurons.

There are still numerous unanswered questions about the exact role of NPAS4 in ARC neurons.

The proposed future experiments above will hopefully add a mechanistic explanation to the phenotype observed when NPAS4 is knocked out from POMC neurons, and further our knowledge of NPAS4 biology by solidifying a role of NPAS4 in regulating food intake and body weight that is distinct from its roles in other brain regions or pancreatic beta cells.

References

1. Obesity and overweight. Accessed March 18, 2023. https://www.who.int/news-room/fact-sheets/detail/obesity-and-overweight

2. Chew NWS, Ng CH, Tan DJH, Kong G, Lin C, Chin YH, Lim WH, Huang DQ, Quek J, Fu CE, Xiao J, Syn N, Foo R, Khoo CM, Wang JW, Dimitriadis GK, Young DY, Siddiqui MS, Lam CSP, Wang Y, Figtree GA, Chan MY, Cummings DE, Noureddin M, Wong VWS, Ma RCW, Mantzoros CS, Sanyal A, Muthiah MD. The global burden of metabolic disease: Data from 2000 to 2019. *Cell Metab*. 2023;35(3):414-428.e3. doi:10.1016/j.cmet.2023.02.003

3. Abarca-Gómez L, Abdeen ZA, Hamid ZA, Abu-Rmeileh NM, Acosta-Cazares B, Acuin C, Adams RJ, Aekplakorn W, Afsana K, Aguilar-Salinas CA, Agyemang C, Ahmadvand A, Ahrens W, Ajlouni K, Akhtaeva N, Al-Hazzaa HM, Al-Othman AR, Al-Raddadi R, Buhairan FA, Dhukair SA, Ali MM, Ali O, Alkerwi A, Alvarez-Pedrerol M, Aly E, Amarapurkar DN, Amouyel P, Amuzu A, Andersen LB, Anderssen SA, Andrade DS, Ängquist LH, Anjana RM, Aounallah-Skhiri H, Araújo J, Ariansen I, Aris T, Arlappa N, Arveiler D, Aryal KK, Aspelund T, Assah FK, Assunção MCF, Aung MS, Avdicová M, Azevedo A, Azizi F, Babu BV, Bahijri S, Baker JL, Balakrishna N, Bamoshmoosh M, Banach M, Bandosz P, Banegas JR, Barbagallo CM, Barceló A, Barkat A, Barros AJ, Barros MV, Bata I, Batieha AM, Batista RL, Batyrbek A, Baur LA, Beaglehole R, Romdhane HB, Benedics J, Benet M, Bennett JE, Bernabe-Ortiz A, Bernotiene G, Bettiol H, Bhagyalaxmi A, Bharadwaj S, Bhargava SK, Bhatti Z, Bhutta ZA, Bi H, Bi Y, Biehl A, Bikbov M, Bista B, Bjelica DJ, Bjerregaard P, Bjertness E, Bjertness MB, Björkelund C, Blokstra A, Bo S, Bobak M, Boddy LM, Boehm BO, Boeing H, Boggia JG, Boissonnet CP, Bonaccio M, Bongard V, et al. Worldwide trends in body-mass index, underweight, overweight, and obesity from 1975 to 2016: a pooled analysis of 2416 population-based measurement studies in 128·9 million children, adolescents, and adults. *The Lancet*. 2017;390(10113):2627-2642. doi:10.1016/S0140-6736(17)32129-3

4. Ogden CL, Carroll MD, Flegal KM. Epidemiologic trends in overweight and obesity. *Endocrinol Metab Clin North Am*. 2003;32(4):741-760, vii. doi:10.1016/s0889-8529(03)00074-4

5. Bray GA, Kim KK, Wilding JPH, Federation WO. Obesity: a chronic relapsing progressive disease process. A position statement of the World Obesity Federation. *Obes Rev*. 2017;18(7):715-723.

6. Colditz GA, Willett WC, Rotnitzky A, Manson JE. Weight gain as a risk factor for clinical diabetes mellitus in women. *Ann Intern Med*. 1995;122(7):481-486. doi:10.7326/0003-4819-122-7-199504010-00001

7. Hu G, Lindström J, Valle TT, Eriksson JG, Jousilahti P, Silventoinen K, Qiao Q, Tuomilehto J. Physical activity, body mass index, and risk of type 2 diabetes in patients with normal or impaired glucose regulation. *Arch Intern Med*. 2004;164(8):892-896. doi:10.1001/archinte.164.8.892

8. Must A, Spadano J, Coakley EH, Field AE, Colditz G, Dietz WH. The disease burden associated with overweight and obesity. *JAMA*. 1999;282(16):1523-1529. doi:10.1001/jama.282.16.1523

9. Zhao X, Gang X, He G, Li Z, Lv Y, Han Q, Wang G. Obesity Increases the Severity and Mortality of Influenza and COVID-19: A Systematic Review and Meta-Analysis. *Front Endocrinol*. 2020;11:595109. doi:10.3389/fendo.2020.595109

10. Padwal R, Leslie WD, Lix LM, Majumdar SR. Relationship Among Body Fat Percentage, Body Mass Index, and All-Cause Mortality: A Cohort Study. *Ann Intern Med*. 2016;164(8):532-541. doi:10.7326/M15-1181

11. Fontaine KR, Redden DT, Wang C, Westfall AO, Allison DB. Years of Life Lost Due to Obesity. *JAMA*. 2003;289(2):187-193. doi:10.1001/jama.289.2.187

12. Prospective Studies Collaboration, Whitlock G, Lewington S, Sherliker P, Clarke R, Emberson J, Halsey J, Qizilbash N, Collins R, Peto R. Body-mass index and cause-specific mortality in 900 000 adults: collaborative analyses of 57 prospective studies. *Lancet Lond Engl*. 2009;373(9669):1083-1096. doi:10.1016/S0140-6736(09)60318-4

13. Arner P, Bernard S, Salehpour M, Possnert G, Liebl J, Steier P, Buchholz BA, Eriksson M, Arner E, Hauner H, Skurk T, Rydén M, Frayn KN, Spalding KL. Dynamics of human adipose lipid turnover in health and metabolic disease. *Nature*. 2011;478(7367):110-113. doi:10.1038/nature10426

14. Berndt J, Kralisch S, Klöting N, Ruschke K, Kern M, Fasshauer M, Schön MR, Stumvoll M, Blüher M. Adipose Triglyceride Lipase Gene Expression in Human Visceral Obesity. *Exp Clin Endocrinol Diabetes*. Published online December 10, 2007:203-210. doi:10.1055/s-2007-993148

15. Jocken JWE, Langin D, Smit E, Saris WHM, Valle C, Hul GB, Holm C, Arner P, Blaak EE. Adipose Triglyceride Lipase and Hormone-Sensitive Lipase Protein Expression Is Decreased in the Obese Insulin-Resistant State. *J Clin Endocrinol Metab*. 2007;92(6):2292-2299. doi:10.1210/jc.2006-1318

16. Spalding KL, Arner E, Westermark PO, Bernard S, Buchholz BA, Bergmann O, Blomqvist L, Hoffstedt J, Näslund E, Britton T, Concha H, Hassan M, Rydén M, Frisén J, Arner P. Dynamics of fat cell turnover in humans. *Nature*. 2008;453(7196):783-787. doi:10.1038/nature06902

17. Sam S, Mazzone T. Adipose tissue changes in obesity and the impact on metabolic function. *Transl Res*. 2014;164(4):284-292. doi:10.1016/j.trsl.2014.05.008

18. Halberg N, Wernstedt-Asterholm I, Scherer PE. The adipocyte as an endocrine cell. *Endocrinol Metab Clin North Am*. 2008;37(3):753-768.

19. Sun K, Kusminski CM, Scherer PE. Adipose tissue remodeling and obesity. *J Clin Invest*. 2011;121(6):2094-2101. doi:10.1172/JCI45887

20. Cnop M, Havel PJ, Utzschneider KM, Carr DB, Sinha MK, Boyko EJ, Retzlaff BM, Knopp RH, Brunzell JD, Kahn SE. Relationship of adiponectin to body fat distribution, insulin sensitivity and plasma lipoproteins: evidence for independent roles of age and sex. *Diabetologia*. 2003;46(4):459-469. doi:10.1007/s00125-003-1074-z

21. Tschritter O, Fritsche A, Thamer C, Haap M, Shirkavand F, Rahe S, Staiger H, Maerker E, Häring H, Stumvoll M. Plasma adiponectin concentrations predict insulin sensitivity of both glucose and lipid metabolism. *Diabetes*. 2003;52(2):239-243. doi:10.2337/diabetes.52.2.239

22. Turer AT, Khera A, Ayers CR, Turer CB, Grundy SM, Vega GL, Scherer PE. Adipose tissue mass and location affect circulating adiponectin levels. *Diabetologia*. 2011;54(10):2515-2524. doi:10.1007/s00125-011-2252-z

23. Banks WA, Kastin AJ, Huang W, Jaspan JB, Maness LM. Leptin enters the brain by a saturable system independent of insulin. *Peptides*. 1996;17(2):305-311.

24. Considine RV, Sinha MK, Heiman ML, Kriauciunas A, Stephens TW, Nyce MR, Ohannesian JP, Marco CC, McKee LJ, Bauer TL, Caro JF. Serum Immunoreactive-Leptin Concentrations in Normal-Weight and Obese Humans. *N Engl J Med*. 1996;334(5):292-295. doi:10.1056/NEJM199602013340503

25. Hotamisligil GS, Shargill NS, Spiegelman BM. Adipose Expression of Tumor Necrosis Factor-α: Direct Role in Obesity-Linked Insulin Resistance. *Science*. 1993;259(5091):87-91. doi:10.1126/science.7678183

26. Lumeng CN, Bodzin JL, Saltiel AR. Obesity induces a phenotypic switch in adipose tissue macrophage polarization. *J Clin Invest*. 2007;117(1):175-184. doi:10.1172/JCI29881

27. Weisberg SP, McCann D, Desai M, Rosenbaum M, Leibel RL, Ferrante AW. Obesity is associated with macrophage accumulation in adipose tissue. *J Clin Invest*. 2003;112(12):1796-1808. doi:10.1172/JCI19246

28. van Vliet S, Koh HCE, Patterson BW, Yoshino M, LaForest R, Gropler RJ, Klein S, Mittendorfer B. Obesity Is Associated With Increased Basal and Postprandial β-Cell Insulin Secretion Even in the Absence of Insulin Resistance. *Diabetes*. 2020;69(10):2112-2119. doi:10.2337/db20-0377

29. Perley M, Kipnis DM. Plasma Insulin Responses to Glucose and Tolbutamide of Normal Weight and Obese Diabetic and Nondiabetic Subjects. *Diabetes*. 1966;15(12):867-874. doi:10.2337/diab.15.12.867

30. Polonsky KS, Given BD, Van Cauter E. Twenty-four-hour profiles and pulsatile patterns of insulin secretion in normal and obese subjects. *J Clin Invest*. 1988;81(2):442-448. doi:10.1172/JCI113339

31. Mittendorfer B, Magkos F, Fabbrini E, Mohammed BS, Klein S. Relationship between body fat mass and free fatty acid kinetics in men and women. *Obes Silver Spring Md*. 2009;17(10):1872-1877. doi:10.1038/oby.2009.224

32. Roden M, Price TB, Perseghin G, Petersen KF, Rothman DL, Cline GW, Shulman GI. Mechanism of free fatty acid-induced insulin resistance in humans. *J Clin Invest*. 1996;97(12):2859-2865. doi:10.1172/JCI118742

33. Santomauro AT, Boden G, Silva ME, Rocha DM, Santos RF, Ursich MJ, Strassmann PG, Wajchenberg BL. Overnight lowering of free fatty acids with Acipimox improves insulin resistance and glucose tolerance in obese diabetic and nondiabetic subjects. *Diabetes*. 1999;48(9):1836-1841. doi:10.2337/diabetes.48.9.1836

34. Unger RH. Lipotoxicity in the pathogenesis of obesity-dependent NIDDM. Genetic and clinical implications. *Diabetes*. 1995;44(8):863-870. doi:10.2337/diab.44.8.863

35. Unger RH, Grundy S. Hyperglycaemia as an inducer as well as a consequence of impaired islet cell function and insulin resistance: implications for the management of diabetes. *Diabetologia*. 1985;28:119-121.

36. Elks CE, den Hoed M, Zhao JH, Sharp SJ, Wareham NJ, Loos RJF, Ong KK. Variability in the

heritability of body mass index: a systematic review and meta-regression. *Front Endocrinol*. 2012;3:29. doi:10.3389/fendo.2012.00029

37. Maes HH, Neale MC, Eaves LJ. Genetic and environmental factors in relative body weight and human adiposity. *Behav Genet*. 1997;27(4):325-351. doi:10.1023/a:1025635913927

38. Malis C, Rasmussen EL, Poulsen P, Petersen I, Christensen K, Beck-Nielsen H, Astrup A, Vaag AA. Total and regional fat distribution is strongly influenced by genetic factors in young and elderly twins. *Obes Res*. 2005;13(12):2139-2145. doi:10.1038/oby.2005.265

39. Stunkard AJ, Foch TT, Hrubec Z. A twin study of human obesity. *JAMA*. 1986;256(1):51-54.

40. Frayling TM, Timpson NJ, Weedon MN, Zeggini E, Freathy RM, Lindgren CM, Perry JR, Elliott KS, Lango H, Rayner NW. A common variant in the FTO gene is associated with body mass index and predisposes to childhood and adult obesity. *Science*. 2007;316(5826):889-894.

41. Yengo L, Sidorenko J, Kemper KE, Zheng Z, Wood AR, Weedon MN, Frayling TM, Hirschhorn J, Yang J, Visscher PM, GIANT Consortium. Meta-analysis of genome-wide association studies for height and body mass index in ∼700000 individuals of European ancestry. *Hum Mol Genet*. 2018;27(20):3641-3649. doi:10.1093/hmg/ddy271

42. Kilpeläinen TO, Zillikens MC, Stančákova A, Finucane FM, Ried JS, Langenberg C, Zhang W, Beckmann JS, Luan J, Vandenput L, Styrkarsdottir U, Zhou Y, Smith AV, Zhao JH, Amin N, Vedantam S, Shin SY, Haritunians T, Fu M, Feitosa MF, Kumari M, Halldorsson BV, Tikkanen E, Mangino M, Hayward C, Song C, Arnold AM, Aulchenko YS, Oostra BA, Campbell H, Cupples LA, Davis KE, Döring A, Eiriksdottir G, Estrada K, Fernández-Real JM, Garcia M, Gieger C, Glazer NL, Guiducci C, Hofman A, Humphries SE, Isomaa B, Jacobs LC, Jula A, Karasik D, Karlsson MK, Khaw KT, Kim LJ, Kivimäki M, Klopp N, Kühnel B, Kuusisto J, Liu Y, Ljunggren Ö, Lorentzon M, Luben RN, McKnight B, Mellström D, Mitchell BD, Mooser V, Moreno JM, Männistö S, O'Connell JR, Pascoe L, Peltonen L, Peral B, Perola M, Psaty BM, Salomaa V, Savage DB, Semple RK, Skaric-Juric T, Sigurdsson G, Song KS, Spector TD, Syvänen AC, Talmud PJ, Thorleifsson G, Thorsteinsdottir U, Uitterlinden AG, van Duijn CM, Vidal-Puig A, Wild SH, Wright AF, Clegg DJ, Schadt E, Wilson JF, Rudan I, Ripatti S, Borecki IB, Shuldiner AR, Ingelsson E, Jansson JO, Kaplan RC, Gudnason V, Harris TB, Groop L, et al. Genetic variation near IRS1 associates with reduced adiposity and an impaired metabolic profile. *Nat Genet*. 2011;43(8):753-760. doi:10.1038/ng.866

43. Lu Y, Day FR, Gustafsson S, Buchkovich ML, Na J, Bataille V, Cousminer DL, Dastani Z, Drong AW, Esko T, Evans DM, Falchi M, Feitosa MF, Ferreira T, Hedman ÅK, Haring R, Hysi PG, Iles MM, Justice AE, Kanoni S, Lagou V, Li R, Li X, Locke A, Lu C, Mägi R, Perry JRB, Pers TH, Qi Q, Sanna M, Schmidt EM, Scott WR, Shungin D, Teumer A, Vinkhuyzen AAE, Walker RW, Westra HJ, Zhang M, Zhang W, Zhao JH, Zhu Z, Afzal U, Ahluwalia TS, Bakker SJL, Bellis C, Bonnefond A, Borodulin K, Buchman AS, Cederholm T, Choh AC, Choi HJ, Curran JE, de Groot LCPGM, De Jager PL, Dhonukshe-Rutten RAM, Enneman AW, Eury E, Evans DS, Forsen T, Friedrich N, Fumeron F, Garcia ME, Gärtner S, Han BG, Havulinna AS, Hayward C, Hernandez D, Hillege H, Ittermann T, Kent JW, Kolcic I, Laatikainen T, Lahti J, Leach IM, Lee CG, Lee JY, Liu T, Liu Y, Lobbens S, Loh M, Lyytikäinen LP, Medina-Gomez C, Michaëlsson K, Nalls MA, Nielson CM, Oozageer L, Pascoe L, Paternoster L, Polašek O, Ripatti S, Sarzynski MA, Shin CS, Narančić NS, Spira D, Srikanth P, Steinhagen-Thiessen E, Sung YJ, Swart KMA, et al. New loci for body fat percentage reveal link between adiposity and cardiometabolic disease risk. *Nat Commun*. 2016;7(1):10495. doi:10.1038/ncomms10495

44. Zillikens MC, Demissie S, Hsu YH, Yerges-Armstrong LM, Chou WC, Stolk L, Livshits G, Broer L, Johnson T, Koller DL, Kutalik Z, Luan J, Malkin I, Ried JS, Smith AV, Thorleifsson G, Vandenput L, Hua Zhao J, Zhang W, Aghdassi A, Åkesson K, Amin N, Baier LJ, Barroso I, Bennett DA, Bertram L, Biffar R, Bochud M, Boehnke M, Borecki IB, Buchman AS, Byberg L, Campbell H, Campos Obanda N, Cauley JA, Cawthon PM, Cederberg H, Chen Z, Cho NH, Jin Choi H, Claussnitzer M, Collins F, Cummings SR, De Jager PL, Demuth I, Dhonukshe-Rutten RAM, Diatchenko L, Eiriksdottir G, Enneman AW, Erdos M, Eriksson JG, Eriksson J, Estrada K, Evans DS, Feitosa MF, Fu M, Garcia M, Gieger C, Girke T, Glazer NL, Grallert H, Grewal J, Han BG, Hanson RL, Hayward C, Hofman A, Hoffman EP, Homuth G, Hsueh WC, Hubal MJ, Hubbard A, Huffman KM, Husted LB, Illig T, Ingelsson E, Ittermann T, Jansson JO, Jordan JM, Jula A, Karlsson M, Khaw KT, Kilpeläinen TO, Klopp N, Kloth JSL, Koistinen HA, Kraus WE, Kritchevsky S, Kuulasmaa T, Kuusisto J, Laakso M, Lahti J, Lang T, Langdahl BL, Launer LJ, Lee JY, Lerch MM, Lewis JR, Lind L, et al. Large meta-analysis of genome-wide association studies identifies five loci for lean body mass. *Nat Commun*. 2017;8(1):80. doi:10.1038/s41467-017-00031-7

45. Kilpeläinen TO, Carli JFM, Skowronski AA, Sun Q, Kriebel J, Feitosa MF, Hedman ÅK, Drong AW, Hayes JE, Zhao J, Pers TH, Schick U, Grarup N, Kutalik Z, Trompet S, Mangino M, Kristiansson K, Beekman M, Lyytikäinen LP, Eriksson J, Henneman P, Lahti J, Tanaka T, Luan J, Greco M FD, Pasko D, Renström F, Willems SM, Mahajan A, Rose LM, Guo X, Liu Y, Kleber ME, Pérusse L, Gaunt T, Ahluwalia TS, Ju Sung Y, Ramos YF, Amin N, Amuzu A, Barroso I, Bellis C, Blangero J, Buckley BM, Böhringer S, I Chen YD, de Craen AJN, Crosslin DR, Dale CE, Dastani Z, Day FR, Deelen J, Delgado GE, Demirkan A, Finucane FM, Ford I, Garcia ME, Gieger C, Gustafsson S, Hallmans G, Hankinson SE, Havulinna AS, Herder C, Hernandez D, Hicks AA, Hunter DJ, Illig T, Ingelsson E, Ioan-Facsinay A, Jansson JO, Jenny NS, Jørgensen ME, Jørgensen T, Karlsson M, Koenig W, Kraft P, Kwekkeboom J, Laatikainen T, Ladwig KH, LeDuc CA, Lowe G, Lu Y, Marques-Vidal P, Meisinger C, Menni C, Morris AP, Myers RH, Männistö S, Nalls MA, Paternoster L, Peters A, Pradhan AD, Rankinen T, Rasmussen-Torvik LJ, Rathmann W, Rice TK, Brent Richards J, Ridker PM, et al. Genome-wide meta-analysis uncovers novel loci influencing circulating leptin levels. *Nat Commun*. 2016;7(1):10494. doi:10.1038/ncomms10494

46. Orthofer M, Valsesia A, Mägi R, Wang QP, Kaczanowska J, Kozieradzki I, Leopoldi A, Cikes D, Zopf LM, Tretiakov EO, Demetz E, Hilbe R, Boehm A, Ticevic M, Nõukas M, Jais A, Spirk K, Clark T, Amann S, Lepamets M, Neumayr C, Arnold C, Dou Z, Kuhn V, Novatchkova M, Cronin SJF, Tietge UJF, Müller S, Pospisilik JA, Nagy V, Hui CC, Lazovic J, Esterbauer H, Hagelkruys A, Tancevski I, Kiefer FW, Harkany T, Haubensak W, Neely GG, Metspalu A, Hager J, Gheldof N, Penninger JM. Identification of ALK in Thinness. *Cell*. 2020;181(6):1246-1262.e22. doi:10.1016/j.cell.2020.04.034

47. Riveros-McKay F, Mistry V, Bounds R, Hendricks A, Keogh JM, Thomas H, Henning E, Corbin LJ, Group USS, O'Rahilly S, Zeggini E, Wheeler E, Barroso I, Farooqi IS. Genetic architecture of human thinness compared to severe obesity. *PLOS Genet*. 2019;15(1):e1007603. doi:10.1371/journal.pgen.1007603

48. Montague CT, Farooqi IS, Whitehead JP, Soos MA, Rau H, Wareham NJ, Sewter CP, Digby JE, Mohammed SN, Hurst JA. Congenital leptin deficiency is associated with severe early-onset obesity in humans. *Nature*. 1997;387(6636):903-908.

49. Clement K, Vaisse C, Lahlou N, Cabrol S, Pelloux V, Cassuto D, Gourmelen M, Dina C, Chambaz J, Lacorte JM. A mutation in the human leptin receptor gene causes obesity and pituitary

dysfunction. *Nature*. 1998;392(6674):398-401.

50. Jackson RS, Creemers JW, Ohagi S, Raffin-Sanson ML, Sanders L, Montague CT, Hutton JC, O'Rahilly S. Obesity and impaired prohormone processing associated with mutations in the human prohormone convertase 1 gene. *Nat Genet*. 1997;16(3):303-306. doi:10.1038/ng0797-303

51. Krude H, Biebermann H, Luck W, Horn R, Brabant G, Grüters A. Severe early-onset obesity, adrenal insufficiency and red hair pigmentation caused by POMC mutations in humans. *Nat Genet*. 1998;19(2):155-157. doi:10.1038/509

52. Krude H, Biebermann H, Schnabel D, Tansek MZ, Theunissen P, Mullis PE, Grüters A. Obesity due to proopiomelanocortin deficiency: three new cases and treatment trials with thyroid hormone and ACTH4–10. *J Clin Endocrinol Metab*. 2003;88(10):4633-4640.

53. Vaisse C, Clement K, Guy-Grand B, Froguel P. A frameshift mutation in human MC4R is associated with a dominant form of obesity. *Nat Genet*. 1998;20(2):113-114. doi:10.1038/2407

54. Yeo GS, Farooqi IS, Aminian S, Halsall DJ, Stanhope RG, O'Rahilly S. A frameshift mutation in MC4R associated with dominantly inherited human obesity. *Nat Genet*. 1998;20(2):111-112. doi:10.1038/2404

55. Spiegelman BM, Flier JS. Obesity and the regulation of energy balance. *cell*. 2001;104(4):531-543.

56. Schwartz MW, Woods SC, Porte Jr D, Seeley RJ, Baskin DG. Central nervous system control of food intake. *Nature*. 2000;404(6778):661-671.

57. Elmquist JK, Elias CF, Saper CB. From lesions to leptin: hypothalamic control of food intake and body weight. *Neuron*. 1999;22(2):221-232.

58. Hetherington AW, Ranson SW. Hypothalamic lesions and adiposity in the rat. *Anat Rec*. 1940;78(2):149-172. doi:10.1002/ar.1090780203

59. Anand BK, Brobeck JR. Localization of a "feeding center" in the hypothalamus of the rat. *Proc Soc Exp Biol Med*. 1951;77(2):323-325.

60. Leibowitz SF, Hammer NJ, Chang K. Hypothalamic paraventricular nucleus lesions produce overeating and obesity in the rat. *Physiol Behav*. 1981;27(6):1031-1040.

61. Hahn TM, Breininger JF, Baskin DG, Schwartz MW. Coexpression of Agrp and NPY in fasting-activated hypothalamic neurons. *Nat Neurosci*. 1998;1(4):271-272.

62. Watson SJ, Akil H. The presence of two [alpha]-MSH positive cell groups in rat hypothalamus. Published online 1979.

63. Elias CF, Lee C, Kelly J, Aschkenasi C, Ahima RS, Couceyro PR, Kuhar MJ, Saper CB, Elmquist JK. Leptin activates hypothalamic CART neurons projecting to the spinal cord. *Neuron*. 1998;21(6):1375-1385.

64. Mountjoy KG, Mortrud MT, Low MJ, Simerly RB, Cone RD. Localization of the melanocortin-4 receptor (MC4-R) in neuroendocrine and autonomic control circuits in the brain. *Mol Endocrinol*.

1994;8(10):1298-1308.

65. Fan W, Boston BA, Kesterson RA, Hruby VJ, Cone RD. Role of melanocortinergic neurons in feeding and the agouti obesity syndrome. *Nature*. 1997;385(6612):165-168.

66. Ollmann MM, Wilson BD, Yang YK, Kerns JA, Chen Y, Gantz I, Barsh GS. Antagonism of central melanocortin receptors in vitro and in vivo by agouti-related protein. *Science*. 1997;278(5335):135-138.

67. Foster MT, Song CK, Bartness TJ. Hypothalamic paraventricular nucleus lesion involvement in the sympathetic control of lipid mobilization. *Obesity*. 2010;18(4):682-689.

68. Xi D, Gandhi N, Lai M, Kublaoui BM. Ablation of Sim1 neurons causes obesity through hyperphagia and reduced energy expenditure. *PloS One*. 2012;7(4):e36453.

69. Kishi T, Aschkenasi CJ, Lee CE, Mountjoy KG, Saper CB, Elmquist JK. Expression of melanocortin 4 receptor mRNA in the central nervous system of the rat. *J Comp Neurol*. 2003;457(3):213-235.

70. Xu B, Goulding EH, Zang K, Cepoi D, Cone RD, Jones KR, Tecott LH, Reichardt LF. Brain-derived neurotrophic factor regulates energy balance downstream of melanocortin-4 receptor. *Nat Neurosci*. 2003;6(7):736-742.

71. Kamitakahara A, Xu B, Simerly R. Ventromedial hypothalamic expression of Bdnf is required to establish normal patterns of afferent GABAergic connectivity and responses to hypoglycemia. *Mol Metab*. 2015;5(2):91-101. doi:10.1016/j.molmet.2015.11.007

72. Krashes MJ, Koda S, Ye C, Rogan SC, Adams AC, Cusher DS, Maratos-Flier E, Roth BL, Lowell BB. Rapid, reversible activation of AgRP neurons drives feeding behavior in mice. *J Clin Invest*. 2011;121(4):1424-1428. doi:10.1172/JCI46229

73. Zhan C, Zhou J, Feng Q, Zhang JE, Lin S, Bao J, Wu P, Luo M. Acute and long-term suppression of feeding behavior by POMC neurons in the brainstem and hypothalamus, respectively. *J Neurosci Off J Soc Neurosci*. 2013;33(8):3624-3632. doi:10.1523/JNEUROSCI.2742-12.2013

74. Cowley MA, Pronchuk N, Fan W, Dinulescu DM, Colmers WF, Cone RD. Integration of NPY, AGRP, and Melanocortin Signals in the Hypothalamic Paraventricular Nucleus: Evidence of a Cellular Basis for the Adipostat. *Neuron*. 1999;24(1):155-163. doi:10.1016/S0896-6273(00)80829-6

75. INGALLS AM, DICKIE MM, SNELL GD. OBESE, A NEW MUTATION IN THE HOUSE MOUSE*. *J Hered*. 1950;41(12):317-318. doi:10.1093/oxfordjournals.jhered.a106073

76. Hummel KP, Dickie MM, Coleman DL. Diabetes, a New Mutation in the Mouse. *Science*. 1966;153(3740):1127-1128. doi:10.1126/science.153.3740.1127

77. Zhang Y, Proenca R, Maffei M, Barone M, Leopold L, Friedman JM. Positional cloning of the mouse obese gene and its human homologue. *Nature*. 1994;372(6505):425-432.

78. Chen H, Charlat O, Tartaglia LA, Woolf EA, Weng X, Ellis SJ, Lakey ND, Culpepper J, Moore KJ, Breitbart RE, Duyk GM, Tepper RI, Morgenstern JP. Evidence that the diabetes gene encodes

the leptin receptor: identification of a mutation in the leptin receptor gene in db/db mice. *Cell*. 1996;84(3):491-495. doi:10.1016/s0092-8674(00)81294-5

79. Halaas JL, Gajiwala KS, Maffei M, Cohen SL, Chait BT, Rabinowitz D, Lallone RL, Burley SK, Friedman JM. Weight-reducing effects of the plasma protein encoded by the obese gene. *Science*. 1995;269(5223):543-546. doi:10.1126/science.7624777

80. Pelleymounter MA, Cullen MJ, Baker MB, Hecht R, Winters D, Boone T, Collins F. Effects of the obese gene product on body weight regulation in ob/ob mice. *Science*. 1995;269(5223):540-543. doi:10.1126/science.7624776

81. Bultman SJ, Michaud EJ, Woychik RP. Molecular characterization of the mouse agouti locus. *Cell*. 1992;71(7):1195-1204. doi:10.1016/s0092-8674(05)80067-4

82. Miller MW, Duhl DM, Vrieling H, Cordes SP, Ollmann MM, Winkes BM, Barsh GS. Cloning of the mouse agouti gene predicts a secreted protein ubiquitously expressed in mice carrying the lethal yellow mutation. *Genes Dev*. 1993;7(3):454-467. doi:10.1101/gad.7.3.454

83. Lu D, Willard D, Patel IR, Kadwell S, Overton L, Kost T, Luther M, Chen W, Woychik RP, Wilkison WO, Cone RD. Agouti protein is an antagonist of the melanocyte-stimulating-hormone receptor. *Nature*. 1994;371(6500):799-802. doi:10.1038/371799a0

84. Yaswen L, Diehl N, Brennan MB, Hochgeschwender U. Obesity in the mouse model of pro-opiomelanocortin deficiency responds to peripheral melanocortin. *Nat Med*. 1999;5(9):1066-1070. doi:10.1038/12506

85. Challis BG, Coll AP, Yeo GSH, Pinnock SB, Dickson SL, Thresher RR, Dixon J, Zahn D, Rochford JJ, White A, Oliver RL, Millington G, Aparicio SA, Colledge WH, Russ AP, Carlton MB, O'Rahilly S. Mice lacking pro-opiomelanocortin are sensitive to high-fat feeding but respond normally to the acute anorectic effects of peptide-YY3-36. *Proc Natl Acad Sci U S A*. 2004;101(13):4695-4700. doi:10.1073/pnas.0306931101

86. Qian S, Chen H, Weingarth D, Trumbauer ME, Novi DE, Guan X, Yu H, Shen Z, Feng Y, Frazier E, Chen A, Camacho RE, Shearman LP, Gopal-Truter S, MacNeil DJ, Van der Ploeg LHT, Marsh DJ. Neither Agouti-Related Protein nor Neuropeptide Y Is Critically Required for the Regulation of Energy Homeostasis in Mice. *Mol Cell Biol*. 2002;22(14):5027-5035. doi:10.1128/MCB.22.14.5027-5035.2002

87. Corander MP, Rimmington D, Challis BG, O'Rahilly S, Coll AP. Loss of Agouti-Related Peptide Does Not Significantly Impact the Phenotype of Murine POMC Deficiency. *Endocrinology*. 2011;152(5):1819-1828. doi:10.1210/en.2010-1450

88. Huszar D, Lynch CA, Fairchild-Huntress V, Dunmore JH, Fang Q, Berkemeier LR, Gu W, Kesterson RA, Boston BA, Cone RD, Smith FJ, Campfield LA, Burn P, Lee F. Targeted disruption of the melanocortin-4 receptor results in obesity in mice. *Cell*. 1997;88(1):131-141. doi:10.1016/s0092-8674(00)81865-6

89. Itoh M, Suganami T, Nakagawa N, Tanaka M, Yamamoto Y, Kamei Y, Terai S, Sakaida I, Ogawa Y. Melanocortin 4 Receptor–Deficient Mice as a Novel Mouse Model of Nonalcoholic Steatohepatitis. *Am J Pathol*. 2011;179(5):2454-2463. doi:10.1016/j.ajpath.2011.07.014

90. Butler AA, Kesterson RA, Khong K, Cullen MJ, Pelleymounter MA, Dekoning J, Baetscher M, Cone RD. A unique metabolic syndrome causes obesity in the melanocortin-3 receptor-deficient mouse. *Endocrinology*. 2000;141(9):3518-3521. doi:10.1210/endo.141.9.7791

91. Chen AS, Marsh DJ, Trumbauer ME, Frazier EG, Guan XM, Yu H, Rosenblum CI, Vongs A, Feng Y, Cao L, Metzger JM, Strack AM, Camacho RE, Mellin TN, Nunes CN, Min W, Fisher J, Gopal-Truter S, MacIntyre DE, Chen HY, Van der Ploeg LH. Inactivation of the mouse melanocortin-3 receptor results in increased fat mass and reduced lean body mass. *Nat Genet*. 2000;26(1):97-102. doi:10.1038/79254

92. Greenman Y, Kuperman Y, Drori Y, Asa SL, Navon I, Forkosh O, Gil S, Stern N, Chen A. Postnatal ablation of POMC neurons induces an obese phenotype characterized by decreased food intake and enhanced anxiety-like behavior. *Mol Endocrinol Baltim Md*. 2013;27(7):1091-1102. doi:10.1210/me.2012-1344

93. Gropp E, Shanabrough M, Borok E, Xu AW, Janoschek R, Buch T, Plum L, Balthasar N, Hampel B, Waisman A, Barsh GS, Horvath TL, Brüning JC. Agouti-related peptide–expressing neurons are mandatory for feeding. *Nat Neurosci*. 2005;8(10):1289-1291. doi:10.1038/nn1548

94. Luquet S, Perez FA, Hnasko TS, Palmiter RD. NPY/AgRP Neurons Are Essential for Feeding in Adult Mice but Can Be Ablated in Neonates. *Science*. 2005;310(5748):683-685. doi:10.1126/science.1115524

95. Cowley MA, Smart JL, Rubinstein M, Cerdán MG, Diano S, Horvath TL, Cone RD, Low MJ. Leptin activates anorexigenic POMC neurons through a neural network in the arcuate nucleus. *Nature*. 2001;411(6836):480-484. doi:10.1038/35078085

96. Schwartz MW, Seeley RJ, Woods SC, Weigle DS, Campfield LA, Burn P, Baskin DG. Leptin increases hypothalamic pro-opiomelanocortin mRNA expression in the rostral arcuate nucleus. *Diabetes*. 1997;46(12):2119-2123.

97. Baver SB, Hope K, Guyot S, Bjørbaek C, Kaczorowski C, O'Connell KMS. Leptin Modulates the Intrinsic Excitability of AgRP/NPY Neurons in the Arcuate Nucleus of the Hypothalamus. *J Neurosci*. 2014;34(16):5486-5496. doi:10.1523/JNEUROSCI.4861-12.2014

98. Elias CF, Aschkenasi C, Lee C, Kelly J, Ahima RS, Bjorbæk C, Flier JS, Saper CB, Elmquist JK. Leptin Differentially Regulates NPY and POMC Neurons Projecting to the Lateral Hypothalamic Area. *Neuron*. 1999;23(4):775-786. doi:10.1016/S0896-6273(01)80035-0

99. Morrison CD, Morton GJ, Niswender KD, Gelling RW, Schwartz MW. Leptin inhibits hypothalamic Npy and Agrp gene expression via a mechanism that requires phosphatidylinositol 3-OH-kinase signaling. *Am J Physiol-Endocrinol Metab*. 2005;289(6):E1051-E1057. doi:10.1152/ajpendo.00094.2005

100. Balthasar N, Coppari R, McMinn J, Liu SM, Lee CE, Tang V, Kenny CD, McGovern RA, Chua SC, Elmquist JK, Lowell BB. Leptin receptor signaling in POMC neurons is required for normal body weight homeostasis. *Neuron*. 2004;42(6):983-991. doi:10.1016/j.neuron.2004.06.004

101. Han Y, He Y, Harris L, Xu Y, Wu Q. Identification of a GABAergic neural circuit governing leptin signaling deficiency-induced obesity. Liberles SD, Wong ML, eds. *eLife*. 2023;12:e82649. doi:10.7554/eLife.82649

102. Könner AC, Janoschek R, Plum L, Jordan SD, Rother E, Ma X, Xu C, Enriori P, Hampel B, Barsh GS, Kahn CR, Cowley MA, Ashcroft FM, Brüning JC. Insulin action in AgRP-expressing neurons is required for suppression of hepatic glucose production. *Cell Metab*. 2007;5(6):438-449. doi:10.1016/j.cmet.2007.05.004

103. Benoit SC, Air EL, Coolen LM, Strauss R, Jackman A, Clegg DJ, Seeley RJ, Woods SC. The Catabolic Action of Insulin in the Brain Is Mediated by Melanocortins. *J Neurosci*. 2002;22(20):9048-9052. doi:10.1523/JNEUROSCI.22-20-09048.2002

104. Plum L, Ma X, Hampel B, Balthasar N, Coppari R, Münzberg H, Shanabrough M, Burdakov D, Rother E, Janoschek R, Alber J, Belgardt BF, Koch L, Seibler J, Schwenk F, Fekete C, Suzuki A, Mak TW, Krone W, Horvath TL, Ashcroft FM, Brüning JC. Enhanced PIP3 signaling in POMC neurons causes KATP channel activation and leads to diet-sensitive obesity. *J Clin Invest*. 2006;116(7):1886-1901. doi:10.1172/JCI27123

105. Williams KW, Margatho LO, Lee CE, Choi M, Lee S, Scott MM, Elias CF, Elmquist JK. Segregation of acute leptin and insulin effects in distinct populations of arcuate proopiomelanocortin neurons. *J Neurosci Off J Soc Neurosci*. 2010;30(7):2472-2479. doi:10.1523/JNEUROSCI.3118-09.2010

106. Dodd GT, Michael NJ, Lee-Young RS, Mangiafico SP, Pryor JT, Munder AC, Simonds SE, Brüning JC, Zhang ZY, Cowley MA, Andrikopoulos S, Horvath TL, Spanswick D, Tiganis T. Insulin regulates POMC neuronal plasticity to control glucose metabolism. *eLife*. 7:e38704. doi:10.7554/eLife.38704

107. Qiu J, Zhang C, Borgquist A, Nestor CC, Smith AW, Bosch MA, Ku S, Wagner EJ, Rønnekleiv OK, Kelly MJ. Insulin Excites Anorexigenic Proopiomelanocortin Neurons via Activation of Canonical Transient Receptor Potential Channels. *Cell Metab*. 2014;19(4):682-693. doi:10.1016/j.cmet.2014.03.004

108. Bewick GA. Bowels control brain: gut hormones and obesity. *Biochem Medica*. 2012;22(3):283-297.

109. Adrian TE, Ferri GL, Bacarese-Hamilton AJ, Fuessl HS, Polak JM, Bloom SR. Human distribution and release of a putative new gut hormone, peptide YY. *Gastroenterology*. 1985;89(5):1070-1077. doi:10.1016/0016-5085(85)90211-2

110. Batterham RL, Cowley MA, Small CJ, Herzog H, Cohen MA, Dakin CL, Wren AM, Brynes AE, Low MJ, Ghatei MA, Cone RD, Bloom SR. Gut hormone PYY(3-36) physiologically inhibits food intake. *Nature*. 2002;418(6898):650-654. doi:10.1038/nature00887

111. Challis BG, Pinnock SB, Coll AP, Carter RN, Dickson SL, O'Rahilly S. Acute effects of PYY3-36 on food intake and hypothalamic neuropeptide expression in the mouse. *Biochem Biophys Res Commun*. 2003;311(4):915-919. doi:10.1016/j.bbrc.2003.10.089

112. Vrang N, Madsen AN, Tang-Christensen M, Hansen G, Larsen PJ. PYY(3-36) reduces food intake and body weight and improves insulin sensitivity in rodent models of diet-induced obesity. *Am J Physiol Regul Integr Comp Physiol*. 2006;291(2):R367-375. doi:10.1152/ajpregu.00726.2005

113. Meeran K, O'Shea D, Edwards CM, Turton MD, Heath MM, Gunn I, Abusnana S, Rossi M, Small CJ, Goldstone AP, Taylor GM, Sunter D, Steere J, Choi SJ, Ghatei MA, Bloom SR. Repeated

intracerebroventricular administration of glucagon-like peptide-1-(7-36) amide or exendin-(9-39) alters body weight in the rat. *Endocrinology*. 1999;140(1):244-250. doi:10.1210/endo.140.1.6421

114. Turton MD, O'Shea D, Gunn I, Beak SA, Edwards CM, Meeran K, Choi SJ, Taylor GM, Heath MM, Lambert PD, Wilding JP, Smith DM, Ghatei MA, Herbert J, Bloom SR. A role for glucagon-like peptide-1 in the central regulation of feeding. *Nature*. 1996;379(6560):69-72. doi:10.1038/379069a0

115. Verdich C, Flint A, Gutzwiller JP, Näslund E, Beglinger C, Hellström PM, Long SJ, Morgan LM, Holst JJ, Astrup A. A meta-analysis of the effect of glucagon-like peptide-1 (7-36) amide on ad libitum energy intake in humans. *J Clin Endocrinol Metab*. 2001;86(9):4382-4389. doi:10.1210/jcem.86.9.7877

116. Shughrue PJ, Lane MV, Merchenthaler I. Glucagon-like peptide-1 receptor (GLP1-R) mRNA in the rat hypothalamus. *Endocrinology*. 1996;137(11):5159-5162. doi:10.1210/endo.137.11.8895391

117. Secher A, Jelsing J, Baquero AF, Hecksher-Sørensen J, Cowley MA, Dalbøge LS, Hansen G, Grove KL, Pyke C, Raun K, Schäffer L, Tang-Christensen M, Verma S, Witgen BM, Vrang N, Bjerre Knudsen L. The arcuate nucleus mediates GLP-1 receptor agonist liraglutide-dependent weight loss. *J Clin Invest*. 2014;124(10):4473-4488. doi:10.1172/JCI75276

118. Bewick GA, Kent A, Campbell D, Patterson M, Ghatei MA, Bloom SR, Gardiner JV. Mice with hyperghrelinemia are hyperphagic and glucose intolerant and have reduced leptin sensitivity. *Diabetes*. 2009;58(4):840-846. doi:10.2337/db08-1428

119. Lawrence CB, Snape AC, Baudoin FMH, Luckman SM. Acute central ghrelin and GH secretagogues induce feeding and activate brain appetite centers. *Endocrinology*. 2002;143(1):155-162. doi:10.1210/endo.143.1.8561

120. Wren AM, Small CJ, Ward HL, Murphy KG, Dakin CL, Taheri S, Kennedy AR, Roberts GH, Morgan DG, Ghatei MA, Bloom SR. The novel hypothalamic peptide ghrelin stimulates food intake and growth hormone secretion. *Endocrinology*. 2000;141(11):4325-4328. doi:10.1210/endo.141.11.7873

121. Briggs DI, Enriori PJ, Lemus MB, Cowley MA, Andrews ZB. Diet-induced obesity causes ghrelin resistance in arcuate NPY/AgRP neurons. *Endocrinology*. 2010;151(10):4745-4755. doi:10.1210/en.2010-0556

122. Tamura H, Kamegai J, Shimizu T, Ishii S, Sugihara H, Oikawa S. Ghrelin stimulates GH but not food intake in arcuate nucleus ablated rats. *Endocrinology*. 2002;143(9):3268-3275. doi:10.1210/en.2002-220268

123. Shiiya T, Nakazato M, Mizuta M, Date Y, Mondal MS, Tanaka M, Nozoe SI, Hosoda H, Kangawa K, Matsukura S. Plasma ghrelin levels in lean and obese humans and the effect of glucose on ghrelin secretion. *J Clin Endocrinol Metab*. 2002;87(1):240-244. doi:10.1210/jcem.87.1.8129

124. Toshinai K, Mondal MS, Nakazato M, Date Y, Murakami N, Kojima M, Kangawa K, Matsukura S. Upregulation of Ghrelin expression in the stomach upon fasting, insulin-induced hypoglycemia, and leptin administration. *Biochem Biophys Res Commun*. 2001;281(5):1220-1225. doi:10.1006/bbrc.2001.4518

125. Jordan SD, Könner AC, Brüning JC. Sensing the fuels: glucose and lipid signaling in the CNS controlling energy homeostasis. *Cell Mol Life Sci CMLS*. 2010;67(19):3255-3273. doi:10.1007/s00018-010-0414-7

126. Mayer J. Glucostatic Mechanism of Regulation of Food Intake. *N Engl J Med*. 1953;249(1):13-16. doi:10.1056/NEJM195307022490104

127. Anand BK, Chhina GS, Sharma KN, Dua S, Singh B. ACTIVITY OF SINGLE NEURONS IN THE HYPOTHALAMIC FEEDING CENTERS: EFFECT OF GLUCOSE. *Am J Physiol*. 1964;207:1146-1154. doi:10.1152/ajplegacy.1964.207.5.1146

128. Oomura Y, Ono T, Ooyama H, Wayner MJ. Glucose and osmosensitive neurones of the rat hypothalamus. *Nature*. 1969;222(5190):282-284. doi:10.1038/222282a0

129. Oomura Y, Yoshimatsu H. Neural network of glucose monitoring system. *J Auton Nerv Syst*. 1984;10(3-4):359-372. doi:10.1016/0165-1838(84)90033-x

130. Yoon NA, Diano S. Hypothalamic glucose-sensing mechanisms. *Diabetologia*. 2021;64(5):985-993. doi:10.1007/s00125-021-05395-6

131. Chrétien C, Fenech C, Liénard F, Grall S, Chevalier C, Chaudy S, Brenachot X, Berges R, Louche K, Stark R. Transient receptor potential canonical 3 (TRPC3) channels are required for hypothalamic glucose detection and energy homeostasis. *Diabetes*. 2017;66(2):314-324.

132. Fioramonti X, Contié S, Song Z, Routh VH, Lorsignol A, Pénicaud L. Characterization of glucosensing neuron subpopulations in the arcuate nucleus: integration in neuropeptide Y and pro-opio melanocortin networks? *Diabetes*. 2007;56(5):1219-1227.

133. Wang R, Liu X, Hentges ST, Dunn-Meynell AA, Levin BE, Wang W, Routh VH. The regulation of glucose-excited neurons in the hypothalamic arcuate nucleus by glucose and feeding-relevant peptides. *Diabetes*. 2004;53(8):1959-1965.

134. Silver IA, Erecińska M. Glucose-induced intracellular ion changes in sugar-sensitive hypothalamic neurons. *J Neurophysiol*. 1998;79(4):1733-1745. doi:10.1152/jn.1998.79.4.1733

135. Mountjoy PD, Bailey SJ, Rutter GA. Inhibition by glucose or leptin of hypothalamic neurons expressing neuropeptide Y requires changes in AMP-activated protein kinase activity. *Diabetologia*. 2007;50(1):168-177. doi:10.1007/s00125-006-0473-3

136. Muroya S, Yada T, Shioda S, Takigawa M. Glucose-sensitive neurons in the rat arcuate nucleus contain neuropeptide Y. *Neurosci Lett*. 1999;264(1-3):113-116.

137. Murphy BA, Fioramonti X, Jochnowitz N, Fakira K, Gagen K, Contie S, Lorsignol A, Penicaud L, Martin WJ, Routh VH. Fasting enhances the response of arcuate neuropeptide Y-glucose-inhibited neurons to decreased extracellular glucose. *Am J Physiol Cell Physiol*. 2009;296(4):C746-756. doi:10.1152/ajpcell.00641.2008

138. Ibrahim N, Bosch MA, Smart JL, Qiu J, Rubinstein M, Rønnekleiv OK, Low MJ, Kelly MJ. Hypothalamic proopiomelanocortin neurons are glucose responsive and express K(ATP) channels. *Endocrinology*. 2003;144(4):1331-1340. doi:10.1210/en.2002-221033

139. Parton LE, Ye CP, Coppari R, Enriori PJ, Choi B, Zhang CY, Xu C, Vianna CR, Balthasar N, Lee CE. Glucose sensing by POMC neurons regulates glucose homeostasis and is impaired in obesity. *Nature*. 2007;449(7159):228-232.

140. Ashford ML, Boden PR, Treherne JM. Glucose-induced excitation of hypothalamic neurones is mediated by ATP-sensitive K+ channels. *Pflüg Arch*. 1990;415:479-483.

141. Ashford ML, Boden PR, Treherne JM. Tolbutamide excites rat glucoreceptive ventromedial hypothalamic neurones by indirect inhibition of ATP-K+ channels. *Br J Pharmacol*. 1990;101(3):531.

142. Dunn-Meynell AA, Routh VH, Kang L, Gaspers L, Levin BE. Glucokinase Is the Likely Mediator of Glucosensing in Both Glucose-Excited and Glucose-Inhibited Central Neurons. *Diabetes*. 2002;51(7):2056-2065. doi:10.2337/diabetes.51.7.2056

143. Schuit FC, Huypens P, Heimberg H, Pipeleers DG. Glucose sensing in pancreatic β-cells: a model for the study of other glucose-regulated cells in gut, pancreas, and hypothalamus. *Diabetes*. 2001;50(1):1-11.

144. Arluison M, Quignon M, Nguyen P, Thorens B, Leloup C, Penicaud L. Distribution and anatomical localization of the glucose transporter 2 (GLUT2) in the adult rat brain--an immunohistochemical study. *J Chem Neuroanat*. 2004;28(3):117-136. doi:10.1016/j.jchemneu.2004.05.009

145. Leloup C, Arluison M, Lepetit N, Cartier N, Marfaing-Jallat P, Ferré P, Pénicaud L. Glucose transporter 2 (GLUT 2): expression in specific brain nuclei. *Brain Res*. 1994;638(1-2):221-226. doi:10.1016/0006-8993(94)90653-x

146. Leloup C, Magnan C, Benani A, Bonnet E, Alquier T, Offer G, Carriere A, Périquet A, Fernandez Y, Ktorza A. Mitochondrial reactive oxygen species are required for hypothalamic glucose sensing. *Diabetes*. 2006;55(7):2084-2090.

147. Louis-Sylvestre J, Le Magnen J. Fall in blood glucose level precedes meal onset in free-feeding rats. *Neurosci Biobehav Rev*. 1980;4 Suppl 1:13-15. doi:10.1016/0149-7634(80)90041-x

148. Davis JD, Wirtshafter D, Asin KE, Brief D. Sustained intracerebroventricular infusion of brain fuels reduces body weight and food intake in rats. *Science*. 1981;212(4490):81-83. doi:10.1126/science.7193909

149. Berthoud HR, Mogenson GJ. Ingestive behavior after intracerebral and intracerebroventricular infusions of glucose and 2-deoxy-D-glucose. *Am J Physiol*. 1977;233(3):R127-133. doi:10.1152/ajpregu.1977.233.3.R127

150. Miselis RR, Epstein AN. Feeding induced by intracerebroventricular 2-deoxy-D-glucose in the rat. *Am J Physiol*. 1975;229(5):1438-1447. doi:10.1152/ajplegacy.1975.229.5.1438

151. Miller JC, Gnaedinger JM, Rapoport SI. Utilization of plasma fatty acid in rat brain: distribution of [14C]palmitate between oxidative and synthetic pathways. *J Neurochem*. 1987;49(5):1507-1514. doi:10.1111/j.1471-4159.1987.tb01021.x

152. Rapoport SI. In vivo labeling of brain phospholipids by long-chain fatty acids: relation to turnover

and function. *Lipids*. 1996;31 Suppl:S97-101. doi:10.1007/BF02637059

153. Rapoport SI. In vivo fatty acid incorporation into brain phosholipids in relation to plasma availability, signal transduction and membrane remodeling. *J Mol Neurosci MN*. 2001;16(2-3):243-261; discussion 279-284. doi:10.1385/JMN:16:2-3:243

154. Colombani AL, Carneiro L, Benani A, Galinier A, Jaillard T, Duparc T, Offer G, Lorsignol A, Magnan C, Casteilla L. Enhanced hypothalamic glucose sensing in obesity: alteration of redox signaling. *Diabetes*. 2009;58(10):2189-2197.

155. Cruciani-Guglielmacci C, Hervalet A, Douared L, Sanders NM, Levin BE, Ktorza A, Magnan C. Beta oxidation in the brain is required for the effects of non-esterified fatty acids on glucose-induced insulin secretion in rats. *Diabetologia*. 2004;47(11):2032-2038. doi:10.1007/s00125-004-1569-2

156. Wang R, Cruciani-Guglielmacci C, Migrenne S, Magnan C, Cotero VE, Routh VH. Effects of oleic acid on distinct populations of neurons in the hypothalamic arcuate nucleus are dependent on extracellular glucose levels. *J Neurophysiol*. 2006;95(3):1491-1498. doi:10.1152/jn.00697.2005

157. Jo YH, Su Y, Gutierrez-Juarez R, Chua S. Oleic Acid Directly Regulates POMC Neuron Excitability in the Hypothalamus. *J Neurophysiol*. 2009;101(5):2305-2316. doi:10.1152/jn.91294.2008

158. Razolli DS, de Araújo TM, Sant'Ana MR, Kirwan P, Cintra DE, Merkle FT, Velloso LA. POMC processing in the hypothalamus is directly regulated by saturated fat − implications for the development of obesity. *Neuroendocrinology*. 2020;110(1-2):92-104. doi:10.1159/000501023

159. Souza GFP, Solon C, Nascimento LF, De-Lima-Junior JC, Nogueira G, Moura R, Rocha GZ, Fioravante M, Bobbo V, Morari J, Razolli D, Araujo EP, Velloso LA. Defective regulation of POMC precedes hypothalamic inflammation in diet-induced obesity. *Sci Rep*. 2016;6(1):29290. doi:10.1038/srep29290

160. Willett WC, Leibel RL. Dietary fat is not a major determinant of body fat. *Am J Med*. 2002;113 Suppl 9B:47S-59S. doi:10.1016/s0002-9343(01)00992-5

161. Wali JA, Jarzebska N, Raubenheimer D, Simpson SJ, Rodionov RN, O'Sullivan JF. Cardio-Metabolic Effects of High-Fat Diets and Their Underlying Mechanisms—A Narrative Review. *Nutrients*. 2020;12(5):1505. doi:10.3390/nu12051505

162. Takahashi M, Ikemoto S, Ezaki O. Effect of the Fat/Carbohydrate Ratio in the Diet on Obesity and Oral Glucose Tolerance in C57BL/6J Mice. *J Nutr Sci Vitaminol (Tokyo)*. 1999;45(5):583-593. doi:10.3177/jnsv.45.583

163. Chu D, Malinowska E, Jura M, Kozak LP. C57BL/6J mice as a polygenic developmental model of diet-induced obesity. *Physiol Rep*. 2017;5(7):e13093. doi:10.14814/phy2.13093

164. De Souza CT, Araujo EP, Bordin S, Ashimine R, Zollner RL, Boschero AC, Saad MJA, Velloso LA. Consumption of a Fat-Rich Diet Activates a Proinflammatory Response and Induces Insulin Resistance in the Hypothalamus. *Endocrinology*. 2005;146(10):4192-4199. doi:10.1210/en.2004-1520

165. Zhang X, Zhang G, Zhang H, Karin M, Bai H, Cai D. Hypothalamic IKKbeta/NF-kappaB and ER stress link overnutrition to energy imbalance and obesity. *Cell*. 2008;135(1):61-73. doi:10.1016/j.cell.2008.07.043

166. Thaler JP, Yi CX, Schur EA, Guyenet SJ, Hwang BH, Dietrich MO, Zhao X, Sarruf DA, Izgur V, Maravilla KR. Obesity is associated with hypothalamic injury in rodents and humans. *J Clin Invest*. 2012;122(1):153-162.

167. Posey KA, Clegg DJ, Printz RL, Byun J, Morton GJ, Vivekanandan-Giri A, Pennathur S, Baskin DG, Heinecke JW, Woods SC, Schwartz MW, Niswender KD. Hypothalamic proinflammatory lipid accumulation, inflammation, and insulin resistance in rats fed a high-fat diet. *Am J Physiol Endocrinol Metab*. 2009;296(5):E1003-1012. doi:10.1152/ajpendo.90377.2008

168. Milanski M, Degasperi G, Coope A, Morari J, Denis R, Cintra DE, Tsukumo DML, Anhe G, Amaral ME, Takahashi HK, Curi R, Oliveira HC, Carvalheira JBC, Bordin S, Saad MJ, Velloso LA. Saturated fatty acids produce an inflammatory response predominantly through the activation of TLR4 signaling in hypothalamus: implications for the pathogenesis of obesity. *J Neurosci Off J Soc Neurosci*. 2009;29(2):359-370. doi:10.1523/JNEUROSCI.2760-08.2009

169. Moraes JC, Coope A, Morari J, Cintra DE, Roman EA, Pauli JR, Romanatto T, Carvalheira JB, Oliveira ALR, Saad MJ, Velloso LA. High-fat diet induces apoptosis of hypothalamic neurons. *PloS One*. 2009;4(4):e5045. doi:10.1371/journal.pone.0005045

170. Obici S, Feng Z, Morgan K, Stein D, Karkanias G, Rossetti L. Central administration of oleic acid inhibits glucose production and food intake. *Diabetes*. 2002;51(2):271-275.

171. Yi CX, Walter M, Gao Y, Pitra S, Legutko B, Kälin S, Layritz C, García-Cáceres C, Bielohuby M, Bidlingmaier M. TNFα drives mitochondrial stress in POMC neurons in obesity. *Nat Commun*. 2017;8(1):15143.

172. Diano S, Liu ZW, Jeong JK, Dietrich MO, Ruan HB, Kim E, Suyama S, Kelly K, Gyengesi E, Arbiser JL, Belsham DD, Sarruf DA, Schwartz MW, Bennett AM, Shanabrough M, Mobbs CV, Yang X, Gao XB, Horvath TL. Peroxisome proliferation–associated control of reactive oxygen species sets melanocortin tone and feeding in diet-induced obesity. *Nat Med*. 2011;17(9):1121-1127. doi:10.1038/nm.2421

173. Ozcan L, Ergin AS, Lu A, Chung J, Sarkar S, Nie D, Myers MG, Ozcan U. Endoplasmic reticulum stress plays a central role in development of leptin resistance. *Cell Metab*. 2009;9(1):35-51. doi:10.1016/j.cmet.2008.12.004

174. Özcan U, Cao Q, Yilmaz E, Lee AH, Iwakoshi NN, Özdelen E, Tuncman G, Görgün C, Glimcher LH, Hotamisligil GS. Endoplasmic Reticulum Stress Links Obesity, Insulin Action, and Type 2 Diabetes. *Science*. 2004;306(5695):457-461. doi:10.1126/science.1103160

175. Won JC, Jang PG, Namkoong C, Koh EH, Kim SK, Park JY, Lee KU, Kim MS. Central administration of an endoplasmic reticulum stress inducer inhibits the anorexigenic effects of leptin and insulin. *Obes Silver Spring Md*. 2009;17(10):1861-1865. doi:10.1038/oby.2009.194

176. Horvath TL, Sarman B, García-Cáceres C, Enriori PJ, Sotonyi P, Shanabrough M, Borok E, Argente J, Chowen JA, Perez-Tilve D, Pfluger PT, Brönneke HS, Levin BE, Diano S, Cowley MA, Tschöp MH. Synaptic input organization of the melanocortin system predicts diet-induced

hypothalamic reactive gliosis and obesity. *Proc Natl Acad Sci*. 2010;107(33):14875-14880. doi:10.1073/pnas.1004282107

177. Horvath TL. Synaptic plasticity in energy balance regulation. *Obes Silver Spring Md*. 2006;14 Suppl 5:228S-233S. doi:10.1038/oby.2006.314

178. In't Veld P, Smeets S. Microscopic Anatomy of the Human Islet of Langerhans. In: Islam MdS, ed. *Islets of Langerhans*. Springer Netherlands; 2015:19-38. doi:10.1007/978-94-007-6686-0_1

179. Noguchi GM, Huising MO. Integrating the inputs that shape pancreatic islet hormone release. *Nat Metab*. 2019;1(12):1189-1201. doi:10.1038/s42255-019-0148-2

180. El-Gohary Y, Sims-Lucas S, Lath N, Tulachan S, Guo P, Xiao X, Welsh C, Paredes J, Wiersch J, Prasadan K, Shiota C, Gittes GK. Three-dimensional analysis of the islet vasculature. *Anat Rec Hoboken NJ 2007*. 2012;295(9):1473-1481. doi:10.1002/ar.22530

181. Henderson JR, Moss MC. A morphometric study of the endocrine and exocrine capillaries of the pancreas. *Q J Exp Physiol Camb Engl*. 1985;70(3):347-356. doi:10.1113/expphysiol.1985.sp002920

182. Lindsay TH, Halvorson KG, Peters CM, Ghilardi JR, Kuskowski MA, Wong GY, Mantyh PW. A quantitative analysis of the sensory and sympathetic innervation of the mouse pancreas. *Neuroscience*. 2006;137(4):1417-1426. doi:10.1016/j.neuroscience.2005.10.055

183. Rodriguez-Diaz R, Abdulreda MH, Formoso AL, Gans I, Ricordi C, Berggren PO, Caicedo A. AUTONOMIC AXONS IN THE HUMAN ENDOCRINE PANCREAS SHOW UNIQUE INNERVATION PATTERNS. *Cell Metab*. 2011;14(1):45-54. doi:10.1016/j.cmet.2011.05.008

184. Tang SC, Baeyens L, Shen CN, Peng SJ, Chien HJ, Scheel DW, Chamberlain CE, German MS. Human pancreatic neuro-insular network in health and fatty infiltration. *Diabetologia*. 2018;61(1):168-181. doi:10.1007/s00125-017-4409-x

185. MacDonald PE, Joseph JW, Rorsman P. Glucose-sensing mechanisms in pancreatic β-cells. *Philos Trans R Soc B Biol Sci*. 2005;360(1464):2211-2225. doi:10.1098/rstb.2005.1762

186. Matschinsky FM. Glucokinase as glucose sensor and metabolic signal generator in pancreatic beta-cells and hepatocytes. *Diabetes.* 1990;39(6):647-652. doi:10.2337/diab.39.6.647

187. McCulloch LJ, van de Bunt M, Braun M, Frayn KN, Clark A, Gloyn AL. GLUT2 (SLC2A2) is not the principal glucose transporter in human pancreatic beta cells: implications for understanding genetic association signals at this locus. *Mol Genet Metab*. 2011;104(4):648-653. doi:10.1016/j.ymgme.2011.08.026

188. Vos AD, Heimberg H, Quartier E, Huypens P, Bouwens L, Pipeleers D, Schuit F. Human and rat beta cells differ in glucose transporter but not in glucokinase gene expression. *J Clin Invest*. 1995;96(5):2489-2495. doi:10.1172/JCI118308

189. Cook DL, Hales CN. Intracellular ATP directly blocks K+ channels in pancreatic B-cells. *Nature*. 1984;311(5983):271-273. doi:10.1038/311271a0

190. Rorsman P, Trube G. Glucose dependent K+-channels in pancreatic beta-cells are regulated by

intracellular ATP. *Pflugers Arch*. 1985;405(4):305-309. doi:10.1007/BF00595682

191. Braun M, Ramracheya R, Bengtsson M, Zhang Q, Karanauskaite J, Partridge C, Johnson PR, Rorsman P. Voltage-gated ion channels in human pancreatic beta-cells: electrophysiological characterization and role in insulin secretion. *Diabetes*. 2008;57(6):1618-1628. doi:10.2337/db07-0991

192. Henquin JC. D-Glucose inhibits potassium efflux from pancreatic islet cells. *Nature*. 1978;271(5642):271-273. doi:10.1038/271271a0

193. Cushman SW, Wardzala LJ. Potential mechanism of insulin action on glucose transport in the isolated rat adipose cell. Apparent translocation of intracellular transport systems to the plasma membrane. *J Biol Chem*. 1980;255(10):4758-4762.

194. Dimitriadis G, Mitrou P, Lambadiari V, Maratou E, Raptis SA. Insulin effects in muscle and adipose tissue. *Diabetes Res Clin Pract*. 2011;93 Suppl 1:S52-59. doi:10.1016/S0168-8227(11)70014-6

195. Stenbit AE, Tsao TS, Li J, Burcelin R, Geenen DL, Factor SM, Houseknecht K, Katz EB, Charron MJ. GLUT4 heterozygous knockout mice develop muscle insulin resistance and diabetes. *Nat Med*. 1997;3(10):1096-1101. doi:10.1038/nm1097-1096

196. MacDonald PE, Marinis YZD, Ramracheya R, Salehi A, Ma X, Johnson PRV, Cox R, Eliasson L, Rorsman P. A KATP Channel-Dependent Pathway within α Cells Regulates Glucagon Release from Both Rodent and Human Islets of Langerhans. *PLOS Biol*. 2007;5(6):e143. doi:10.1371/journal.pbio.0050143

197. Briant L, Salehi A, Vergari E, Zhang Q, Rorsman P. Glucagon secretion from pancreatic α-cells. *Ups J Med Sci*. 2016;121(2):113-119. doi:10.3109/03009734.2016.1156789

198. Vieira E, Salehi A, Gylfe E. Glucose inhibits glucagon secretion by a direct effect on mouse pancreatic alpha cells. *Diabetologia*. 2007;50(2):370-379. doi:10.1007/s00125-006-0511-1

199. Walker JN, Ramracheya R, Zhang Q, Johnson PRV, Braun M, Rorsman P. Regulation of glucagon secretion by glucose: paracrine, intrinsic or both? *Diabetes Obes Metab*. 2011;13 Suppl 1:95-105. doi:10.1111/j.1463-1326.2011.01450.x

200. Rorsman P, Huising MO. The somatostatin-secreting pancreatic δ-cell in health and disease. *Nat Rev Endocrinol*. 2018;14(7):404-414. doi:10.1038/s41574-018-0020-6

201. Itoh Y, Kawamata Y, Harada M, Kobayashi M, Fujii R, Fukusumi S, Ogi K, Hosoya M, Tanaka Y, Uejima H, Tanaka H, Maruyama M, Satoh R, Okubo S, Kizawa H, Komatsu H, Matsumura F, Noguchi Y, Shinohara T, Hinuma S, Fujisawa Y, Fujino M. Free fatty acids regulate insulin secretion from pancreatic beta cells through GPR40. *Nature*. 2003;422(6928):173-176. doi:10.1038/nature01478

202. Kristinsson H, Bergsten P, Sargsyan E. Free fatty acid receptor 1 (FFAR1/GPR40) signaling affects insulin secretion by enhancing mitochondrial respiration during palmitate exposure. *Biochim Biophys Acta*. 2015;1853(12):3248-3257. doi:10.1016/j.bbamcr.2015.09.022

203. Ferdaoussi M, Bergeron V, Zarrouki B, Kolic J, Cantley J, Fielitz J, Olson EN, Prentki M, Biden

T, MacDonald PE, Poitout V. G protein-coupled receptor (GPR)40-dependent potentiation of insulin secretion in mouse islets is mediated by protein kinase D1. *Diabetologia*. 2012;55(10):2682-2692. doi:10.1007/s00125-012-2650-x

204. Kristinsson H, Smith DM, Bergsten P, Sargsyan E. FFAR1 is involved in both the acute and chronic effects of palmitate on insulin secretion. *Endocrinology*. 2013;154(11):4078-4088. doi:10.1210/en.2013-1352

205. Hoppa MB, Collins S, Ramracheya R, Hodson L, Amisten S, Zhang Q, Johnson P, Ashcroft FM, Rorsman P. Chronic palmitate exposure inhibits insulin secretion by dissociation of Ca(2+) channels from secretory granules. *Cell Metab*. 2009;10(6):455-465. doi:10.1016/j.cmet.2009.09.011

206. Nolan CJ, Madiraju MSR, Delghingaro-Augusto V, Peyot ML, Prentki M. Fatty acid signaling in the beta-cell and insulin secretion. *Diabetes*. 2006;55 Suppl 2:S16-23. doi:10.2337/db06-s003

207. Tang C, Ahmed K, Gille A, Lu S, Gröne HJ, Tunaru S, Offermanns S. Loss of FFA2 and FFA3 increases insulin secretion and improves glucose tolerance in type 2 diabetes. *Nat Med*. 2015;21(2):173-177. doi:10.1038/nm.3779

208. Villa SR, Priyadarshini M, Fuller MH, Bhardwaj T, Brodsky MR, Angueira AR, Mosser RE, Carboneau BA, Tersey SA, Mancebo H, Gilchrist A, Mirmira RG, Gannon M, Layden BT. Loss of Free Fatty Acid Receptor 2 leads to impaired islet mass and beta cell survival. *Sci Rep*. 2016;6(1):28159. doi:10.1038/srep28159

209. Kristinsson H, Sargsyan E, Manell H, Smith DM, Göpel SO, Bergsten P. Basal hypersecretion of glucagon and insulin from palmitate-exposed human islets depends on FFAR1 but not decreased somatostatin secretion. *Sci Rep*. 2017;7(1):4657. doi:10.1038/s41598-017-04730-5

210. Olofsson CS, Salehi A, Göpel SO, Holm C, Rorsman P. Palmitate stimulation of glucagon secretion in mouse pancreatic alpha-cells results from activation of L-type calcium channels and elevation of cytoplasmic calcium. *Diabetes*. 2004;53(11):2836-2843. doi:10.2337/diabetes.53.11.2836

211. Gerich JE, Langlois M, Schneider V, Karam JH, Noacco C. Effects of alternations of plasma free fatty acid levels on pancreatic glucagon secretion in man. *J Clin Invest*. 1974;53(5):1284-1289. doi:10.1172/JCI107675

212. Arntfield ME, van der Kooy D. β-Cell evolution: How the pancreas borrowed from the brain: The shared toolbox of genes expressed by neural and pancreatic endocrine cells may reflect their evolutionary relationship. *BioEssays*. 2011;33(8):582-587. doi:10.1002/bies.201100015

213. Schwartz MW, Guyenet SJ, Cirulli V. The Hypothalamus and β-Cell Connection in the Gene-Targeting Era. *Diabetes*. 2010;59(12):2991-2993. doi:10.2337/db10-1149

214. Atouf F, Czernichow P, Scharfmann R. Expression of neuronal traits in pancreatic beta cells. Implication of neuron-restrictive silencing factor/repressor element silencing transcription factor, a neuron-restrictive silencer. *J Biol Chem*. 1997;272(3):1929-1934. doi:10.1074/jbc.272.3.1929

215. van Arensbergen J, García-Hurtado J, Moran I, Maestro MA, Xu X, Van de Casteele M, Skoudy AL, Palassini M, Heimberg H, Ferrer J. Derepression of Polycomb targets during pancreatic

organogenesis allows insulin-producing beta-cells to adopt a neural gene activity program. *Genome Res*. 2010;20(6):722-732. doi:10.1101/gr.101709.109

216. Cruz SA, Tseng YC, Kaiya H, Hwang PP. Ghrelin affects carbohydrate-glycogen metabolism via insulin inhibition and glucagon stimulation in the zebrafish (Danio rerio) brain. *Comp Biochem Physiol A Mol Integr Physiol*. 2010;156(2):190-200. doi:10.1016/j.cbpa.2010.01.019

217. Devaskar SU, Giddings SJ, Rajakumar PA, Carnaghi LR, Menon RK, Zahm DS. Insulin gene expression and insulin synthesis in mammalian neuronal cells. *J Biol Chem*. 1994;269(11):8445-8454.

218. Pelling M, Anthwal N, McNay D, Gradwohl G, Leiter AB, Guillemot F, Ang SL. Differential requirements for neurogenin 3 in the development of POMC and NPY neurons in the hypothalamus. *Dev Biol*. 2011;349(2):406-416. doi:10.1016/j.ydbio.2010.11.007

219. Rukstalis JM, Habener JF. Neurogenin3: a master regulator of pancreatic islet differentiation and regeneration. *Islets*. 2009;1(3):177-184. doi:10.4161/isl.1.3.9877

220. Hart AW, Mella S, Mendrychowski J, van Heyningen V, Kleinjan DA. The Developmental Regulator Pax6 Is Essential for Maintenance of Islet Cell Function in the Adult Mouse Pancreas. *PLoS ONE*. 2013;8(1):e54173. doi:10.1371/journal.pone.0054173

221. Thakurela S, Tiwari N, Schick S, Garding A, Ivanek R, Berninger B, Tiwari VK. Mapping gene regulatory circuitry of Pax6 during neurogenesis. *Cell Discov*. 2016;2(1):1-22. doi:10.1038/celldisc.2015.45

222. Aigha II, Abdelalim EM. NKX6.1 transcription factor: a crucial regulator of pancreatic β cell development, identity, and proliferation. *Stem Cell Res Ther*. 2020;11(1):459. doi:10.1186/s13287-020-01977-0

223. Sander M, Paydar S, Ericson J, Briscoe J, Berber E, German M, Jessell TM, Rubenstein JLR. Ventral neural patterning by Nkx homeobox genes: Nkx6.1 controls somatic motor neuron and ventral interneuron fates. *Genes Dev*. 2000;14(17):2134-2139.

224. Wicksteed B, Brissova M, Yan W, Opland DM, Plank JL, Reinert RB, Dickson LM, Tamarina NA, Philipson LH, Shostak A, Bernal-Mizrachi E, Elghazi L, Roe MW, Labosky PA, Myers MG, Gannon M, Powers AC, Dempsey PJ. Conditional gene targeting in mouse pancreatic ß-Cells: analysis of ectopic Cre transgene expression in the brain. *Diabetes*. 2010;59(12):3090-3098. doi:10.2337/db10-0624

225. Yang XJ, Kow LM, Funabashi T, Mobbs CV. Hypothalamic glucose sensor: similarities to and differences from pancreatic beta-cell mechanisms. *Diabetes*. 1999;48(9):1763-1772. doi:10.2337/diabetes.48.9.1763

226. Maechler P, Wollheim CB. Mitochondrial glutamate acts as a messenger in glucose-induced insulin exocytosis. *Nature*. 1999;402(6762):685-689. doi:10.1038/45280

227. Gonoi T, Mizuno N, Inagaki N, Kuromi H, Seino Y, Miyazaki J, Seino S. Functional neuronal ionotropic glutamate receptors are expressed in the non-neuronal cell line MIN6. *J Biol Chem*. 1994;269(25):16989-16992. doi:10.1016/S0021-9258(17)32507-3

228. Reetz A, Solimena M, Matteoli M, Folli F, Takei K, De Camilli P. GABA and pancreatic beta-cells: colocalization of glutamic acid decarboxylase (GAD) and GABA with synaptic-like microvesicles suggests their role in GABA storage and secretion. *EMBO J*. 1991;10(5):1275-1284. doi:10.1002/j.1460-2075.1991.tb08069.x

229. Berridge MJ, Bootman MD, Roderick HL. Calcium signalling: dynamics, homeostasis and remodelling. *Nat Rev Mol Cell Biol*. 2003;4(7):517-529. doi:10.1038/nrm1155

230. Greer PL, Greenberg ME. From Synapse to Nucleus: Calcium-Dependent Gene Transcription in the Control of Synapse Development and Function. *Neuron*. 2008;59(6):846-860. doi:10.1016/j.neuron.2008.09.002

231. Sabatini PV, Speckmann T, Lynn FC. Friend and foe: β-cell Ca2+ signaling and the development of diabetes. *Mol Metab*. 2019;21:1-12. doi:10.1016/j.molmet.2018.12.007

232. Berridge MJ. Neuronal calcium signaling. *Neuron*. 1998;21(1):13-26. doi:10.1016/s0896-6273(00)80510-3

233. Jonas P, Burnashev N. Molecular mechanisms controlling calcium entry through AMPA-type glutamate receptor channels. *Neuron*. 1995;15(5):987-990. doi:10.1016/0896-6273(95)90087-x

234. Royo M, Escolano BA, Madrigal MP, Jurado S. AMPA Receptor Function in Hypothalamic Synapses. *Front Synaptic Neurosci*. 2022;14:833449. doi:10.3389/fnsyn.2022.833449

235. Liu T, Kong D, Shah BP, Ye C, Koda S, Saunders A, Ding JB, Yang Z, Sabatini BL, Lowell BB. Fasting activation of AgRP neurons requires NMDA receptors and involves spinogenesis and increased excitatory tone. *Neuron*. 2012;73(3):511-522. doi:10.1016/j.neuron.2011.11.027

236. Suyama S, Ralevski A, Liu ZW, Dietrich MO, Yada T, Simonds SE, Cowley MA, Gao XB, Diano S, Horvath TL. Plasticity of calcium-permeable AMPA glutamate receptors in Pro-opiomelanocortin neurons. *eLife*. 2017;6:e25755. doi:10.7554/eLife.25755

237. Chin D, Means AR. Calmodulin: a prototypical calcium sensor. *Trends Cell Biol*. 2000;10(8):322-328. doi:10.1016/S0962-8924(00)01800-6

238. Shen X, Valencia CA, Szostak J, Dong B, Liu R. Scanning the human proteome for calmodulin-binding proteins. *Proc Natl Acad Sci*. 2005;102(17):5969-5974. doi:10.1073/pnas.0407928102

239. Easom RA. CaM kinase II: a protein kinase with extraordinary talents germane to insulin exocytosis. *Diabetes*. 1999;48(4):675-684. doi:10.2337/diabetes.48.4.675

240. Persaud SJ, Liu B, Sampaio HB, Jones PM, Muller DS. Calcium/calmodulin-dependent kinase IV controls glucose-induced Irs2 expression in mouse beta cells via activation of cAMP response element-binding protein. *Diabetologia*. 2011;54(5):1109-1120. doi:10.1007/s00125-011-2050-7

241. Wang X, Li H, De Leo D, Guo W, Koshkin V, Fantus IG, Giacca A, Chan CB, Der S, Wheeler MB. Gene and Protein Kinase Expression Profiling of Reactive Oxygen Species-Associated Lipotoxicity in the Pancreatic β-Cell Line MIN6. *Diabetes*. 2004;53(1):129-140. doi:10.2337/diabetes.53.1.129

242. Wayman GA, Lee YS, Tokumitsu H, Silva A, Soderling TR. Calmodulin-Kinases: Modulators of

Neuronal Development and Plasticity. *Neuron*. 2008;59(6):914-931. doi:10.1016/j.neuron.2008.08.021

243. Jhala US, Canettieri G, Screaton RA, Kulkarni RN, Krajewski S, Reed J, Walker J, Lin X, White M, Montminy M. cAMP promotes pancreatic beta-cell survival via CREB-mediated induction of IRS2. *Genes Dev*. 2003;17(13):1575-1580. doi:10.1101/gad.1097103

244. Mao Z, Wiedmann M. Calcineurin enhances MEF2 DNA binding activity in calcium-dependent survival of cerebellar granule neurons. *J Biol Chem*. 1999;274(43):31102-31107. doi:10.1074/jbc.274.43.31102

245. Wu H, Rothermel B, Kanatous S, Rosenberg P, Naya FJ, Shelton JM, Hutcheson KA, DiMaio JM, Olson EN, Bassel-Duby R, Williams RS. Activation of MEF2 by muscle activity is mediated through a calcineurin-dependent pathway. *EMBO J*. 2001;20(22):6414-6423. doi:10.1093/emboj/20.22.6414

246. Graef IA, Mermelstein PG, Stankunas K, Neilson JR, Deisseroth K, Tsien RW, Crabtree GR. L-type calcium channels and GSK-3 regulate the activity of NF-ATc4 in hippocampal neurons. *Nature*. 1999;401(6754):703-708. doi:10.1038/44378

247. Macian F. NFAT proteins: key regulators of T-cell development and function. *Nat Rev Immunol*. 2005;5(6):472-484. doi:10.1038/nri1632

248. Bernal-Mizrachi E, Wen W, Shornick M, Permutt MA. Activation of nuclear factor-kappaB by depolarization and Ca(2+) influx in MIN6 insulinoma cells. *Diabetes*. 2002;51 Suppl 3:S484-488. doi:10.2337/diabetes.51.2007.s484

249. Meffert MK, Chang JM, Wiltgen BJ, Fanselow MS, Baltimore D. NF-kappa B functions in synaptic signaling and behavior. *Nat Neurosci*. 2003;6(10):1072-1078. doi:10.1038/nn1110

250. Sheng M, Greenberg ME. The regulation and function of c-fos and other immediate early genes in the nervous system. *Neuron*. 1990;4(4):477-485. doi:10.1016/0896-6273(90)90106-P

251. Morgan JI, Curran T. Calcium as a modulator of the immediate-early gene cascade in neurons. *Cell Calcium*. 1988;9(5-6):303-311.

252. LOEBRICH S, NEDIVI E. The Function of Activity-Regulated Genes in the Nervous System. *Physiol Rev*. 2009;89(4):1079-1103. doi:10.1152/physrev.00013.2009

253. Yap EL, Greenberg ME. Activity-Regulated Transcription: Bridging the Gap between Neural Activity and Behavior. *Neuron*. 2018;100(2):330-348. doi:10.1016/j.neuron.2018.10.013

254. Abraham WC, Dragunow M, Tate WP. The role of immediate early genes in the stabilization of long-term potentiation. *Mol Neurobiol*. 1991;5(2-4):297-314. doi:10.1007/BF02935553

255. Greenberg ME, Ziff EB, Greene LA. Stimulation of Neuronal Acetylcholine Receptors Induces Rapid Gene Transcription. *Science*. 1986;234(4772):80-83. doi:10.1126/science.3749894

256. Spiegel I, Mardinly AR, Gabel HW, Bazinet JE, Couch CH, Tzeng CP, Harmin DA, Greenberg ME. Npas4 regulates excitatory-inhibitory balance within neural circuits through cell-type-specific gene programs. *Cell*. 2014;157(5):1216-1229.

257. Tyssowski KM, DeStefino NR, Cho JH, Dunn CJ, Poston RG, Carty CE, Jones RD, Chang SM, Romeo P, Wurzelmann MK, Ward JM, Andermann ML, Saha RN, Dudek SM, Gray JM. Different Neuronal Activity Patterns Induce Different Gene Expression Programs. *Neuron*. 2018;98(3):530-546.e11. doi:10.1016/j.neuron.2018.04.001

258. Maxwell MA, Muscat GEO. The NR4A Subgroup: Immediate Early Response Genes with Pleiotropic Physiological Roles. *Nucl Recept Signal*. 2006;4(1):nrs.04002. doi:10.1621/nrs.04002

259. Josefsen K, Sørensen LR, Buschard K, Birkenbach M. Glucose induces early growth response gene (Egr-1) expression in pancreatic beta cells. *Diabetologia*. 1999;42(2):195-203. doi:10.1007/s001250051139

260. Ohsugi M, Cras-Méneur C, Zhou Y, Warren W, Bernal-Mizrachi E, Permutt MA. Glucose and insulin treatment of insulinoma cells results in transcriptional regulation of a common set of genes. *Diabetes*. 2004;53(6):1496-1508. doi:10.2337/diabetes.53.6.1496

261. Susini S, Roche E, Prentki M, Schlegel W. Glucose and glucoincretin peptides synergize to induce c-fos, c-jun, junB, zif-268, and nur-77 gene expression in pancreatic beta(INS-1) cells. *FASEB J Off Publ Fed Am Soc Exp Biol*. 1998;12(12):1173-1182.

262. Glauser DA, Brun T, Gauthier BR, Schlegel W. Transcriptional response of pancreatic beta cells to metabolic stimulation: large scale identification of immediate-early and secondary response genes. *BMC Mol Biol*. 2007;8(1):54. doi:10.1186/1471-2199-8-54

263. McIntosh BE, Hogenesch JB, Bradfield CA. Mammalian Per-Arnt-Sim proteins in environmental adaptation. *Annu Rev Physiol*. 2010;72:625-645.

264. Kewley RJ, Whitelaw ML, Chapman-Smith A. The mammalian basic helix–loop–helix/PAS family of transcriptional regulators. *Int J Biochem Cell Biol*. 2004;36(2):189-204.

265. Taylor BL, Zhulin IB. PAS domains: internal sensors of oxygen, redox potential, and light. *Microbiol Mol Biol Rev MMBR*. 1999;63(2):479-506. doi:10.1128/MMBR.63.2.479-506.1999

266. Sabatini PV, Lynn FC. All-encomPASsing regulation of β-cells: PAS domain proteins in β-cell dysfunction and diabetes. *Trends Endocrinol Metab*. 2015;26(1):49-57. doi:10.1016/j.tem.2014.11.002

267. Shimizu I, Yoshida Y, Minamino T. A role for circadian clock in metabolic disease. *Hypertens Res*. 2016;39(7):483-491. doi:10.1038/hr.2016.12

268. Gonzalez FJ, Xie C, Jiang C. The role of hypoxia-inducible factors in metabolic diseases. *Nat Rev Endocrinol*. 2018;15(1):21-32. doi:10.1038/s41574-018-0096-z

269. Sangoram AM, Saez L, Antoch MP, Gekakis N, Staknis D, Whiteley A, Fruechte EM, Vitaterna MH, Shimomura K, King DP, Young MW, Weitz CJ, Takahashi JS. Mammalian Circadian Autoregulatory Loop: A Timeless Ortholog and mPer1 Interact and Negatively Regulate CLOCK-BMAL1-Induced Transcription. *Neuron*. 1998;21(5):1101-1113. doi:10.1016/S0896-6273(00)80627-3

270. Lowrey PL, Shimomura K, Antoch MP, Yamazaki S, Zemenides PD, Ralph MR, Menaker M, Takahashi JS. Positional Syntenic Cloning and Functional Characterization of the Mammalian

Circadian Mutation tau. *Science*. 2000;288(5465):483-491. doi:10.1126/science.288.5465.483

271. Lee H, Chen R, Lee Y, Yoo S, Lee C. Essential roles of CKIδ and CKIε in the mammalian circadian clock. *Proc Natl Acad Sci*. 2009;106(50):21359-21364. doi:10.1073/pnas.0906651106

272. Challet E. The circadian regulation of food intake. *Nat Rev Endocrinol*. 2019;15(7):393-405. doi:10.1038/s41574-019-0210-x

273. McHill AW, Phillips AJ, Czeisler CA, Keating L, Yee K, Barger LK, Garaulet M, Scheer FA, Klerman EB. Later circadian timing of food intake is associated with increased body fat. *Am J Clin Nutr*. 2017;106(5):1213-1219. doi:10.3945/ajcn.117.161588

274. Bray MS, Ratcliffe WF, Grenett MH, Brewer RA, Gamble KL, Young ME. Quantitative analysis of light-phase restricted feeding reveals metabolic dyssynchrony in mice. *Int J Obes*. 2013;37(6):843-852. doi:10.1038/ijo.2012.137

275. Strubbe JH, van Dijk G. The temporal organization of ingestive behaviour and its interaction with regulation of energy balance. *Neurosci Biobehav Rev*. 2002;26(4):485-498. doi:10.1016/S0149-7634(02)00016-7

276. Rivera-Estrada D, Aguilar-Roblero R, Alva-Sánchez C, Villanueva I. The homeostatic feeding response to fasting is under chronostatic control. *Chronobiol Int*. 2018;35(12):1680-1688. doi:10.1080/07420528.2018.1507036

277. De Araujo LD, Roa SL, Bueno AC, Coeli-Lacchini FB, Martins CS, Uchoa ET, Antunes-Rodrigues J, Elias LL, Elias PC, Moreira AC, De Castro M. Restricted Feeding Schedules Modulate in a Different Manner the Expression of Clock Genes in Rat Hypothalamic Nuclei. *Front Neurosci*. 2016;10. Accessed April 19, 2023. https://www.frontiersin.org/articles/10.3389/fnins.2016.00567

278. Guilding C, Hughes AT, Brown TM, Namvar S, Piggins HD. A riot of rhythms: neuronal and glial circadian oscillators in the mediobasal hypothalamus. *Mol Brain*. 2009;2(1):28. doi:10.1186/1756-6606-2-28

279. Tan K, Knight ZA, Friedman JM. Ablation of AgRP neurons impairs adaption to restricted feeding. *Mol Metab*. 2014;3(7):694-704. doi:10.1016/j.molmet.2014.07.002

280. Henry FE, Sugino K, Tozer A, Branco T, Sternson SM. Cell type-specific transcriptomics of hypothalamic energy-sensing neuron responses to weight-loss. Elmquist JK, ed. *eLife*. 2015;4:e09800. doi:10.7554/eLife.09800

281. Cedernaes J, Huang W, Ramsey KM, Waldeck N, Cheng L, Marcheva B, Omura C, Kobayashi Y, Peek CB, Levine DC, Dhir R, Awatramani R, Bradfield CA, Wang XA, Takahashi JS, Mokadem M, Ahima RS, Bass J. Transcriptional Basis for Rhythmic Control of Hunger and Metabolism within the AgRP Neuron. *Cell Metab*. 2019;29(5):1078-1091.e5. doi:10.1016/j.cmet.2019.01.023

282. Semenza GL, Wang GL. A nuclear factor induced by hypoxia via de novo protein synthesis binds to the human erythropoietin gene enhancer at a site required for transcriptional activation. *Mol Cell Biol*. 1992;12(12):5447-5454.

283. Tian H, McKnight SL, Russell DW. Endothelial PAS domain protein 1 (EPAS1), a transcription

factor selectively expressed in endothelial cells. *Genes Dev*. 1997;11(1):72-82. doi:10.1101/gad.11.1.72

284. Gu YZ, Moran SM, Hogenesch JB, Wartman L, Bradfield CA. Molecular characterization and chromosomal localization of a third alpha-class hypoxia inducible factor subunit, HIF3alpha. *Gene Expr*. 1998;7(3):205-213.

285. Ivan M, Kondo K, Yang H, Kim W, Valiando J, Ohh M, Salic A, Asara JM, Lane WS, Kaelin WG. HIFalpha targeted for VHL-mediated destruction by proline hydroxylation: implications for O2 sensing. *Science*. 2001;292(5516):464-468. doi:10.1126/science.1059817

286. Jaakkola P, Mole DR, Tian YM, Wilson MI, Gielbert J, Gaskell SJ, von Kriegsheim A, Hebestreit HF, Mukherji M, Schofield CJ, Maxwell PH, Pugh CW, Ratcliffe PJ. Targeting of HIF-alpha to the von Hippel-Lindau ubiquitylation complex by O2-regulated prolyl hydroxylation. *Science*. 2001;292(5516):468-472. doi:10.1126/science.1059796

287. Salceda S, Caro J. Hypoxia-inducible factor 1alpha (HIF-1alpha) protein is rapidly degraded by the ubiquitin-proteasome system under normoxic conditions. Its stabilization by hypoxia depends on redox-induced changes. *J Biol Chem*. 1997;272(36):22642-22647. doi:10.1074/jbc.272.36.22642

288. Wenger RH, Stiehl DP, Camenisch G. Integration of oxygen signaling at the consensus HRE. *Sci STKE Signal Transduct Knowl Environ*. 2005;2005(306):re12. doi:10.1126/stke.3062005re12

289. Moreau JM, Ciriello J. Effects of acute intermittent hypoxia on energy balance and hypothalamic feeding pathways. *Neuroscience*. 2013;253:350-360. doi:10.1016/j.neuroscience.2013.09.007

290. Tschöp M, Strasburger CJ, Töpfer M, Hautmann H, Riepl R, Fischer R, Hartmann G, Morrison K, Appenzeller M, Hildebrandt W, Biollaz J, Bärtsch P. Influence of hypobaric hypoxia on leptin levels in men. *Int J Obes*. 2000;24(2):S151-S151. doi:10.1038/sj.ijo.0801309

291. Tschöp M, Strasburger CJ, Hartmann G, Biollaz J, Bärtsch P. Raised leptin concentrations at high altitude associated with loss of appetite. *The Lancet*. 1998;352(9134):1119-1120. doi:10.1016/S0140-6736(05)79760-9

292. Ciriello J, Moreau JM, McCoy A, Jones DL. Effect of intermittent hypoxia on arcuate nucleus in the leptin-deficient rat. *Neurosci Lett*. 2016;626:112-118. doi:10.1016/j.neulet.2016.05.029

293. Gaspar JM, Mendes NF, Corrêa-da-Silva F, Lima-Junior JC de, Gaspar RC, Ropelle ER, Araujo EP, Carvalho HM, Velloso LA. Downregulation of HIF complex in the hypothalamus exacerbates diet-induced obesity. *Brain Behav Immun*. 2018;73:550-561. doi:10.1016/j.bbi.2018.06.020

294. Zhang H, Zhang G, Gonzalez FJ, Park S min, Cai D. Hypoxia-inducible factor directs POMC gene to mediate hypothalamic glucose sensing and energy balance regulation. *PLoS Biol*. 2011;9(7):e1001112.

295. Chandel NS, Maltepe E, Goldwasser E, Mathieu CE, Simon MC, Schumacker PT. Mitochondrial reactive oxygen species trigger hypoxia-induced transcription. *Proc Natl Acad Sci U S A*. 1998;95(20):11715-11720. doi:10.1073/pnas.95.20.11715

296. Chandel NS, McClintock DS, Feliciano CE, Wood TM, Melendez JA, Rodriguez AM,

Schumacker PT. Reactive oxygen species generated at mitochondrial complex III stabilize hypoxia-inducible factor-1alpha during hypoxia: a mechanism of O2 sensing. *J Biol Chem*. 2000;275(33):25130-25138. doi:10.1074/jbc.M001914200

297. Andrews ZB, Liu ZW, Walllingford N, Erion DM, Borok E, Friedman JM, Tschöp MH, Shanabrough M, Cline G, Shulman GI, Coppola A, Gao XB, Horvath TL, Diano S. UCP2 mediates ghrelin's action on NPY/AgRP neurons by lowering free radicals. *Nature*. 2008;454(7206):846-851. doi:10.1038/nature07181

298. Moser M, Knoth R, Bode C, Patterson C. LE-PAS, a novel Arnt-dependent HLH-PAS protein, is expressed in limbic tissues and transactivates the CNS midline enhancer element. *Mol Brain Res*. 2004;128(2):141-149.

299. Ooe N, Saito K, Mikami N, Nakatuka I, Kaneko H. Identification of a novel basic helix-loop-helix-PAS factor, NXF, reveals a Sim2 competitive, positive regulatory role in dendritic-cytoskeleton modulator drebrin gene expression. *Mol Cell Biol*. 2004;24(2):608-616.

300. Lin Y, Bloodgood BL, Hauser JL, Lapan AD, Koon AC, Kim TK, Hu LS, Malik AN, Greenberg ME. Activity-dependent regulation of inhibitory synapse development by Npas4. *Nature*. 2008;455(7217):1198-1204. doi:10.1038/nature07319

301. Bersten DC, Bruning JB, Peet DJ, Whitelaw ML. Human Variants in the Neuronal Basic Helix-Loop-Helix/Per-Arnt-Sim (bHLH/PAS) Transcription Factor Complex NPAS4/ARNT2 Disrupt Function. *PLOS ONE*. 2014;9(1):e85768. doi:10.1371/journal.pone.0085768

302. Bersten DC, Wright JA, McCarthy PJ, Whitelaw ML. Regulation of the neuronal transcription factor NPAS4 by REST and microRNAs. *Biochim Biophys Acta BBA - Gene Regul Mech*. 2014;1839(1):13-24. doi:10.1016/j.bbagrm.2013.11.004

303. Sun X, Jing L, Li F, Zhang M, Diao X, Zhuang J, Rastinejad F, Wu D. Structures of NPAS4-ARNT and NPAS4-ARNT2 heterodimers reveal new dimerization modalities in the bHLH-PAS transcription factor family. *Proc Natl Acad Sci U S A*. 2022;119(46):e2208804119. doi:10.1073/pnas.2208804119

304. Brigidi GS, Hayes MGB, Delos Santos NP, Hartzell AL, Texari L, Lin PA, Bartlett A, Ecker JR, Benner C, Heinz S, Bloodgood BL. Genomic Decoding of Neuronal Depolarization by Stimulus-Specific NPAS4 Heterodimers. *Cell*. 2019;179(2):373-391.e27. doi:10.1016/j.cell.2019.09.004

305. Damborsky JC, Slaton GS, Winzer-Serhan UH. Expression of Npas4 mRNA in telencephalic areas of adult and postnatal mouse brain. *Front Neuroanat*. 2015;9:145.

306. Ramamoorthi K, Fropf R, Belfort GM, Fitzmaurice HL, McKinney RM, Neve RL, Otto T, Lin Y. Npas4 regulates a transcriptional program in CA3 required for contextual memory formation. *Science*. 2011;334(6063):1669-1675.

307. Zhang SJ, Zou M, Lu L, Lau D, Ditzel DAW, Delucinge-Vivier C, Aso Y, Descombes P, Bading H. Nuclear Calcium Signaling Controls Expression of a Large Gene Pool: Identification of a Gene Program for Acquired Neuroprotection Induced by Synaptic Activity. Orr H, ed. *PLoS Genet*. 2009;5(8):e1000604. doi:10.1371/journal.pgen.1000604

308. Coba MP, Valor LM, Kopanitsa MV, Afinowi NO, Grant SGN. Kinase Networks Integrate

Profiles of N-Methyl-d-aspartate Receptor-mediated Gene Expression in Hippocampus*. *J Biol Chem*. 2008;283(49):34101-34107. doi:10.1074/jbc.M804951200

309. Kuzniewska B, Nader K, Dabrowski M, Kaczmarek L, Kalita K. Adult Deletion of SRF Increases Epileptogenesis and Decreases Activity-Induced Gene Expression. *Mol Neurobiol*. 2016;53(3):1478-1493. doi:10.1007/s12035-014-9089-7

310. Speckmann T, Sabatini PV, Nian C, Smith RG, Lynn FC. Npas4 Transcription Factor Expression Is Regulated by Calcium Signaling Pathways and Prevents Tacrolimus-induced Cytotoxicity in Pancreatic Beta Cells. *J Biol Chem*. 2016;291(6):2682-2695. doi:10.1074/jbc.M115.704098

311. Shamloo M, Soriano L, Von Schack D, Rickhag M, Chin DJ, Gonzalez-Zulueta M, Gido G, Urfer R, Wieloch T, Nikolich K. Npas4, a novel helix–loop–helix PAS domain protein, is regulated in response to cerebral ischemia. *Eur J Neurosci*. 2006;24(10):2705-2720.

312. Ooe N, Motonaga K, Kobayashi K, Saito K, Kaneko H. Functional characterization of basic helix-loop-helix-PAS type transcription factor NXF in vivo: putative involvement in an “on demand” neuroprotection system. *J Biol Chem*. 2009;284(2):1057-1063.

313. Hester I, McKee S, Pelletier P, Thompson C, Storbeck C, Mears A, Schulz JB, Hakim AA, Sabourin LA. Transient expression of Nxf, a bHLH–PAS transactivator induced by neuronal preconditioning, confers neuroprotection in cultured cells. *Brain Res*. 2007;1135:1-11.

314. Klaric TS, Thomas PQ, Dottori M, Leong WK, Koblar SA, Lewis MD. A reduction in Npas4 expression results in delayed neural differentiation of mouse embryonic stem cells. *Stem Cell Res Ther*. 2014;5(3):1-14.

315. Bloodgood BL, Sharma N, Browne HA, Trepman AZ, Greenberg ME. The activity-dependent transcription factor NPAS4 regulates domain-specific inhibition. *Nature*. 2013;503(7474):121-125. doi:10.1038/nature12743

316. Sun X, Lin Y. Npas4: linking neuronal activity to memory. *Trends Neurosci*. 2016;39(4):264-275.

317. Choy FC, Klarić TS, Leong WK, Koblar SA, Lewis MD. Reduction of the neuroprotective transcription factor Npas4 results in increased neuronal necrosis, inflammation and brain lesion size following ischaemia. *J Cereb Blood Flow Metab*. 2016;36(8):1449-1463. doi:10.1177/0271678X15606146

318. Esser JS, Charlet A, Schmidt M, Heck S, Allen A, Lother A, Epting D, Patterson C, Bode C, Moser M. The neuronal transcription factor NPAS4 is a strong inducer of sprouting angiogenesis and tip cell formation. *Cardiovasc Res*. 2017;113(2):222-223. doi:10.1093/cvr/cvw248

319. Sabatini PV, Krentz NAJ, Zarrouki B, Westwell-Roper CY, Nian C, Uy RA, Shapiro AMJ, Poitout V, Lynn FC. Npas4 Is a Novel Activity–Regulated Cytoprotective Factor in Pancreatic b-Cells.

320. Sabatini PV, Speckmann T, Nian C, Glavas MM, Wong CK, Yoon JS, Kin T, Shapiro AMJ, Gibson WT, Verchere CB, Lynn FC. Neuronal PAS Domain Protein 4 Suppression of Oxygen Sensing Optimizes Metabolism during Excitation of Neuroendocrine Cells. *Cell Rep*. 2018;22(1):163-174. doi:10.1016/j.celrep.2017.12.033

321. Berglund ED, Liu C, Sohn JW, Liu T, Kim MH, Lee CE, Vianna CR, Williams KW, Xu Y,

Elmquist JK. Serotonin 2C receptors in pro-opiomelanocortin neurons regulate energy and glucose homeostasis. *J Clin Invest*. 2013;123(12):5061-5070. doi:10.1172/JCI70338

322. Chen R, Wu X, Jiang L, Zhang Y. Single-Cell RNA-Seq Reveals Hypothalamic Cell Diversity. *Cell Rep*. 2017;18(13):3227-3241. doi:10.1016/j.celrep.2017.03.004

323. Huang LT (Helen), Zhang D, Nian C, C LF. Truncated CD19 as a selection marker for the isolation of stem cell derived β-cells. Published online April 6, 2023:2023.04.05.535733. doi:10.1101/2023.04.05.535733

324. Butler A, Hoffman P, Smibert P, Papalexi E, Satija R. Integrating single-cell transcriptomic data across different conditions, technologies, and species. *Nat Biotechnol*. 2018;36(5):411-420. doi:10.1038/nbt.4096

325. Chen EY, Tan CM, Kou Y, Duan Q, Wang Z, Meirelles GV, Clark NR, Ma'ayan A. Enrichr: interactive and collaborative HTML5 gene list enrichment analysis tool. *BMC Bioinformatics*. 2013;14(1):128. doi:10.1186/1471-2105-14-128

326. Kuleshov MV, Jones MR, Rouillard AD, Fernandez NF, Duan Q, Wang Z, Koplev S, Jenkins SL, Jagodnik KM, Lachmann A, McDermott MG, Monteiro CD, Gundersen GW, Ma'ayan A. Enrichr: a comprehensive gene set enrichment analysis web server 2016 update. *Nucleic Acids Res*. 2016;44(W1):W90-W97. doi:10.1093/nar/gkw377

327. Xie Z, Bailey A, Kuleshov MV, Clarke DJB, Evangelista JE, Jenkins SL, Lachmann A, Wojciechowicz ML, Kropiwnicki E, Jagodnik KM, Jeon M, Ma'ayan A. Gene Set Knowledge Discovery with Enrichr. *Curr Protoc*. 2021;1(3). doi:10.1002/cpz1.90

328. Segerstolpe Å, Palasantza A, Eliasson P, Andersson EM, Andréasson AC, Sun X, Picelli S, Sabirsh A, Clausen M, Bjursell MK, Smith DM, Kasper M, Ämmälä C, Sandberg R. Single-Cell Transcriptome Profiling of Human Pancreatic Islets in Health and Type 2 Diabetes. *Cell Metab*. 2016;24(4):593-607. doi:10.1016/j.cmet.2016.08.020

329. Muraro MJ, Dharmadhikari G, Grün D, Groen N, Dielen T, Jansen E, van Gurp L, Engelse MA, Carlotti F, de Koning EJP, van Oudenaarden A. A Single-Cell Transcriptome Atlas of the Human Pancreas. *Cell Syst*. 2016;3(4):385-394.e3. doi:10.1016/j.cels.2016.09.002

330. Lawlor N, George J, Bolisetty M, Kursawe R, Sun L, Sivakamasundari V, Kycia I, Robson P, Stitzel ML. Single-cell transcriptomes identify human islet cell signatures and reveal cell-type-specific expression changes in type 2 diabetes. *Genome Res*. 2017;27(2):208-222. doi:10.1101/gr.212720.116

331. Avrahami D, Wang YJ, Schug J, Feleke E, Gao L, Liu C, Naji A, Glaser B, Kaestner KH. Single-cell transcriptomics of human islet ontogeny defines the molecular basis of β-cell dedifferentiation in T2D. *Mol Metab*. 2020;42:101057. doi:10.1016/j.molmet.2020.101057

332. Camunas-Soler J, Dai XQ, Hang Y, Bautista A, Lyon J, Suzuki K, Kim SK, Quake SR, MacDonald PE. Patch-Seq Links Single-Cell Transcriptomes to Human Islet Dysfunction in Diabetes. *Cell Metab*. 2020;31(5):1017-1031.e4. doi:10.1016/j.cmet.2020.04.005

333. Tritschler S, Theis FJ, Lickert H, Böttcher A. Systematic single-cell analysis provides new insights into heterogeneity and plasticity of the pancreas. *Mol Metab*. 2017;6(9):974-990.

doi:10.1016/j.molmet.2017.06.021

334. Li J, Klughammer J, Farlik M, Penz T, Spittler A, Barbieux C, Berishvili E, Bock C, Kubicek S. Single-cell transcriptomes reveal characteristic features of human pancreatic islet cell types. *EMBO Rep*. 2016;17(2):178-187. doi:10.15252/embr.201540946

335. Wang YJ, Schug J, Lin J, Wang Z, Kossenkov A, Consortium the H, Kaestner KH. Comparative analysis of commercially available single-cell RNA sequencing platforms for their performance in complex human tissues. Published online February 5, 2019:541433. doi:10.1101/541433

336. Bernal-Mizrachi E, Cras-Méneur C, Ye BR, Johnson JD, Permutt MA. Transgenic overexpression of active calcineurin in beta-cells results in decreased beta-cell mass and hyperglycemia. *PloS One*. 2010;5(8):e11969. doi:10.1371/journal.pone.0011969

337. Hoeflich KP, Ikura M. Calmodulin in Action: Diversity in Target Recognition and Activation Mechanisms. *Cell*. 2002;108(6):739-742. doi:10.1016/S0092-8674(02)00682-7

338. Wayman GA, Tokumitsu H, Davare MA, Soderling TR. Analysis of CaM-kinase signaling in cells. *Cell Calcium*. 2011;50(1):1-8. doi:10.1016/j.ceca.2011.02.007

339. Yu X, Murao K, Sayo Y, Imachi H, Cao WM, Ohtsuka S, Niimi M, Tokumitsu H, Inuzuka H, Wong NCW, Kobayashi R, Ishida T. The role of calcium/calmodulin-dependent protein kinase cascade in glucose upregulation of insulin gene expression. *Diabetes*. 2004;53(6):1475-1481. doi:10.2337/diabetes.53.6.1475

340. Dang D, Taheri S, Das S, Ghosh P, Prince LS, Sahoo D. Computational Approach to Identifying Universal Macrophage Biomarkers. *Front Physiol*. 2020;11. Accessed March 18, 2023. https://www.frontiersin.org/articles/10.3389/fphys.2020.00275

341. Rodnoi P, Rajkumar M, Moin ASM, Georgia SK, Butler AE, Dhawan S. Neuropeptide Y expression marks partially differentiated **β** cells in mice and humans. *JCI Insight*. 2017;2(12). doi:10.1172/jci.insight.94005

342. Augsornworawat P, Maxwell KG, Velazco-Cruz L, Millman JR. Single-Cell Transcriptome Profiling Reveals β Cell Maturation in Stem Cell-Derived Islets after Transplantation. *Cell Rep*. 2020;32(8):108067. doi:10.1016/j.celrep.2020.108067

343. Westwell-Roper C, Dai DL, Soukhatcheva G, Potter KJ, van Rooijen N, Ehses JA, Verchere CB. IL-1 blockade attenuates islet amyloid polypeptide-induced proinflammatory cytokine release and pancreatic islet graft dysfunction. *J Immunol Baltim Md 1950*. 2011;187(5):2755-2765. doi:10.4049/jimmunol.1002854

344. Bensellam M, Shi YC, Chan JY, Laybutt DR, Chae H, Abou-Samra M, Pappas EG, Thomas HE, Gilon P, Jonas JC. Metallothionein 1 negatively regulates glucose-stimulated insulin secretion and is differentially expressed in conditions of beta cell compensation and failure in mice and humans. *Diabetologia*. 2019;62(12):2273-2286. doi:10.1007/s00125-019-05008-3

345. van der Meulen T, Mawla AM, DiGruccio MR, Adams MW, Nies V, Dólleman S, Liu S, Ackermann AM, Cáceres E, Hunter AE, Kaestner KH, Donaldson CJ, Huising MO. Virgin Beta Cells Persist throughout Life at a Neogenic Niche within Pancreatic Islets. *Cell Metab*. 2017;25(4):911-926.e6. doi:10.1016/j.cmet.2017.03.017

346. Denwood G, Tarasov A, Salehi A, Vergari E, Ramracheya R, Takahashi H, Nikolaev VO, Seino S, Gribble F, Reimann F, Rorsman P, Zhang Q. Glucose stimulates somatostatin secretion in pancreatic δ-cells by cAMP-dependent intracellular Ca2+ release. *J Gen Physiol*. 2019;151(9):e201912351. doi:10.1085/jgp.201912351

347. Aguayo-Mazzucato C, Andle J, Lee TB, Midha A, Talemal L, Chipashvili V, Hollister-Lock J, van Deursen J, Weir G, Bonner-Weir S. Acceleration of β Cell Aging Determines Diabetes and Senolysis Improves Disease Outcomes. *Cell Metab*. 2019;30(1):129-142.e4. doi:10.1016/j.cmet.2019.05.006

348. Helman A, Klochendler A, Azazmeh N, Gabai Y, Horwitz E, Anzi S, Swisa A, Condiotti R, Granit RZ, Nevo Y, Fixler Y, Shreibman D, Zamir A, Tornovsky-Babeay S, Dai C, Glaser B, Powers AC, Shapiro AMJ, Magnuson MA, Dor Y, Ben-Porath I. p16Ink4a-induced senescence of pancreatic beta cells enhances insulin secretion. *Nat Med*. 2016;22(4):412-420. doi:10.1038/nm.4054

349. Li N, Liu F, Yang P, Xiong F, Yu Q, Li J, Zhou Z, Zhang S, Wang CY. Aging and stress induced β cell senescence and its implication in diabetes development. *Aging*. 2019;11(21):9947-9959. doi:10.18632/aging.102432

350. Pullen TJ, Khan AM, Barton G, Butcher SA, Sun G, Rutter GA. Identification of genes selectively disallowed in the pancreatic islet. *Islets*. 2010;2(2):89-95. doi:10.4161/isl.2.2.11025

351. Dorrell C, Schug J, Canaday PS, Russ HA, Tarlow BD, Grompe MT, Horton T, Hebrok M, Streeter PR, Kaestner KH, Grompe M. Human islets contain four distinct subtypes of β cells. *Nat Commun*. 2016;7(1):11756. doi:10.1038/ncomms11756

352. Olsen HL, Theander S, Bokvist K, Buschard K, Wollheim CB, Gromada J. Glucose stimulates glucagon release in single rat alpha-cells by mechanisms that mirror the stimulus-secretion coupling in beta-cells. *Endocrinology*. 2005;146(11):4861-4870. doi:10.1210/en.2005-0800

353. Dickerson MT, Dadi PK, Altman MK, Verlage KR, Thorson AS, Jordan KL, Vierra NC, Amarnath G, Jacobson DA. Glucose-mediated inhibition of calcium-activated potassium channels limits α-cell calcium influx and glucagon secretion. *Am J Physiol Endocrinol Metab*. 2019;316(4):E646-E659. doi:10.1152/ajpendo.00342.2018

354. Lai BK, Chae H, Gómez-Ruiz A, Cheng P, Gallo P, Antoine N, Beauloye C, Jonas JC, Seghers V, Seino S, Gilon P. Somatostatin Is Only Partly Required for the Glucagonostatic Effect of Glucose but Is Necessary for the Glucagonostatic Effect of KATP Channel Blockers. *Diabetes*. 2018;67(11):2239-2253. doi:10.2337/db17-0880

355. Teo AKK, Lim CS, Cheow LF, Kin T, Shapiro JA, Kang NY, Burkholder W, Lau HH. Single-cell analyses of human islet cells reveal de-differentiation signatures. *Cell Death Discov*. 2018;4(1):1-11. doi:10.1038/s41420-017-0014-5

356. Johnston NR, Mitchell RK, Haythorne E, Pessoa MP, Semplici F, Ferrer J, Piemonti L, Marchetti P, Bugliani M, Bosco D, Berishvili E, Duncanson P, Watkinson M, Broichhagen J, Trauner D, Rutter GA, Hodson DJ. Beta Cell Hubs Dictate Pancreatic Islet Responses to Glucose. *Cell Metab*. 2016;24(3):389-401. doi:10.1016/j.cmet.2016.06.020

357. Thompson PJ, Shah A, Ntranos V, Van Gool F, Atkinson M, Bhushan A. Targeted Elimination of Senescent Beta Cells Prevents Type 1 Diabetes. *Cell Metab*. 2019;29(5):1045-1060.e10.

doi:10.1016/j.cmet.2019.01.021

358. Sharma N, Pollina EA, Nagy MA, Yap EL, DiBiase FA, Hrvatin S, Hu L, Lin C, Greenberg ME. ARNT2 Tunes Activity-Dependent Gene Expression through NCoR2-Mediated Repression and NPAS4-Mediated Activation. *Neuron*. 2019;102(2):390-406.e9. doi:10.1016/j.neuron.2019.02.007

359. Woitecki AMH, Müller JA, van Loo KMJ, Sowade RF, Becker AJ, Schoch S. Identification of Synaptotagmin 10 as Effector of NPAS4-Mediated Protection from Excitotoxic Neurodegeneration. *J Neurosci*. 2016;36(9):2561-2570. doi:10.1523/JNEUROSCI.2027-15.2016

360. Xu P, Berto S, Kulkarni A, Jeong B, Joseph C, Cox KH, Greenberg ME, Kim TK, Konopka G, Takahashi JS. NPAS4 regulates the transcriptional response of the suprachiasmatic nucleus to light and circadian behavior. *Neuron*. 2021;109(20):3268-3282.e6. doi:10.1016/j.neuron.2021.07.026

361. Paeger L, Pippow A, Hess S, Paehler M, Klein AC, Husch A, Pouzat C, Brüning JC, Kloppenburg P. Energy imbalance alters Ca2+ handling and excitability of POMC neurons. Elmquist JK, ed. *eLife*. 2017;6:e25641. doi:10.7554/eLife.25641

362. Quarta C, Fioramonti X, Cota D. POMC Neurons Dysfunction in Diet-induced Metabolic Disease: Hallmark or Mechanism of Disease? *Neuroscience*. 2020;447:3-14. doi:10.1016/j.neuroscience.2019.09.031

363. Heyward FD, Liu N, Jacobs C, Ivison R, Machado N, Uner A, Srinivasan H, Patel SJ, Gulko A, Sermersheim T, Orkin SH, Tsai L, Rosen ED. Integrated genomic analysis of AgRP neurons reveals that IRF3 regulates leptin's hunger-suppressing effects. Published online January 3, 2022:2022.01.03.474708. doi:10.1101/2022.01.03.474708

364. Martin EW, Sung MH. Challenges of Decoding Transcription Factor Dynamics in Terms of Gene Regulation. *Cells*. 2018;7(9):132. doi:10.3390/cells7090132

365. Liu Y, Beyer A, Aebersold R. On the Dependency of Cellular Protein Levels on mRNA Abundance. *Cell*. 2016;165(3):535-550. doi:10.1016/j.cell.2016.03.014

366. Tong Q, Ye CP, Jones JE, Elmquist JK, Lowell BB. Synaptic release of GABA by AgRP neurons is required for normal regulation of energy balance. *Nat Neurosci*. 2008;11(9):998-1000. doi:10.1038/nn.2167

367. Padilla SL, Carmody JS, Zeltser LM. Pomc-expressing progenitors give rise to antagonistic neuronal populations in hypothalamic feeding circuits. *Nat Med*. 2010;16(4):403-405. doi:10.1038/nm.2126

368. Yang Y, He Y, Liu H, Zhou W, Wang C, Xu P, Cai X, Liu H, Yu K, Pei Z, Hyseni I, Fukuda M, Tong Q, Xu J, Sun Z, O'Malley BW, Xu Y. Hypothalamic steroid receptor coactivator-2 regulates adaptations to fasting and overnutrition. *Cell Rep*. 2021;37(10):110075. doi:10.1016/j.celrep.2021.110075

369. Yu M, Bean JC, Liu H, He Y, Yang Y, Cai X, Yu K, Pei Z, Liu H, Tu L, Conde KM, Wang M, Li Y, Yin N, Zhang N, Han J, Scarcelli NA, Xu P, He Y, Xu Y, Wang C. SK3 in POMC neurons plays a sexually dimorphic role in energy and glucose homeostasis. *Cell Biosci*. 2022;12(1):170. doi:10.1186/s13578-022-00907-2

370. Rau AR, Hentges ST. The Relevance of AgRP Neuron-Derived GABA Inputs to POMC Neurons Differs for Spontaneous and Evoked Release. *J Neurosci Off J Soc Neurosci*. 2017;37(31):7362-7372. doi:10.1523/JNEUROSCI.0647-17.2017

371. Biglari N, Gaziano I, Schumacher J, Radermacher J, Paeger L, Klemm P, Chen W, Corneliussen S, Wunderlich CM, Sue M, Vollmar S, Klöckener T, Sotelo-Hitschfeld T, Abbasloo A, Edenhofer F, Reimann F, Gribble FM, Fenselau H, Kloppenburg P, Wunderlich FT, Brüning JC. Functionally distinct POMC-expressing neuron subpopulations in hypothalamus revealed by intersectional targeting. *Nat Neurosci*. 2021;24(7):913-929. doi:10.1038/s41593-021-00854-0

372. Campbell JN, Macosko EZ, Fenselau H, Pers TH, Lyubetskaya A, Tenen D, Goldman M, Verstegen AMJ, Resch JM, McCarroll SA, Rosen ED, Lowell BB, Tsai LT. A molecular census of arcuate hypothalamus and median eminence cell types. *Nat Neurosci*. 2017;20(3):484-496. doi:10.1038/nn.4495

373. Lam BY, Cimino I, Polex-Wolf J, Kohnke SN, Rimmington D, Iyemere V, Heeley N, Cossetti C, Schulte R, Saraiva LR. Heterogeneity of hypothalamic pro-opiomelanocortin-expressing neurons revealed by single-cell RNA sequencing. *Mol Metab*. 2017;6(5):383-392.

374. Busetto V, Barbosa I, Basquin J, Marquenet É, Hocq R, Hennion M, Paternina JA, Namane A, Conti E, Bensaude O, Le Hir H. Structural and functional insights into CWC27/CWC22 heterodimer linking the exon junction complex to spliceosomes. *Nucleic Acids Res*. 2020;48(10):5670-5683. doi:10.1093/nar/gkaa267

375. Huisman C, Norgard MA, Levasseur PR, Krasnow SM, van der Wijst MGP, Olson B, Marks DL. Critical changes in hypothalamic gene networks in response to pancreatic cancer as found by single-cell RNA sequencing. *Mol Metab*. 2022;58:101441. doi:10.1016/j.molmet.2022.101441

376. Beattie JH, Wood AM, Newman AM, Bremner I, Choo KH, Michalska AE, Duncan JS, Trayhurn P. Obesity and hyperleptinemia in metallothionein (-I and -II) null mice. *Proc Natl Acad Sci U S A*. 1998;95(1):358-363. doi:10.1073/pnas.95.1.358

377. Minelli A, DeBiasi S, Brecha NC, Zuccarello LV, Conti F. GAT-3, a high-affinity GABA plasma membrane transporter, is localized to astrocytic processes, and it is not confined to the vicinity of GABAergic synapses in the cerebral cortex. *J Neurosci Off J Soc Neurosci*. 1996;16(19):6255-6264. doi:10.1523/JNEUROSCI.16-19-06255.1996

378. Gong S, Shao H, Cai X, Zhu J. Astrocyte-Derived Neuronal Transdifferentiation as a Therapy for Ischemic Stroke: Advances and Challenges. *Brain Sci*. 2022;12(9):1175. doi:10.3390/brainsci12091175

379. Burke LK, Doslikova B, D'Agostino G, Greenwald-Yarnell M, Georgescu T, Chianese R, Martinez de Morentin PB, Ogunnowo-Bada E, Cansell C, Valencia-Torres L, Garfield AS, Apergis-Schoute J, Lam DD, Speakman JR, Rubinstein M, Low MJ, Rochford JJ, Myers MG, Evans ML, Heisler LK. Sex difference in physical activity, energy expenditure and obesity driven by a subpopulation of hypothalamic POMC neurons. *Mol Metab*. 2016;5(3):245-252. doi:10.1016/j.molmet.2016.01.005

380. Wang C, Xu Y. Mechanisms for sex differences in energy homeostasis. *J Mol Endocrinol*. 2019;62(2):R129-R143. doi:10.1530/JME-18-0165

381. Wang C, He Y, Xu P, Yang Y, Saito K, Xia Y, Yan X, Hinton Jr A, Yan C, Ding H, Yu L, Shu G, Gupta R, Wu Q, Tong Q, Lagor WR, Flores ER, Xu Y. TAp63 contributes to sexual dimorphism in POMC neuron functions and energy homeostasis. *Nat Commun*. 2018;9:1544. doi:10.1038/s41467-018-03796-7

Appendices

Appendix A | Calcium-regulated genes in human islet alpha, beta, and delta cells

From Positive vs Negative transcriptome comparisons, all genes below have an adjusted p-value < 0.05. Negative average Log fold change (Avg LogFC) values indicate the gene is expressed higher in the Negative over the Positive condition.

Cluster	Gene	Avg LogFC	Adj p-value	Cluster	Gene	Avg LogFC	Adj p-value
β1	ZNF331	1.20462	1.41E-57	β3	NPAS4	0.37160	3.18E-27
β1	SIK2	0.84501	7.19E-89	β3	HIVEP2	0.37119	1.21E-15
β1	NR4A2	0.72848	1.72E-57	β3	CREM	0.35695	1.74E-13
β1	C2CD4B	0.72449	4.28E-41	β3	AOPEP	0.35333	1.26E-16
β1	ELL2	0.65640	1.24E-50	β3	MIA2	0.34658	3.59E-15
β1	IER3	0.59867	5.34E-22	β3	RGS16	0.34331	1.86E-08
β1	GADD45B	0.55290	6.69E-14	β3	PHTF2	0.33256	1.57E-15
β1	SNAP25-AS1	0.54515	6.14E-31	β3	C2CD4A	0.32003	2.80E-04
β1	PDE10A	0.54222	1.58E-31	β3	TET2	0.31382	7.43E-13
β1	SGMS2	0.51856	3.62E-49	β3	MT-ND6	0.31122	9.79E-12
β1	CPE	0.51025	2.40E-36	β3	PDK4	0.31096	7.06E-03
β1	NR4A3	0.50950	2.85E-43	β3	MAR4.	0.30812	1.62E-15
β1	SIK3	0.49752	2.17E-43	β3	INHBA	0.30332	9.13E-03
β1	RGS16	0.49278	1.08E-11	β3	VAT1L	0.30061	5.37E-08
β1	BTG2	0.48786	1.08E-04	β3	UNC13A	0.30007	1.61E-14
β1	NPAS4	0.47756	9.66E-32	β3	SLC7A5	0.29258	5.23E-09
β1	FOS	0.46161	8.74E-13	β3	PAPSS2	0.28903	7.54E-04
β1	ELMO1	0.44917	4.43E-18	β3	MT-ND3	0.28066	3.84E-22
β1	INHBA	0.44770	3.51E-20	β3	PAM	0.27598	8.29E-09
β1	NR4A1	0.43181	1.42E-28	β3	DENND4A	0.27594	1.02E-09
β1	C2CD4A	0.41640	2.50E-16	β3	SNAP25	0.26385	4.99E-06
β1	CREM	0.41159	2.26E-19	β3	JUNB	0.25889	2.11E-03
β1	JUNB	0.40105	2.10E-12	β3	ELAVL4	-0.25264	3.14E-05
β1	PAM	0.39829	8.36E-25	β3	DHRS2	-0.25833	7.91E-07
β1	FNDC3A	0.39069	7.02E-27	β3	UBB	-0.25857	7.82E-07
β1	DENND4A	0.38680	5.50E-27	β3	RPL27A	-0.25904	5.41E-22
β1	SNAP25	0.38372	1.14E-23	β3	RPS5	-0.26016	3.03E-18
β1	UNC13A	0.37996	3.91E-26	β3	LINC00486	-0.26026	1.05E-06
β1	HIVEP2	0.37800	2.22E-17	β3	RPS18	-0.26140	5.36E-24
β1	PDK4	0.36597	1.62E-07	β3	RPS16	-0.26218	5.41E-20
β1	IAPP	0.36505	7.21E-10	β3	RPS6	-0.26719	3.41E-25
β1	PARM1	0.36119	4.11E-23	β3	RPS3	-0.26887	7.72E-26

β1	TET2	0.36012	8.45E-22	β3	STMN2	-0.26990	8.03E-04
β1	ATF6	0.35115	5.64E-11	β3	RPL17	-0.27066	5.71E-28
β1	MT-ND6	0.34533	2.86E-11	β3	OLMALINC	-0.27194	9.56E-10
β1	PHTF2	0.33276	1.01E-17	β3	EEF1G	-0.27268	9.96E-21
β1	AOPEP	0.32071	5.22E-12	β3	RPL9	-0.27614	3.29E-26
β1	MT-ND3	0.30989	1.13E-31	β3	RPL7A	-0.27917	1.86E-32
β1	ST18	0.30652	1.35E-08	β3	TUBA1B	-0.28043	3.23E-17
β1	PLK2	0.29458	1.17E-13	β3	RPL7	-0.28249	2.32E-24
β1	AC096564.1	0.29351	8.37E-21	β3	RAB11FIP1	-0.28620	4.15E-06
β1	FOXO1	0.28920	3.97E-10	β3	RPSA	-0.28644	3.28E-22
β1	SLC7A5	0.28893	3.85E-11	β3	RPS11	-0.28679	8.06E-26
β1	CITED2	0.28775	3.75E-12	β3	RPL18A	-0.28913	6.63E-26
β1	ALPK3	0.28521	6.26E-15	β3	HSPB1	-0.29130	5.50E-03
β1	TP53BP1	0.28279	4.69E-18	β3	GAPDH	-0.29246	3.10E-15
β1	PAPSS2	0.27434	4.11E-08	β3	FTH1	-0.29330	9.85E-10
β1	MAR4.	0.27221	4.70E-11	β3	JUN	-0.29430	1.49E-06
β1	TMEM200A	0.26877	9.83E-17	β3	EGR1	-0.29460	6.72E-07
β1	MIA2	0.26736	8.66E-07	β3	RPL13A	-0.30055	1.50E-32
β1	MTRNR2L12	0.26587	9.49E-16	β3	RPL10A	-0.30208	2.00E-22
β1	CPEB4	0.26305	1.46E-09	β3	RPS17	-0.30804	4.23E-18
β1	WWC1	0.25177	4.53E-03	β3	RPS20	-0.30864	1.69E-22
β1	RAPGEF1	0.25172	1.69E-14	β3	KLF6	-0.31220	6.63E-09
β1	STMN2	-0.25195	3.17E-05	β3	RPS4X	-0.31461	4.87E-30
β1	MYO1E	-0.25598	3.44E-06	β3	MYO1E	-0.31483	3.35E-08
β1	TUBA1B	-0.25626	7.05E-14	β3	GLCCI1	-0.33224	2.26E-10
β1	RPL13A	-0.26034	2.30E-23	β3	RPL13	-0.33561	4.40E-38
β1	RPL10A	-0.26585	1.42E-21	β3	TXNIP	-0.34169	6.00E-08
β1	RPS20	-0.26734	3.22E-18	β3	DACH1	-0.34316	3.88E-13
β1	ACTG1	-0.27487	1.07E-05	β3	TMSB4X	-0.37527	3.71E-03
β1	RPL13	-0.27625	3.05E-27	β3	PTPRD	-0.37631	1.10E-02
β1	RPS11	-0.28019	8.50E-29	β3	RPS2	-0.38353	6.89E-35
β1	FMN2	-0.28981	1.36E-15	β3	DEPP1	-0.60058	2.89E-19
β1	TXNIP	-0.29468	1.09E-03	β4	GADD45B	0.71455	5.14E-12
β1	LINC01619	-0.31071	9.67E-14	β4	MT-ND3	0.67729	1.25E-02
β1	EGR1	-0.34842	1.67E-11	β4	JUNB	0.56106	4.38E-04
β1	RPS2	-0.34979	8.02E-45	β4	ZNF331	0.52677	3.71E-24
β1	NPY	-0.36246	6.05E-06	β4	SIK2	0.48114	5.87E-16
β1	DEPP1	-0.37698	1.22E-13	β4	PDE10A	0.43277	2.44E-07
β2	ZNF331	1.24091	3.41E-52	β4	FOS	0.42297	1.10E-05
β2	SIK2	0.78023	2.84E-80	β4	SNAP25-AS1	0.39349	1.25E-13
β2	NR4A2	0.72460	3.66E-52	β4	RPS29	0.38735	5.52E-03
β2	SNAP25-AS1	0.55385	5.97E-31	β4	MT-ND4L	0.36382	3.05E-02
β2	IER3	0.54271	8.68E-18	β4	NR4A1	0.35053	7.37E-16

β2	CPE	0.54190	4.22E-43	β4	ELMO1	0.32920	3.82E-04
β2	PAM	0.50309	3.18E-26	β4	RASD1	0.32454	5.90E-03
β2	NR4A3	0.49276	7.72E-37	β4	PHTF2	0.32005	2.09E-05
β2	PDE10A	0.49178	5.22E-20	β4	MAN1A1	0.31591	2.55E-04
β2	ELMO1	0.48968	1.71E-23	β4	HSPA1A	0.31116	3.94E-06
β2	ELL2	0.47449	4.80E-22	β4	SIK3	0.30692	9.28E-08
β2	C2CD4B	0.47081	4.87E-18	β4	ZFP36	0.30436	7.05E-07
β2	SGMS2	0.43914	2.55E-32	β4	NR4A2	0.30388	1.82E-08
β2	NR4A1	0.43807	3.74E-37	β4	TP53BP1	0.29715	3.66E-08
β2	SIK3	0.41477	2.84E-32	β4	MTLN	0.29666	8.93E-05
β2	PDK4	0.40081	1.43E-07	β4	ABHD3	0.29411	1.14E-02
β2	PARM1	0.36440	2.08E-23	β4	KDELR2	0.29064	3.20E-05
β2	SNAP25	0.36160	1.41E-16	β4	RANBP1	0.28977	1.22E-05
β2	FNDC3A	0.35588	1.95E-17	β4	CPEB4	0.28803	1.09E-05
β2	GADD45B	0.35207	6.26E-03	β4	PET100	0.28370	5.97E-05
β2	MT-ND6	0.34493	8.45E-12	β4	MAP2	0.28362	3.93E-02
β2	PHTF2	0.34204	5.08E-19	β4	HIVEP2	0.28333	1.33E-05
β2	DENND4A	0.32249	3.02E-19	β4	ST18	0.28295	2.58E-06
β2	CREM	0.31740	5.58E-13	β4	MTRNR2L12	0.28223	1.07E-06
β2	RGS16	0.31131	1.17E-04	β4	VAT1L	0.28167	8.47E-05
β2	UNC13A	0.31114	1.78E-17	β4	NDUFA3	0.28161	1.13E-03
β2	MIA2	0.30754	3.95E-14	β4	PAM	0.28149	2.20E-03
β2	FOS	0.30013	5.74E-03	β4	UNC13A	0.27938	8.06E-07
β2	HIVEP2	0.28922	1.98E-13	β4	MCF2L2	0.27882	2.24E-02
β2	VAT1L	0.27133	1.36E-07	β4	TARDBP	0.27525	5.37E-06
β2	NPAS4	0.27117	1.61E-20	β4	ATP9A	0.27502	6.54E-05
β2	MT-ND3	0.27065	7.99E-24	β4	SAMD3	0.27409	1.17E-03
β2	CPEB4	0.26891	1.31E-12	β4	GBF1	0.27395	2.31E-06
β2	DAPK1	0.26080	1.61E-05	β4	PAPSS2	0.27313	8.30E-03
β2	WWC1	0.26047	2.07E-03	β4	BTG2	0.27290	1.71E-04
β2	TP53BP1	0.25983	1.32E-15	β4	C2CD4B	0.27090	1.41E-03
β2	MAN1A1	0.25611	1.93E-08	β4	GABRB3	0.27053	1.74E-06
β2	STXBP1	0.25416	7.47E-10	β4	TNFRSF21	0.26696	3.58E-08
β2	AC096564.1	0.25273	3.53E-12	β4	ELL2	0.26667	4.95E-04
β2	DYRK1A	0.25179	8.88E-11	β4	M6PR	0.26616	3.36E-06
β2	RPL27A	-0.25023	2.32E-26	β4	NDUFA9	0.26305	4.60E-03
β2	PEMT	-0.25126	2.46E-08	β4	STXBP1	0.26062	1.29E-02
β2	RPS27A	-0.25144	3.71E-32	β4	BRAF	0.25927	3.11E-05
β2	EIF4A2	-0.25245	2.00E-12	β4	MARK1	0.25844	5.50E-04
β2	RPL29	-0.25279	4.83E-25	β4	STAT3	0.25714	6.68E-04
β2	RPS9	-0.25395	1.83E-31	β4	DENND4A	0.25514	3.82E-06
β2	TPT1	-0.25420	1.18E-29	β4	SMIM4	0.25203	1.19E-02
β2	GLCCI1	-0.25627	8.07E-07	β4	TTR	-0.56055	3.49E-10

β2	RACK1	-0.25630	3.33E-26	β5	ZNF331	1.20359	5.81E-13
β2	RPS3A	-0.25653	4.27E-37	β5	NR4A2	0.72569	3.73E-12
β2	RPL3	-0.25720	1.54E-34	β5	ELL2	0.59399	7.02E-11
β2	RPL18	-0.25772	1.69E-32	β5	SIK2	0.57245	3.37E-10
β2	FTH1	-0.25788	6.78E-08	β5	NR4A3	0.51455	6.87E-09
β2	RPL31	-0.25921	2.08E-16	β5	C2CD4B	0.48797	4.09E-08
β2	RPL11	-0.25970	2.36E-33	β5	PARM1	0.46291	1.41E-08
β2	ELAVL4	-0.26130	6.47E-11	β5	PDE10A	0.46274	3.13E-03
β2	RPL23A	-0.26205	1.22E-34	β5	SNAP25-AS1	0.45965	3.98E-06
β2	RPLP2	-0.26239	7.32E-22	β5	NR4A1	0.44149	7.50E-11
β2	HSPA8	-0.26292	4.97E-12	β5	GADD45B	0.42471	3.73E-02
β2	RPS18	-0.26429	5.69E-35	β5	NPAS4	0.42199	5.86E-09
β2	TUBA1B	-0.26951	2.96E-19	β5	IER3	0.41782	1.13E-05
β2	RPL15	-0.26951	1.10E-37	β5	ELMO1	0.36605	1.37E-02
β2	RPL7A	-0.27047	2.45E-40	β5	CPE	0.35511	3.08E-03
β2	RPL5	-0.27081	5.59E-33	β5	DENND4A	0.35483	2.05E-04
β2	RPL23	-0.27115	1.48E-23	β5	MIA2	0.33749	1.63E-02
β2	RPS16	-0.27316	8.14E-26	β5	SIK3	0.32737	1.09E-03
β2	HSPB1	-0.27568	4.35E-07	β5	PHTF2	0.31759	1.47E-02
β2	LINC00486	-0.27913	1.40E-06	β5	MT-ND6	0.30610	3.85E-02
β2	RPS5	-0.27931	2.23E-27	β5	UNC13A	0.29831	3.02E-02
β2	ARL15	-0.28095	2.25E-08	β5	GCH1	0.28536	1.70E-02
β2	RPSA	-0.28234	2.04E-26	β5	FNDC3A	0.28320	2.43E-02
β2	STMN2	-0.28324	4.96E-05	β5	MT-ND3	0.25832	4.29E-03
β2	RPL8	-0.28494	7.09E-36	β5	PFN2	-0.26924	2.23E-03
β2	RPL6	-0.28788	1.40E-33	β5	LGR4	-0.27060	4.94E-04
β2	LRRTM4	-0.28804	5.39E-06	β5	GAPDH	-0.28085	1.37E-02
β2	RPL32	-0.28904	2.60E-32	β5	FTH1	-0.34921	1.44E-03
β2	ACTG1	-0.29026	1.40E-05	β5	MYO1E	-0.36647	2.54E-06
β2	RPL18A	-0.29187	2.18E-28	β5	TXNIP	-0.45558	2.59E-03
β2	RPS3	-0.29428	1.62E-37	β6	MT-ND3	0.30896	1.07E-02
β2	UBB	-0.30012	5.78E-11	β6	ZNF331	0.27550	5.99E-03
β2	RPL17	-0.30150	2.26E-39	β6	ELMO1	0.26247	4.78E-02
β2	RPS6	-0.30435	1.24E-36	β7	ZNF331	1.10090	1.09E-10
β2	RPL9	-0.30858	2.63E-37	β7	PPP1R1A	0.76184	7.39E-04
β2	RPS11	-0.31277	1.54E-37	β7	SIK2	0.72566	1.47E-10
β2	FMN2	-0.31449	2.08E-17	β7	KRT10	0.67753	4.90E-06
β2	RPL10A	-0.31508	5.76E-25	β7	YBX1	0.61926	9.92E-03
β2	EEF1G	-0.31817	3.75E-30	β7	ELL2	0.61531	1.28E-04
β2	RPS17	-0.31832	1.85E-26	β7	H1FX	0.60718	7.84E-05
β2	RPL19	-0.32050	7.10E-35	β7	INHBA	0.58202	1.24E-04
β2	RPL7	-0.32344	1.33E-32	β7	ELMO1	0.57566	1.08E-04
β2	EGR1	-0.33073	9.19E-18	β7	IER3	0.52510	5.55E-05

β2	GAPDH	-0.33581	1.31E-18	β7	NR4A2	0.48427	1.57E-02
β2	RPL13	-0.33805	2.56E-50	β7	AOPEP	0.47738	8.88E-04
β2	RPL13A	-0.33883	4.00E-40	β7	BRI3	0.47294	1.40E-02
β2	RPS20	-0.33927	2.20E-31	β7	NR4A3	0.47229	2.57E-06
β2	RPS4X	-0.34638	6.59E-42	β7	PTMS	0.46360	2.13E-04
β2	CNTN5	-0.35107	3.63E-05	β7	PARM1	0.45600	3.14E-04
β2	MYO1E	-0.35201	9.62E-20	β7	CAMK2N1	0.44370	4.14E-02
β2	RPS2	-0.36072	1.95E-44	β7	SGMS2	0.44229	4.51E-04
β2	TXNIP	-0.38275	2.00E-17	β7	YWHAH	0.42291	4.45E-02
β2	DEPP1	-0.64229	2.06E-30	β7	PAM	0.41775	3.52E-03
β3	ZNF331	1.18702	1.33E-43	β7	LCOR	0.41609	3.08E-02
β3	SIK2	0.76981	7.06E-71	β7	USP6NL	0.40822	1.06E-02
β3	NR4A2	0.69312	1.65E-39	β7	SIK3	0.39903	7.93E-03
β3	C2CD4B	0.62066	1.84E-25	β7	CREM	0.39663	8.08E-03
β3	NR4A3	0.60886	9.99E-38	β7	C2CD4B	0.37539	5.60E-04
β3	ELL2	0.58795	7.01E-32	β7	C2CD4A	0.37481	1.32E-02
β3	GADD45B	0.58201	3.58E-18	β7	PRRC2C	0.37445	4.36E-04
β3	PDE10A	0.53046	8.31E-27	β7	YWHAZ	0.31824	4.52E-03
β3	IER3	0.49809	2.95E-22	β7	MT-ND3	0.27641	2.60E-02
β3	CPE	0.48220	3.06E-37	β7	TTR	-0.26769	2.39E-02
β3	SNAP25-AS1	0.47650	1.04E-14	β7	TMED10	-0.29497	1.29E-02
β3	BTG2	0.45067	9.99E-03	β7	SCG3	-0.35018	6.42E-04
β3	SGMS2	0.43022	7.00E-24	β7	ATP6V0E1	-0.35788	1.30E-02
β3	IAPP	0.42576	2.50E-09	β7	CD63	-0.35978	1.10E-04
β3	NR4A1	0.41704	4.40E-30	β7	SSR4	-0.36262	2.44E-04
β3	ELMO1	0.40419	3.28E-12	β7	SCG5	-0.36535	6.78E-05
β3	WWC1	0.39624	8.43E-12	β7	HLA-A	-0.36703	1.60E-02
β3	PARM1	0.39231	4.56E-23	β7	TMED9	-0.36947	1.14E-02
β3	SIK3	0.38442	5.94E-23	β7	TIMP1	-0.37079	1.56E-04
				β7	B2M	-0.38423	5.25E-05
Cluster	**Gene**	**Avg LogFC**	**Adj p-value**	**Cluster**	**Gene**	**Avg LogFC**	**Adj p-value**
α1	FOS	0.67761	3.06E-38	α2	MTRNR2L1	0.26776	6.71E-33
α1	MCU	0.66549	1.56E-65	α2	TMEM163	0.26760	1.17E-09
α1	RFX2	0.64605	1.84E-71	α2	MIA2	0.26284	1.46E-14
α1	INS	0.59435	7.07E-38	α2	GRAMD4	0.25662	6.59E-07
α1	IAPP	0.50047	3.96E-13	α2	SOCS1	0.25330	5.32E-20
α1	RFX3	0.47267	4.43E-40	α2	PCSK1N	0.25254	1.36E-11
α1	MT-ND3	0.46711	4.25E-63	α2	MT-ND1	0.25142	2.87E-26
α1	SIK2	0.46244	2.61E-39	α2	MT-ATP6	0.25138	6.77E-15
α1	IER3	0.40442	9.20E-16	α2	GNAS	0.25123	1.92E-22
α1	SGMS2	0.40318	1.43E-32	α2	ELAVL4	-0.26643	2.30E-08
α1	SLC7A2	0.38864	4.69E-25	α2	HSPB1	-0.28211	1.21E-11
α1	MBNL2	0.37355	8.17E-24	α2	MYO1E	-0.29865	2.04E-11

α1	SIK3	0.37267	5.08E-32	α2	JUN	-0.31292	5.25E-14
α1	NLK	0.36484	2.60E-19	α3	ZNF331	0.88107	1.98E-09
α1	ZNF331	0.36417	1.77E-07	α3	NR4A3	0.61060	8.34E-06
α1	PAM	0.36078	7.54E-31	α3	WWC1	0.51422	4.49E-02
α1	ELL2	0.34432	1.60E-23	α3	ELL2	0.45495	1.61E-08
α1	ANKRD28	0.32916	2.07E-10	α3	SCG2	0.42327	1.72E-02
α1	AC096564.1	0.32720	1.09E-39	α3	ST18	0.40834	6.92E-06
α1	PHTF2	0.31838	5.28E-23	α3	PAM	0.40618	2.98E-04
α1	CPE	0.30241	4.37E-24	α3	NR4A1	0.38738	2.54E-06
α1	CACNB2	0.28573	6.63E-22	α3	MTMR7	0.38246	1.08E-03
α1	PDE10A	0.28420	3.95E-09	α3	SIK2	0.37769	1.66E-05
α1	CDON	0.28104	2.50E-20	α3	IER3	0.37600	1.69E-08
α1	ZCCHC14	0.28028	2.30E-17	α3	ATP2B1	0.33478	1.39E-02
α1	TRAK1	0.27974	1.17E-14	α3	PDE10A	0.33241	4.05E-03
α1	ST18	0.27303	3.68E-09	α3	CREM	0.32102	1.05E-02
α1	TRPM3	0.27108	1.33E-06	α3	MT-ND3	0.26291	2.11E-04
α1	SEMA3E	0.26974	3.49E-04	α3	ZBTB20	-0.27894	4.23E-02
α1	TBC1D9	0.26775	7.60E-09	α3	DACH1	-0.34587	3.16E-02
α1	MICU1	0.26617	1.31E-17	α3	SPDYA	-0.36771	1.08E-03
α1	MTRNR2L1	0.26551	1.54E-26	α3	COX10-AS1	-0.37246	1.91E-02
α1	GADD45B	0.26109	1.79E-09	α3	RAD23B	-0.38355	9.29E-04
α1	FLNB	0.26023	7.06E-14	α3	ACOT12	-0.39722	4.27E-02
α1	C2CD4B	0.25869	6.97E-10	α3	RRAS2	-0.47479	7.99E-04
α1	INHBA	0.25676	5.40E-04	α3	SQSTM1	-0.51307	1.36E-07
α1	ZSWIM6	0.25668	8.27E-10	α3	LINC01619	-0.56784	8.08E-06
α1	MUC13	0.25631	4.37E-05	α4	RFX2	1.07647	1.91E-27
α1	MAN1A1	0.25188	6.57E-07	α4	FOS	0.90203	2.47E-13
α1	MT-ND4L	0.25180	3.73E-13	α4	MCU	0.85028	1.39E-20
α1	RPS2	-0.25616	6.27E-35	α4	RFX3	0.70101	9.28E-10
α1	MYO10	-0.26856	9.05E-03	α4	NLK	0.64999	6.56E-11
α1	HERPUD1	-0.28862	3.47E-20	α4	PAM	0.64347	1.06E-14
α1	SYN2	-0.34024	4.91E-14	α4	MBNL2	0.57688	1.17E-09
α1	HSPB1	-0.43511	1.14E-18	α4	SIK2	0.56062	3.30E-09
α2	INS	0.70513	1.76E-57	α4	SGMS2	0.54206	1.57E-08
α2	IAPP	0.62107	5.23E-07	α4	SLC7A2	0.52724	3.40E-06
α2	NR4A3	0.54453	2.30E-19	α4	ANKRD28	0.51328	3.92E-05
α2	MT-ND3	0.50010	6.30E-74	α4	LINC01091	0.49074	6.47E-03
α2	C2CD4B	0.49365	5.67E-18	α4	CDON	0.46154	1.15E-06
α2	ZCCHC14	0.42513	5.93E-36	α4	INHBA	0.45461	2.30E-02
α2	GADD45B	0.42144	1.05E-11	α4	MICU1	0.44530	2.64E-07
α2	PDK4	0.40246	1.00E-12	α4	SIK3	0.40873	1.40E-04
α2	ZFP36	0.37734	1.67E-04	α4	TACC1	0.37829	1.47E-03
α2	IER3	0.36097	8.11E-13	α4	TRAK1	0.35684	6.40E-03

α2	PLOD2	0.34154	2.99E-15	α4	ATP6V1A	0.35407	7.15E-03
α2	ST3GAL6	0.33685	4.19E-11	α4	AC096564.1	0.35204	1.75E-04
α2	ELL2	0.33516	2.34E-24	α4	CRY1	0.34638	2.27E-02
α2	ST18	0.33401	2.88E-20	α4	CACNB2	0.34420	6.41E-03
α2	ZNF331	0.33377	1.49E-04	α4	ATP2B1	0.34222	3.65E-02
α2	MTRNR2L12	0.33181	1.19E-27	α4	GLUD1	0.32767	1.44E-02
α2	SIK3	0.32951	9.51E-23	α4	IER3	0.32474	2.43E-04
α2	NPAS4	0.32522	6.92E-17	α4	CPE	0.30330	6.93E-03
α2	SLC7A2	0.32074	4.65E-26	α4	RLF	0.27000	3.94E-02
α2	SMOC1	0.31952	5.15E-12	α4	RPL13	-0.28942	1.69E-02
α2	FNIP2	0.31190	2.89E-07	α4	RPL13A	-0.31139	7.02E-03
α2	MUC13	0.31118	4.73E-08	α4	SQSTM1	-0.32698	2.26E-02
α2	MCU	0.30835	4.64E-06	α4	RPS11	-0.32720	6.34E-06
α2	PAM	0.30164	2.03E-10	α5	ZNF331	0.67155	8.24E-06
α2	SIRT1	0.29881	1.27E-14	α5	RFX3	0.65430	2.89E-02
α2	CPE	0.29368	5.63E-21	α5	RFX2	0.64617	3.98E-04
α2	ZNRF1	0.29107	1.02E-05	α5	SIK3	0.58032	4.18E-04
α2	NR4A1	0.28317	6.35E-21	α5	SIK2	0.54766	1.09E-04
α2	NR4A2	0.28064	2.91E-06	α5	MT-ND3	0.52759	9.68E-05
α2	PDE10A	0.28011	5.56E-07	α5	PAPPA2	0.51857	3.55E-03
α2	RPS29	0.27809	4.53E-17	α5	PAM	0.50793	3.20E-02
α2	PAPSS2	0.27717	6.55E-14	α5	MT-ND6	0.47200	1.42E-02
α2	SGMS2	0.27620	8.73E-14	α5	ZSCAN18	0.42679	1.70E-03
α2	XPR1	0.27619	8.61E-10	α5	AOPEP	0.33369	2.11E-02
α2	MT-CYB	0.27247	5.69E-26	α5	AF111167.1	0.25986	3.25E-02
α2	MT-ND4L	0.26813	1.54E-13	α5	CHMP2A	-0.29104	3.16E-02
α2	VGF	0.26812	3.34E-17	α5	TTR	-0.31282	1.03E-02
				α5	TRIR	-0.37705	1.10E-02
Cluster	**Gene**	**Avg LogFC**	**Adj p-value**	**Cluster**	**Gene**	**Avg LogFC**	**Adj p-value**
δ	NR4A3	0.89108	8.77E-14	δ	UBE2QL1	0.25705	1.09E-05
δ	ZNF331	0.76793	2.33E-16	δ	KLHL24	-0.26423	3.67E-02
δ	INS	0.66980	1.05E-10	δ	RAP1B	-0.27364	3.05E-03
δ	PDE10A	0.60028	2.75E-10	δ	AGPAT4	-0.28290	9.95E-03
δ	SLC7A5	0.50703	2.81E-15	δ	ACTG1	-0.28850	3.68E-05
δ	IAPP	0.50673	2.66E-03	δ	FERMT2	-0.29259	7.40E-03
δ	NR4A2	0.50186	5.92E-07	δ	ST3GAL5	-0.29604	5.83E-04
δ	GCH1	0.46399	9.08E-06	δ	AC112196.1	-0.31945	1.19E-04
δ	IER3	0.42191	1.60E-10	δ	GRAMD2B	-0.32827	8.91E-03
δ	MAR4.	0.41541	2.17E-09	δ	AC017101.1	-0.33361	2.32E-12
δ	CPE	0.40479	4.27E-12	δ	HSPB1	-0.33745	4.41E-03
δ	SMOC1	0.40284	6.07E-06	δ	CORO1C	-0.33792	2.54E-05
δ	SIK3	0.37695	4.63E-10	δ	RAB11FIP1	-0.34499	3.29E-03
δ	FOXO1	0.35257	4.22E-06	δ	ZEB1	-0.36977	7.10E-03

δ	SIK2	0.34349	2.16E-04	δ	KLF7	-0.37540	4.56E-04
δ	SLC7A2	0.34189	6.69E-04	δ	VCL	-0.40792	6.41E-07
δ	MT-ND3	0.33831	1.89E-11	δ	RSU1	-0.40820	3.84E-06
δ	C2CD4B	0.32014	5.81E-06	δ	DAAM1	-0.40880	2.10E-05
δ	STX17-AS1	0.30871	4.32E-02	δ	TMCC3	-0.41057	4.66E-07
δ	ELL2	0.30704	1.29E-02	δ	TANC2	-0.41981	1.25E-06
δ	C4orf48	0.29937	1.20E-04	δ	ITGAV	-0.43057	4.13E-02
δ	KRT10	0.29476	6.44E-03	δ	STX12	-0.44825	7.96E-07
δ	PCSK1N	0.29238	6.95E-03	δ	ZNF608	-0.45856	2.39E-07
δ	MARK1	0.28178	1.55E-05	δ	GCNT1	-0.45863	1.06E-05
δ	PPP1R1A	0.28109	2.76E-02	δ	STXBP5L	-0.46802	8.13E-03
δ	KLF10	0.27675	6.70E-06	δ	JUN	-0.50454	1.09E-08
δ	GNAS	0.27396	8.95E-04	δ	ELAVL4	-0.57629	7.55E-14
δ	NPHP4	0.27274	1.37E-05	δ	CBR4	-0.58001	2.25E-09
δ	TMEM51	0.27158	7.74E-05	δ	MYO1E	-0.58201	1.38E-17
δ	RAP1GAP2	0.26422	1.49E-02	δ	ERRFI1	-0.61428	1.32E-03
δ	STAT3	0.26246	1.64E-03	δ	KLF6	-0.65854	1.55E-13
δ	PHC2	0.26157	5.35E-03	δ	PALLD	-0.71772	2.65E-13
δ	SGMS2	0.25964	2.14E-03	δ	PDLIM5	-0.71787	1.43E-10
				δ	DEPP1	-0.83559	7.87E-08

Appendix B | Analysis of single cell RNA sequencing data in chapter 3

```
#Replace Directory with appropriate destination
#Remember to check cell counts at each key step
#load packages in Rstudio

library(Seurat)
library(dplyr)
library(ggplot2)
library(cowplot)
library(patchwork)
library(sctransform)

#Create Seurat object from raw data – downstream outputs of Cell Ranger v7
#Replace object name and repeat until all 9 samples have been completed
#Samples are donorID_condition (example: R253_low)
#Save copies of the newly generated raw Seurat objects

R253_Low_data <- Read10X(data.dir = "Directory/R253_low/outs/filtered_feature_bc_matrix/")
R253_Low <- CreateSeuratObject(counts = R253_Low_data, project = "R253_Low", min.cells
= 3, min.features = 200)
saveRDS(R253_Low, file = "Directory/objects/raw_objects/R253_Low_RAW.rds")

#For QC, make new column in metadata for percentage of mitochondrial genes per cell
#Visualize QC metrics nFeature_RNA, nCounts_RNA, percent.mt for each sample
#Save QC plots for metrics – determine QC cutoff
#Repeat for all samples – make sure same QC cutoffs are appropriate for all

R253_Low[["percent.mt"]] <- PercentageFeatureSet(R253_Low, pattern = "^MT-")
R253_Low_QC <- VlnPlot(R253_Low, features = c("nFeature_RNA", "nCount_RNA",
"percent.mt"), ncol = 3)
ggsave("R253_Low_unfilt_QC.pdf", plot = R253_Low_QC, device = "pdf", width = 11, height
= 11, units = "in")
R253_Low_featureVSmt_unfilt <- FeatureScatter(R253_Low, feature1 = "nFeature_RNA",
feature2 = "percent.mt")
ggsave("R253_Low_unfilt_featureVSmt.pdf", plot = R253_Low_featureVSmt_unfilt, device =
"pdf", width = 11, height = 11, units = "in")

#Keep cells that have less than 6000 genes/cell, less than 20% percent.mt
#Check filtered object QC and save plots after filtering

R253_Low <- subset(R253_Low, subset = nFeature_RNA < 6000 & percent.mt < 20)
R253_Low_QC_filt <- VlnPlot(R253_Low, features = c("nFeature_RNA", "nCount_RNA",
"percent.mt"), ncol = 3)
ggsave("R253_Low_filt_QC.pdf", plot = R253_Low_QC_filt, device = "pdf", width = 11, height
= 11, units = "in")
```

```
#Run SCTransform for normalization on each sample separately
#Make sure to save each SCT object

R253_Low <- SCTransform(R253_Low, verbose = FALSE)
saveRDS(R253_Low, file = "Directory/objects/SCT_objects/R253_Low_SCT.rds")

#Turn all objects into list for efficient integration

hislet_list <- list(R253_Low, R253_Positive, R253_Negative, R282_Low, R282_Positive,
R282_Negative, R317_Low, R317_Positive, R317_Negative)

#Select integration features and prep for integration

hislet_int_features <- SelectIntegrationFeatures(object.list = hislet_list, nfeatures = 3000)
hislet_list <- PrepSCTIntegration(object.list = hislet_list, anchor.features = hislet_int_features)

#Continue by finding anchors, then integrate

hislet_anchors <- FindIntegrationAnchors(object.list = hislet_list, normalization.method =
"SCT", anchor.features = hislet_int_features)
hislet <- IntegrateData(anchorset = hislet_anchors, normalization.method = "SCT")

#Save the freshly integrated object

saveRDS(hislet, file = "Directory/objects/hislet.rds")

#Add sample metadata based on orig.ident – donor ID and condition
#Start by setting the active identity to orig.ident

Idents(hislet) <- "orig.ident"

#All metadata renaming follows the exact same 3 lines of code
#First, specify which cells, identified by a level of the active identity you are in with
#cells.use <- WhichCells(object = hislet, idents = "identity_value")
#Next, decide on the new metadata value to assign to these cells
#hislet <- SetIdent(object = hislet, cells = cells.use, value = "new_value")
#Finally, move all that informatin into the new (or old, if being renamed) metadata column
hislet[["target_column_name"]] <- Idents(object = hislet)

#Starting from orig.ident, create new column called Donor and input donor ID information
#example for donor R253

cells.use <- WhichCells(object = hislet, idents = c("R253_Low", "R253_Positive",
"R253_Negative"))
hislet <- SetIdent(object = hislet, cells = cells.use, value = "R253")
hislet[["Donor"]] <- Idents(object = hislet)
```

```
#Starting from orig.ident, create new column for experimental conditions
#example for Low condition samples:

Idents(hislet) <- "orig.ident"
levels(hislet)

cells.use <- WhichCells(object = hislet, idents = c("R253_Low", "R282_Low", "R317_Low"))
hislet <- SetIdent(object = hislet, cells = cells.use, value = "Low")
hislet[["Condition"]] <- Idents(object = hislet)

#Save object with newly added metadata

saveRDS(hislet, file = "Directory/objects/hislet.rds")

#Run PCA, check dimensions with elbow plot and heatmaps
#Save object before continuing so clustering resolution can be changed if needed

hislet <- RunPCA(hislet, verbose = FALSE)

elbowplot <- ElbowPlot(hislet, ndims = 50, reduction = "pca")
elbowplot
ggsave("hislet_elbow.pdf", plot = elbowplot, device = "pdf", path = "Directory/", width = 11,
height = 11, units = "in")

dimHM1 <- DimHeatmap(hislet, dims = 25:35, cells = 500, balanced = TRUE)
dimHM1
ggsave("hislet_DimHeatmap1.pdf", plot = dimHM1, device = "pdf", path = "Directory/", width =
11, height = 11, units = "in")

dimHM2 <- DimHeatmap(hislet, dims = 35:45, cells = 500, balanced = TRUE)
dimHM2
ggsave("hislet_DimHeatmap2.pdf", plot = dimHM2, device = "pdf", path = "Directory/", width =
11, height = 11, units = "in")

hislet <- RunUMAP(hislet, reduction = "pca", dims = 1:40, verbose = FALSE)
hislet <- FindNeighbors(hislet, dims = 1:40, verbose = FALSE)

saveRDS(hislet, file = ""Directory/objects/hislet_precluster.rds")

#Specify cluster resolution, go back to hislet_precluster object if resolution needs to be altered
#Start with resolution 0.8, try 0.7, 0.6, 0.5, and 0.4
#Plot gene expression for each cell type to roughly determine number of clusters per cell type

hislet <- FindClusters(hislet, resolution = 0.6)
umap_clusters <- DimPlot(hislet, reduction = "umap", label = TRUE) + NoLegend()
umap_clusters
```

```
ggsave("hislet_clusters.pdf", plot = umap_clusters, device = "pdf", path = "Directory/umaps/",
width = 11, height = 11, units = "in")

islet.genes <- c("INS", "GCG", "SST", "PPY", "GHRL", "CPA1", "KRT19", "PECAM1",
"PDGFRB", "FCER1G")
endo.genes <- c("INS", "GCG", "SST", "PPY")
nonendo.genes <- c("CPA1", "KRT19", "PECAM1", "PDGFRB", "FCER1G")

DefaultAssay(hislet) <- "SCT"
cluster_test <- FeaturePlot(hislet, features = islet.genes, min.cutoff = 0)
cluster_test
ggsave("clustertest_umap.pdf", plot = cluster_test, device = "pdf", path = "Directory/umaps/",
width = 11, height = 11, units = "in")
endo_test <- FeaturePlot(hislet, features = endo.genes, min.cutoff = 0)
endo_test
ggsave("endotest_umap.pdf", plot = endo_test, device = "pdf", path = "Directory/umaps/", width
= 11, height = 11, units = "in")
nonendo_test <- FeaturePlot(hislet, features = nonendo.genes, min.cutoff = 0)
nonendo_test
ggsave("nonendotest_umap.pdf", plot = nonendo_test, device = "pdf", path =
"Directory/umaps/", width = 11, height = 11, units = "in")

#Save once ideal clustering resolution is determined for now – can always go back and change

saveRDS(hislet, file = "Directory/objects/hislet_cluster.rds")

#Get number of cells in each cluster, from each sample and condition

donor.per.cluster <- table(hislet$seurat_clusters, hislet$Donor)
write.csv(donor.per.cluster, file = "Directory/donor_per_cluster.csv")
condition.per.cluster <- table(hislet$seurat_clusters, hislet$Condition)
write.csv(condition.per.cluster, file = "Directory/condition_per_cluster.csv")

#Find all markers per cluster for cluster identity identification

DefaultAssay(hislet) <- "SCT"
cluster.deg <- FindAllMarkers(hislet, assay = "SCT", only.pos = TRUE, min.pct = 0.50,
logfc.threshold = 0.50, verbose = TRUE)
write.csv(cluster.deg, file = "Directory/DEG/hislet_cluster_deg.csv")

#Label clusters based on cell types by creating a new column in metadata
#Make sure to save object after assigning cell type labels
#Example for alpha cells:

Idents(hislet) <- "seurat_clusters"
levels(hislet)
```

```
cells.use <- WhichCells(object = hislet, idents = c("0", "1", "9", "12", "14", "16", "17", "20",
"24"))
hislet <- SetIdent(object = hislet, cells = cells.use, value = "Alpha")
hislet[["Cell_Type"]] <- Idents(object = hislet)

saveRDS(hislet, file = "Directory/objects/hislet_cluster.rds")

#Find all markers per cluster for cluster identity identification

celltype_deg <- FindAllMarkers(hislet, assay = "SCT", only.pos = TRUE, min.pct = 0.50,
logfc.threshold = 0.50, verbose = TRUE)
write.csv(celltype_deg, file = "Directory/DEG/hislet_celltype_deg.csv")

#Featureplots for individual genes – markers for endocrine and non-endocrine cell types
#Example for INS:

DefaultAssay(hislet) <- "SCT"
INS <- FeaturePlot(hislet, "INS", min.cutoff = 0)
ggsave("INS_umap.pdf", plot = INS, device = "pdf", path = "Directory/Featureplots/", width =
11, height = 11, units = "in")

#Subset non-endocrine clusters from hislet
#Generate heatmap with top 5 DEGs for each non-endocrine cell type

Idents(hislet) <- “Cell_Type”
hislet_nonendo <- subset(hislet, idents = c("Duct", "Acinar", "Mesenchymal", "Endothelial",
"Immune"))
saveRDS(hislet_nonendo, file = "Directory/objects/hislet_new_nonendo.rds")

nonendo_hm_genes <- c("MMP7", "KRT19", "LAMC2", "KRT18", "KRT7",
                      "CELA3B", "CELA3A", "REG1B", "REG1A", "CPB1",
                      "MMP1", "TIMP1", "TIMP3", "TFPI2", "INHBA",
                      "ANGPT2", "TCF4", "FLT1", "ENG", "ESM1",
                      "ANXA1", "SRGN", "SAMSN1", "FCER1G")

nonendohm <- DoHeatmap(hislet_nonendo, features = nonendo_hm_genes, assay = "SCT") +
scale_fill_gradientn(colors = c("blue4", "white", "red"))
ggsave("nonendo_genes_heatmap.pdf", plot = nonendohm, device = "pdf", path =
"Directory/DEG/", width = 11, height = 8, units = "in")

#Subset endocrine cells, recluster, and save as new object

DefaultAssay(hislet) <- "integrated"
endo <- subset(hislet, idents = c("Alpha", "Beta", "Delta", "PP", "Unknown", "Polyhormonal"))
endo
```

```
elbowplot <- ElbowPlot(endo, ndims = 50, reduction = "pca")
elbowplot
endo <- RunUMAP(endo, reduction = "pca", dims = 1:40, verbose = FALSE)
endo <- FindNeighbors(endo, dims = 1:40, verbose = FALSE)
saveRDS(endo, file = "Directory/objects/endo_precluster.rds")

endo <- FindClusters(object = endo, resolution = 0.6)
endoumap <- DimPlot(endo, label = TRUE, label.size = 6) + NoLegend()
endoumap
ggsave("endo_umap.pdf", plot = endoumap, device = "pdf", path = "Directory/umaps/", width =
11, height = 11, units = "in")

#Plot featureplots for endocrine marker genes INS, GCG, SST, PPY

DefaultAssay(endo) <- "SCT"
endo_feat <- FeaturePlot(endo, features = endo.genes, min.cutoff = 0)
endo_feat

saveRDS(endo, file = "Directory/objects/endo_cluster.rds")

#Get number of cells in each cluster and each cell type, from each sample
#Determine which clusters need to get removed due to poor integration across samples

endo.donor.cluster <- table(endo$seurat_clusters, endo$Donor)
write.csv(endo.donor.cluster, file = "Directory/endo_donor_per_cluster.csv")
endo.condition.cluster <- table(endo$seurat_clusters, endo$Condition)
write.csv(endo.condition.cluster, file = "Directory/endo_condition_per_cluster.csv")
endo.donor.celltype <- table(endo$Cell_Type, endo$Donor)
write.csv(endo.donor.celltype, file = "Directory/endo_donor_per_celltype.csv")
endo.condition.celltype <- table(endo$Cell_Type, endo$Condition)
write.csv(endo.condition.celltype, file = "Directory/endo_condition_per_celltype.csv")

#UMAP plot by cell types

Idents(endo) <- "Cell_Type"
endo_celltype_umap <- DimPlot(endo, label = TRUE, label.size = 6) + NoLegend()
ggsave("endo_celltypes.pdf", plot = endo_celltype_umap, device = "pdf", path =
"Directory/umaps/", width = 11, height = 11, units = "in")

#Remove clusters that are poorly integrated between donors
#clusters 8, 9, 13, 14, 15, 19, 21
#Therefore, give a list of cluster numbers EXCEPT the above numbers
#Save the newly generated umap with cluster labels

Idents(endo) <- "seurat_clusters"
levels(endo)
```

```
endo <- subset(endo, idents = c("0", "1", "2", "3", "4", "5", "6", "7", "10", "11", "12", "16", "17",
"18", "20"))
endo_filt <- DimPlot(endo, label = TRUE, label.size = 6)
ggsave("endo_clusters_filt.pdf", plot = endo_filt, device = "pdf", path = "Directory/umaps/",
width = 11, height = 11, units = "in")

#Plot featureplots for endocrine marker genes INS, GCG, SST, PPY

DefaultAssay(endo) <- "SCT"
endo_feat <- FeaturePlot(endo, features = endo.genes, min.cutoff = 0)
endo_feat
ggsave("endo_features.pdf", plot = endo_feat, device = "pdf", path = "Directory/Featureplots/",
width = 22, height = 22, units = "in")

#Save endocrine cells object with poorly integrated clusters removed

saveRDS(endo, file = "Directory/objects/endo_filter.rds")

#Create new column in metadata for cluster names post-filtering
#Starting from cluster 0, name all clusters
#Example for cluster 0 = Alpha1

Idents(endo) <- "seurat_clusters"
levels(endo)

cells.use <- WhichCells(object = endo, idents = "0")
endo <- SetIdent(object = endo, cells = cells.use, value = "Alpha1")
endo[["cluster_name"]] <- Idents(object = endo)

#UMAP plot with the new cluster names

endo_umap_named <- DimPlot(endo, label = TRUE, label.size = 6) + NoLegend()
endo_umap_named
ggsave("endo_umap_named.pdf", plot = endo_umap_named, device = "pdf", path =
"Directory/umaps/", width = 11, height = 11, units = "in")

#Create metadata column for cell types only for cells in the endo object
#Example for alpha cells

Idents(endo) <- "cluster_name"
levels(endo)

cells.use <- WhichCells(object = endo, idents = c("Alpha1", "Alpha2", "Alpha3", "Alpha4",
"Alpha5"))
endo <- SetIdent(object = endo, cells = cells.use, value = "Alpha")
endo[["endo_celltype"]] <- Idents(object = endo)
```

```
#Save the object with the new metadata
#At this point, metadata should have Donor, Condition, Cell_Type (from hislet), cluster_name (endo), and endo_celltype

saveRDS(endo, file = "Directory/objects/endo_filter.rds")

#Identifying DEGs in each cluster for alpha and beta cells
#For alpha, beta, delta, and polyhormonal cells
#Split objects into cell types first, obtain top DEGs in each alpha and beta cell cluster
#Example for beta cells:

Idents(endo) <- "endo_celltype"
levels(endo)
DefaultAssay(endo) <- "integrated"

beta <- subset(endo, idents = "Beta")
DimPlot(beta)
saveRDS(beta, file = "Directory/objects/beta.rds")

Idents(beta) <- "cluster_name"
levels(beta)
levels(beta) <- c("Beta1", "Beta2", "Beta3", "Beta4", "Beta5", "Beta6", "Beta7")
DefaultAssay(beta) <- "SCT"
beta_cluster_deg <- FindAllMarkers(beta, assay = "SCT", only.pos = TRUE, logfc.threshold = 2.0, verbose = TRUE)
write.csv(beta_cluster_deg, file = "Directory/DEG/beta_clusters_deg.csv")

beta_cluster_top10 <- c("CNTN5", "PTPRD", "TRMP3", "UNC5D", "LSAMP", "DGKB", "MEG3", "SPP1", "NPY", "IGFBP5",
                        "GRAMD2B", "TMED6", "MYL6", "LINC01091", "MARK1", "TBC1D4", "FTH1", "LINC01146", "GNAS", "IAPP",
                        "RBP4", "TIMP1", "HSPA5", "PAPSS2", "NEAT1", "MT-ND1", "HS6ST3", "PCSK1N", "FGF14", "PRG4", "KCNMA1",
                        "HERPUD1", "CHGB", "MGRN1", "SERP1", "ARF4", "SLC25A36", "CEBPG", "GLRX5", "CLTRN", "SLC9A3R1",
                        "MT1X", "MT2A", "MT1E", "MT1F", "MT1M", "MT1G", "SOD2", "DNAJC12", "TNFRSF12A", "PTMS",
                        "AC106793.1", "EGLN3", "AC112206.2", "AL138828.1", "AL163541.1", "LINC02542", "AC021192.1", "IKZF3", "TSBP1-AS1", "MEIKIN",
                        "DMD", "PRUNE2", "SAT1", "TMEM176B", "UBE2D3", "OAZ1", "H1F0", "TBL1XR1", "CCDC288")

betahm <- DoHeatmap(beta, features = beta_cluster_top10, assay = "SCT") + scale_fill_gradientn(colors = c("blue4", "white", "red"))
betahm
ggsave("beta_cluster_DEG_heatmap.pdf", plot = betahm, device = "pdf", path =
```

```
"Directory/DEG/", width = 8, height = 11, units = "in")

#Identifying calcium-regulated and glucose-regulated genes in each cluster
#Split the cell type objects into paired conditions for conditional comparisons
#Positive and Negative for calcium-regulated genes, Low and Positive for glucose-regulated
#For alpha cells only, use Low and Negative instead of Low and Positive
#Example for beta cells

Idents(beta) <- "Condition"
levels(beta)
beta_pn <- subset(beta, idents = c("Positive", "Negative"))
Idents(beta_pn) <- "Condition"
levels(beta_pn)
saveRDS(beta_pn, file = "Directory/objects/beta_pn.rds")

Idents(beta) <- "Condition"
levels(beta)
beta_lp <- subset(beta, idents = c("Low", "Positive"))
Idents(beta_lp) <- "Condition"
levels(beta_lp)
saveRDS(beta_lp, file = "Directory/objects/beta_lp.rds")

#Obtain DEG in each cluster using the split objects, comparing the 2 conditions
#For delta cells, there are no clusters – use the delta_pn and delta_lp objects
#Must perform function in each cluster one by one
#Example for Positive vs Negative comparison in cluster Beta1:

Idents(beta_pn) <- "cluster_name"
levels(beta_pn)

beta1_pn_deg <- FindMarkers(beta_pn, ident.1 = "Positive", ident.2 = "Negative", group.by =
'Condition', subset.ident = "Beta1")
write.csv(beta1_pn_deg, file = "Directory/DEG/Beta1_PvN_deg.csv")

#Generate split violin plots for calcium-regulated or glucose-regulated genes
#Example:

beta_calcium_genes <- c("NPAS4", "IAPP", "ZNF331", "NR4A1")
Calcium_vln <- VlnPlot(beta_pn, features = beta_calcium_genes, cols = c("dodgerblue",
"forestgreen"), pt.size = 0, split.by = "Condition", split.plot = TRUE, ncol = 2)
ggsave("beta_calcium_vln.pdf", plot = Calcium_vln, device = "pdf", path = "Directory/Violins/",
width = 11, height = 8, units = "in")

#Split beta cells into PCDH7-high and PCDH7-low
#Obtain DEG lists for PCDH7-high vs PCDH7-low
#Set cutoff for PCDH7-high based on ridge plot of PCDH7 expression in beta cells
```

```
Idents(beta) <- "cluster_name"
levels(beta)
DefaultAssay(beta) <- "SCT"

ridgeplot <- RidgePlot(beta, features = "PCDH7", assay = "SCT")
ggsave("beta_PCDH7_ridge.pdf", plot = ridgeplot, device = "pdf", path = "Directory/", width =
8, height = 8, units = "in")

pcdh7_high <- WhichCells(beta, expression = PCDH7 > 1)
beta$PCDH7_status <- ifelse(colnames(beta) %in% pcdh7_high, "PCDH7_HIGH",
"PCDH7_LOW")

Idents(beta) <- "PCDH7_status"
DotPlot(beta, features = "PCDH7")

saveRDS(beta, file = "Directory/objects/beta.rds")

pcdh7_deg <- FindMarkers(beta, ident.1 = "PCDH7_HIGH", ident.2 = "PCDH7_LOW")
write.csv(pcdh7_deg, file = "Directory/pcdh7/PCDH7_high_vs_low_deg.csv")

PCDH7_dot <- DotPlot(beta, features = "PCDH7", cols = c("blue", "red"), dot.scale = 20)
ggsave("PCDH7_dotplot.pdf", plot = PCDH7_dot, device = "pdf", path = "Directory/pcdh7/",
width = 8, height = 11, units = "in")

PCDH7_feature <- FeaturePlot(endo, "PCDH7", order = TRUE)
ggsave("PCDH7_featureplot.pdf", plot = PCDH7_feature, device = "pdf", path =
"Directory/pcdh7/", width = 11, height = 11, units = "in")

#Subset polyhormonal cells + alpha or polyhormonal cells + beta cells from endo
#Generate heatmaps comparing alpha and beta maturity markers
#Use average expression of genes per cluster for cleaner heatmap
#Example for polyhormonal cells + beta cells

mature.beta <- c("INS", "IAPP", "MAFA", "UCN3", "PDX1", "ERO1B", "NKX2-2", "NKX6-
1")
DefaultAssay(endo) <- "integrated"
Idents(endo) <- “Cell_Type”
polybeta <- subset(endo, idents = c("Beta", "Polyhormonal"))
saveRDS(polybeta, file = "Directory/objects/polybeta.rds")
avg_polybeta <- AverageExpression(polybeta, return.seurat = TRUE)
saveRDS(avg_polybeta, file = "Directory/objects/avg_polybeta.rds")
polyvsbeta <- DoHeatmap(avg_polybeta, features = mature.beta, draw.lines = FALSE) +
scale_fill_gradientn(colors = c("blue", "white", "red"))
ggsave("polybeta_hm.pdf", plot = polyvsbeta, device = "pdf", path = "Directory/DEG/", width =
8, height = 8, units = "in")
```

Appendix C | Analysis of single cell RNA sequencing data in chapter 6

```
#Replace Directory with appropriate destination
#Remember to check cell counts at each key step
#load packages in Rstudio

library(Seurat)
library(dplyr)
library(ggplot2)
library(cowplot)
library(patchwork)
library(sctransform)

#Create Seurat object from raw data – downstream outputs of Cell Ranger v7
#Replace object name and repeat until all 13 samples have been completed
#Samples are genotype and sample number (example: CT1)
#CT1-CT4, KO1-KO3 are refed; CT5-CT7, KO4-KO6 are fasted
#Save copies of the newly generated raw Seurat objects
#Example for CT1:

CT1_raw <- Read10X(data.dir = "Directory/CT1/outs/filtered_feature_bc_matrix/")
CT1 <- CreateSeuratObject(counts = CT1_raw, project = "CT1", min.cells = 3, min.features =
200)
saveRDS(CT1, file = "Directory/Objects/CT1_RAW.rds")

#For QC, make new column in metadata for percentage of mitochondrial genes per cell
#Visualize QC metrics nFeature_RNA, nCounts_RNA, percent.mt for each sample
#Save QC plots for metrics – determine QC cutoff
#Repeat for all samples – make sure same QC cutoffs are appropriate for all

CT1[["percent.mt"]] <- PercentageFeatureSet(CT1, pattern = "^mt-")
CT1.QC <- VlnPlot(CT1, features = c("nFeature_RNA", "nCount_RNA", "percent.mt"), ncol =
3)
ggsave("CT1_prefilter.pdf", plot = CT1.QC, device = "pdf", path = "Directory/QCplots/", width
= 11, height = 11, units = "in")

#Set Threshold for filtering cells - all objects
#Only keep cells with percent.mt < 20% and nFeature < 7500
#Re-plot the QC metrics after filtering and save the plots

CT1 <- subset(CT1, subset = nFeature_RNA < 7500 & percent.mt < 20)
CT1.filter.QC <- VlnPlot(CT1, features = c("nFeature_RNA", "nCount_RNA", "percent.mt"),
ncol = 3)
ggsave("CT1_filter.pdf", plot = CT1.filter.QC, device = "pdf", path = "Directory/QCplots/",
width = 11, height = 11, units = "in")
```

```
#Run SCTransform for normalization on each sample separately
#Make sure to save each SCT object

CT1 <- SCTransform(CT1, verbose = FALSE)
saveRDS(CT1, file = "Directory/Objects/CT1_SCT.rds")

#Turn objects into list and integrate
arc.all.list <- list(CT1, CT2, CT3, CT4, CT5, CT6, CT7, KO1, KO2, KO3, KO4, KO5, KO6)

#Select integration features and prep for integration
#Then find anchors and integrate

arc.all.features <- SelectIntegrationFeatures(object.list = arc.all.list, nfeatures = 3000)
arc.all.list <- PrepSCTIntegration(object.list = arc.all.list, anchor.features = arc.all.features)

arc.all.anchors <- FindIntegrationAnchors(object.list = arc.all.list, normalization.method =
"SCT", anchor.features = arc.all.features)
arc.all <- IntegrateData(anchorset = arc.all.anchors, normalization.method = "SCT")

#Save the integrated object
saveRDS(arc.all, file = "Directory/Objects/ARC_all.rds")

#Run PCA, determine number of dimensions
#Use elbow plot and confirm with heatmaps
#Run UMAP dimensional reduction and find neighbours for clustering
#Save the object before clustering so it can be re-loaded for clustering at a different resolution

arc.all <- RunPCA(arc.all, verbose = FALSE)
elbowplot <- ElbowPlot(arc.all, ndims = 50, reduction = "pca")
elbowplot
ggsave("arc_all_elbow.pdf", plot = elbowplot, device = "pdf", path = "Directory/QCplots/",
width = 11, height = 8.5, units = "in")

DimHeatmap(arc.all, dims = 35:45, cells = 500, balanced = TRUE)
arc.all <- RunUMAP(arc.all, reduction = "pca", dims = 1:40, verbose = FALSE)
arc.all <- FindNeighbors(arc.all, dims = 1:40, verbose = FALSE)

saveRDS(arc.all, file = "Directory/Objects/ARC_all_precluster.rds")

#Continue with specifying cluster resolution
#Save object once cluster resolution is finalized

arc.all <- FindClusters(arc.all, resolution = 0.6)
clusters.umap <- DimPlot(arc.all, reduction = "umap", label = TRUE) + NoLegend()
ggsave("ARC_seurat_clusters.pdf", plot = clusters.umap, device = "pdf", path =
"Directory/umaps/", width = 11, height = 11, units = "in")
```

```
quick.genes <- c("Snap25", "Syt1", "Olig1", "Agt")
extra.genes <- c("Ccdc153","Rax","Cldn5","Myh11","Cx3cr1","C1qa","Mrc1")

cluster.test <- FeaturePlot(arc.all, features = quick.genes, order = TRUE, min.cutoff = 0)
ggsave("clustertest_umap.pdf", plot = cluster.test, device = "pdf", path = "Directory/umaps/",
width = 11, height = 11, units = "in")
cluster.test2 <- FeaturePlot(arc.all, features = extra.genes, order = TRUE, min.cutoff = 0)
ggsave("clustertest2_umap.pdf", plot = cluster.test2, device = "pdf", path = "Directory/umaps/",
width = 11, height = 11, units = "in")

saveRDS(arc.all, file = "Directory/Objects/ARC_all_res0.6.rds")

#Get number of cells in each cluster, from each sample

cells.per.cluster <- table(arc.all$seurat_clusters, arc.all$genotype)
write.csv(cells.per.cluster, file = "Directory/cells_per_cluster.csv")
condition.per.cluster <- table(arc.all$seurat_clusters, arc.all$condition)
write.csv(condition.per.cluster, file = "Directory/condition_per_cluster.csv")

#Find all markers per cluster for further cluster identity identification

DefaultAssay(arc.all) <- "RNA"
cluster.deg <- FindAllMarkers(arc.all, assay = "RNA", only.pos = TRUE, min.pct = 0.50,
logfc.threshold = 0.25)
write.csv(cluster.deg, file = "Directory/DEG/all_cluster_deg.csv")

#UMAP plot of all clusters in object

Idents(arc.all) <- "seurat_clusters"
levels(arc.all)
seurat_umap <- DimPlot(arc.all, reduction = "umap", label = FALSE) + NoLegend()
seurat_umap
ggsave("ARC_seurat_clusters_nolabel.pdf", plot = seurat_umap, device = "pdf", path = "~/",
width = 11, height = 11, units = "in")

#UMAP plot split by genotype

arc_splitgeno <-DimPlot(arc.all, split.by = "genotype") + NoLegend()
arc_splitgeno
ggsave("ARC_umap_split_geno.pdf", plot = arc_splitgeno, device = "pdf", path = "~/", width =
22, height = 11, units = "in")

#UMAP plot split by condition

arc_splitcond <- DimPlot(arc.all, split.by = "condition") + NoLegend()
arc_splitcond
```

```
ggsave("ARC_umap_split_cond.pdf", plot = arc_splitcond, device = "pdf", path = "~/", width = 22, height = 11, units = "in")

#Metadata labelling
#orig.ident content values will be RENAMED to the format condition_genotype_sampleID
#R = Refed, F = Fasted; CT = control, KO = knockout
#Example for CT1:

Idents(arc.all) <- "orig.ident"
levels(arc.all)
cells.use <- WhichCells(object = arc.all, idents = "CT1")
arc.all <- SetIdent(object = arc.all, cells = cells.use, value = "R_CT_1")
arc.all[["orig.ident"]] <- Idents(object = arc.all)

#cluster_name column will be made to label cells with a specific cluster name in a cell type
#Example for Neuron1 cluster (cluster 5)

Idents(arc.all) <- "seurat_clusters"
levels(arc.all)
cells.use <- WhichCells(object = arc.all, idents = 5)
arc.all <- SetIdent(object = arc.all, cells = cells.use, value = "Neuron1")
arc.all[["cluster_name"]] <- Idents(object = arc.all)

#cell_type column will be made to label cells with a cell type
#Example for Neurons

Idents(arc.all) <- "seurat_clusters"
levels(arc.all)
cells.use <- WhichCells(object = arc.all, idents = c("5", "15", "16", "21", "22", "25", "32"))
arc.all <- SetIdent(object = arc.all, cells = cells.use, value = "Neurons")
arc.all[["cell_type"]] <- Idents(object = arc.all)

#genotype column will be made to label cells with either CT (control) or KO (knockout)

Idents(arc.all) <- "orig.ident"
levels(arc.all)

cells.use <- WhichCells(object = arc.all, idents = c("R_CT_1", "R_CT_2", "R_CT_3",
"R_CT_4", "F_CT_5", "F_CT_6", "F_CT_7"))
arc.all <- SetIdent(object = arc.all, cells = cells.use, value = "CT")
arc.all[["genotype"]] <- Idents(object = arc.all)
cells.use <- WhichCells(object = arc.all, idents = c("R_KO_8", "R_KO_9", "R_KO_10",
"F_KO_11", "F_KO_12", "F_KO_13"))
arc.all <- SetIdent(object = arc.all, cells = cells.use, value = "KO")
arc.all[["genotype"]] <- Idents(object = arc.all)
```

```
#condition column will be made to label cells with either fasted or refed

Idents(arc.all) <- "orig.ident"
levels(arc.all)

cells.use <- WhichCells(object = arc.all, idents = c("R_CT_1", "R_CT_2", "R_CT_3",
"R_CT_4", "R_KO_8", "R_KO_9", "R_KO_10"))
arc.all <- SetIdent(object = arc.all, cells = cells.use, value = "Refed")
arc.all[["condition"]] <- Idents(object = arc.all)
cells.use <- WhichCells(object = arc.all, idents = c("F_CT_5", "F_CT_6", "F_CT_7",
"F_KO_11", "F_KO_12", "F_KO_13"))
arc.all <- SetIdent(object = arc.all, cells = cells.use, value = "Fasted")
arc.all[["condition"]] <- Idents(object = arc.all)

#sample_number will be made to label cells coming from a unique biological sample
#numbers 1 through 13 will be used
#Example for sample R_CT_1 (sample 1)

Idents(arc.all) <- "orig.ident"

cells.use <- WhichCells(object = arc.all, idents = "R_CT_1")
arc.all <- SetIdent(object = arc.all, cells = cells.use, value = "1")
arc.all[["sample_number"]] <- Idents(object = arc.all)

saveRDS(arc.all, file = "Directory/Objects/ARC_all_res0.6.rds")

#Generate UMAP plot of all cells coloured by cell type

Idents(arc.all) <- "cell_type"
arc.umap.celltypes <- DimPlot(arc.all) + NoLegend()
arc.umap.celltypes
ggsave("ARC_umap_celltypes_nolabel.pdf", plot = arc.umap.celltypes, device = "pdf", path =
"~/", width = 11, height = 11, units = "in")

#Generate dot plot of marker genes for each cell type

levels(arc.all) <- c("Astrocytes", "Neurons", "Tanycytes", "Ependymocytes",
"Oligodendrocytes", "Endothelial", "Microglia", "Mystery")
celltype_genes <- c("Agt", "Gfap", "Snap25", "Resp18", "Syt1", "Rbfox3",
                    "Slc17a6", "Slc32a1", "Rax", "Gpr50", "Ccdc153", "Tmem212",
                    "Olig1", "Mag", "Pllp", "Mobp", "Cldn5", "Myh11", "Slc38a5",
                    "Slco1c1", "C1qa", "Mrc1", "Cx3cr1", "Aif1", "Pdgfra", "Lum", "Dcn", "Col15a1")
celltype_dotplot <- DotPlot(arc.all, assay = "SCT", features = celltype_genes, dot.scale = 10) +
RotatedAxis()
ggsave("arc_celltype_dot.pdf", plot = celltype_dotplot, device = "pdf", path = "~/arc_umap",
width = 22, height = 11, units = "in")
```

```
#From arc.all, subset out only cells that are Neurons, and express Pomc
#Save the subsetted Pomc+ neurons as a separate object

theme_set(theme_cowplot())
Idents(arc.all) <- "cell_type"
DefaultAssay(arc.all) <- "integrated"

pomc.neurons <- subset(arc.all, subset = Pomc > 0, idents = "Neurons")
saveRDS(pomc.neurons, file = "Directory/Objects/ARC_all_POMC.rds")

#Add metadata column within pomc.neurons so both condition and genotype are included

Idents(pomc.neurons) <- "orig.ident"
levels(pomc.neurons)

cells.use <- WhichCells(object = pomc.neurons, idents = c("R_CT_1", "R_CT_2", "R_CT_3",
"R_CT_4"))
pomc.neurons <- SetIdent(object = pomc.neurons, cells = cells.use, value = "Refed_CT")
pomc.neurons[["condition_genotype"]] <- Idents(object = pomc.neurons)

cells.use <- WhichCells(object = pomc.neurons, idents = c("R_KO_8", "R_KO_9",
"R_KO_10"))
pomc.neurons <- SetIdent(object = pomc.neurons, cells = cells.use, value = "Refed_KO")
pomc.neurons[["condition_genotype"]] <- Idents(object = pomc.neurons)

cells.use <- WhichCells(object = pomc.neurons, idents = c("F_CT_5", "F_CT_6", "F_CT_7"))
pomc.neurons <- SetIdent(object = pomc.neurons, cells = cells.use, value = "Fasted_CT")
pomc.neurons[["condition_genotype"]] <- Idents(object = pomc.neurons)

cells.use <- WhichCells(object = pomc.neurons, idents = c("F_KO_11", "F_KO_12",
"F_KO_13"))
pomc.neurons <- SetIdent(object = pomc.neurons, cells = cells.use, value = "Fasted_KO")
pomc.neurons[["condition_genotype"]] <- Idents(object = pomc.neurons)

saveRDS(pomc.neurons, file = "Directory/Objects/ARC_all_POMC.rds")

#General DEGs between KO and CT in all POMC neurons

DefaultAssay(pomc.neurons) <- "SCT"
Idents(pomc.neurons) <- "genotype"
levels(pomc.neurons)
pomc.geno.deg <- FindAllMarkers(pomc.neurons, assay = "SCT", only.pos = TRUE)
write.csv(pomc.geno.deg, file = "Directory/AllPomcNeurons_KOvsCT_deg.csv")

geno.deg <- c("Cwc22", "Agt", "Mt2", "Slc6a11",
          "Rpl21", "Prkg1", "Marchf1", "Snhg11", "Kcnip4", "Pcdh9")
```

```
dot.geno <- DotPlot(pomc.neurons, assay = "SCT", features = geno.deg, dot.scale = 20, col.min = 0)
ggsave("CT_KO_DEG_dotplot.pdf", plot = dot.geno, device = "pdf", path = "~/arc_data", width = 11, height = 11, units = "in")

#Identifying refeeding-regulated genes in CT POMC neurons only

Idents(pomc.neurons) <- "condition_genotype"
refeed.CT.genes <- FindMarkers(pomc.neurons, ident.1 = "Refed_CT", ident.2 = "Fasted_CT")
write.csv(refeed.CT.genes, file = "Directory/CT_POMC_Refed_vs_Fasted_genes.csv")

#Refeeding-regulated genes within KO POMC neurons only

Idents(pomc.neurons) <- "condition_genotype"
refeed.KO.genes <- FindMarkers(pomc.neurons, ident.1 = "Refed_KO", ident.2 = "Fasted_KO")
write.csv(refeed.KO.genes, file = "Directory/KO_POMC_Refed_vs_Fasted_genes.csv")

#Refed_CT vs Refed_KO

Idents(pomc.neurons) <- "condition_genotype"
Refed.CTvsKO.genes <- FindMarkers(pomc.neurons, ident.1 = "Refed_CT", ident.2 = "Refed_KO")
write.csv(Refed.CTvsKO.genes, file = "Directory/Refed_POMC_CT_vs_KO_genes.csv")

#Gene Ontology using DEenrichRPlot
#Use Biological Process and Molecular Function 2021
#Generate barplots of top 20 terms and CSV outputs
#For general CT vs KO (all POMC neurons) and for Refed_CT vs Refed_KO only

POMC_CT_KO_BP <- DEenrichRPlot(pomc.neurons, ident.1 = "CT", ident.2 = "KO", assay = "SCT", max.genes = 800, enrich.database = "GO_Biological_Process_2021", num.pathway = 20, return.gene.list = TRUE)
write.csv(POMC_CT_KO_BP, file = "Directory/enrichR/POMC_CT_KO_BiolProc.csv")

plot_POMC_CT_KO_BP <- DEenrichRPlot(pomc.neurons, ident.1 = "CT", ident.2 = "KO", assay = "SCT", max.genes = 800, enrich.database = "GO_Biological_Process_2021", num.pathway = 20)
ggsave("POMC_CT_KO_BP_barplot.pdf", plot = plot_POMC_CT_KO_BP, device = "pdf", path = "Directory/enrichR", width = 22, height = 11, units = "in")

POMC_CT_KO_MF <- DEenrichRPlot(pomc.neurons, ident.1 = "CT", ident.2 = "KO", assay = "SCT", max.genes = 800, enrich.database = "GO_Molecular_Function_2021", num.pathway = 20, return.gene.list = TRUE)
write.csv(POMC_CT_KO_MF, file = "Directory/enrichR/POMC_CT_KO_MolFunc.csv")

plot_POMC_CT_KO_MF <- DEenrichRPlot(pomc.neurons, ident.1 = "CT", ident.2 = "KO",
```

```
assay = "SCT", max.genes = 800, enrich.database = "GO_Molecular_Function_2021",
num.pathway = 20)
ggsave("POMC_CT_KO_MF_barplot.pdf", plot = plot_POMC_CT_KO_MF, device = "pdf",
path = "Directory/enrichR", width = 22, height = 11, units = "in")

RefedCT_KO_BP <- DEenrichRPlot(pomc.neurons, ident.1 = "Refed_CT", ident.2 =
"Refed_KO", assay = "SCT", max.genes = 600, enrich.database =
"GO_Biological_Process_2021", num.pathway = 20, return.gene.list = TRUE)
write.csv(RefedCT_KO_BP, file = "Directory/enrichR/Refed_CT_KO_BioProc.csv")

plot_RefedCT_KO_BP <- DEenrichRPlot(pomc.neurons, ident.1 = "Refed_CT", ident.2 =
"Refed_KO", assay = "SCT", max.genes = 600, enrich.database =
"GO_Biological_Process_2021", num.pathway = 20)
ggsave("Refed_CT_KO_BP_barplot.pdf", plot = plot_RefedCT_KO_BP, device = "pdf", path =
"Directory/enrichR", width = 22, height = 11, units = "in")

#Split violin plots for genes showing all four conditions and genotypes
#Example for IEG

ieg <- c("Fos", "Egr1", "Jund", "Fosb", "Junb", "Jun","Npas4", "Arc")
pomc.ieg.cond <- VlnPlot(pomc.neurons, features = ieg, pt.size = 0, ncol = 3)
ggsave("IEG_split_vlns.pdf", plot = pomc.ieg.cond, device = "pdf", path = "~/", width = 11,
height = 8, units = "in")

#Dot plots for DEG between CT and KO POMC neurons
#Example for GABA receptor subunit genes from GO analysis

dot.gabar.geno <- DotPlot(pomc.neurons, assay = "SCT", c("Gabrb3", "Gabrb1", "Gabrg3",
"Gabra2", "Gabrg1", "Gabrg2", "Gabra3"), dot.scale = 20, col.min = 0)

ggsave("CT_KO_gabar_genes_dotplot.pdf", plot = dot.gabar.geno, device = "pdf", path = "~/",
width = 11, height = 11, units = "in")
```